MAGNETIC, STRUCTURAL AND SEDIMENTOLOGICAL ANALYSIS OF GLACIAL SEDIMENTS: INSIGHTS FROM MODERN, QUATERNARY AND NEOPROTEROZOIC ENVIRONMENTS

by

Edward James Fleming

A thesis submitted to
The University of Birmingham
For the degree of
DOCTOR OF PHILOSOPHY

Department of Earth Sciences
School of Geography, Earth and
Environmental Sciences
The University of Birmingham
January 2014

ABSTRACT

Glacial sediments, particularly diamicts, can be ambiguous to interpret. Fabric analyses, such as anisotropy of magnetic susceptibility (AMS), have been shown to provide specific information on the formation and subsequent deformation of glacial sediments. In this thesis, detailed investigations utilising the AMS technique have been combined with traditional sedimentological and structural techniques, to help resolve a number of current problems in glacial geology. At the same time, limitations of such uses of AMS have been established. In the modern environment (Tunabreen, Svalbard), magnetic lineations develop parallel to glacier flow and reveal dynamic behaviour during past surges. In a Quaternary glaciotectonite (Bacton Green Till Member, Norfolk, UK), AMS fabric develop in response to glacial deformation and reveal strain vectors that can be related to ice flow from contrasting directions. Finally in Neoproterozoic diamictites (Wilsonbreen Formation, Svalbard), despite local tectonic overprinting and diagenetic change, AMS can be used to reveal a dominant ice-flow to direction to the north. In combination with other sedimentological techniques, this has allowed the identification of glaciotectonic features and an ice-marginal, terrestrial and subaqueous model is proposed. These results support the use of AMS as a fast, objective and accurate technique that can facilitate the interpretation of cryptic glacial sediments.

ACKNOWLEDGEMENTS

In doing this PhD, I have been the envy of many of my peers. Not only have I had the opportunity to work in some of the wildest and most beautiful landscapes on Earth, I have been supported by a world-renowned supervisory team. Without whom, this PhD would not have been completed.

I would like to start by thanking my supervisors at the University of Birmingham (Dr. Carl Stevenson and Professor Ian Fairchild) for their guidance, help and support at every single stage of this PhD. Carl – your in-depth knowledge of structural geology and anything AMS-related have been a real help. Thanks for always showing interest in my work and for encouraging me to delve into new areas. Ian - thanks for devoting so much of your time to me. Despite becoming Head of school, you have somehow always found time to be there to offer your experience and wisdom, whenever I needed help or advice. Thanks for supporting my varied academic interests and ideas but also for keeping me on the straight and narrow when it was needed.

In addition, I would like to thank my external supervisors, Professor Mike Hambrey and Professor Doug Benn. Mike - thanks for your help with all glacial things glacial related and for sharing your vast editorial knowledge with me. Thanks also for teaching me the 'correct' way to pronounce glacier (gla-ssy-er) and for trying to rid me of my Americanisms and bad grammatical habits. Doug - thanks for your extensive support whilst in Svalbard and for setting up my work at UNIS. I also owe special thanks to my (unofficial) supervisor, Dr. Mike Petronis. Thanks for the extensive guidance and support whilst in New Mexico and for financially supporting me during my inevitable disasters (like losing my Wallet!). I would like to extend this thanks to Mike's colleagues and students at New Mexico Highlands University, for making me feel so welcome during my visits.

I have been fortunate in my research to have met many amazing people. I've had the pleasure of meeting and working with Dr. Tony Spencer, who as well as introducing me to Scottish diamictites, has included me in (and funded!) several trips to the Garvellachs. In addition, I have made many friends on my extensive visits to Longyearbyen, Svalbard. Thanks to all the staff and students at UNIS - I will definitely miss the Friday gatherings! I would also like to take this

opportunity to thank Harold Lovell, who shared many of the trials, tribulations and triumphs of Svalbard fieldwork with me.

I would like to thank both staff and students within Earth Sciences at the University of Birmingham for making my time there so enjoyable. Whilst there, I was fortunate to have been introduced into the legacy of Room 116. I would like to thank the other former inhabitants: Paul Anderson, Plaman Andreev, Craig Magee, Andy Rees, Ken McDermott and Ben Slater for the many fascinating discussions and situations that have provided a welcome break from PhD work. I would like to thank the other PhD students of the department and the various students that have visited. in particular, I'd like to thank William McCarthy for providing various discussions on AMS both during his visits and elsewhere.

I also owe thanks to the technical and administrative staff: Gretchel Coldicott, Aruna Mistry, and in particular Paul hands. Thanks Paul for your always prompt preparation of thin-sections and for putting up with my seemingly endless sawing whilst preparing samples for AMS (I can assure you Paul - it was worse for me than it was you!).

On a funding note, this PhD was undertaken with financial support from the Natural Environment Research Council (NERC). The PhD was a tied-studentship to the GAINS (Glacial Activity in Neoproterozoic Svalbard) grant (NE/H004963/1). In addition, the Research Council of Norway Arctic Field Grant program is thanked for the additional funding they provided for fieldwork at Tunabreen in Svalbard and the QRA for providing funding for my the participation at the European Geosciences Union, General Assembly 2013.

Penultimately, I would like to thank my friends and family. Special thanks go to Tara Grove, for always being there and for putting up with the late-evenings (and very early mornings) that writing this thesis entailed. In addition, thanks to my father (Alan Fleming) for always encouraging me to do what I enjoy. Thanks both for your unconditional support (both moral and financial) - and for proof-reading parts of this thesis!

Finally, I owe thanks to my examiners (Dr. Dan Le Heron and Professor Tim Reston) for examining (and passing!) this thesis.

TABLE OF CONTENTS

LIST OF FIGURES

Photo caption *- Carl Stevenson on a nunnatack of diamictite at Pinnsvinfjellet, Olav V land, Svalbard*

LIST OF TABLES

LIST OF ABBREVIATIONS

AF	Alternating Field
A/M	Ampere-meter
ARM	Anhysteretic remanent magnetisation
P_j	Anisotropy degree
AARM	Anisotropy of anhysteretic remanent magnetization
AMS	Anisotropy of Magnetic Susceptibility
H	Applied magnetic field
BIRM	Back-field isothermal remanent magnetisation
cm	Centimetre
c.f.	Compare with
dm	Decimetre
S_2	Eigenvalue of the intermediate eigenvector
S_3	Eigenvalue of the minimum eigenvector
S_1	Eigenvalue of the principle eigenvector
F	Foliation parameter
W3	Gropbreen Member
Hz	Hertz
M	Induced magnetisation
V_2	Intermediate eigenvector
K_2	Intermediate susceptibility axis
IRM	Isothermal remanent magnetisation
km	Kilometre
Fl	Laminated fines
L	Lineation parameter
J/J_{max}	Magnetisation, normalised to maximum magnetisation
Dm	Massive diamictite
Fm	Massive fines
Gm	Massive gravel
Sm	Massive sand
K_1	Maximum susceptibility axis
K_{mean}	Mean susceptibility
MDF	Medium destructive field
Ma	Mega-annum (million years)
µm	Micrometre
W2	Middle Carbonate Member
mT	Millitesla
V_3	Minimum eigenvector

K_3	Minimum susceptibility axis
MD	Multi-domain
NRM	Natural remanent magnetisation
K_0/K	Normalised reciprocal susceptibility
K/K_0	Normalised susceptibility
W1	Ormen Member
E2	Petrovbreen Member
V_1	Principal eigenvector
PSD	Pseudo single domain
SIRM	Saturation isothermal remanent magnetisation
s.s.	Senso stricto
T	Shape parameter
SD	Single-domain
E4	Slangen Member
Ds	Stratified diamictite
Gs	Stratified gravel
Ss	Stratified/laminated sand
K	Susceptibility
K_0	Susceptibility at room temperature
T	Tesla
SI	The International System of Units

IJF	Professor Ian J. Fairchild (supervisor)[1]
CTS	Dr. Carl Stevenson (supervisor)[1]
MJH	Professor Michael Hambrey (supervisor)[2]
DB	Professor Douglas I. Benn (supervisor)[3]
MSP	Dr. Michael S. Petronis (collaborator) [4]
HL	Harold Lovell (collaborator)[3,5]
EAM	Emily McMillan (collaborator)[1]

[1] School of Geography, Earth and Environmental Sciences, University of Birmingham, Birmingham B15 2TT, UK

[2] Institute of Geography and Earth Sciences, Aberystwyth University, Aberystwyth, UK

[3] Department of Geology, The University Centre in Svalbard (UNIS), Longyearbyen, Norway

[4] Natural Resource Management, New Mexico Highlands University, Las Vegas, NM, USA

[5]School of Geography, Queen Mary University of London, London, E1 4NS, UK

STATEMENT OF CONTRIBUTION

This study forms part of the NERC funded GAINS (Glacial Activity in Neoproterozoic Svalbard) grant (NE/H004963/1), the aims of which are to strengthen our understanding of the nature of extreme Neoproterozoic glaciation in Svalbard. This has involved the collection of a large pool of data by a number of national and international partners. However, all of the work presented in this thesis is my own, unless otherwise stated. In addition, Chapters 3 and 4 form part of co-authored published papers. However, I am the primary author in these, and I am responsible for the content. General guidance and proof-reading have been provided by my supervisors throughout.

In Chapter 3 (forming part of Fleming et al., in press), I am responsible for all of the planning, data collection, data analysis and writing. Field work was undertaken in combination with HL who was working on a separate project (Lovell, 2014). DB provided guidance during fieldwork and MSP provided guidance whilst carrying out rock magnetic experiments. IJF, CTS and MJH provided general supervision and all the co-authors helped with proof-reading.

In Chapter 4 (forming part of Fleming et al., 2013), I am responsible for all of the planning, data collection, data analysis and writing. MSP provided guidance whilst carrying out rock magnetic experiments and CTS provided general supervision and in addition MJH and IJF helped with proof-reading.

In Chapters 5, and 6, some of the data from two sites (Dracoisen and Ditlovtoppen) were obtained by my supervisors (CTS, MJH, DB, IJF and MPS) prior to the start of my PhD studentship. At these sites, apart from the collection itself, I am responsible for all of the subsequently analysis, and all of the interpretations are my own.

CHAPTER 1.

INTRODUCTION

1.1. Introduction

Glaciers and ice sheets have, today and in the past, had an enormous influence on all aspects of the earth system. It is suggested that there have been at least 11 epochs in the earth's history where there has been extensive and long lasting glaciation (Hambrey and Harland, 1981). As the ice from these periods has long since melted, clues to its existence has to be drawn from the sedimentary record. Glacial environments are inherently dynamic and deposition can result in a wide range of sedimentary environments through a variety of processes. No other sedimentary environment exhibits such rapid and spatially variable changes of processes which can make it very difficult to interpret. Furthermore, the sediment types most frequently associated with glaciation are enigmatic diamictites. The term diamictite (diamicton for the unlithified equivalent) follows the mis-named symmictite (Flint et al., 1960b) and is defined as a non-sorted terrigenous sediment or rock that contains a wide range of particle sizes, regardless of genesis (Flint et al., 1960a; Flint, 1971). These sediments are often structureless, therefore compounding the overall difficulty, which has lead to major controversies in the interpretation of the geological record.

A great deal of research has previously been carried out on glacial sediments using classic sedimentological and structural techniques. In this thesis, key issues of glacial sedimentology are examined through the novel use of the anisotropy of magnetic susceptibility (AMS) technique. The study has been carried out in conjunction with classic sedimentological and structural techniques to establish a comparative basis for assessing the potential of AMS as an effective tool in the interpretation of glacial sediments.

1.2. Glacial sedimentary environments

For the purposes of this study, environments of glacial sedimentation can be broadly divided into three main types: forming beneath the ice (subglacial), forming within water (subaqueous - glaciomarine or glaciolacustrine) and forming on the land surface (proglacial). For detailed

reviews on glacial depositional environments, see Menzies (2002) Evans (2005), and Benn and Evans (2010).

Subglacial environments (Fig. 1.1) occur where the ice is in direct contact with the glacier bed. Despite subglacial tills covering large parts of North America and Northern Europe, the subglacial environment is one of the least understood depositional environments, largely

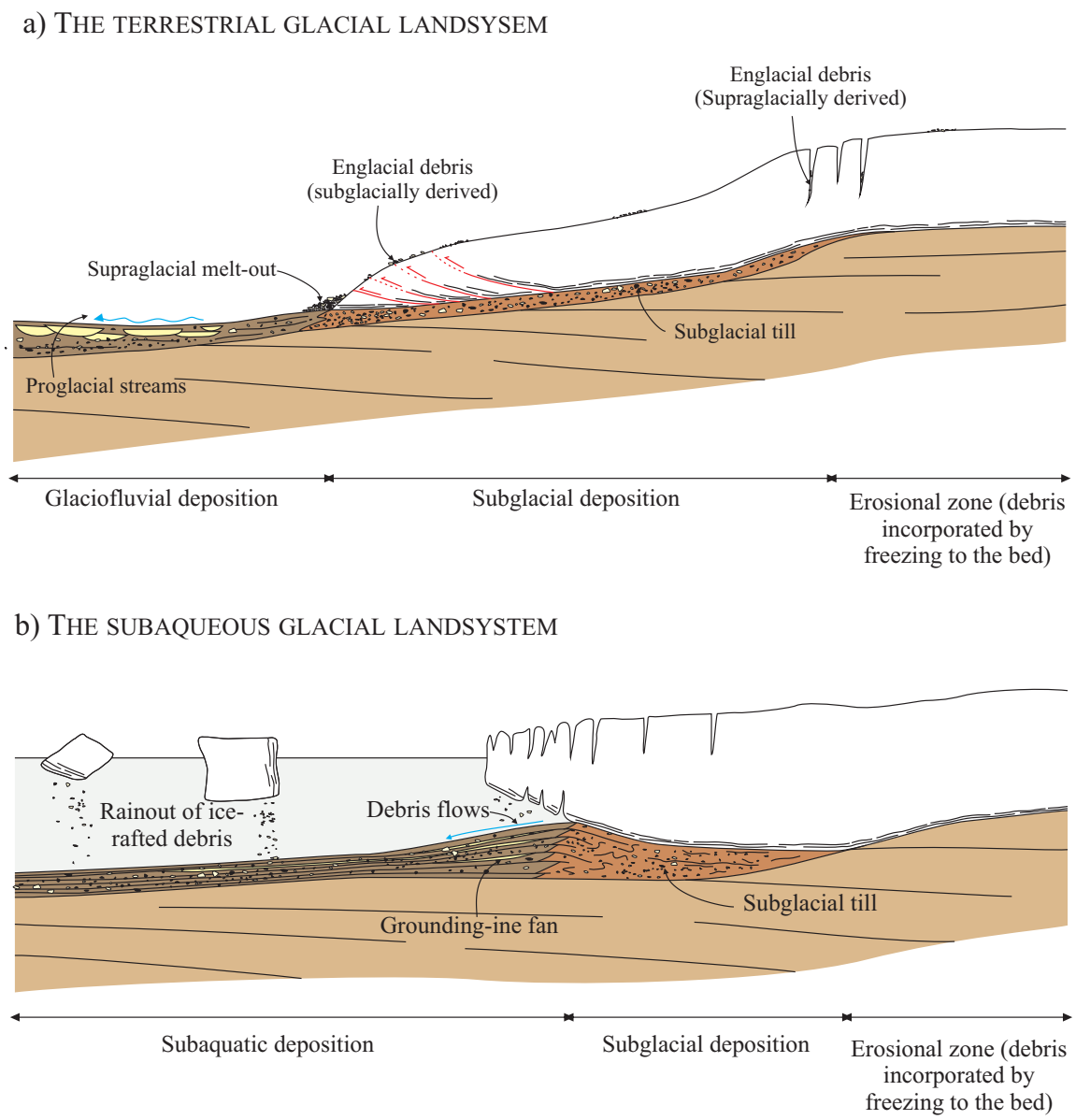

Fig. 1.1 - Longitudinal (flow-parallel) models of glacier termini from glaciers with bases at the pressure melting point, based on diagrams of Hambrey and Harland (1981) with modification. (a) Terrestrial glacial deposition showing subglacial and glaciofluvial environments. (b) Glaciomarine depositional environment, with the inclusion of a grounding-line fan (after Powell and Domack, 1995; Powell, 2003).

stemming from the fact that the bed is mostly inaccessible. As such, many of the processes leading to the formation of subglacial sediments are poorly understood. Deposition in this environment occurs through a combination of lodgement, ploughing, melt out and bed deformation (Dreimanis, 1988). However, it is becoming increasingly apparent that most till lies between these simplistic end members, resulting from a combination of all four processes along with erosion (Evans et al., 2006) and the term *subglacial traction till* is commonly used. Diamicton is the most commonly associated deposit, and can be massive or stratified, but a variety of other deposits can be recognised. These include lenses of sand and gravel (Menzies, 1990), boulder pavements (e.g. Boyce and Eyles, 2000) and clastic dykes (e.g. Le Heron et al., 2005).

Subaqueous environments (Fig. 1.1b) occur where the ice reaches a water body such as the sea (glaciomarine environment) or a lake (glaciolacustrine environment). A plethora of processes and sediment sources occur owing to the combined action of ice and water (Powell and Domack, 1995). Close to the ice margin, the efflux of meltwater from subglacial channels can deposit large quantities of sediment. In addition, floating debris-laden icebergs or ice-shelves deliver sediment through ice rafting (Thomas and Connell, 1985). Floating ice can travel for considerable distances, depositing ice-rafted debris as dropstones in locations far away from the ice margin. Rapid spatial variation in sedimentation rates can result in the development of grounding-line fans (Fig. 1.1b) (Powell, 1990). Depositional palaeoslopes are common in such environments, leading to frequent resedimentation events e.g. mass-flows. These can travel considerable distances, even on shallow slopes (Dowdeswell et al., 1996).

Proglacial environments (Fig. 1.1a) form at and beyond the ice margin, where glaciers are land-terminating. Here, a variety of sediments can be produced which are mostly deposited by meltwater from debris derived from the ice mass itself (see review by Maizels, 2002). Large quantities of meltwater can result in the development of glaciofluvial systems, for example, large proglacial outwash plains or sandurs can develop which are characterised by complex braided channel networks.

The depositional processes occurring in these three environments are further complicated by

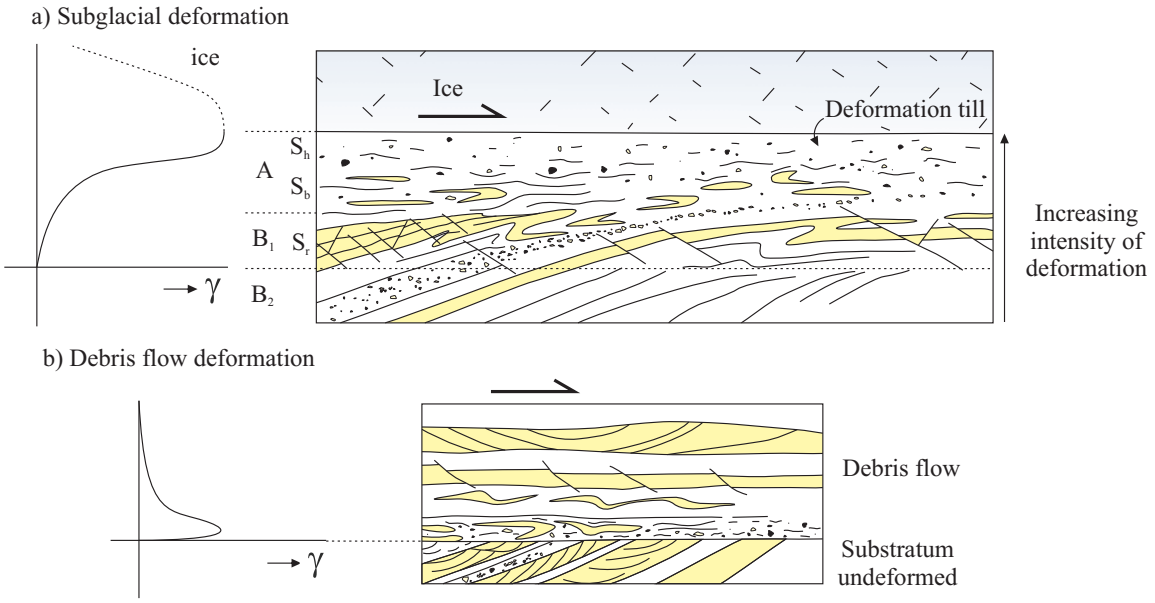

Fig. 1.2 - Comparisons of structures found in typical soft-sediment shear zones (after van der Wateren, 2002 and the sources cited therein). (a) The subglacial shear zone in subglacial sediments showing a progressive increase in strain and deformation towards the ice-bed interface. Sr is the minimal strain, S_b contains boudins, detached folds and transposed foliation, S_h is the maximum strain, homogenised central horizon of the shear zone. Horizons A, B_1, B_2 refer to those described in Boulton's (1987) deformation till model. (b) The shear zone at the base of a debris flow, showing an abrupt change in deformation from the debris flow to the undeformed stratum.

the fact that glaciers are highly dynamic systems which can respond significantly to even slight changes in temperature or sea-level. Many glaciers are also subject to complex internal cycles (e.g. surge behaviour, see Meier and Post, 1969), which result in oscillation of the ice margin, but are not primarily controlled by external processes. Complex feedback mechanisms can also occur, particularly in marine-terminating glaciers and ice sheets; therefore, advance-retreat cycles are common, leading to sharp changes in depositional environments (Mercer, 1978).

Deformation occurs at a variety of locations in glacial environments. These include the bulldozing of sediment at the ice margin, shear at the subglacial bed, and slumping and mass-flow at the glacier snout (Fig. 1.2). Glacial deformation has attracted an extensive literature (see van der Wateren, 2002) largely owing to its role in influencing the formation of geomorphic features, its use in reconstructing former ice flow directions and in the understanding of processes operating at the bed.

Of particular interest for this study is the process of glaciotectonism. Glaciotectonism is the structural deformation of the upper horizon of the lithosphere by glacial stresses (Slater, 1926). This process can lead to a variety of soft-sediment structures that can appear analogous to deformation in rocks and can produce a deposit known as a glaciotectonite. Glaciotectonites were originally described as referring to a subglacially sheared sediment, analogous to mylonites; however, a wider definition is commonly used which covers any body of unlithified or weakly lithified sediment deformed by glacial stresses (van der Wateren, 2002). Deformation can be described as both brittle and ductile (Fig. 1.2). Brittle deformation results in the production of discrete undeformed blocks separated by narrow shear corridors. In contrast, ductile deformation is referred to as the pervasive deformation of sediment by folding and faulting through cataclastic processes; however, in contrast to ductile deformation in metamorphic rocks occurring through crystal lattice deformation, grains remain essentially intact.

Glaciotectonism is largely controlled by the flow of the overriding ice. Glaciers and ice sheets can exhibit a number of deformational regimes, demonstrated beautifully through structures on the surface of glaciers and ice sheets (Hambrey and Lawson, 2000). In a subglacial environment, sediments are subjected to horizontal simple shearing, coupled with extension (Fig. 1.3). Depending on hydrological conditions, confining pressure and shear strains, a variety of both brittle (e.g. faults) and ductile (e.g. folds) structures can be produced, often with increasing intensity of deformation towards the ice-bed interface (Fig. 1.2a). High shear strains can result in sediment remobilisation and the formation of a subglacial till. In proglacial settings, glaciotectonic compression may facilitate the formation of structures analogous to fold and thrust belts in an orogenic foreland setting (Fig. 1.3).

1.3. Research issues

The recognition of glacial sediments in the sedimentary record has caused significant debate and controversy since they were first described. Throughout history, glacial sediment sections have been continually interpreted and reinterpreted (e.g. Schermerhorn, 1974). Although a wide

range of lithofacies and characters pertaining to distinct glacial environments exist (e.g. Eyles et al., 1983), their origin is often debated. In some cases, the same sequence has been interpreted as forming under strikingly different environments, e.g. the glacial sequence at Scarborough Bluffs, Ontario (Eyles and Eyles, 1983b; Dreimanis, 1984) and the formation of the Precambrian Port Askaig Formation of Scotland (Spencer, 1971; Eyles and Eyles, 1983a; Fairchild, 1985).

The most common sediment associated with glacial deposition, diamicton, is usually structureless and can form in a variety of environments. For example, massive diamict is common in subglacial environments (Evans et al., 2006) forming through processes of lodgement, ploughing, melt out and bed deformation as a subglacial traction till. Such deposits are also a feature of many glaciomarine sequences, occurring through the rainout of ice rafted debris (e.g. Dowdeswell et al., 1994). Furthermore, sediment remobilisation events can result in homogenisation and the production of diamicton, which may or may not have originally been produced by glacial activity (e.g. Eyles and Eyles, 2000).

Where structures can be seen, the application of structural geological approaches to the investigation and understanding of glacially deformed sequences has been particularly useful.

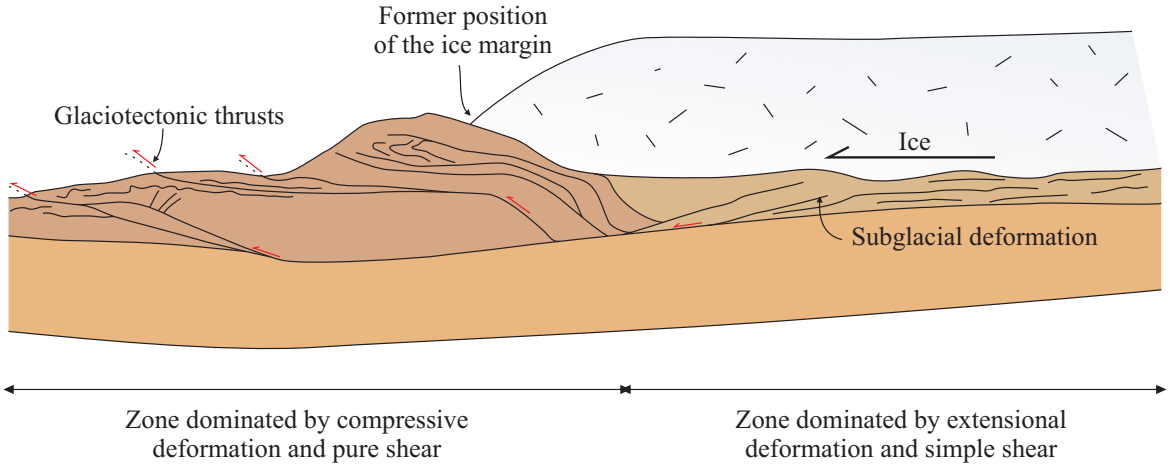

Fig. 1.3 – Glaciotectonic regimes associated with a terrestrial land-terminating glacier (after Aber and Ber, 2007 and the sources cited therein), based on the composite-ridge set in front of Eyjabakkajökull, Iceland. Shown are the subglacial zone dominated by extensional glaciotectonics, contrasted with the proglacial zone dominated by compressive deformation.

Structures can be analysed on both macroscopic and microscopic scales and can provide considerable information about the genetic environment and deformational history. However, fold structures, similar to those found in glaciotectonic environments, are also found in other environments, e.g. slumping on glaciomarine slopes (Arnaud and Eyles, 2002). Some authors have suggested key differences in the nature of sediments deformed through resedimentation and those formed through subglacial shear. For example, Hiemstra et al. (2004) observed that whilst subglacial sediments displayed a progressive increase in intensity of deformation, discrete failure planes developed in slide deposits above which sediment was largely undeformed. However, slide deposits only represent one of many types of mass movement deposit and a robust set of criteria for each environment has not yet been established.

Clast fabric analysis can provide constraints over depositional processes and is considered by many to be a fundamental tool in the analysis of glacial sediments. The technique is long established and is normally used as a means for deriving past ice flow directions (Holmes, 1941) through the measurement of the preferred alignment of the long axis (a-axis) of visible clasts. By the statistical analysis of eigenvalues, the fabric strength can be calculated, and this has recently been used as a means to distinguish different modes of deposition (e.g. Hart and Roberts, 1994) as well as the analysis of strain magnitude within deformed sediments (Benn, 1994; Hart and Roberts, 1994; Benn and Evans, 1996). However, others have doubted the use of clast fabrics alone to determine deposition environment (e.g. Bennett et al., 1999). This is because deformation processes occur in a range of settings and there is considerable overlap between depositional environments.

1.4. The AMS technique

One alternative fabric technique, which is becoming increasingly used in the analysis of glacial sediments, involves the measurement of Anisotropy of Magnetic Susceptibility (AMS). AMS is a technique that utilises the magnetic behaviour of minerals to determine their spatial arrangement and geometric configuration (fabric) within rock or sediment. This technique is routinely used in

other areas of geology, mostly to examine flow mechanisms within igneous rocks or to characterise deformation within tectonically deformed rocks. However, despite a strong promise, relatively few examples exist of the application of AMS to glacial materials.

Fuller (1962) first attempted the use of AMS in the fabric characterisation of glacial diamicton. Subsequently, AMS analysis has been applied to tills by several authors (e.g. Stupavsky and Gravenor, 1975; Eyles et al., 1987) and it has been shown that, in conjunction with other petrofabric techniques, AMS can provide invaluable information on the formation and subsequent deformation of glacial sediments. Recent advances in the technique, largely because of increased speed in acquisition of AMS data, and novel advances in laboratory testing of the technique (Iverson et al., 2008), have led to a resurgence of publications in this area (Hooyer et al., 2008; Shumway and Iverson, 2009; Thomason and Iverson, 2009; Gentoso et al., 2012).

As well as simply characterising flow directions, the AMS of glacial sediments has been suggested to provide information regarding highly debated topics such as the deforming bed model of glacier flow and the manner of particle rotation during shear (Hooyer et al., 2008; Shumway and Iverson, 2009). A link between AMS and shear strain was recognised in ring-shear experiments by Iverson et al. (2008) and suggestions were made for its diagnostic use. However, compared to the vast literature available on applications for examining deformation in rock (see references in Borradaile and Jackson, 2010), the AMS of glacial sediments is understudied.

1.5. Particular issues

In order for the promise of the technique to be assessed, several questions have been identified which are yet be fully addressed. These questions are considered important and are addressed in the main body of the thesis.

Q1. What is the relationship between AMS and the deformation within glacier ice?
Although most studies interpret the maximum susceptibility axis of the AMS fabric to lie parallel to the direction of ice flow, the relationship between the AMS fabric and deformation within the

overriding ice is poorly understood. It is yet to be explored whether AMS fabrics can be detected within the basal ice of glaciers and how these relate to the laboratory results of Iverson et al. (2008) and the interpretation of the AMS in Quaternary tills.

Q2. How does the magnetic signal of sediment with different magnetic mineralogies respond to subglacial shear? Different minerals can produce very different AMS fabric characteristics (see Chapter 2, section 2.3.3). The experimental work of Iverson et al. (2008) largely focussed on tills with a magnetic mineralogy dominated by silt-sized magnetite particles. Sediments dominated by paramagnetic minerals are also common; however, it is not known how these behave in response to subglacial shear.

Q3. Can AMS be applied to the study of glaciotectonites? The majority of AMS studies have focussed on determining ice flow directions and bed dynamics from fabrics within tills. No published data exists for the application of AMS to glaciotectonites, where pre-existing unconsolidated sediment has been glacially deformed such that relics of the original structure remain.

Q4. Are primary fabrics preserved in the pre-Quaternary glacial sediments? In other areas of sedimentology, AMS is routinely applied to the pre-Quaternary (e.g. Schieber and Ellwood, 1993; Dall'olio et al., 2013); however the growth of new diagenetic minerals can disrupt the original fabric (e.g. Schieber and Ellwood, 1993). The preservation of magnetic fabrics during diagenesis is yet to be established.

Q5. Can AMS be used as a genetic indicator of depositional and deformational processes? It has been suggested that the AMS could be used as a genetic indicator of depositional or deformational processes (Eyles et al., 1987; Iverson et al., 2008). Further investigation is needed before the use of AMS in this way can be verified.

1.6. Thesis outline

In this thesis, a combined magnetic, sedimentological and structural approach is taken for the

analysis of glacial sediments. This thesis is written as a series of papers, each addressing a different aspect of glacial sedimentology and connected by the use of the AMS technique. Each chapter has its own aims and objectives that address both the research questions relating to AMS (outlined above) and other current problems in glacial sedimentology. Chapter 3 has already been published (Fleming et al., 2013), Chapter 4 is in press (Fleming et al., in press), and Chapters 5 and 6 are intended for publication.

Where possible, the contents of these chapters are left as they were or intend to be submitted for publication, so that each will function as a stand-alone contribution; however, to avoid repetition, most of the theoretical discussion and background on the AMS has been removed and is included in Chapter 2. In addition, details of the AMS methods are removed and are included in Appendix A. Additional analytical methods are described where they are used. However, where the same methods are used in subsequent chapters, the reader is referred back to the relevant chapter.

Chapter 2 - The theoretical background behind the technique is described and the current literature on the AMS technique is reviewed.

Chapter 3 - Results are presented from the first-ever application of AMS to examine deformation within the basal ice of a polythermal surge-type glacier in Svalbard. As well as addressing Q1, this chapter reveals interesting insights into the dynamic behaviour of the glacier during the last surge.

Chapter 4 - Results are presented from the analysis of a classic glaciotectonised section in North Norfolk, UK. In addition to AMS measurements from a lithology dominated by paramagnetic minerals (addressing Q2), a detailed, systematic structural investigation is undertaken to provide a second proxy of strain direction, thereby addressing Q3. Finally, the relationships of the fabrics to ice-flow across North Norfolk are established.

Chapter 5 - Results are presented of a detailed AMS study of Neoproterozoic diamictites from the Wilsonbreen Formation in NE Svalbard. In this chapter, through extensive rock

magnetic experiments and comparisons with clast macrofabric data, the origin of the diamictites and their relationship to palaeoflow across the basin are assessed (addressing Q4).

Chapter 6 - Presented in this chapter are the results of a detailed analysis of deformation structures within certain parts of the Wilsonbreen Formation through a combination of sedimentology, structural geology and magnetic fabrics (addressing Q3, Q4 and Q5). In this chapter, the origins of unusual deformational structures are established and a depositional model suggested.

Chapter 7 - The results are synthesised, the main conclusions drawn and suggestions of future work are made.

CHAPTER 2.

ANISOTROPY OF MAGNETIC SUSCEPTIBILITY

2.1. Introduction

Anisotropy of magnetic susceptibility (AMS) is one of a group of techniques used to measure the petrofabric of rock or sediment. It was first measured in minerals more than a century ago (e.g. Voight and Kinoshita, 1907), but it was not until the pioneering work of Graham (1954) that its use as a petrofabric tool was first suggested. After this, AMS was applied to a range of geological materials, such as the analysis of sediments (e.g. Rees, 1961; Rees, 1965) and igneous and metamorphic rocks (e.g. Stacey, 1960; Stone, 1963). AMS is now routinely applied to measure the mineral orientation fabric in a variety of geological situations. Throughout the years, the ultimate goal of AMS work has remained essentially the same (Martín-Hernández et al., 2004): to establish principal directions of finite or incremental strains in order to determine flow/emplacement directions or deformation in sediments and intrusive/extrusive igneous rocks.

Whilst a variety of other petrofabric techniques exist (e.g. clast fabric analysis, microfabric analysis, neutron texture analysis), AMS has a number of key advantages over these. It can be measured relatively quickly and is less labour intensive than alternatives. For example, with modern equipment, the AMS can be characterised in a matter of minutes as opposed to several hours for optical measurement of a fabric on a universal stage microscope. In addition, AMS reflects the bulk average of many grains within a sample and several samples make up a site, therefore making the technique highly representative. It can also be used in settings where other structures or structural indicators are lacking. However, like many other techniques, AMS is not without its caveats. The magnetic response of minerals can be highly variable. Whilst in many cases the AMS fabric is directly comparable to grain fabric, there are various reasons why this may not necessarily be the case (Tarling and Hrouda, 1993). Therefore, a complete understanding is needed before the results can be fully interpreted.

In this chapter, an introduction to the theory of AMS is presented and how it can be used to characterise a fabric within rock or sediment (Sections 2.2 - 2.5). The techniques commonly used to characterise the mineralogy are explained in Section 2.6. A review of how AMS can be used to investigate sedimentary rocks is given in Section 2.7, and an introduction into the current state of

research into the AMS of glacial sediments is given in Section 2.8. Finally, an outline of how AMS is used in this thesis is presented in Section 2.9.

2.2. Diamagnetism, paramagnetism and ferromagnetism

Magnetic susceptibility is a dimensionless proportionality constant that indicates the degree of magnetisation of a material in response to a magnetic field. All materials are magnetic in the fact that they all are affected by magnetic fields in some way; however, some are more magnetic than others. Materials can be classed as having diamagnetic, paramagnetic and ferromagnetic behaviours (Dunlop and Özdemir, 1997). At an atomic scale, diamagnetism occurs when a magnetic field is applied to a substance where the electron shells are complete (no net magnetic moments). The paired electrons effectively cancel each other out and weak magnetisation is produced in the opposite direction to that of the applied field (Fig. 2.1a), resulting in a negative

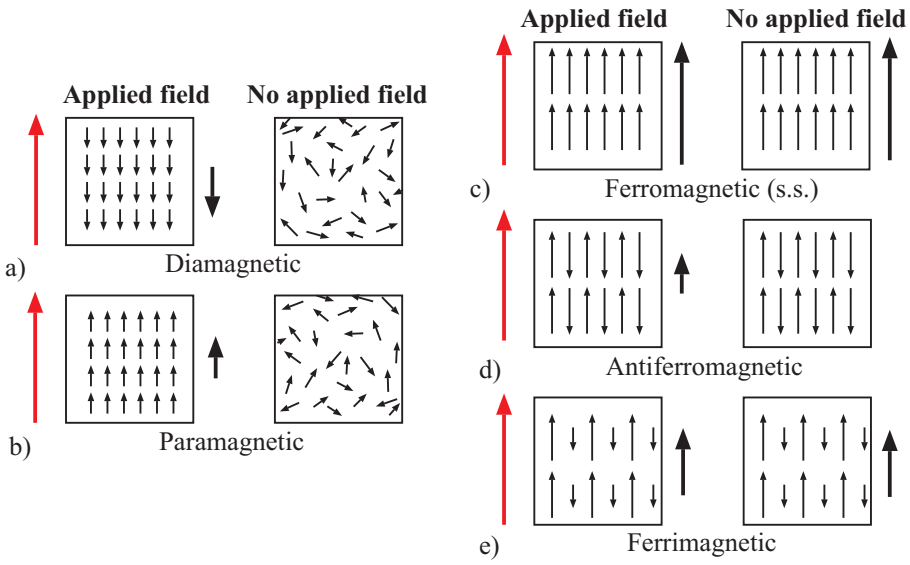

Fig. 2.1 – The response of different materials to magnetisation (after Tarling and Hrouda, 1993). The left column shows the magnetisation that a substance receives when in a magnetic field (red arrows) whilst the right column shows the magnetisation after the field has been removed (black arrows). (a) Diamagnetic minerals showing a weak magnetisation in the opposite direction. (b) Paramagnetic minerals showing weak field in the same direction. (c) Ferromagnetic (s.s.) minerals showing a strong field in the same direction both with and without an external magnetic field. (d) Antiferromagnetic minerals showing a weak field but no magnetisation. (e) Ferrimagnetic minerals showing an induced and remanent magnetisation in the same direction to the external field but weaker than ferromagnetic (s.s.) minerals.

susceptibility. In contrast, paramagnetic materials are somewhat more affected by a magnetic field. They display a slightly stronger, non-permanent magnetisation parallel to the applied field, resulting in a positive susceptibility. This occurs because of the presence of unpaired electrons at the atomic scale. However, the individual magnetic ions do not interact magnetically. As such, the alignment is subsequently lost when the external magnetic field is removed. In both paramagnetic and diamagnetic minerals, the strength of the induced magnetisation is directly related to the strength of the applied field. This is represented by the equation $M=KH$ where M is the induced magnetisation, H is the applied field and K is the susceptibility measured in SI units (Tarling and Hrouda, 1993).

Ferromagnetic substances include those commonly thought of as magnetic (e.g. iron, nickel and magnetite). They have much higher susceptibilities than paramagnetic and diamagnetic minerals as the atomic moments exhibit very strong interactions. Ferromagnetism is a behaviour typical of the first transition series of elements (NB. ferromagnetism *senso lato* is commonly used to describe this behaviour, but ferromagnetism *senso stricto* is also used as a subdivision, discussed below).These substances are able to retain a magnetisation after the external field has been removed, a property known as spontaneous magnetism. This happens because the electron spins become spontaneously coupled and all of the individual spin magnetisations become aligned (Dunlop and Özdemir, 1997). In some elements, the electron spins of adjacent cations become directly coupled (ferromagnetism (s.s.), Fig. 2.1c); however, when other elements of the transition metals combine, such as the oxides, the presence of an intermediate anion results in a linkage, where the directions of the electron spins in the adjacent cations are reversed. This results in no net magnetism in the absence of an external field, and a slight positive magnetisation when a field is applied (Fig. 2.1d). Substances that behave in this way are termed antiferromagnetic. If one lattice is more strongly magnetised, a net magnetic field can be created in the mineral grain in the absence of an external magnetic field (Fig. 2.1e). These substances are known as ferrimagnetic.

One of the remarkable properties of ferromagnetic grains is their ability to be influenced by very low magnetic fields. This can occur because the magnetisation within a grain can divide

into a number of small regions called domains, separated by transition zones called Bloch walls, in order to keep magnetostatic energy to a minimum (Fig. 2.2). For a full discussion on domain theory see O'Reilly (1984), Tarling and Hrouda (1993) and Dunlop and Özdemir (1997). In the absence of an external magnetic field, domains would ideally be arranged in such a way that the direction of magnetisation is opposite, thereby cancelling each other out. However, crystal imperfections can serve to 'pin' Bloch walls allowing a net magnetisation to be retained. In the presence of an external magnetic field, translation of the Bloch walls can cause the domains to become progressively aligned until the saturation magnetisation is reached (the maximum magnetisation a ferromagnetic grain can accommodate).

The number of domains that can form in a ferromagnetic grain is primarily affected by its

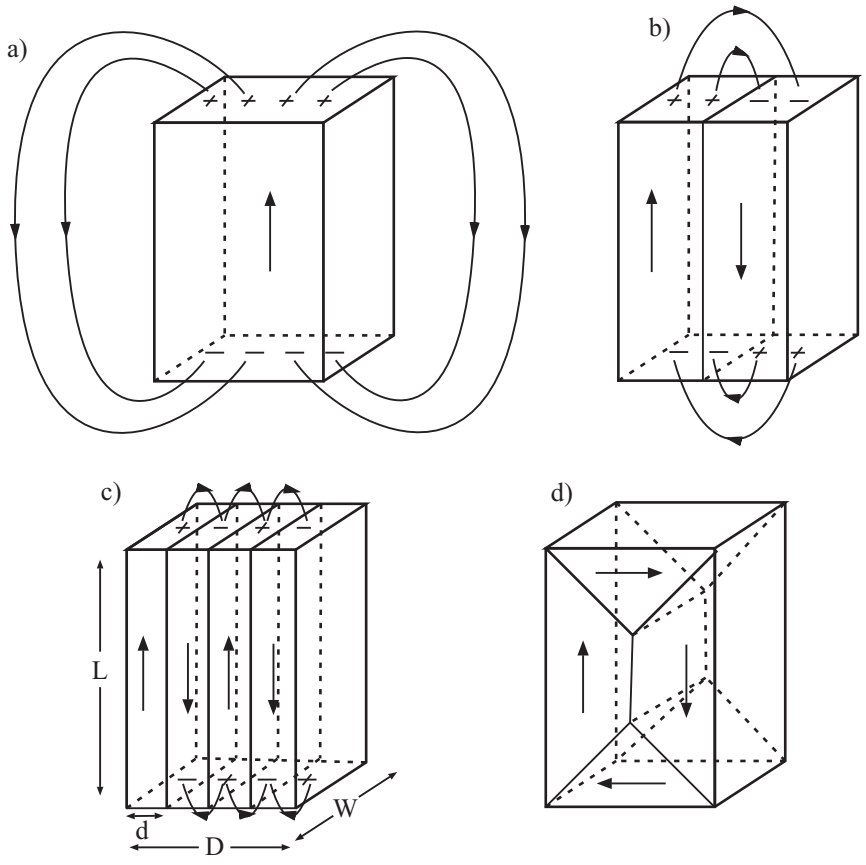

Fig. 2.2 – Responses to the change in domain structure of ferromagnetic minerals (after Dunlop and Özdemir, 1997). (a) SD structure with widely separated positive and negative poles. (b) Two domain structure with less pole separation and more localised flux linkages. (c) Four domain structure. (d) Closure domains in a two-domain structure.

size. In larger grains, more than one domain may form. This type of grain is therefore called a multi-domain (MD) grain (Fig. 2.2c and d). The Bloch wall translations allow these grains to be easily affected by magnetisation even at low magnetic fields, and they are generally referred to as being magnetically 'soft'. The energy required to form domains increases as grain size decreases. Below a certain size (1μm for magnetite) only one domain will form. This type of grain is referred to as a single-domain (SD) grain (Fig. 2.2a). It is magnetically easy to change the magnetisation in an MD grain as all that is required is Bloch wall translation. SD grains, in contrast, can only be changed by rotating the magnetisation axis itself which is a magnetically difficult process that requires high field strengths (Moskowitz, 1991). As such, these grains are generally referred to as being magnetically 'hard'. In addition, crystal lattice imperfections can affect some MD grains. These reduce the ability of neighbouring grains to interact. This can cause behaviour more similar to SD grains and is therefore termed pseudo-single domain (PSD).

2.3. Types of anisotropy

Whilst in the majority of cases, AMS is used as a direct measurement of the petrofabric of rock or sediment. In reality, AMS is highly complex and controlled by a number of factors. Hence, the AMS may not always directly reflect the grain fabric. These factors are discussed below:

2.3.1. Shape

Shape anisotropy is common in ferromagnetic minerals and occurs when the susceptibility ellipsoid has the same orientation and aspect ratio as the grain itself (Borradaile and Jackson, 2010). This is because of the presence of self-demagnetising fields which strongly affect the susceptibility. In the presence of an external magnetic field, the alignment of the electron spins result in the creation of north and south magnetic poles at opposite ends on the grain surface. These poles move as far apart as possible to keep magnetostatic forces to a minimum. Consequently, the susceptibility ellipsoid has the same shape as the grain (Tarling and Hrouda,

1993). This effect becomes increasing prevalent in smaller grains. As such, SD grains are usually completely dominated by shape anisotropy (Dunlop and Özdemir, 1997). However, even larger MD grains are affected by shape anisotropy as spontaneous magnetisation will always generate a demagnetising field.

2.3.2. Magnetocrystalline Anisotropy

Crystalline anisotropy occurs mostly in paramagnetic minerals, but it can also form in some ferromagnetic (s.s.) and ferrimagnetic grains when the south-demagnetising fields are absent or too low to be important (Borradaile and Jackson, 2010). It arises because the magnetic ions in the crystal lattice interact with one another and with neighbouring non-magnetic ions. The nature and strength of this interaction depends on the orientation in the crystal lattice (Dunlop and Özdemir, 1997). As result, the magnetic moment is greatest along specific directions. This direction is referred to as the 'easy axis' or 'easy plane' of magnetisation (Tarling and Hrouda, 1993). Most minerals, especially chain and sheet silicates, tend to form elongate or platy grains. As a result, the crystallography determines both the AMS and the grain-shape. They have greatest susceptibility in an orientation subparallel to their long axis and a minimum susceptibility at a high angle to the basal plane (Borradaile and Werner, 1994). Therefore, the AMS fabric and grain fabric are not necessarily mutually exclusive (e.g. Cifelli et al., 2005; Cifelli et al., 2009) but commonly yield compatible AMS fabric patterns (see Section 2.5.2).

2.3.3. Effects of grain size

Grain size can have a significant impact on the anisotropy of the grain. The AMS of MD grains is largely controlled by shape or magnetocrystalline anisotropy. As such, the principal susceptibility axes normally coincide with the grain shape. SD grains, on the other hand, can cause problems as they can display inverse magnetic fabrics (Potter and Stephenson, 1988). When a weak field is applied along the long axis of the grain (the normal AMS procedure), it cannot induce a magnetisation as only high strength fields can change the magnetisation (Section 2.2).

Therefore, the grain effectively has zero susceptibility along its long axis but greatest susceptibility when a field is applied at an angle perpendicular to it. This is effectively the inverse of the pattern seen in the shape anisotropy of MD grains. The effects of SD grains on AMS fabrics has been investigated in several cases (e.g. Stephenson et al., 1986; Potter and Stephenson, 1988) and if not recognised, erroneous interpretations may result.

2.3.4. Magnetic interactions

In some igneous rocks, magnetic interactions between the individual ferromagnetic grains can be important (Hargraves et al., 1991). It was seen that, even if the grains within the rock are isotropic, an anisotropic AMS fabric can still be produced because of the ability of ferromagnetic grains to interact when sufficiently close to each other. However, Gaillot et al. (2006) examined this further and discovered that magnetic interactions are negligible once grains are spaced by a distance larger than the mean grain size. The vastly lower ferromagnetic components of most sedimentary rocks (Tarling and Hrouda, 1993) mean the effects of distribution anisotropy are likely to be negligible.

2.4. Determination of the AMS Fabric

AMS is calculated by lowering a specimen (cube or cylinder) into an induction coil assemblage through which a weak AC current is applied (see Appendix A). This current creates a temporary magnetic field around the sample, therefore inducing a magnetisation. At the same time, a neighbouring sensory coil measures changes in the ambient magnetic field. The sample is rotated about an axis in three orthogonal orientations. As almost all rocks are anisotropic, the induced magnetisation will vary depending on the orientation of the sample with respect to the magnetic field. This results in variation in the induced magnetic field measured by the sensory coil. By this means, the ability of the sample to become magnetised (magnetic susceptibility) and variation depending on the direction of the applied field (anisotropy) can be quantified.

Once recorded, this susceptibility data can be resolved through a variety of matrix equations (e.g. Girdler, 1961; Jelínek and Kropáček, 1978; Tauxe, 1998; Owens, 2000) which serve to calculate the eigenvalues and eigenvectors, and resolve the six independent elements of the second-rank tensor that defines the AMS of a sample. This can be represented by a magnitude ellipsoid (Nye, 1964) with minimum (K_3), intermediate (K_2) and maximum (K_1) susceptibility axes, such that $K_1 \geq K_2 \geq K_3$ (Fig. 2.3). This can be compared to the strain ellipse used in structural geology and, in many cases, the orientation of the AMS ellipsoid and the strain ellipse can be very similar (Borradaile and Jackson, 2010).

2.4.1. Susceptibility parameters

A variety of statistical calculations have been proposed to deal with susceptibility data (see Tarling and Hrouda, 1993 for review). In all studies, mean susceptibility (K_{mean}) is calculated by the equation:

$$K_{mean} = \frac{K_1 + K_2 + K_3}{3}.$$

This provides a mean value of the integral of the directional susceptibility over the entire specimen (Nagata, 1961). It allows the direct comparison of susceptibility between different samples, and may be used to indicate the dominant magnetic mineralogy within the specimen (Tarling and Hrouda, 1993).

A variety of parameters have been developed for characterising the fabric (see Tarling, 1983 pp. 18). In this thesis, the shape of the ellipsoid is characterised using the lineation (L) and foliation (F) parameters of Khan (1962) and are calculated as:

$$L = \frac{(K_1 - K_2)}{K_{mean}}$$

and

$$F = \frac{(K_2 - K_3)}{K_{mean}}.$$

These values are based on the lineation of Balsley and Buddington (1960) and foliation of Stacey (1960) but have subsequently been normalised against the mean susceptibility, following

the work of Khan (1962). These values effectively represent a ratio between the principal susceptibility axes. They can be readily plotted and displayed visually on a Flinn-type plot, similar to those typically used in structural geology (Flinn, 1962; Flinn, 1965) (Fig. 2.4a).

As an alternative to F/L parameters, the shape parameter (T), is also used to define the shape of the susceptibility ellipsoid (Jelínek, 1981), given by:

$$T = \left[\frac{2\ln\frac{K_2}{K_3}}{\ln\frac{K_1}{K_3}}\right] - 1.$$

This is commonly preferentially used over other shape parameters as all three principal susceptibility axes are used in its calculation. T will always return a value between -1 and 1. Oblate (disk-shaped) ellipsoids will correspond to $0 < T \leq 1$ whilst prolate (rod-shaped) correspond to negative values $-1 < T \leq 0$.

The degree of anisotropy of a sample was traditionally measured by the anisotropy degree (P) (Nagata, 1961). This was altered, however, by Jelínek (1981) to include all the principal susceptibility values and the mean value rather than just the maximum and minimum values. The corrected anisotropy degree (P_j) is now universally adopted and is given by:

$$P_j = exp\left(\sqrt{2\left[\left(\ln\left(\frac{K_1}{K_3}\right)\right)^2 + \left(\ln\left(\frac{K_1}{K}\right)\right)\right]}\right).$$

T and P_j are commonly plotted together to give a graph (e.g. Fig. 2.4b) that displays comparable information on both shape and magnitude. These diagrams allow a clear distinction between magnitude and shape and are generally considered an alternative to L/F Flinn-type plots (Fig. 2.4a). To allow direct comparison with pre-existing studies, both P_j-T and L/F plots are used in this thesis.

2.4.2. Graphical representation of AMS directional data

Direction data is commonly plotted onto lower-hemisphere, equal-area stereographic projection allowing three dimensional representations of the data (Fig. 2.3). The orthogonal

orientations of the maximum (K_1), intermediate (K_2) and minimum (K_3) susceptibility axes are plotted as squares, triangles and circles respectively. It is considered good practise to analyse 8 – 12 subsamples per site where possible in order to get a good representative AMS fabric. Every subsample from each site is typically plotted on to the stereonet which can be used to display a first approximation of the shape of the ellipsoid. Rapid distinction can subsequently be made between oblate, triaxial and prolate ellipsoids (Fig. 2.3). Other data (e.g. cleavage, striations, fold axes, bedding etc.) can be simultaneously plotted for comparison. In addition, 95% confidence ellipsoids and the mean susceptibility axes are commonly plotted for each site.

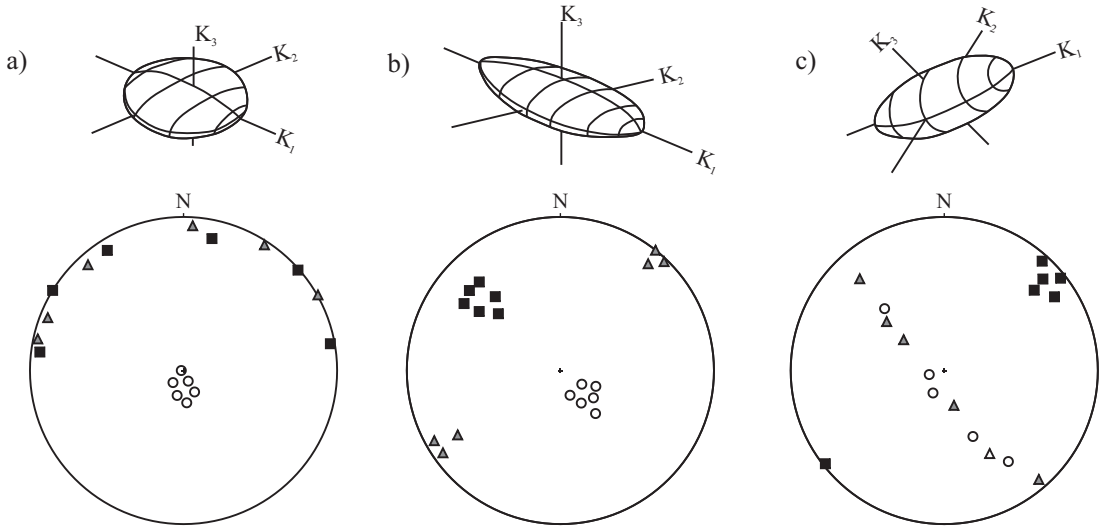

Fig. 2.3 - The plotting of anisotropy directional data on a stereographic projection showing an oblate (a), triaxial (b) and prolate fabric (c) (after Tarling and Hrouda, 1993). The maximum (K_1), intermediate (K_2) and minimum (K_3) susceptibility axes are plotted as squares, triangles and circles respectively.

Data on the stereonet can be rapidly analysed visually and will typically lie between three forms (Fig. 2.3). Where the susceptibility ellipsoid is prolate, the K_1 axes will tend to group whilst K_2 and K_3 axes will form a girdle 90° from the maximum direction (Fig. 2.3c). Oblate ellipsoids typically show well grouped K_3 axes, whilst K_1 and K_2 axes form a girdle 90° from the minimum direction (Fig. 2.3a). In most cases, this girdling defines a magnetic 'foliation' which may follow a cleavage or bedding plane. Triaxial ellipsoids typically form distinct groups of axes with no girdling of the data (Fig. 2.3b).

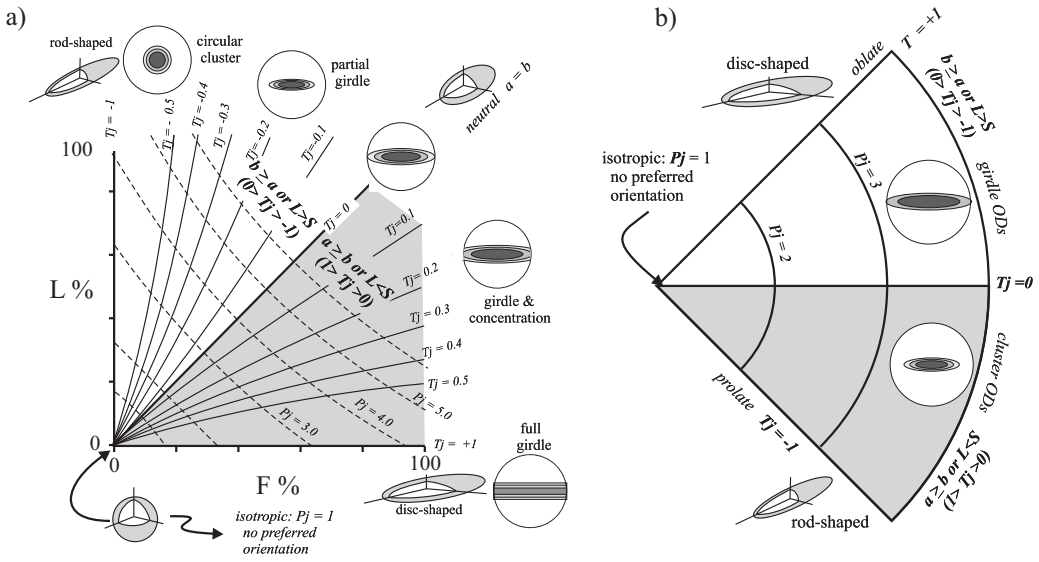

Fig. 2.4 – The graphical representation of AMS parameters (after Tarling and Hrouda, 1993; Borradaile and Jackson, 2010). (a) Plot of the degree of lineation (L) and foliation (F) based on the classic Flinn plot used in structural geology (Flinn, 1962; Flinn, 1965). The relationship to P_j and T_j are also shown. (b) Plot of T and P_j. Oblate ellipsoids have positive values whilst prolate ellipsoids have negative values.

2.5. Magnetic properties of sedimentary rocks and rock-forming minerals

Sedimentary rocks are normally made of a variety of minerals, each with different magnetic properties. Ferromagnetic minerals (e.g. haematite and magnetite) have the greatest susceptibility. If these are present in a rock, they normally control both the anisotropy and susceptibility (Fig. 2.5). When these minerals are almost absent, the magnetic fabric is normally controlled by the crystal lattice orientations of paramagnetic or diamagnetic minerals (Rochette, 1987). In very weakly magnetic rocks that are absent of ferromagnetic minerals and have very low concentrations of paramagnetic minerals, diamagnetic minerals can dominate (Owens and Rutter, 1978), and the susceptibilities will be negative.

Tarling and Hrouda (1993) suggested that, as a general rule of thumb and assuming paramagnetic minerals are common constituents (>10%), the anisotropy and susceptibility will be controlled by the following:

1. The ferromagnetic fraction if the susceptibility is higher than 5000 $\times 10^{-6}$.

2. The paramagnetic fraction if susceptibility is lower than 500 $\times 10^{-6}$.

3. Both the ferromagnetic and paramagnetic fraction, if the susceptibility is between 500 and 5000 $\times 10^{-6}$.

The diamagnetic fraction if the susceptibility is negative (Hrouda and Kahan, 1991).

Interpretation of the magnetic mineralogy in this way is only a first-order guide as rocks can be more complex. As such, it is essential that analysis of the individual components be undertaken.

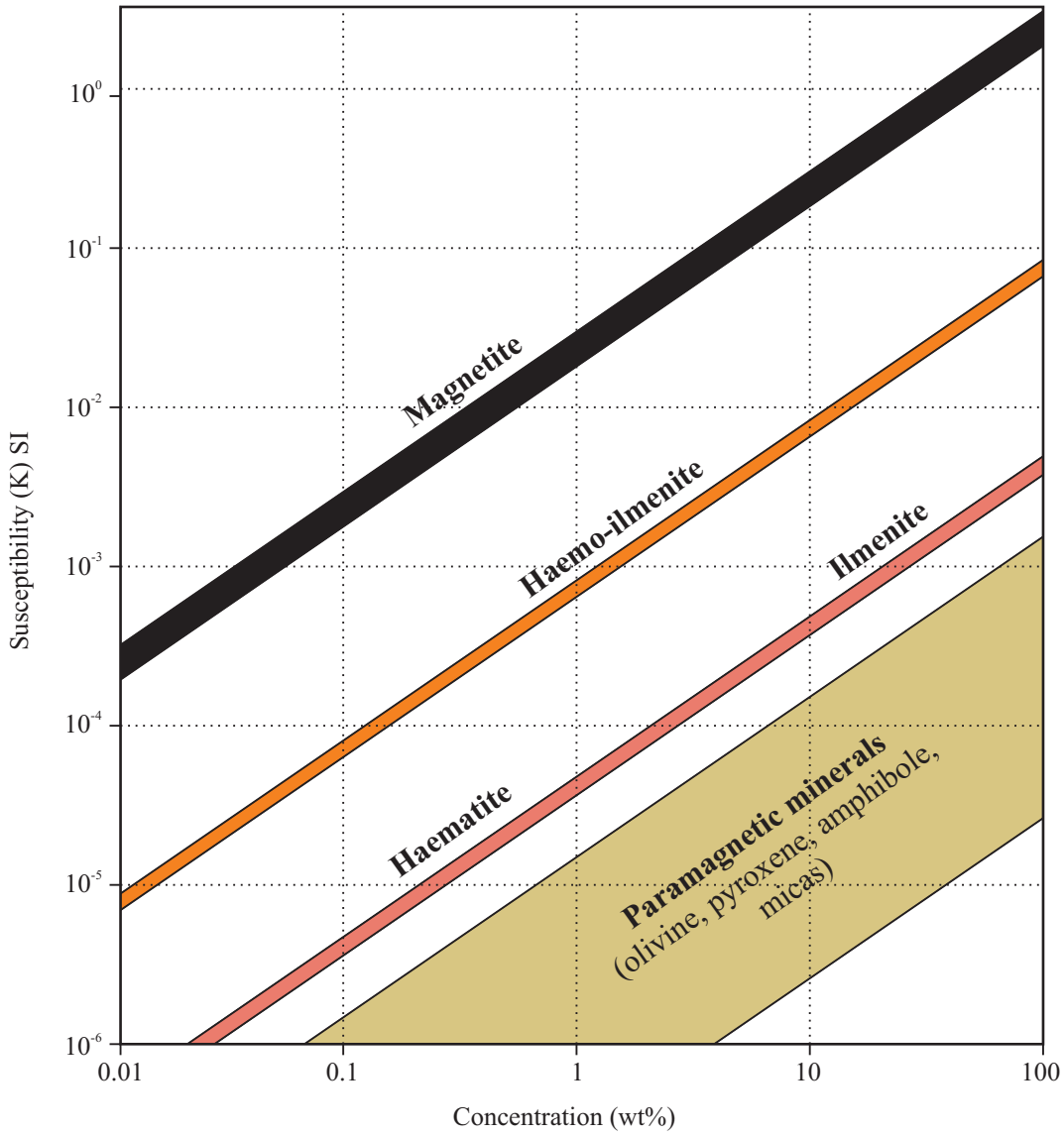

Fig. 2.5 – The contribution of various minerals to the mean susceptibility (K_{mean}) of a sample depending on their concentration (after Hrouda and Kahan, 1991 and the references within).

2.5.1. Ferromagnetic minerals

Most ferromagnetic grains originate in igneous or metamorphic rocks but are subsequently eroded and incorporated into sediments as detrital grains. In addition, ferromagnetic minerals can also grow in sediment during diagenesis (e.g. Rathore, 1979; Schieber and Ellwood, 1988) or can be produced by micro-organisms (e.g. Moskowitz et al., 1993). Of particular importance for this study are magnetite and haematite. Magnetite is a common detrital mineral in sedimentary rocks, particularly where basic igneous rocks are being eroded (Tarling and Hrouda, 1993). Haematite is much more chemically stable in oxidising conditions and can form either as a detrital mineral, commonly associated with partial haematisation of other iron-bearing minerals in oxidizing environments, or it can form as an authigenic coating around detrital grains.

Magnetite (Fe_3O_4) is a common mineral in sedimentary rocks. It will dominate both the susceptibility and anisotropy even if only present at low concentrations (≥ 0.5 %) because of its high susceptibilities (e.g. 2.8 S.I. for MD magnetite)(Tarling and Hrouda, 1993). The Curie temperature of pure magnetite is 578 °C; however, this falls if impurities are present. For example, the Curie temperature of some titanomagnetites is 150 °C (Dunlop and Özdemir, 1997). An important feature of pure magnetite is the presence of the Verwey transition (Verwey, 1939; Verwey and Haayman, 1941) at -155 °C. Below this temperature, magnetite will transform from a cubic to orthorhombic structure and subsequently displays a lowered magnetic susceptibility.

Magnetite grains display shape anisotropy. When present in sedimentary rocks, their

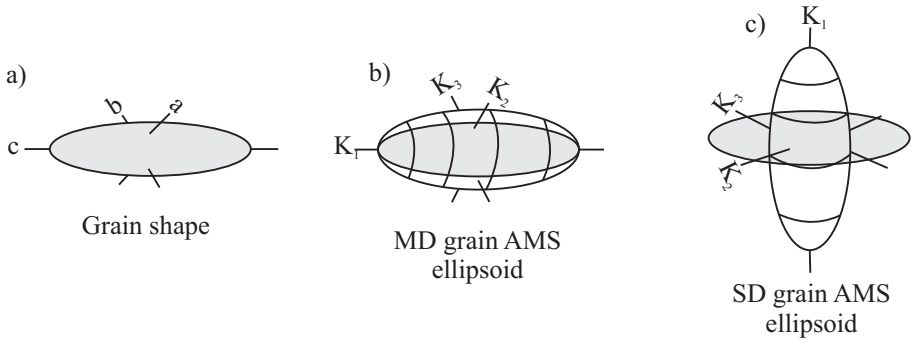

Fig. 2.6 – The effect of the domain shape on the susceptibility ellipsoid. (a) The original grain shape. (b) The AMS ellipsoid of MD grains showing normal behaviour. (c) The AMS ellipsoid of SD grains showing inverse behaviour.

interpretation is therefore relatively straightforward (e.g. Rees, 1965; Ellwood, 1980). However, as discussed in Section 2.3.3, grain size can have a significant effect on the AMS and the subsequent interpretation of the fabric. Small magnetite grains (<1 μm) only possess a single-domain. This results in principal susceptibility axes that are reversed (Potter and Stephenson, 1988; Borradaile and Puumala, 1989) (Fig. 2.6). The susceptibility axes can switch, as such an oblate fabric (Fig. 2.7a) where K_3 sits perpendicular to the foliation/lineation (defined by the K_1 and K_2) can become a linear fabric where K_1 lies perpendicular to K_2 and K_3 (Fig. 2.7b). This, if not correctly recognised, can have drastic implications for the interpretation of the AMS fabric. Inverse fabrics can normally be easily identified through comparisons with macroscopic sedimentological or structural indicators (e.g. palaeoflow indicators, bedding, cleavage etc.). Where this is not

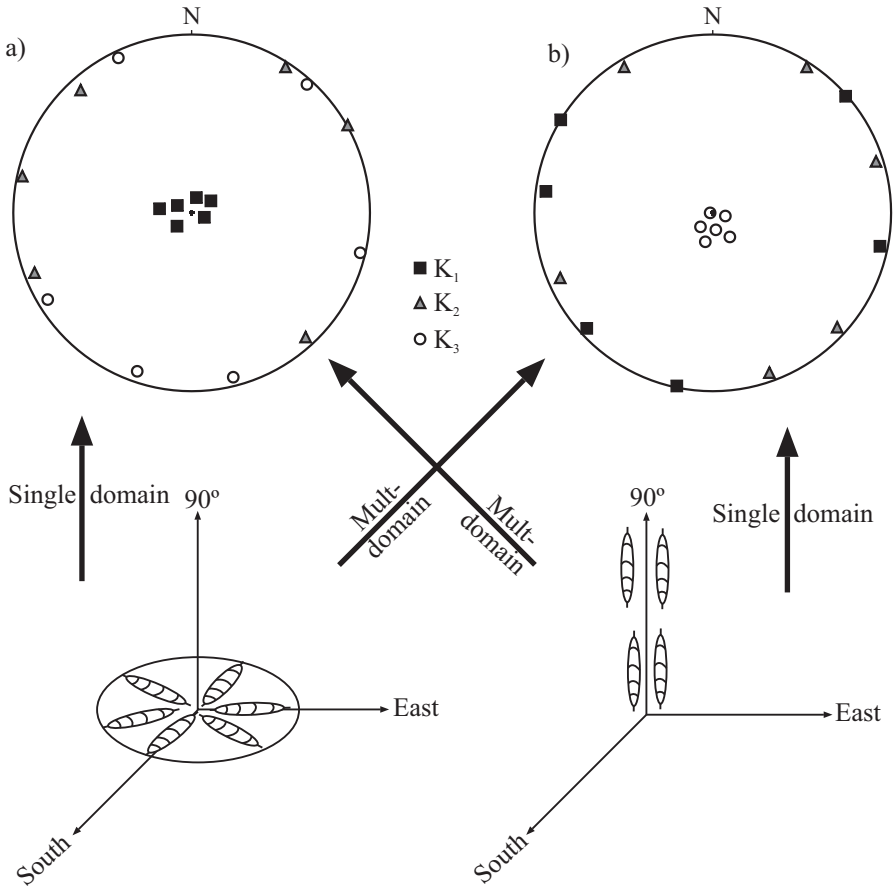

Fig. 2.7 – The behaviour of SD and MD ferromagnetic grains and their appearance on a stereonet (after Tarling and Hrouda, 1993). Where the long axes of grains are randomly distributed within a plane (a), MD behaviour would result in an oblate AMS fabric whereas SD behaviour would result in a prolate AMS fabric. Where the long axis of grains are aligned vertically (b) MD behaviour would result in a prolate fabric whilst SD behaviour would result in an oblate fabric.

possible, the unique response of SD grains to an external magnetic field (as discussed in Section 2.2) can be used to determine its presence through rock magnetic experiments (see Section 2.6).

2.5.2. Paramagnetic minerals

Weathering causes the physical and chemical breakdown of rocks. This process can lead to a concentration of particulate residues (e.g. quartz) and the formation of secondary minerals, such as paramagnetic phyllosilicates (clay minerals). As such, clay minerals (e.g. chlorite, illite, kaolinite etc.) are very common in sedimentary rocks. Being paramagnetic, these minerals do not carry a magnetic remanence but can be effectively used in AMS studies (e.g. Borradaile et al., 1986; Hirt et al., 1993; Lüneburg et al., 1999). Paramagnetic minerals typically have low susceptibilities (around 5×10^{-4} SI) (Tarling and Hrouda, 1993). As such, their properties can easily be obscured if ferromagnetic minerals are present. An important feature of paramagnetic minerals is that susceptibility decreases with temperature according to the Curie-Weiss law. However, pure examples of paramagnetic minerals are rare. Impurities are common and, if present during heating, they can result in the growth of new minerals (Just and Kontny, 2012).

Paramagnetic minerals display crystalline anisotropy. Although this is not a direct function of the shape of the grain, they can readily be used as petrofabric indicators. This is because they split readily along crystallographic axes. This is particularly useful in the case of the mineral biotite, where the arrangement of the cleavage planes produces anisotropic crystals, and the AMS is a direct reflection of the shape of the grain (Ballet et al., 1985). Other phyllosilicate minerals (e.g. chlorite) have dominantly oblate anisotropies where K_3 lies within 5° of the basal planes (c-axis). This was shown by Cifelli et al. (2005) and (2009) who compared the AMS fabric of clay minerals with the analysis of neutron diffraction poles (a direct petrofabric indicator). It was found that the K_3 axes of the AMS fabric coincided perfectly with the poles to the basal planes of the chlorite minerals.

2.5.3. Diamagnetic minerals

Diamagnetic minerals (e.g. quartz and calcite), despite being very common and normally making up the bulk of rock or sediment, have very weak, negative susceptibilities (typically -1 × 10^{-5}). They therefore only become important when ferromagnetic minerals are completely absent and paramagnetic minerals are virtually absent (less than 1% of the total volume) (Tarling and Hrouda, 1993). Diamagnetic minerals produce inverse AMS fabrics in a similar way to those produced in SD magnetite (Section 2.5.1). As such, the susceptibility axes are switched. The K_1 axis lies at 90° to the foliation plane defined by the K_2 and K_3 axes. Therefore, erroneous interpretation can result if diamagnetic fabrics are not properly recognised.

The identification of a diamagnetic contribution is relatively straightforward as susceptibility values of such minerals are always negative (because of reasons explained in Section 2.2). However, interpretation can be more problematic when minute paramagnetic or ferromagnetic contributions exist (e.g. Rochette, 1988; Hrouda, 2004). Anisotropy values near zero can be anomalously high (Hrouda and Kapička, 1986; Rochette, 1987; Biedermann et al., 2013), because of the way anisotropy is calculated. Although this is not thought to affect fabric orientations (Hrouda, 2004; Callot et al., 2010), its effect can cause problems when calculating the anisotropy parameters. In addition, the crystallographic structure of some diamagnetic minerals (e.g. calcite) can cause further complications (Rochette, 1988; de Wall et al., 2000). In spite of this, various studies have effectively characterised tectonic deformation in diamagnetic rocks (e.g. Hamilton et al., 2004; Callot et al., 2010; Borradaile et al., 2012).

2.5.4. Summary

Although AMS is held as a fast, objective method of measuring the petrofabric of rock or sediment, its interpretation can be complex because of the variety of different behaviours of different magnetic minerals. Ferromagnetic minerals normally display shape anisotropy (e.g. MD magnetite) and can provide a direct reflection of the petrofabric, often both in terms of direction and degree of alignment. Paramagnetic minerals (e.g. clays) display crystalline

anisotropy. Although this is not a direct reflection of grain shape, it is often directly comparable to the petrofabric. However, fine grained ferromagnetic minerals (e.g. SD magnetite) can produce inverse fabrics which, if not correctly recognised, could result in erroneous interpretations.

As such, identification of the contributors to the fabric is vital in all AMS studies. In this thesis, a suite of rock magnetic experiments are employed. The primary aim is to determine the relationship of the AMS fabrics to the depositional processes occurring within the sediment. Additional fabric measurements (e.g. clast fabric analysis) and the analysis of structural and sedimentological features (e.g. folds, faults, stretching lineations and striations) are undertaken where possible, so that the validity of the AMS technique can be determined.

2.6. Determination of the magnetic mineralogy

A first order approximation of the mineralogy can be given from the mean susceptibility of the samples (see Fig. 2.5 and Section 2.5). However, it is often the case that more detailed magnetic mineralogical investigations are needed before the source of the fabric can be determined. The rock magnetic experiments used in this thesis to evaluate the magnetic mineralogy of the samples are discussed below. In these experiments, the magnetic induction is measured by Tesla (T) or millitesla (mT), whilst the magnetisation (J), is measured in ampere-metre (A/M).

2.6.1. Temperature versus low field susceptibility

The investigation of the variation of bulk magnetic susceptibility with temperature can be used as a powerful technique for the identification of magnetic minerals (e.g. Hrouda et al., 1997a; Stevenson et al., 2007; Petronis et al., 2011). High-temperature susceptibility investigations typically involve the bulk susceptibility measurements of powdered specimens in a non-magnetic furnace. The sample is heated in a stepwise manner from room temperature. At each increment, the low field magnetic susceptibility is measured. The variation in susceptibility

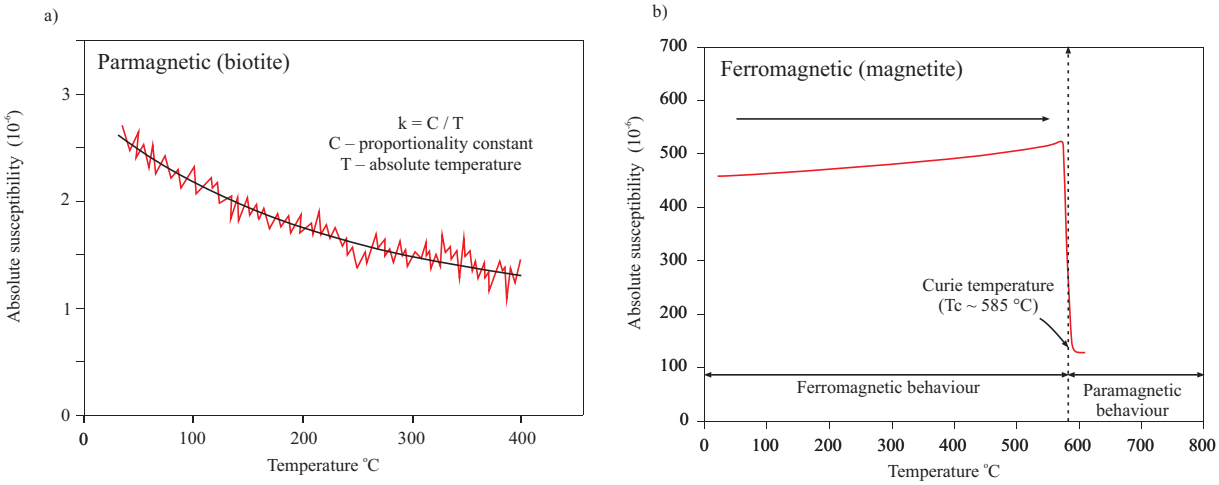

Fig. 2.8 – The variation of susceptibility with temperature for different minerals (after Hrouda et al., 1997a). (a) Typical thermomagnetic curve for a pure paramagnetic minerals (biotite) showing a decrease in susceptibility with increasing temperature according to the Curie-Weiss hyperbola (black). (b) Typical thermomagnetic curve for magnetite showing an increase in susceptibility with increasing temperature up to the Curie temperature (Tc), after which the material behaves paramagnetically.

can subsequently be used as a proxy for the magnetic mineralogy or to investigate compositional and phase changes that take place on heating or cooling (Pokorný et al., 2011).

Paramagnetic minerals (e.g. biotite) normally display a decrease in susceptibility with increasing temperature following a hyperbola (in accordance with the Curie-Weiss law, Fig. 2.8a, 2.9a and 2.10b). If ferromagnetic minerals are present, the Curie point can usually be approximated (Fig. 2.8b). The Curie point is the temperature at which super exchange forces are

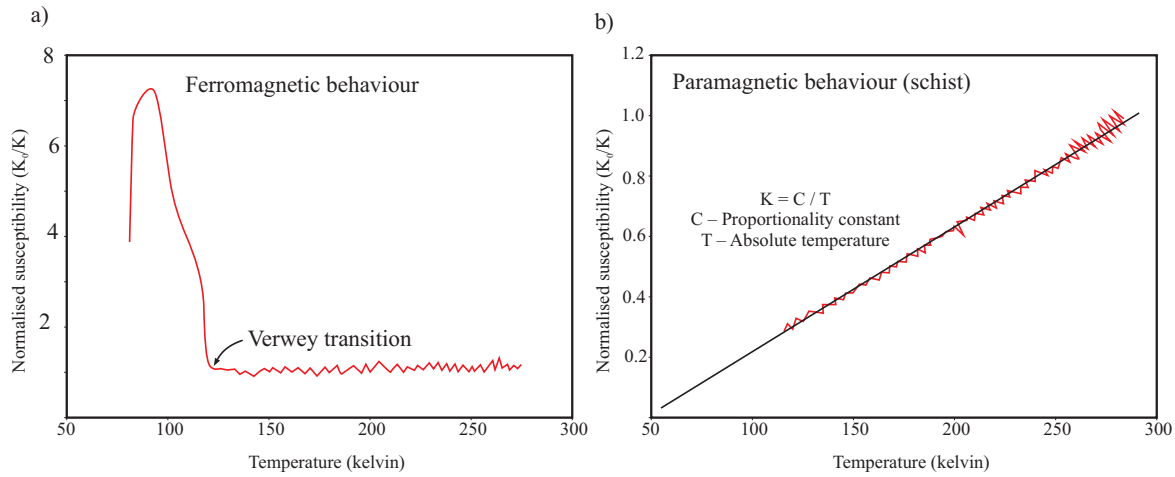

Fig. 2.9 – Low temperature variation of susceptibility plotted as the normalised reciprocal (K_0/K) (after Richter and van der Pluijm, 1994). (a) Ferromagnetic behaviour in magnetite showing the Verwey transition at 188 K and no temperature dependence between 120 K and 273 K. (b) Paramagnetic behaviour in a mica dominated schist, plotting as a straight line, obeying the Curie-Weiss law perfectly.

no longer effective and the substance behaves paramagnetically. For example, pure magnetite (Fig. 2.8b) has a Curie point of 580 ˚C. Above this temperature, susceptibility drops and the mineral behaves paramagnetically. However, the Curie temperature for ferrimagnetic grains is variable and can gradually decrease with increasing impurities in the matrix (e.g. falling to 150 ˚C for some titanomagnetites).

Temperature versus low field susceptibility analysis can also give a crude proxy of grain size. Some minerals, particularly fine grained (SD) magnetite and haematite, show enhanced susceptibility just prior to the Curie point; a feature known as a Hopkinson peak (Hopkinson, 1890). The recognition of this peak can be an indicator of SD sized grains. However, an increase in susceptibility prior to the Curie point can also result from the growth of new magnetic mineral phases on heating (Just and Kontny, 2012). This effect can be minimized by flooding the sample chamber with argon gas during heating to prevent oxidation reactions. Even if this is done, however, mineral reactions can still be observed (e.g. Just and Kontny, 2012). The growth of new magnetic phases is also seen on heating samples dominated by paramagnetic minerals (Fig. 2.10a). This can cause an increase in susceptibility with increasing temperature, in spite of the

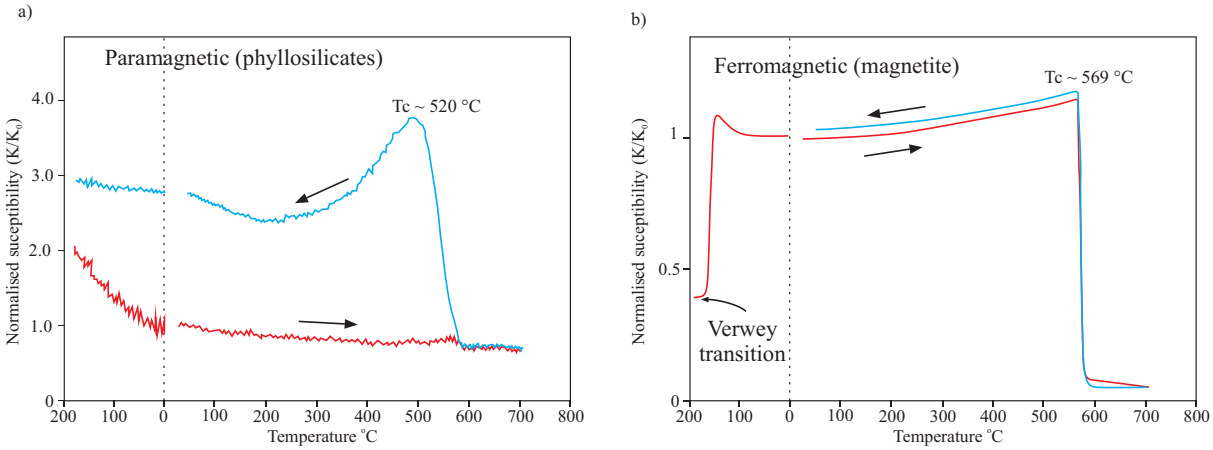

Fig. 2.10 – Combined susceptibility variation at low and high temperatures on heating (red line) and cooling (blue line) (after Just and Kontny, 2012). (a) Paramagnetic (illite) sample displaying the Curie-Weiss behaviour at low temperatures; however, on cooling a sharp increase in susceptibility is seen past a curie temperature of 520 °C reflecting the growth of a new ferrimagnetic phase at high temperatures. (b) Typical ferromagnetic behaviour in a granite sample dominated by MD magnetite. On heating from low temperatures, the Verwey transition is seen at -150 °C and a drop in susceptibility is seen at the Curie temperature signifying a change to paramagnetic behaviour. The cooling curve displays a similar behaviour indicating no alteration on heating or cooling during the experiment.

sample being dominantly paramagnetic at room temperature. This effect of this is also seen on cooling where significantly higher susceptibility curves can be observed. As such, the presence of a Hopkinson peak is not necessarily diagnostic of SD behaviour, but it is enough to warrant further investigation if present.

Investigations into the variation of low-field susceptibility at low temperatures is also used as a technique for the identification if magnetic minerals. Following the procedure of Richter and van der Pluijm (1994), this is undertaken by cooling a sample to 77 K (Kelvin) in liquid nitrogen and measuring the bulk susceptibility every 18 seconds during warming to room temperature. Paramagnetic minerals will display a hyperbola (following the Curie-Weiss law). This results in a decrease in susceptibility with increasing temperature (Fig. 2.9b). In contrast, ferromagnetic minerals (e.g. magnetite) are characterised by a Verwey Transition (Verwey, 1939). For example, magnetite will pass through the Verwey Tranition at approximately -152 °C on cooling, during which it will undergo a change in crystal structure that results in an abrupt decrease in susceptibility (Fig. 2.9a). Above the Verwey Transition, ferromagnetic minerals behave independently of temperature (Richter and van der Pluijm, 1994).

Temperature versus low field susceptibility data is normally displayed on standard line graphs either with absolute or normalised susceptibility. Low-temperature susceptibility data is traditionally displayed as separate graphs that plot the normalised reciprocal (K_0/K) versus temperature (Fig. 2.9). This effectively inverts the shape of the curve and transforms it into a straight line (e.g. Richter and van der Pluijm, 1994). However, it can also be shown on the same graph (e.g. Fig. 2.10) to allow direct comparison with the high temperature versus susceptibility data.

2.6.2. Varying field susceptibility

The variation of field strength with susceptibility can also be used to provide constraints on the interpretation of the magnetic mineralogy. The theory of low-field AMS is based on the assumption that there is a linear relationship between magnetisation and the magnetising field

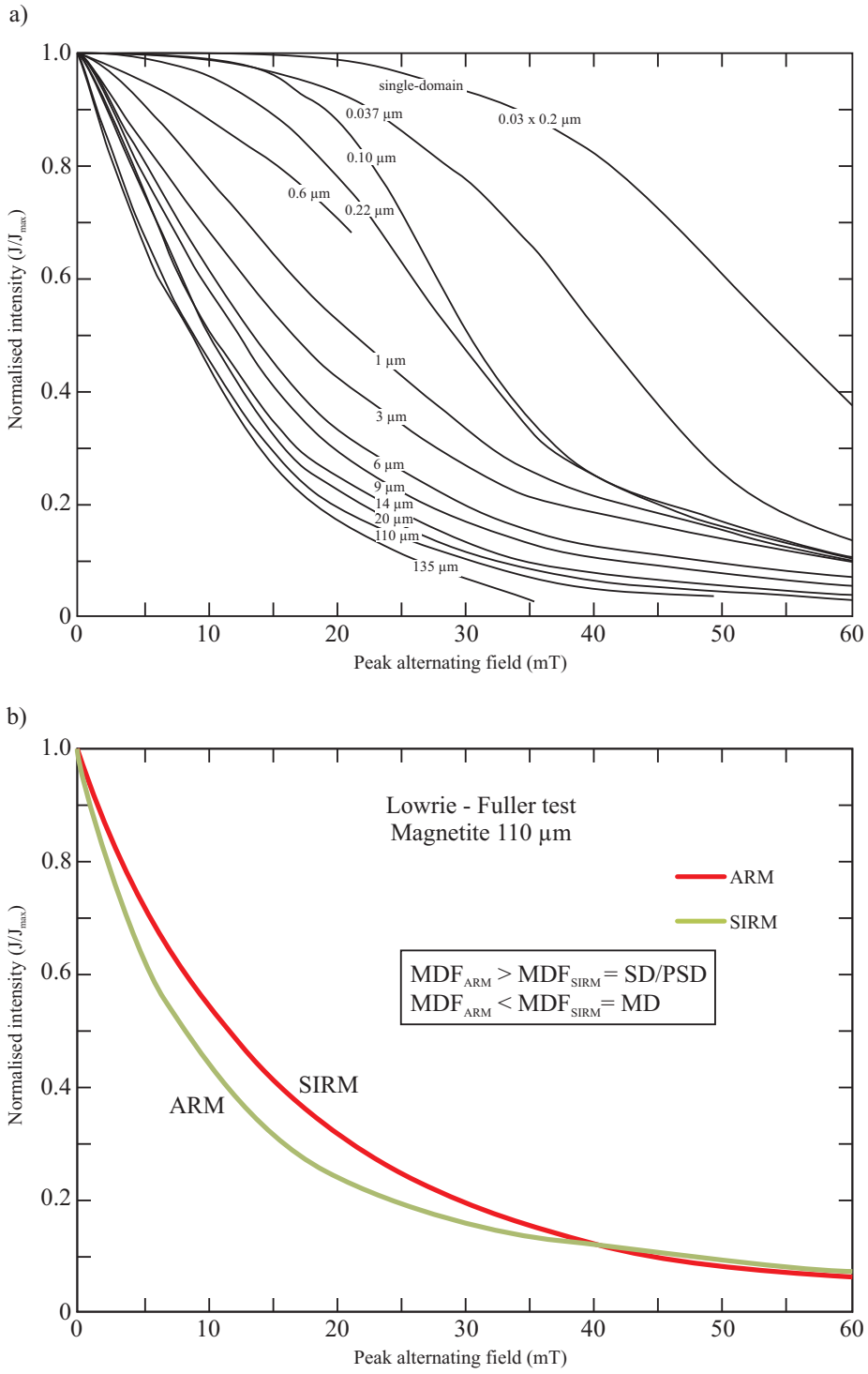

Fig. 2.11 – AF demagnetisation curves for the characterisation of grain size (after Dunlop and Özdemir, 1997). (a) Comparison of AF demagnetisation curves with widely different grain sizes. The shape of the curve changes from sigmoidal in the SD grain size range to exponential in the MD grain size range. (b) Experimental Lowrie Fuller test for MD magnetite grains (110 µm) showing the demagnetisation curves of the SIRM and ARM. The MDF of the ARM is less than the MDF of the SIRM therefore following the predictions of the Lowrie-Fuller test.

(Hrouda, 2011). Whilst this is valid for diamagnetic minerals, paramagnetic minerals and pure magnetite, some minerals (e.g. titanomagnetite, haematite and pyrrhotite) can show very strong field variation (Hrouda, 2002; Hrouda, 2009). Therefore, by measuring the bulk susceptibility at incremental field strengths, ranging from 5 – 700 A/M, an indication of the presence of these minerals can be determined. Whilst this method is not diagnostic, it is a rapid, non-destructive way of indicating the presence of some ferromagnetic phases.

2.6.3. AF, ARM and SIRM demagnetisation and the Lowrie-Fuller test

The ferromagnetic component of the susceptibility can be further investigated through remanence based methods (see Dunlop and Özdemir, 1997 for review). Of these, alternating field (AF) demagnetisation techniques can be used to examine the coercivity of a sample (how easily it can be magnetised). During AF demagnetisation, a sample is exposed to an alternating magnetic field, with a waveform that progressively decreases in magnitude with time. This peak field is applied at progressively higher levels up to 120 mT or until the sample is demagnetised. The AF demagnetisation value needed to half the original remanence value is called the medium destructive field (MDF).

Manipulation of the remanent magnetism is brought about either by realigning the domain grain walls (magnetically easy) or by rotating the magnetisation (magnetically difficult). As such, grains which have multiple domains are relatively easy to magnetise whilst grains with just a single domain are much harder (see Section 2.2). Therefore, the coercivity of a mineral can directly reflect its grain size (Fig. 2.11a). The maximum coercivity for a given mineral occurs within the SD range and normally decreases with increasing grain size as the grain subdivides into domains. However, composition can also affect coercivity as some minerals (e.g. haematite) display much higher values. Minerals with low coercivities (e.g. MD magnetite) can be referred to as magnetically ‘soft’ and display a low MDF. In contrast, minerals with high coercivities (e.g. SD magnetite and haematite) are referred to as being magnetically ‘hard’ and have much higher MDFs or may not respond at all to AF demagnetisation.

To examine the coercivity spectra, the natural remanent magnetisation (NRM) can be demagnetised. Alternatively, a magnetisation can be induced into the sample and subsequently demagnetised with an AF field. Applying a magnetic field to a sample under isothermal conditions will result in an isothermal remanent magnetisation (IRM). A large magnetic field will force grain rotation in SD particles or domain wall rotation in MD particles and saturation may be reached. This is referred to as the saturation isothermal remanent magnetisation (SIRM). In addition, an anhysteretic remanent magnetisation (ARM) can be imparted on a sample by applying a progressively decaying large alternating field (AF) whilst at the same time applying a smaller constant DC field across the sample. ARM is often used as an analogue for thermoremanent magnetisation, which involves the application of an external magnetic field during cooling from temperatures above the Curie point of the minerals (Moskowitz, 1991). The randomising effects of the AF are thought to be similar in each (Dunlop and Özdemir, 1997). As such, ARM is often used to eliminate the need for heating and the risk of associated chemical alterations (e.g. Banerjee and Mellema, 1974).

The experimental results of Lowrie and Fuller (1971) revealed distinct differences in the shape of the demagnetisation curve of the SIRM and TRM (or ARM) depending on whether SD or MD grains were present (Fig. 2.11b). A subsequent Lowrie-Fuller test was proposed to permit a rapid identification of rocks dominated by SD grains (which were desirable carriers of the NRM for palaeomagnetic studies). It was suggested that if the MDF of the ARM was less than the MDF of the SIRM, MD grains were dominant. In contrast, if the MDF of the ARM was greater that the MDF of the SIRM, SD grains would be dominant in the sample.

In practice, the test is not totally reliable. Subsequent studies (e.g. Dunlop et al., 1973; Johnson et al., 1975; Bailey and Dunlop, 1983) revealed that grains much larger than SD size gave an SD-type Lowrie-Fuller test. Importantly, Heider et al. (1992) observed this behaviour in grains up to 100 μm, leading to the conclusion that the test result is not a simple indicator of grain size or domain state as was originally hoped. However, the exact conditions of Heider et al.'s test are unlikely in natural settings, and the Lowrie-Fuller test is still considered a useful grain

size discriminator for magnetite (Xu and Dunlop, 1995; Dunlop and Özdemir, 1997). It is used in this thesis to complement the other rock magnetic experiments. Similar information on grain size can also be obtained from analysis of the shape of the demagnetisation curves themselves (Fig. 2.11a).

2.6.4. IRM acquisition curves

An alternative means to examine the coercivity spectrum of the sample can be undertaken through analysis of the IRM acquisition (Fig.2.12). This involves exposing a sample to an external magnetising field for a short time and measuring the magnetic moment. The strength of the field is increased in a stepwise manor until the sample reaches saturation (SIRM) (Butler, 1992). The magnetic field is then reversed along the same axes, and a field is applied in the opposite direction in the same manor until the magnetic moment returns to zero; a procedure known as the back

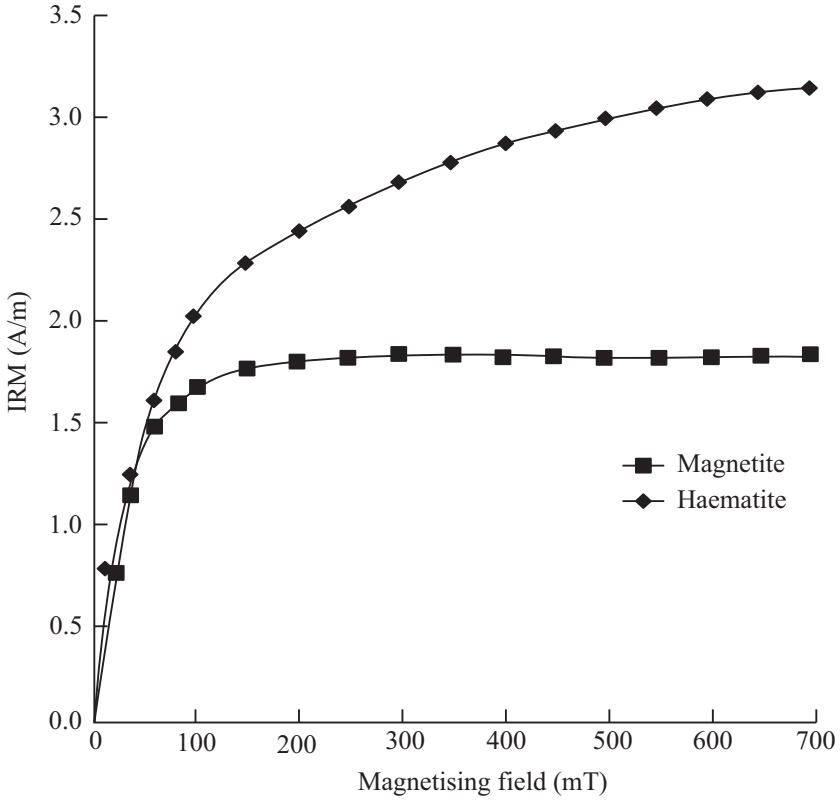

Fig. 2.12 – IRM acquisition curves of magnetite and haematite (after Moskowitz, 1991; Butler, 1992). MD magnetite has a low coercivity and reaches saturation at relatively low magnetising fields. In contrast, haematite has a high coercivity and does not reach saturation until much higher field strengths.

field IRM (BIRM). The results are often considered comparable to full hysteresis measurements and can be used when the equipment needed for this is not available.

Magnetically 'soft' minerals (e.g. MD magnetite) will typically reach saturation at relatively low strength magnetic fields. In contrast, high coercivity, magnetically 'hard' minerals will reach saturation at much higher field strengths (e.g. Day et al., 1977; Argyle and Dunlop, 1990). For example, magnetite will generally reach the saturation magnetisation at 300 mT, whilst haematite requires fields in excess of 2.5 T (Lowrie and Heller, 1982)(Fig. 2.12). As such, IRM acquisition curves can be used as a useful indication of the presence of haematite in a sample.

2.6.5. Summary

Determination of the magnetic mineralogy is crucial in any AMS study. A first order approximation can be obtained from analysis of the mean susceptibility; however, more detailed rock magnetic experiments are often required, particularly where a mixed magnetic mineralogy is suspected. The investigation of temperature versus susceptibility can be used as a reliable distinction between paramagnetic and ferromagnetic components, particularly when cryogenic methods are used. The growth of new mineral phases can obscure the results from high temperatures, but the Curie-Weiss parabola can normally readily be distinguished from the ferromagnetic Verwey transition at low temperatures. If ferromagnetic components are suspected, either through relatively high mean susceptibility values, Curie-point estimates or the presence of anomalous 'inverse' fabrics, then remanence based investigations can be used. AF demagnetisation and IRM acquisition can provide excellent indications of domain state (SD or MD) and can reveal the presence of haematite. Only once the origin of the magnetic fabric is determined can reliable interpretations be made as to the physical processes that formed it.

2.7. AMS of sedimentary rocks

AMS has been used as a technique for determining three-dimensional petrofabric in

sedimentary rocks by various authors (Rees, 1961; Griffiths et al., 1962; Hamilton, 1963; Rees, 1965). There is now a good understanding of the application of AMS to a variety of sedimentary deposits, including those from marine (e.g. Piper et al., 1996; Kissel et al., 1997), glacial (e.g. Shumway and Iverson, 2009; Thomason and Iverson, 2009) and aeolian environments (e.g. Lagroix and Banerjee, 2002; Bradák, 2009). In almost all cases, the AMS fabric directly reflects the conditions and processes that formed the sediment (Tarling and Hrouda, 1993). However, fabrics from sedimentary rocks are prone to secondary alteration and remagnetisation. Shortly after deposition, a variety of factors (both diagenetic and tectonic) can affect the fabrics (see Tarling and Hrouda, 1993 for review). What follows is a review of the current literature behind the formation and preservation of AMS fabrics in the sedimentary record.

2.7.1. Primary sedimentary AMS fabrics

In a subaqueous environment, the alignment of minerals is controlled primarily by gravitational and hydrodynamic processes. When deposition occurs in still water on a flat surface, gravitational settling is the only significant force and causes platy grains to become aligned parallel to the depositional surface. This gives rise to a strongly oblate fabric confined to the bedding plane. The K_1 and K_2 axes will girdle about the bedding plane, whilst the K_3 axes will lie perpendicular to this surface (Hamilton and Rees, 1970).

In nature, completely still water is rare and hydrodynamic disruption is common. For example, currents acting on the sea floor can greatly affect grain alignment. This process has been investigated experimentally under laboratory conditions (e.g. Rees, 1961; Rees and Woodall, 1975). Typically, if a current is present, the long axis of grains will rotate and become preferentially aligned parallel to the direction of flow. As such, magnetic lineations (K_1 axes) will develop which subsequently reflect current flow directions. Strong currents may result in an imbrication of K_1 axes away from the bedding plane. This can produce a magnetic lineation in an up-flow dip (King, 1955; Rees and Woodall, 1975; Parés et al., 2007). In some cases, K_1 axes have been observed lying normal to the palaeoflow direction (e.g. Piper et al., 1996). This has

been interpreted to reflect grain rolling on its long axes perpendicular to flow under certain flow regimes and is considered rare. Hence, AMS has effectively been used to reconstruct palaeoflow directions in a variety of settings (e.g. Rees et al., 1968; Ellwood, 1980; Kissel et al., 1997; Parés et al., 2007; Pueyo Anchuela et al., 2013).

Soft-sediment deformational processes can also have a significant impact on primary depositional fabrics, e.g. slumping (Schwehr and Tauxe, 2003). Here, stress acting on the sediment can cause grains to rotate. This results in the alignment of long axes parallel to and short axes perpendicular to the shear plane. AMS has also been particularly useful in determining palaeoflow from debris flows (e.g. Gravenor, 1986; Archanjo et al., 2006). AMS lineations were observed to form parallel with palaeoflow directions of the debris flow, and an imbrication of K_1 away from palaeoflow is often seen. This pattern is similar to those produced in some extrusive igneous rocks, particularly tuffs which can give 'sedimentary' fabric patterns (e.g. Ellwood, 1982; Incoronato et al., 1983). There have been various studies of the AMS fabrics of deep sea turbidites (e.g. Ellwood and Ledbetter, 1977; Taira and Lienert, 1979; Dall'olio et al., 2013). In these situations, lineations are typically seen interpreted to form parallel to the depositing current.

2.7.2. Post-depositional effects

Whilst most AMS fabrics are controlled by the primary depositional mechanisms, post-depositional processes can have a significant impact on fabrics formed during sedimentary processes (e.g. Borradaile and Tarling, 1981; Borradaile and Tarling, 1984; Kissel et al., 1986; Averbuch et al., 1992). This can result from a variety of complex biological, chemical and physical factors (see Tarling and Hrouda, 1993 for review). For example, bioturbation within the sediment can result in a weakening of the fabric strength (Chernow et al., 1986), although in these situations, the original magnetic lineation is often still preserved.

With increasing depth, gravity continues to try to rotate grains towards the horizontal which can act to make a fabric more oblate. As the sediment becomes increasing compacted, pore space and permeability are reduced and the grains' ability to rotate is restricted. After this, the most

significant mechanism that will affect the fabric are diagenetic changes in the mineralogy. The growth of new minerals during diagenesis can affect AMS fabrics even if not strongly magnetic themselves. For example, they may disrupt adjacent grains if their growth exceeds the available space (Tarling and Hrouda, 1993). However, the original palaeocurrent can still be extracted in most cases even if this has occurred (e.g. Schieber and Ellwood, 1988). New magnetic minerals can also form from iron-bearing paramagnetic minerals (e.g. biotite and hornblende). In many cases, these can fill the pre-existing shape of the original mineral and provide fabric orientations that are often the same as the original grain (Tarling, 1983).

2.7.3. Tectonism

AMS has been shown to be very sensitive to tectonic reorientation, especially if it takes place prior to cementation (Tarling and Hrouda, 1993). In these situations, deformation is solely a result of the mechanical rotation of grains at low hydrostatic pressures and temperatures (e.g. Kissel et al., 1986; Cifelli et al., 2009). In this way, tectonic fabrics can be observed in sediments that otherwise show no other evidence of deformation. Grain rotation is more restricted if the rocks are cemented. In these situations, greater pressure and more intense deformation is generally required to modify primary fabrics. Phyllosilicate minerals are particularly prone to this and can more readily rotate into new stress fields than larger ferromagnetic grains. In some cases, it has even been possible to link AMS to strain in a quantitative way (e.g. Kligfield et al., 1981; Borradaile, 1987, 1988; Hrouda et al., 1997b). In higher-grade metamorphic rocks, the original mineralogy can be modified completely and new minerals can form whose fabrics are controlled by the ambient stress field at the time of metamorphism.

Various studies have been undertaken to show how sedimentary fabrics are affected by tectonic deformation (e.g. Borradaile and Tarling, 1981; Borradaile and Tarling, 1984; Kissel et al., 1986; Averbuch et al., 1992; Borradaile and Henry, 1997) (Fig. 2.13). The incipient deformation of mudrocks from the Southern Pyrenean Foreland Basin was investigated by Parés et al. (1999). They showed that the progressive development of an overprinting tectonic fabric

could be identified in rocks that otherwise showed no mesoscopic evidence of deformation. Starting with an oblate sedimentary fabric (Fig. 2.13, Type I), the first evidence of tectonic deformation is characterised by the clustering of K_1 axes normal to the tectonic shortening direction (Fig. 2.13, Type II) and preservation of the K_3 axes perpendicular to bedding. This results in a dominantly triaxial fabric pattern, even in rocks dominated by phyllosilicate minerals. This is because a magnetic lineation can be produced through the intersection of basal planes (as discussed in Section 2.5.2). Subsequent deformation at higher tectonic strain results in the deviation of K_1 and K_2 axes away from the bedding plane, ultimately forming a 'tectonic' fabric (Fig. 2.13, Type III – VI). If strain is purely compressional, then this tectonic fabric may form a circular girdle parallel to the rock cleavage (Fig. 2.13, Type V). However, lineations may also form in an orientation perpendicular to the direction of horizontal shortening (Fig. 2.13, Type IV and VI).

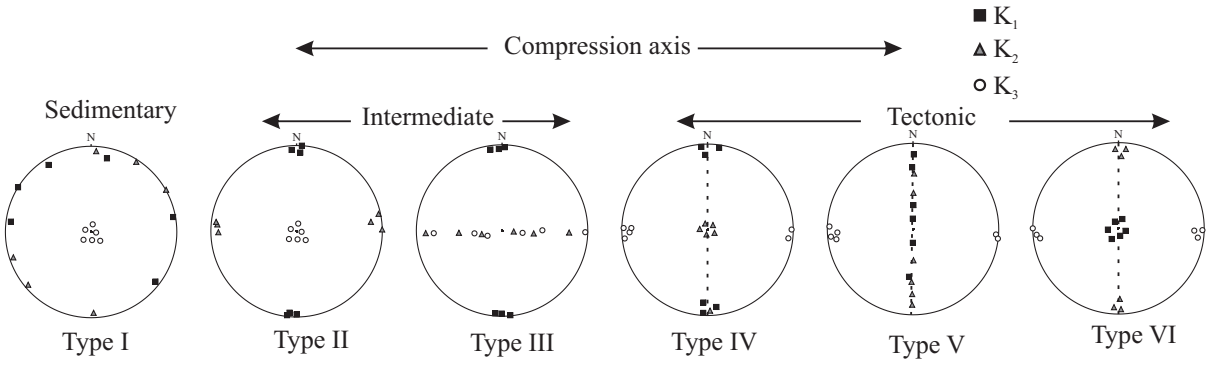

Fig. 2.13 – The effect of incipient deformation on primary AMS fabrics. Sedimentary fabrics (Type I) typically display oblate AMS fabrics. In response to horizontal compression, K_1 axes will cluster parallel to fold axes (Type II). If horizontal extension occurs associated with the compression, a girdle fabric may form between K_2 and K_3 axes (Type III). Tectonic fabrics (Type IV to VI) are when the K_1 axes have migrated 90° from bedding to sit normal to cleavage plane.

2.8. Applications to glacial sediments

A summary of literature where AMS has been applied to glacial sediments is presented in Table 2.1. The AMS technique was first applied to glacial sediments by Fuller (1962). In this study, AMS fabrics of till were compared with clast macrofabrics (widely considered an

Reference	Title	Deposit	Location	Techniques used	Magnetic carrier	Synopsis
(Fuller, 1962)	A magnetic fabric in till	Barrington chalk pit	Cambridge, UK	AMS, clast fabrics	?Magnetite	First ever application of AMS to till. AMS fabrics have the same orientation as clast fabrics. Suggests that magnetic fabric could prove a useful tool in glacial sediments and provide an indication of flow direction in the parent glacier or ice sheet.
(Stupavsky et al., 1974a)	Paleomagnetism and magnetic fabric of the Leaside and Sunnybrook Tills near Toronto, Ontario	Leaside till and Sunnybrook till	Toronto, Canada	Palaemagnetism, AMS	Unknown	A stable primary remanent magnetism of detrital origin (DRM) can be measured from the till to characterise the pole at deposition. North and NW K_1 orientations in the same orientation as previous clast macrofabrics suggesting ice flow to the NW
(Stupavsky et al., 1974b)	Paleomagnetism of the Port Stanley Till, Ontario	Port Stanley till	Wheatley, Ontario, Canada	Palaemagnetism, AMS	Unknown	A stable DRM is measured to provide pole at deposition. AMS lineations occurred parallel to the interpreted ice flow direction and is unrelated to the DRM.
(Stupavsky and Gravenor, 1975)	Magnetic fabric around boulders in till	Port Stanley till	Port Alma, Ontario, Canada	AMS	Unknown	AMS was measured in the till surrounding a large boulder. Variation in strength of the fabric lead the authors to an interpretation that pressure on the upstream of the boulder caused the release of a water slurry resulting in the preferred orientation of clasts and AMS fabric patterns.
(Boulton, 1976)	The origin of glacially fluted surfaces - observations and theory	Various Recent deposits	Iceland, Spitsbergen, Norway, and the Alps	Clast fabrics, AMS	Unknown	Uses magnetic fabrics and clast fabrics to investigate flute formation. Dipping magnetic fabrics on the flute crest were interpreted to represent the movement of material horizontally and upwards during flute formation.
(Eyles et al., 1987)	Depositional controls on the magnetic characteristics of lodgement tills and other glacial diamict facies	Various sites from around Lake Ontario	Canada	Facies analysis, clast fabrics, Palaemagnetism, AMS	Unknown	Investigated the AMS characteristics of tills produced by lodgement, rainout and resedimentation processes. Concluded that AMS can offer considerable assistance in genetic studies of massive diamictite facies.
(Stewart et al., 1988)	Nature and origin of corrugated ground moraine of the Des Moines lobe, Story County, Iowa	late Wisconsinan till	Story County, Iowa	Facies analysis, clast fabrics, AMS	Unknown	Investigated the origin of corrugated ground. Till and pebble fabric were found to be similar and strong. Along with the presence of other indicators (e.g. striations, boulder pavements) indicated a lodgement origin.
(Principato et al., 2005)	Glacial-Marine or Subglacial Origin of Diamicton Units from the Southwest and North Iceland Shelf: Implications for the Glacial History of Iceland	Various recent	Southwest and north Iceland shelf	Facies analysis, microfabric, radiocarbon dating, foraminiferal assemblage data.	Unknown	Used a range of proxies to investigate the origin of the diamicton. Subglacial tills were observed to have a low inclination K_3 axes in a consistent direction whilst the K_3 axes of glaciomarine diamictites were steeper and more random.

(Archanjo et al., 2006)	AMS and grain shape fabric of the Late Palaeozoic diamictites of the Southeastern Parana Basin, Brazil	Late Palaeozoic Itararé Group	South-eastern Paraná Basin, Brazil	AMS, microfabric, rock magnetic experiments	phyllosilicates, minor SD magnetite	Observed scattered magnetic lineations around a subhorizontal foliation plane. Interpreted the diamictites to be sub-aqueous mass flow, largely base on previous publications. AMS fabrics were therefore interpreted to represent palaeoflow directions of the mass flows.
(Hooyer et al., 2008)	Magnetic fabric of sheared till: A strain indicator for evaluating the bed deformation model of glacier flow	Various late Wisconsin-age basal tills	Lab-based	AMS (ring shear deformation), rock magnetic experiments	Magnetite with minor haematite	AMS fabric progressively increased in strength with increasing shear strains up to a point where 'steady state' fabrics were reached. K_1 axes clustered strongly in the direction of shear plunging up glacier.
(Iverson et al., 2008)	The experimental basis for interpreting particle and magnetic fabrics of sheared till	Various late Wisconsin-age basal tills	Lab-based	AMS (ring shear deformation)	Magnetite with minor haematite	The experimental procedure behind with interpretations (above) and their significance of the results in terms of theories of particle rotation.
(Shumway and Iverson, 2009)	Magnetic fabrics of the Douglas Till of the Superior lobe: exploring bed-deformation kinematics	Douglas Till, Miller Creek Formation	Douglas County, Wisconsin, USA	AMS, microfabric	Magnetite (after Hooyer et al., 2008)	Based on comparisons with Hooyer et al. (2008), the tills were interpreted to have been subglacially deformed under variable strains. K_1 axes were generally parallel to flow but large variation over short distances is interpreted to represent a heterogeneous deforming bed.
(Thomason and Iverson, 2009)	Deformation of the Batestown till of the Lake Michigan lobe, Laurentide ice sheet	Batestown Member, Lemont Formation	Illinois, USA	AMS, microfabric, micromorphology	Magnetite (after Hooyer et al., 2008)	Highly variable fabric strengths were observed. Based on comparisons Hooyer et al. (2008), parts of the till do not contain fabrics strong enough to have been deformed under the bed deformation model.
(Gentoso et al., 2012)	Exploring till bed kinematics using AMS magnetic fabrics and pebble fabrics: the Weedsport drumlin field, New York State, USA	Late Wisconsin Furnaceville Till	New York State, USA	AMS, clast fabrics, rock magnetic experiments	maghaemite	K_1 axes were observed to be parallel to pebble long-axis orientations, plunging gently up-glacier. These were both parallel to the drumlin long axes but deviating moderately from flute direction.
(Tylmann et al., 2012)	The ice/bed interface mosaic: deforming spots intervening with stable areas under the fringe of the Scandinavian Ice Sheet at Sampława, Poland	Unnamed Late Weichselian tills	Sampława, Poland	Facies analysis, AMS	unknown	AMS and clast fabrics are compared in interbedded subglacial tills and outwash sediments. K_1 axes lie parallel to mean clast fabric orientations. The authors use the fabric strength to quantify the strain based on comparisons with Hooyer et al. (2008)

Table 2.1 – Comparison of the published literature on the AMS of glacial sediments.

alternative fabric indicator), and a magnetic lineation was seen that lay parallel to the mean clast fabric orientation. Fuller subsequently suggested that AMS could be used as a proxy for ice flow direction. The work of Stupavsky and Gravenor (1975), Stupavsky et al. and (1974a) Stupavsky et al. (1974b) supported this idea. As well as investigating the natural remanent magnetisation, these authors used AMS to determine the flow directions in Late Wisconsinan tills around Lake Ontario.

Apart from reference to the technique in Boulton (1976), Eyles et al. (1987) was the first to apply the technique to till from modern glacial settings. These authors compared AMS fabrics produced from modern subglacial tills in Iceland and Pleistocene tills in England with submarine rainout diamicton from Pleistocene sediments around Lake Ontario. The subglacial diamictons analysed displayed a weakly-developed, flow-parallel AMS fabric, whilst in subaqueous, rainout diamictons, a range of fabrics were observed, from oblate to strongly clustered. Tightly clustered fabrics were interpreted as resedimented debris flow deposits. From this, Eyles et al. (1987) tentatively concluded that subglacial tills display a weaker AMS fabric than diamicton produced through mass-flow processes. However, the authors admitted that the results were provisional and did not take into account the variables when dealing with tills of different ages and with vastly different compositions.

The first application of AMS to pre-Quaternary diamictites was carried out by Archanjo et al. (2006). These authors analysed Late Palaeozoic diamictites of the Itararé Group, Brazil. Archanjo et al. were also the first to systematically carry out rock magnetic investigations into the AMS of diamicts. Instead of a ferromagnetic contribution, which is often assumed, the results revealed that paramagnetic clay minerals were controlling both the anisotropy and susceptibility. In spite of possibly having a very different magnetic carrier to the AMS, the authors made comparisons to the fabric characteristics of Eyles et al. (1987) and interpreted deposition through debris flows.

Since the late 1980s, it has become increasingly accepted that widespread subsole deformation occurs beneath glaciers (Boulton, 1986; Boulton and Hindmarsh, 1987). In addition to processes of lodgement and melt-out, subsole deformation is now considered to play a major role in

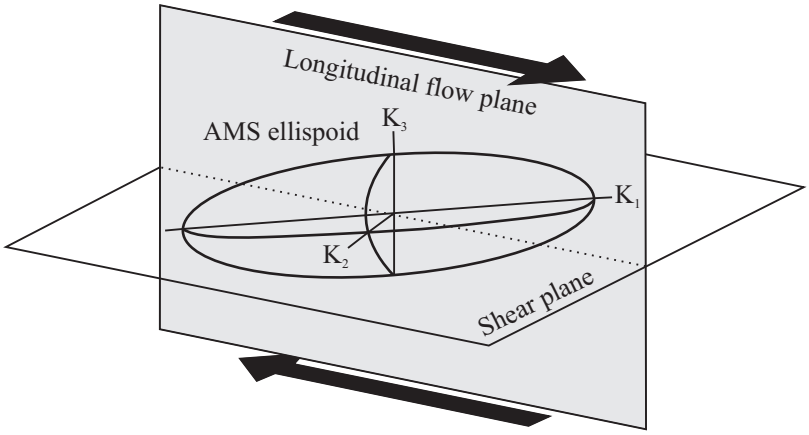

Fig. 2.14 – Schematic relationship between the AMS ellipsoid and the flow of glacier (after Hooyer et al., 2008; Iverson et al., 2008; Shumway and Iverson, 2009), showing an up glacier K_1 dip orientated parallel to the longitudinal flow plane.

the formation of till (Benn and Evans, 2010). The deforming bed can be thought of as a soft-sediment shear zone, with similarities to shear zones in tectonically deformed metamorphic rock.

The work of Iverson et al. (2008) and Hooyer et al. (2008) made a significant contribution to the idea that AMS could be used to investigate deformation in subglacial tills. These authors used ring-shear experiments to investigate fabric development in tills. When an intact till sample was sheared under conditions similar to those expected to be operating at the ice-bed interface, it was found that micro-faults develop that facilitate the rotation of the long axis of particles into the plane of shear. This gave rise to a preferential alignment of grains (Fig. 2.14) and resulted in the formation of K_1 axes parallel to the direction of shear and a magnetic foliation plane dipping gently up glacier.

It was noted that, although the fabrics became more clustered with increasing shear strains, the anisotropy values (P_j) did not appear to change significantly with increasing shear strains. To facilitate the interpretation of this clustering, the authors adapted the eigenvalue method of Mark (1973). This technique is routinely used in clast fabric analysis to determine fabric strength (e.g. Benn, 1994; Benn, 1995; Benn and Ringrose, 2001). Using this analysis, the shape and strength of the fabric is represented by the eigenvalue S_1, S_2 and S_3. The strength of the clustering of the magnetic lineation is represented by the S_1 eigenvalue, where a value of 0.33 means no alignment

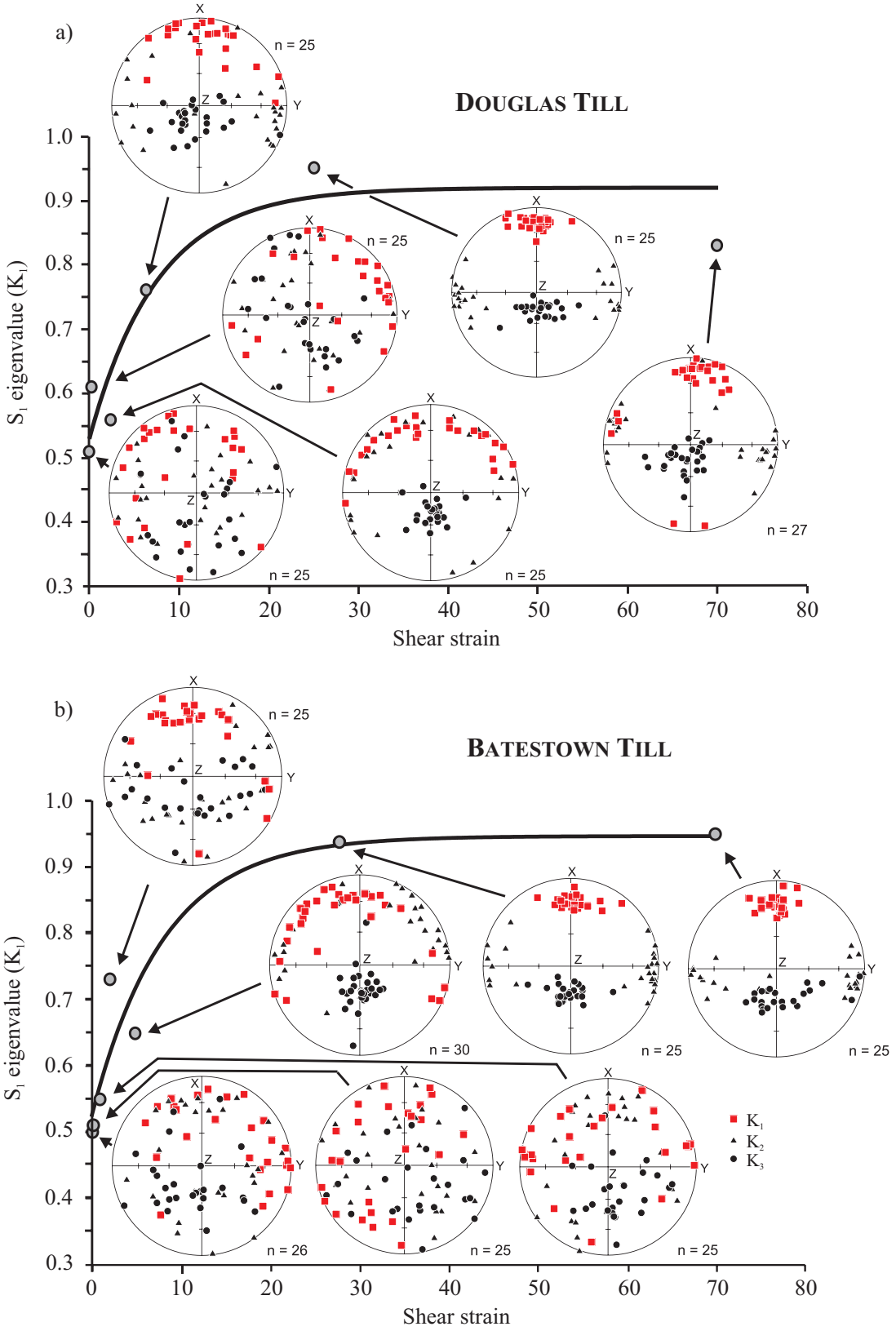

Fig. 2.15 – S_1 eigenvalue strengths and AMS fabrics in the Douglas (a) and Batestown (b) Tills versus shear strain (after Hooyer et al., 2008; Iverson et al., 2008), obtained by shearing the tills to progressively higher strains in a ring shear device. AMS results are presented on to lower-hemisphere, equal-area stereographic projections.

whilst and eigenvalue of 1.0 indicates perfect alignment.

By deforming till in a ring shear device, Iverson et al. (2008) and Hooyer et al. (2008) measured AMS fabrics at progressively increasing shear strengths (Fig. 2.15). The S_1 eigenvalue was observed to increase with increasing shear strains up to moderate values (6–25) where a steady state fabric was reached. Using this method, the authors suggested that direct comparisons could be made between the AMS fabric and shear strengths of the deforming bed. As such, tills that have not been sheared sufficiently to fit in with the bed-deformation model (Boulton, 1986) could be detected. This theory was applied to Late Wisconsinan tills from Wisconsin and Illinois (Shumway and Iverson, 2009; Thomason and Iverson, 2009). These authors directly compared eigenvalues with the ring shear experiments of Iverson et al. (2008). From this, certain tills were identified with fabrics that were not strong enough to be consistent with deformation through the deforming bed model.

Whilst the eigenvalue method is useful in clast fabrics analysis, its use in the characterisation of AMS fabrics should be applied with great caution. Clast fabric analysis involves the direct measurement of the long axis of clasts. The eigenvalues reflect this alone. In contrast, the eigenvalue of AMS fabrics, as well as being controlled by the degree of alignment, are also controlled by the relative proportions of ferromagnetic, paramagnetic and diamagnetic grains. Each of these can display both crystalline and shape anisotropy with possible inverse and normal fabric patterns. Even in the same section, it is likely that a minor deviation in composition may have a significant effect on the eigenvalue and is not necessarily linked to strain.

As such, doubts can be clast over the ability of the eigenvalue method to quantify strain through AMS and genetically identify tills in this manner proposed by Hooyer et al. (2008), Iverson et al. (2008) and Shumway and Iverson (2009). Direct comparisons with Iverson et al. (2008) and Hooyer et al. (2008) should not be made, especially where the mineralogy has not been investigated (e.g. Tylmann et al., 2012). This point is also applicable for the use of AMS as a diagnostic tool to distinguish between different facies, such as those presented in Eyles et al. (1987). As minor variation in mineralogy can significantly affect the fabric, the strength of

sediment from different sources (debris flow and subglacial) should not be directly compared unless the magnetic mineralogy is fully investigated.

In spite of this, AMS can provide a reliable indicator of ice-flow direction. In almost all cases, magnetic lineations are well correlated with clast other fabric indicators (clast fabrics and microfabric investigation) and other flow indicators. The speed, accuracy and objectiveness of the technique give it significant potential over other petrofabric indicators, and the technique therefore has the potential to make a significant contribution to glacial sedimentology. However, before reliable links between AMS and strain and AMS and depositional processes can be made, significantly more study is needed.

2.9. Use of AMS in this thesis

In this thesis, AMS samples are collected from three distinct areas, each addressing a different aspect of glacial sedimentology, and each connected by the use of the AMS technique. Many aspects of this thesis are entirely novel. As such, new methodologies have had to be developed. The collection of AMS samples was through a combination of field-based drilling and block sampling (as outlined in Appendix A). AMS samples of basal ice (Chapter 3) were collected using a portable rock drill. Unconsolidated diamicton from the Pleistocene of North Norfolk (Chapter 4) were collected through block sampling, followed by laboratory hardening and preparation. Finally, Neoproterozoic diamictites of NE Svalbard (Chapters 5 and 6) were collected using a combination of field drilling and block sampling. In total 140 sites were sampled with 1690 individual subsamples. Normally between 8 and 12 subsamples were used to make up a site following the procedure outlined in Appendix A.

Because of the large variation in the strength and shape of the AMS in different minerals, particular attention was paid to fully characterising the magnetic mineralogy in each chapter (Section 2.6). Thermomagnetic experiments were undertaken by measuring variation in magnetic susceptibility through the heating of powdered samples at 6 °C intervals, from room temperature

(21 °C) to 700 °C, using the AGICO MFK-1A Kappabridge with a CS4 high-temperature susceptibility attachment. Low-temperature susceptibility experiments were conducted using an in-house built cryostat system coupled with the MFK-1A Kappabridge. Samples were cooled to 77 K in liquid nitrogen, and the bulk susceptibility was measured every 18 seconds during warming to room temperature.

The ferromagnetic contribution to the fabric was analysed through IRM acquisition curves, AF demagnetisation curves and varying field susceptibility. IRM and BIRM experiments (i.e. partial hysteresis loops) were conducted by inducing an external applied field at progressive stronger strengths up to a peak of 2.5 T where saturation was obtained. Once saturated, BIRM demagnetisation was carried out by applying an increasing field along the –Z axis until the +Z magnetisation reached zero. AF-demagnetisation of the NRM, ARM and SIRM experiments were conducted by exposing the sample to an alternating magnetic field in a progressive stepwise manner up to a 120 mT peak applied field. Both the AF-demagnetisation and IRM/BIRM acquisition were measured on an AGICO JR6-A dual-speed spinner magnetometer, in a magnetically shielded room. The low-field variation of AC susceptibly was measured at fields between 5 and 700 A/M following the procedure of Hrouda et al. (2006).

CHAPTER 3.

MAGNETIC FABRICS IN THE BASAL ICE OF A SURGE-TYPE GLACIER

3.1. Introduction

In this chapter, a novel application of the anisotropy of magnetic susceptibility (AMS) technique is presented to examine debris-rich basal ice. The flow of glacier ice can produce similar structures to those produced in ductile deformation within rocks (Maltman et al., 2000). The analysis of these structures and smaller-scale ice fabrics can provide insight concerning the strain history and deformation of glacier ice, since ice crystals are anisotropic (Castelnau et al., 1998) and tend to develop a preferred orientation in response to strain.

The most commonly used method to examine fabrics within glacier ice is the analysis of c-axis crystallographic orientations of ice crystals in thin section (e.g. Bader, 1951; Rigsby, 1958). This has been particularly useful in understanding how ice deforms under stress (Wilson, 2000; Wilson and Sim, 2002). More recently, the development of automated techniques have introduced greater speed and objectivity (Wilen et al., 2003). However, Tison and Lorrain (1987) showed that glacier ice can recrystallise over quite short timescales. This can occur either through subsequent deformation, or the ice can recrystallise under ambient conditions (Samyn et al., 2008). As such, the final measured fabric may not represent the cumulative strain but rather a more recent recrystallisation event.

Fabric analysis involving the measurement of the AMS (Tarling and Hrouda, 1993) has provided considerable insight into depositional (e.g. Ellwood and Ledbetter, 1977; Lagroix and Banerjee, 2002; Hooyer et al., 2008) and deformation histories (e.g. Parés et al., 1999; Borradaile and Jackson, 2004; Cifelli et al., 2009) of rock and sediment. In recent years the technique has provided new and interesting information about various aspects of glaciology, including facilitating the interpretation of bed deformation (Hooyer et al., 2008; Iverson et al., 2008), glacier flow direction (Shumway and Iverson, 2009; Thomason and Iverson, 2009) and glaciotectonic history (Fleming et al., 2013) of deformed glacial sediment. Despite the links between styles of deformation seen in glaciers to those of rocks and sediment, there is (to our knowledge) no published research on the AMS of glacier ice.

Glacier ice formed by the firnification of snow, often termed englacial ice (e.g. Hubbard et al., 2000), is dominated by H_2O and is therefore diamagnetic (negative susceptibility) (Lanci et al., 2001). While the AMS of rock dominated by diamagnetic minerals has been used to investigate structural deformation (e.g. Owens and Rutter, 1978; de Wall et al., 2000; Borradaile et al., 2012), compared to rock that is dominated by ferromagnetic and paramagnetic minerals, the relationship to strain is not as well understood, and research into the magnetic anisotropy of H_2O ice has not been carried out. Unlike englacial ice, there is a zone of ice at the base of glaciers and ice sheets which exhibits a distinct set of physical and chemical properties formed by processes operating at the bed, commonly referred to as basal ice (Hubbard and Sharp, 1989; Knight, 1997; Hubbard et al., 2009). This ice is thought to have predominantly formed through processes including adfreezing, regelation and hydraulic supercooling (Hubbard, 1991; Hubbard and Sharp, 1993; Cook et al., 2006) at the base of glaciers and ice sheets. As such, it has the ability to incorporate significant amounts of detrital minerals or subglacial sediment en masse (Hambrey et al., 2005). Depending on the composition of the source material, this detrital material is expected to contain paramagnetic and ferromagnetic grains that will overwhelm the diamagnetic signal and create fabrics which retain more of a signal related to ice deformation. The basal ice of glaciers and ice sheets therefore represents a suitable candidate for potential AMS investigations.

Glacier ice flows in response to gravitational forces acting on a sloping ice body; however, this flow is resisted by friction at the bed and lateral margins. Being located in the zone between the bed and the bulk of the glacier ice, basal ice is shown to be strongly affected by glacial motion and is commonly highly deformed (Souchez et al., 2000; Larsen et al., 2010; Samyn et al., 2010). As such, a variety of structures are produced reflecting compression, extension or simple shear, depending on the flow regime of the glacier. Basal ice commonly exhibits a strong ice-crystal c-axis fabric (Samyn et al., 2008). As a result, one may expect fabrics associated with such deformation, as well as being recorded in the diamagnetic ice, to be preserved through a preferred orientation of grains within the detrital sediment. In theory, an AMS fabric should therefore develop within the detrital component of basal ice that reflects the cumulative strain history.

AMS has been used to characterise and quantify very weak or subtle mineral fabrics and has been widely used in geology as a means for investigating the processes involved in the formation of rocks and sediments (see references in Tarling and Hrouda, 1993). It is an important tool in understanding how a material deforms in response to tectonic deformation as stress acting on the sediment can cause grains to rotate resulting in a preferential alignment (Chapter 2, Section 2.7.3). In glacial sedimentology, the AMS of subglacial sediments has the ability to reveal subtle fabrics relating to ice deformation (Eyles et al., 1987; Shumway and Iverson, 2009; Thomason and Iverson, 2009; Gentoso et al., 2012). As well as various field-based applications, the technique has been verified through laboratory testing (Hooyer et al., 2008; Iverson et al., 2008). Basal ice generally lies immediately above subglacial sediment and plays an important role in its formation through melt-out or lodgement (Benn and Evans, 2010). However, the way that sediment particles within the ice respond to strain is not well understood. The application of AMS to basal ice offers excellent opportunity for some of these ideas to be investigated.

In this study, the AMS technique is applied to basal ice exposed at the margin of a surge-type tidewater glacier in Svalbard. The aims of this study are to (i) characterise the AMS fabric by determining the orientation, degree of alignment and shape of the susceptibility ellipsoid, as well as the carrier of the magnetic signal (through rock magnetic experiments); (ii) determine the relationship of the fabric to other visible strain indicators within the ice at both outcrop scale and through the analysis of aerial photographs; and finally (iii) examine the relationship of the fabric to the recent surge activity of the glacier. Through these investigations, the potential of the AMS technique for the analysis of basal ice is evaluated and future areas in which the technique could be applied are suggested.

3.2. Glaciological and geological setting

Tunabreen is a 33 km-long tidewater glacier located in central Svalbard (Fig. 3.1). The glacier drains from the Filchnerfonna and Lomonosovfonna ice caps and flows into Tempelfjorden. The surrounding bedrock geology consists of undeformed, gently dipping Permian and Carboniferous

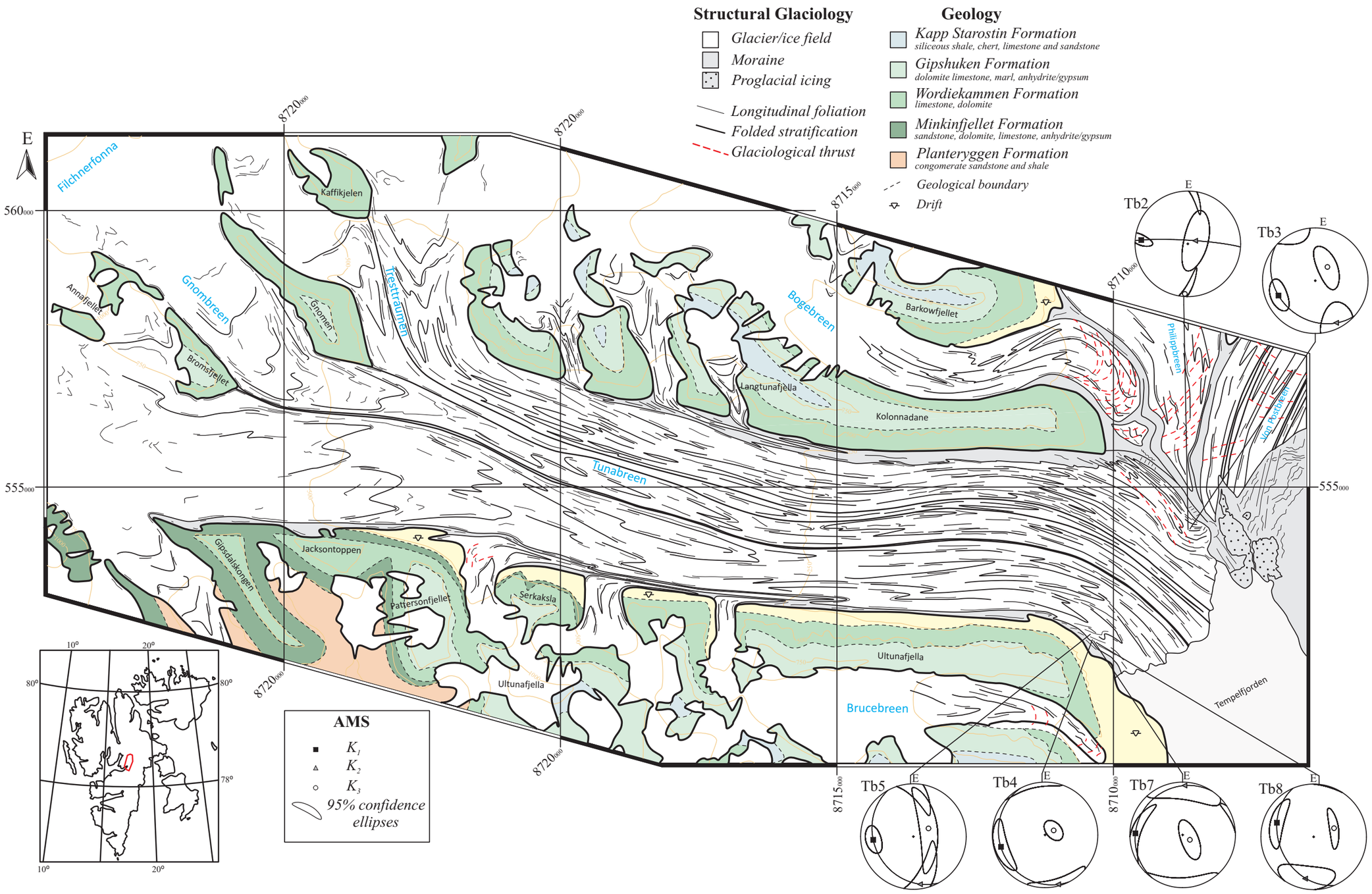

Fig. 3.1 - Geological map of Tunabreen and surrounding area, with glaciological structures and magnetic fabric results. Geology redrawn after Dallmann et al. (2009) and Dallmann et al. (2011). Glaciological structures drawn from aerial photographs dated July 2004. AMS results are plotted onto lower-hemisphere, equal-area stereographic projections showing the mean susceptibility ellipsoids with the 95% confidence ellipsoids and the magnetic foliation (great circles) derived from the K_3 orientation. Inset map shows location of study area within Svalbard.

sediments composed of conglomerate, sandstone and shale of the Billefjorden Group. In turn, these are overlain by locally fossiliferous sandstones, carbonates, shales and cherts of the Dickson Land Subgroup (Cutbill and Challinor, 1965). These strata were mostly deposited on a stable carbonate platform under shallow marine conditions (Harland et al., 1997).

Radio echo-sounding records indicate that the glacier is polythermal (Bamber, 1987). Tunabreen is a surge-type glacier and is the only one in Svalbard known to have surged three times, producing a consistent return period of approximately 40 years (Mansell et al., 2012). Tunabreen last surged in 2003-2005, during which the terminus advanced by up to two km into Tempelfjorden (Benn et al., 2009). Since surge termination, Tunabreen has calved back to its present-day position, revealing spectacular and easily accessible exposures of the basal zone of the glacier at the lateral margins, including the glacier-bed interface. There are three dominant ice facies within the exposures: (i) a banded debris-rich facies composed of alternating bands or laminae (1-10 mm thick) of ice containing diamicton and clean bubble-free ice; (ii) a solid debris-rich facies composed of diamicton with some stratification (hereafter referred to as 'banded facies' and 'solid facies', respectively (after Hubbard et al., 2009)); and (iii) a clean, bubbly facies, hereafter termed 'englacial facies' (after Hubbard et al., 2000).

The flow regimes of Tunabreen are indicated through structures exposed at the surface of the glacier (see mapped foliation in Fig. 3.1). Ice stratification and longitudinal foliation (utilising glaciological terminology of Hambrey and Lawson (2000)) is clearly seen in aerial photographs. This stratification, which originates in an orientation defined by the margins of the flow boundaries in the accumulation zone, becomes folded as the ice flows. Fold tightness increases down-glacier, evolving to isoclinal towards the terminus. Fold limbs are rotated parallel to the glacier margins and axial planes lie parallel to glacier flow direction, creating flow-parallel structures trending at 5°. These are commonly referred to as longitudinal foliation (Hambrey and Lawson, 2000), a phenomenon well known from Svalbard glaciers (e.g. Hambrey and Glasser, 2003; Hambrey et al., 2005).

At the height of the most recent surge in 2004, almost the entire length of Tunabreen

exhibited intense surface crevassing. Transverse crevasses dominated the pattern, forming perpendicular to the longitudinal foliation and glacier flow direction. Tunabreen has a tidewater margin and is dominated by a strong extensional flow regime during surges. This is a characteristic often seen in other Svalbard tidewater surge-type glaciers (cf. Hodgkins and Dowdeswell, 1994; Murray et al., 2003) without the compressional deformation commonly exhibited at the terminus of land-terminating Svalbard glaciers (Hambrey et al., 2005). However, towards the terminus, the eastern margin of Tunabreen reaches a confluence with the neighbouring Bogebreen, Phillippbreen and Von Postbreen. Here, a component of oblique compressional deformation is seen through the presence of structures that crop out at the surface which truncate foliation and crevasse patterns, interpreted as thrusts (Fig. 3.1). This, combined with a changing coastal morphology, results in the deviation of flow at this location from a predominantly southwards direction into a SSW direction.

3.3. Methods

Two sections were analysed at the lateral margins of Tunabreen, hereafter referred to as the northwest (NW) and southeast (SE) sections (Fig. 3.2). Six sites were chosen from the banded basal ice facies, covering both lateral and vertical changes. In order to increase the chances of the acquisition of reliable fabrics, sites were chosen where the sediment concentration was greater than 10% by volume. Cores were collected during April 2011, utilising the methodology described in Appendix A. Sedimentological and structural data were collected in the field using standard procedures (cf. Evans and Benn, 2004). Structural data from the measurement of mineral lineations were collected in March 2012.

AMS samples were measured following the methodology outlined in Chapter 2, Section 2.9. The AMS data was analysed using standard statistical analysis (see Section 2.4.1) involving the calculation of the mean susceptiblity in SI units (K_{mean}), corrected anisotropy degree (P_j), lineation (L) and foliation (F) parameters and the shape parameter (T) (Jelínek, 1981).

Fig. 3.2 - Field photographs of Tunabreen and the sections sampled. (a) NW section at the lateral margin of Tunabreen. Blue ice in the right of the photograph represents englacial ice while the basal ice is shown by the darker brown horizon in the centre (snowmobile in foreground = 1 metre). Height of section = 15 metres. (b) Photograph showing the locations of the NW and SE sections taken from the lateral moraine of Von Postbreen. (c) SE section showing englacial ice (blue) overlying basal ice (brown and banded). Height of section = 30 metres.

Because of the low susceptibility of the samples, careful cleaning and calibration of the sample holder was undertaken between each site, as even small amounts of ferromagnetic or paramagnetic dust may swamp the susceptibility signal of the samples (Borradaile et al., 2012). In spite of the Kappabridge being sensitive to 0.5×10^{-8} with an accuracy of 0.1%, the

anisotropy values near zero can be anomalously high (Hrouda and Kapička, 1986; Rochette, 1987; Biedermann et al., 2013). Although this is not thought to affect fabric orientations (Hrouda, 2004; Callot et al., 2010), its effect can cause problems when calculating the anisotropy parameters. As such, any subsamples with susceptibilities in the range of -5 to 5×10^{-6}were discounted, as recommended by Hrouda (2004).

In all AMS investigations, determination of the magnetic mineralogy is of importance because of the different fabric characteristics which can be produced by different minerals. The detrital component, typically 10-40% volume of sample volume, was extracted from the diamagnetic H_2O by sublimation, and investigations of the magnetic mineralogy were conducted following the methodology outlined in Chapter 2, Section 2.9. The ferromagnetic and paramagnetic contributions were analysed through examining the variation of low-field magnetic susceptibility with temperature (Section 2.6.1) and the low-field variation of AC susceptibility (Section 2.6.2) following the procedure of Hrouda et al. (2006). In addition, the ferromagnetic fraction of six samples was analysed through the acquisition of Isothermal Remanent Magnetisation (IRM) experiments (Section 2.6.4).

3.4. Results

3.4.1. Magnetic mineralogy

The mean susceptibility (K_{mean}) of the samples range from 9 to 23×10^{-6} (average 20×10^{-6}, Table 3.1). This is well within the paramagnetic realm (see Fig. 2.4, Chapter 2). The magnetic susceptibility of the samples in which the detrital sediment was separated from the ice are 96×10^{-6} for TB3 and 38×10^{-6} for TB5, reflecting the absence of diamagnetic H_2O.

Low-temperature susceptibility measurements (Fig. 3.3c) can be used to distinguish between the contribution of paramagnetic from ferromagnetic phases, since antiferromagnetic, diamagnetic and most ferromagnetic minerals have a temperature-independent susceptibility in

Site	N	K_m	K_1	*K_1 95% Error*	K_2	*K_2 95% Error*	K_3	*K_3 95% Error*	L	F	P_j	T
TB2	6	9.04E-06	**4/12.5**	*22/6*	**160/76**	49/19	**273/6**	49/4	1.018	1.052	1.077	-0.046
TB3	13	2.28E-05	**338/26**	*36/21*	**243/11**	36/21	**132/62**	35/16	1.017	1.009	1.027	-0.303
TB4	7	1.28E-05	**345/15**	*34/13*	**254/3**	35/12	**152/75**	18/12	1.022	1.035	1.058	0.227
TB5	12	2.37E-05	**355/25**	*19/14*	**261/9**	71/13	**152/63**	71/14	1.076	1.024	1.107	-0.512
TB7	11	1.87E-05	**2/11**	*46/9*	**93/7**	46/26	**214/77**	33/13	1.012	1.025	1.038	0.335
TB8	12	1.89E-05	**21/26**	*35/12*	**280/21**	38/22	**157/56**	31/7	1.037	1.028	1.066	-0.142

Table 3.1 - Mean site AMS data (see Chapter 2, Section 2.4.1 for calculation): N = number of samples; K_m = mean susceptibility; K_1, K_2, K_3 = orientations (declination and inclination) of the principal susceptibility axes with 95% confidence ellipses; L = lineation ($L = K_1/K_2$); F = foliation ($F= K_2/K_3$); P_j = anisotropy degree; T = shape parameter.

the 77 to 295 K temperature range (Richter and van der Pluijm, 1994). The curves show good Curie-Weiss temperature dependence, where susceptibility decreases with increasing temperature (Nagata, 1961). The ratio of low-temperature/room-temperature versus the mean value of room temperature susceptibility are plotted (Fig. 3.3c) and the ratio of all samples is above 3.2, indicating a substantial paramagnetic component to the low-field AMS.

The variation of low-field susceptibility with temperatures from 20 to 700 °C (Fig. 3.3b) shows a decreasing susceptibility with increase of temperature on some curves within the range of 20 to 250 °C, following Curie-Weiss behaviour (Fig. 3.3bi), whereas others show an independent or slight increase in susceptibility within this range (Fig. 3.3bii). Above 250 °C all samples show an increase in susceptibility with increasing temperature and exhibit strong peaks at 560 °C, presumably indicating either the growth of new ferromagnetic phases on heating or the 'Hopkinson peak' owing to a minor amount of Fe-Ti oxide present within the sample (See Chapter 2, Section 2.6.1).

The variation of field strength with susceptibility can also be used to provide constraints on the magnetic mineralogy (Fig. 3.3c). This experiment works on the principle that diamagnetic and paramagnetic minerals exhibit a linear relationship between magnetisation and the magnetisation field, whereas the susceptibility of some ferromagnetic minerals exhibit a strong field-dependent susceptibility (Hrouda et al., 2006). Non-systematic behaviour is seen in all samples in the 0 to 200 A/M range reflecting the high error margin in the measurement of susceptibility at these frequencies in low-susceptibility samples. However, above 200 A/M all

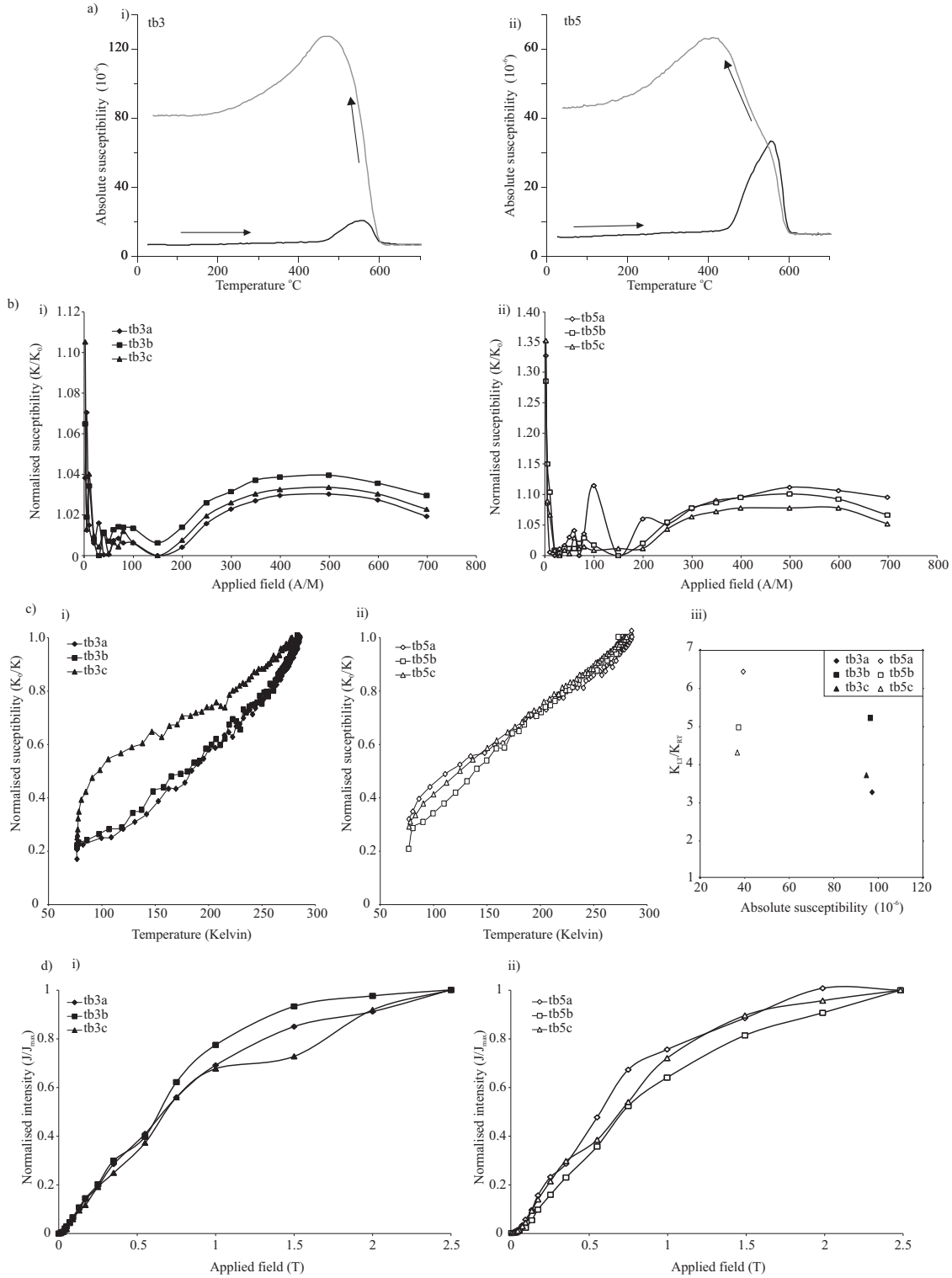

Fig. 3.3 - Rock magnetic experiments. (a) Low-field susceptibility (K) vs. temperature curves for (i) NW and (ii) SE sections. In each case, the heating curve is black and the cooling curve is grey. (b) Low-field susceptibility vs. Applied field (A/M) curves normalised to the lowest susceptibility value (K/K_0) for (i) NW and (ii) SE sections. (c) The normalised reciprocal (K/K_0) susceptibility vs. temperature for (i) NW and (ii) SE sections and (iii) the ratio of the susceptibility at the lowest temperature to the susceptibility at room temperature (K_{LT}/K_{RT}), plotted against magnetic susceptibility. (d) IRM experiments showing variation in normalised magnetic intensity (J/J_{max}) with applied field (T) for (i) NW and (ii) SE sections.

samples show a field-dependent susceptibility, which increases up to 500 A/M before decreasing. This presumably represents a minor contribution to the susceptibility by a ferromagnetic component.

This ferromagnetic component is investigated further through the acquisition of IRM (Fig. 3.3d). This works on the principle that the coercivity of a mineral varies with composition and grain size (see Chapter 2, Section 2.6.4). For example, the saturation magnetisation of haematite is near 3 T while magnetite is fully saturated by 300 mT (Fig. 2.12, Chapter 2). The IRM acquisition curves all fail to show complete saturation at 2.5 T indicating the presence of a high-coercivity phase, presumably haematite.

3.4.2. Anisotropy of magnetic susceptibility (AMS)

Samples yield susceptibility ellipsoids that are predominantly triaxial (Fig. 3.4), where F is roughly equal to L, although variation exists between subsamples, ranging from strongly oblate to

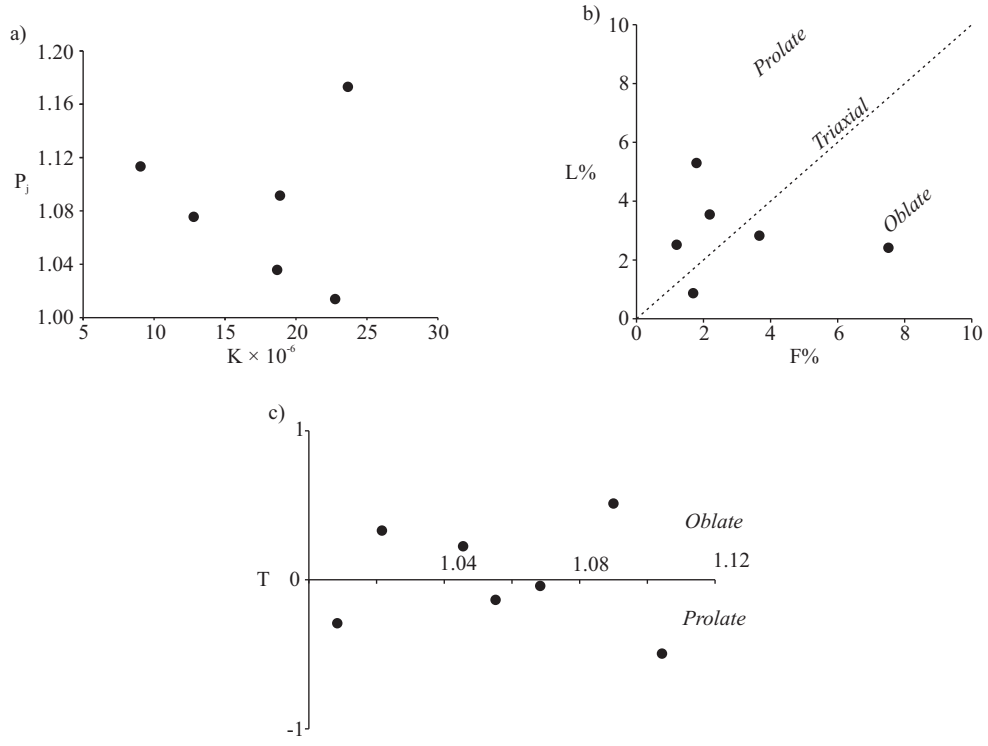

Fig. 3.4 - Variation of AMS parameters for all sites. (a) Anisotropy parameter (P_j) vs. susceptibility (K). (b) L% vs. F% (magnetic lineation vs. magnetic foliation). (c) Shape parameter (T) vs. Anisotropy parameter (P_j).

strongly prolate (possibly in part arising from the high error margins when calculating parameters at low susceptibilities (Hrouda, 2004; Biedermann et al., 2013)). The mean corrected anisotropy degree (P_j) is relatively high (1.05) (Fig. 3.4a) compared with the typical values within sediments dominated by paramagnetic minerals. However, haematite can have very high (>100) anisotropies (Tarling and Hrouda, 1993; Guerrero-Suarez and Martín-Hernández, 2012), and this high value may reflect the presence of a minor amount of haematite contributing to the anisotropy.

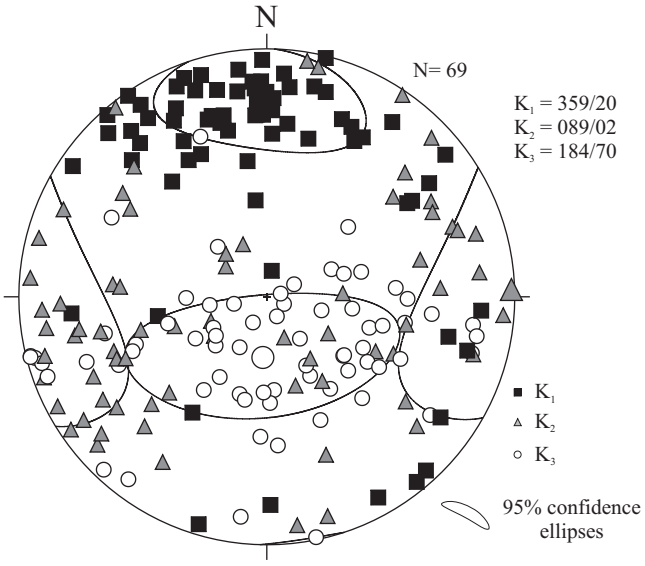

Fig. 3.5 - Stereographic projection of AMS results from all samples showing K_1 (black squares), K_2 (grey triangles) and K_3 (white circles) with 95% confidence ellipses.

AMS results are shown on lower-hemisphere, equal-area stereographic projections (Fig. 3.5), and the corresponding AMS results from individual sites and their sampled locations are shown in Figure 3.6. The mean maximum susceptibility orientation (K_1) plunges gently (20°) to the north, with a general north-south trend (mean = 359°) (Fig. 3.5). This is subparallel to the dominant glacier flow direction, as calculated from the trend of the glacier and the orientation of the macroscopic longitudinal foliation. The minimum susceptibility axes (K_3) are subvertical, defining the pole to the magnetic foliation (K_1-K_2 plane). At the NW section (close to the western margin of the glacier), K_1 axes cluster at 20° to 001°, and K_3 axes cluster at 30° to 188°. The SE section, despite being close to the opposite margin of the glacier, gives broadly similar fabric orientations to the SE section, with K_1 axes clustering at 20° to 355° and K_3 axes clustering at 27° to 097°.

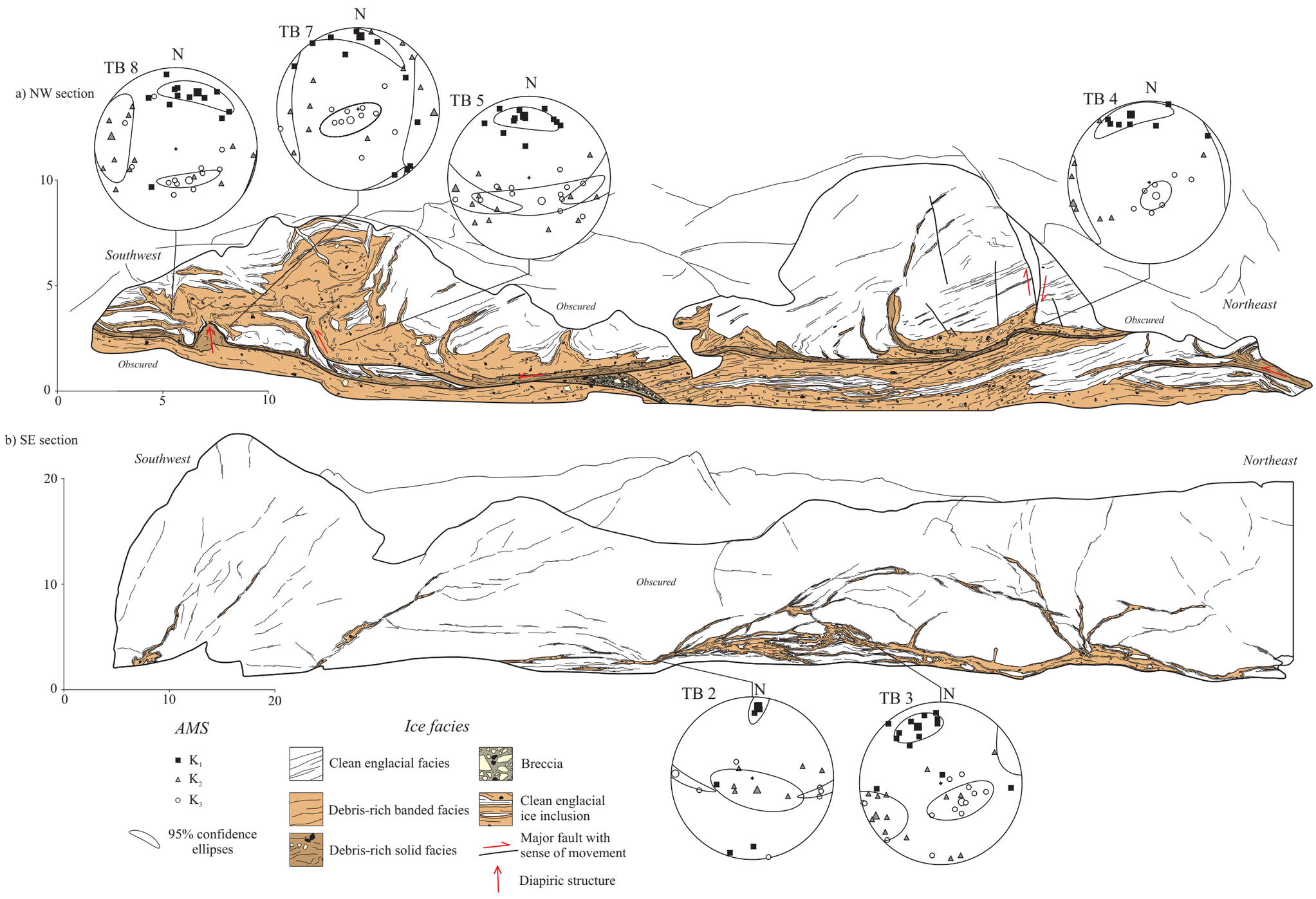

Fig. 3.6 - Two-dimensional section logs of (a) the NW section and (b) the SE section (no vertical exaggeration), with magnetic fabrics for all sites showing the three mean principal susceptibility axes plotted onto lower-hemisphere stereographic projections. See Figs. 3.1 and 3.2 for locations.

3.4.3. Analysis of visible structures

In subglacial sediments investigated at other sites, the orientation of magnetic fabrics have been shown to reflect glacier-induced simple shear relating to the flow direction of glacier ice (Hooyer et al., 2008; Iverson et al., 2008; Shumway and Iverson, 2009; Thomason and Iverson, 2009; Fleming et al., 2013). Basal ice lies at this crucial boundary between the bulk glacier ice and deforming bed, and it has been interpreted to deform similarly in a way. This is strongly related to the flow of the glacier (Knight, 1997). Evidence for deformation is seen at both sections as a variety of structures including folds, faults and lineations (Fig. 3.7). One of the unique features of the study of deformation within glacier ice is that, as opposed to most other geological materials, ice is often translucent or transparent. This allows structures to be seen in three dimensions through the ice face (e.g. Fig. 3.7f, g and h), aiding analysis and interpretation. These structures can be analysed to provide insight into the kinematics of deformation thus providing independent verification of the state of strain within the basal ice. As such, comparisons can be made with the magnetic fabric to determine its relationship to strain within the ice.

Folding and boudinage are common within the basal ice at both sections, especially at the SE section. Here, the banded ice facies (Fig. 3.7a), which presumably formed at an orientation parallel to the glacier bed or overriding obstacles, is highly folded in places (Fig. 3.7d, e and f). Folds are typically steeply inclined to recumbent and strongly asymmetric, with inter-limb angles ranging from tight to isoclinal. One interesting, and at first somewhat confusing, aspect of these folds is that vergence direction can appear on the two-dimensional ice face to be in both directions (e.g. Fig. 3.7d). Folds also occasionally form concentric augen-like rings (Fig. 3.9a). The axes of these folds lie in a north-south orientation, generally parallel to the glacier flow direction and parallel to the maximum susceptibility orientations (K_1). This indicates that rather than being purely cylindrical, which is often assumed, folds are highly non-cylindrical in a style often referred to as sheath folding (Alsop and Holdsworth, 2004; Alsop and Carreras, 2007; Alsop et al., 2007).

The fabric of the debris and bubbles within the banded ice facies is not planar. In contrast,

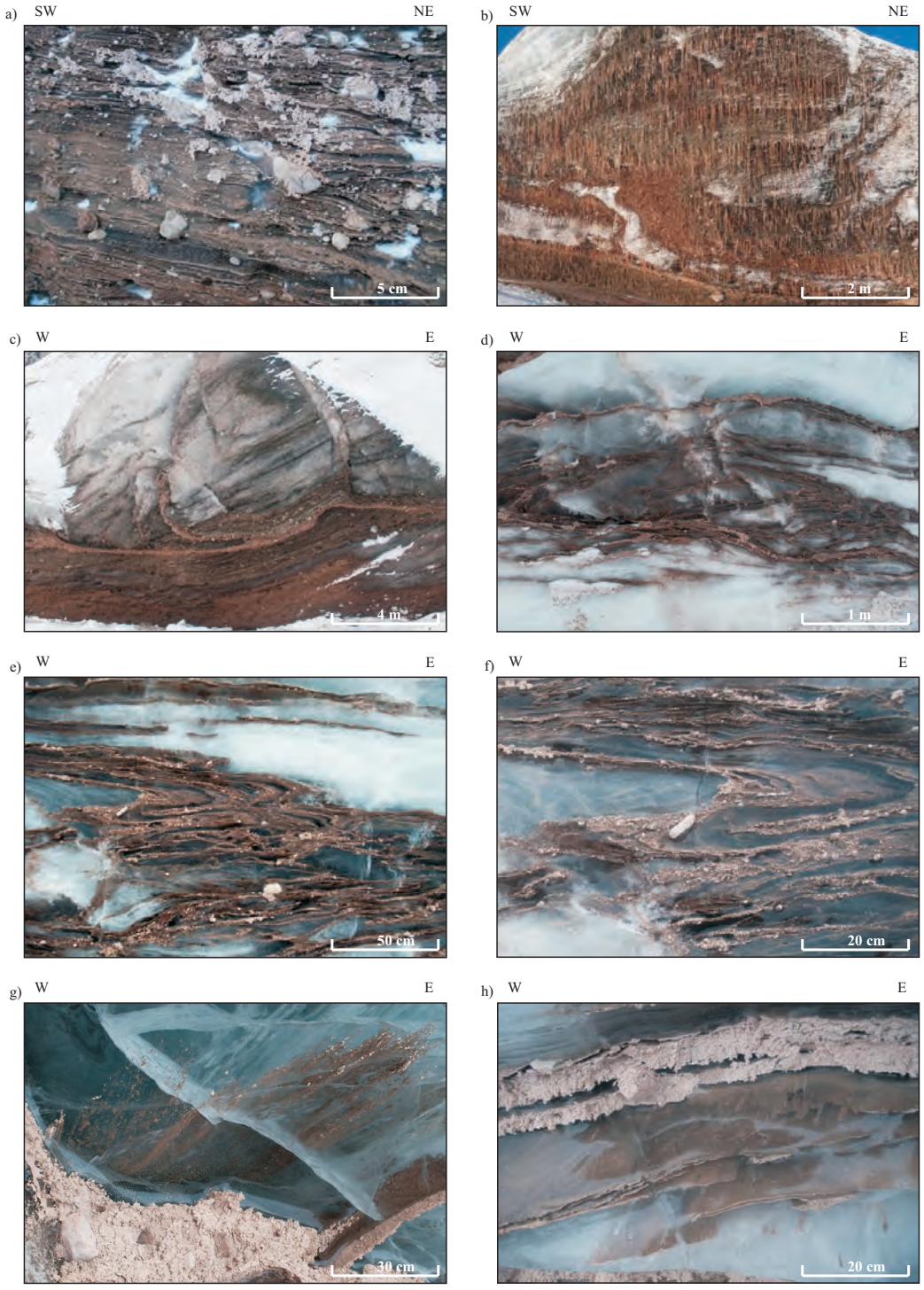

Fig. 3.7 - Field photographs of typical structures present within the basal ice. (a) Banded debris-rich ice facies from which most of the samples were collected showing subhorizontal alternating bands (>1-10 mm) of debris-rich and debris-poor ice. (b) Thick (8 metre) section of basal ice at NW section with lenses of clean bubbly (englacial) ice. The basal ice is partially obscured by icicles. (c) Banded and solid debris-rich basal ice facies thrust over blocks of clean englacial ice. (d) Folded banded ice showing a double vergence pattern in the folds. (e) Isoclinal recumbent folds verging to the right. (f) Close up of isoclinal "Z" fold showing vergence to the right. The fold axis can be traced through the ice giving a three-dimensional view of the fold. (g) Mineral stretching lineations in debris-poor basal ice above debris-rich horizon. (h) Mineral stretching lineations and elongated bubbles on the surface of debris-rich horizons within clean ice.

a strong linear component is present (Fig. 3.7g and h). Debris is observed to be arranged in linear aggregates and is often observed to be strongly smeared along an axis. Lineations, measured at the SW section, cluster at 10° to 005° (Fig. 3.8). In places, strongly elongated bubbles are orientated in the same direction as the debris lineations (Fig. 3.7h). Debris lineations are also seen to form generally parallel to fold axes and almost completely parallel to the magnetic lineation which, in most previous studies of AMS of deformed sediments, represents the direction of stretching (e.g. Liss et al., 2002; Parés and van der Pluijm, 2002; Cifelli et al., 2005).

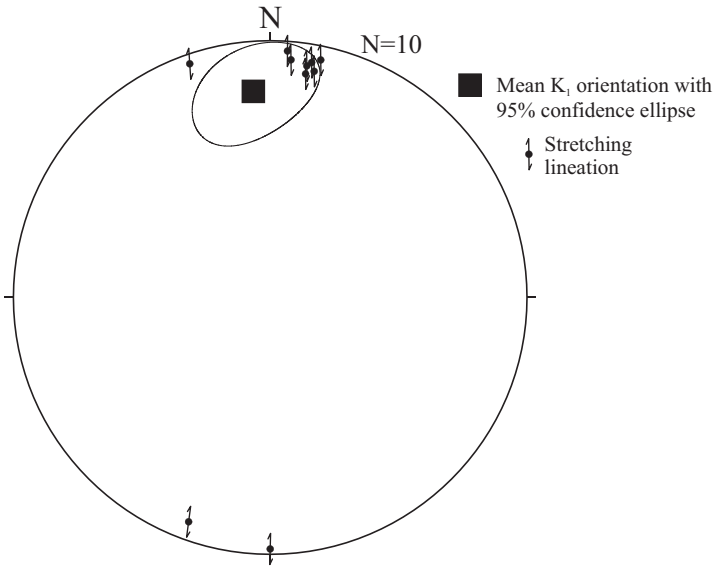

Fig. 3.8 - Mineral stretching lineations and mean K_1 orientation for SE exposure with 95% confidence ellipses.

Faulting is common which illustrates that, as well as ductile folding, brittle deformation has also occurred within the basal ice at both sections (Fig. 3.7b, c). The NW section contains a number of faults that are typically orientated north-south to NE-SW, shallow to moderately dipping to the east, parallel or subparallel to the glacier margins. At the SE section, faults strike in a north-south orientation; however, both dip angle and dip direction are variable. The majority of the faults have a reverse offset, but many contain subhorizontal debris lineations on their surface. This indicates oblique or even transverse slip in some cases and suggests a transpressional glaciotectonic regime. Thrusting has clearly resulted in the tectonic thickening of basal ice. For example, this can be seen in Figure 3.7c where banded debris-rich ice has been thrust up over

blocks of clean englacial ice.

3.5. Discussion

3.5.1. Control on AMS fabric

The low susceptibility of the samples indicates a volumetrically significant proportion of diamagnetic minerals, presumably quartz, calcite and ice. Yet, the presence of paramagnetic and ferromagnetic phases provide a positive susceptibility which probably controls the magnetic fabric (Tarling and Hrouda, 1993). The dependence of susceptibility on temperature follows Curie-Weiss behaviour at low temperatures (cf. Fig 2.9, Chapter 2), suggesting a dominance of paramagnetic minerals (Richter and van der Pluijm, 1994). At high temperatures, the increase in susceptibility can be attributed to the growth of new ferromagnetic minerals with the peak at 550 °C, possibly representing a suppressed 'Hopkinson peak' of a minor ferromagnetic contribution (Chapter 2, Section 2.6.1). The dependence of the susceptibility on field strength could be attributed to a ferromagnetic contribution, since pure paramagnetic minerals yield field-independent behaviour (Hrouda et al., 2006), but given the low susceptibility and the strong dependence of susceptibility with temperature, its influence on the AMS is considered minor. The high coercivity picked out by the IRM experiments indicates that haematite most likely controls this ferromagnetic contribution. Therefore, the origin of the AMS signal is interpreted as having a mixed magnetic mineralogy. This is dominated by paramagnetic phases which, given the composition of the material, are likely to be phyllosilicate clays with possibly a minor contribution of a high-coercivity ferromagnetic phase, presumably haematite.

The presence of flow parallel magnetic lineations associated with sediment dominated by phyllosilicate clay minerals and haematite may at first seem counter-intuitive as both minerals typically display crystalline anisotropy, where the maximum susceptibility axis lies in the basal plane of the mineral (Chapter 2, Section 2.5.2). As such, K_1 orientations are not parallel to the long axis of grains but rather depend on the crystallographic structure, with the minimum

susceptibility perpendicular to the basal plane. In spite of this, magnetic lineations are common in rocks dominated by phyllosilicate minerals and are shown to form parallel to the direction of stretching (Parés and van der Pluijm, 2002; Cifelli et al., 2005; Cifelli et al., 2009). Phyllosilicate minerals tend break along their basal plane, which when under extensional stresses, become disposed about an axis parallel to stretching thus creating a magnetic lineation that is directly compatible with fabrics created through shape anisotropy.

3.5.2. Relationship of structures to AMS

The magnetic fabrics show strong apparent correspondence with the orientations of macroscopic structures present within the ice. The stratification (mapped in Fig. 3.1 and schematically drawn in Fig. 3.9), which would have originally formed in an orientation parallel to flow boundaries in the accumulation zone, has been tightly folded forming a longitudinal foliation (Fig. 3.9a) under a strong extensional regime. This foliation generally lies parallel to the AMS lineation. The close relationship of the strike of the longitudinal foliation and the AMS lineation within the basal ice suggests that, as one would expect, the basal ice has been deformed by glacier motion.

At the outcrop scale, the banded ice facies within the basal ice have been folded under non-coaxial stretching and simple shear (Fig. 3.10d). In these conditions, folding initiates during the initial stage of shear where the field of compression occurs at a high angle to bedding (Fig. 3.9dii). As deformation continues, the strain ellipse rotates to a low angle to bedding and extensional processes become dominant, resulting in boudinage (e.g. Fig. 3.10diii). The folds created within the basal ice at Tunabreen have axes which are strongly curvilinear (Fig. 3.9a). This represents a non-cylindrical style of folding, commonly referred to as sheath folding (Alsop et al., 2007). Sheath folds normally form when perturbations during the initial stages of folding are greatly exaggerated in high-strain conditions (Cobbold and Quinquis, 1980). As folding progresses, fold noses become stretched and elongated, and fold axes rotate towards the direction of shear within the ice. Fold axes can eventually becomes parallel or subparallel to the main stretching direction

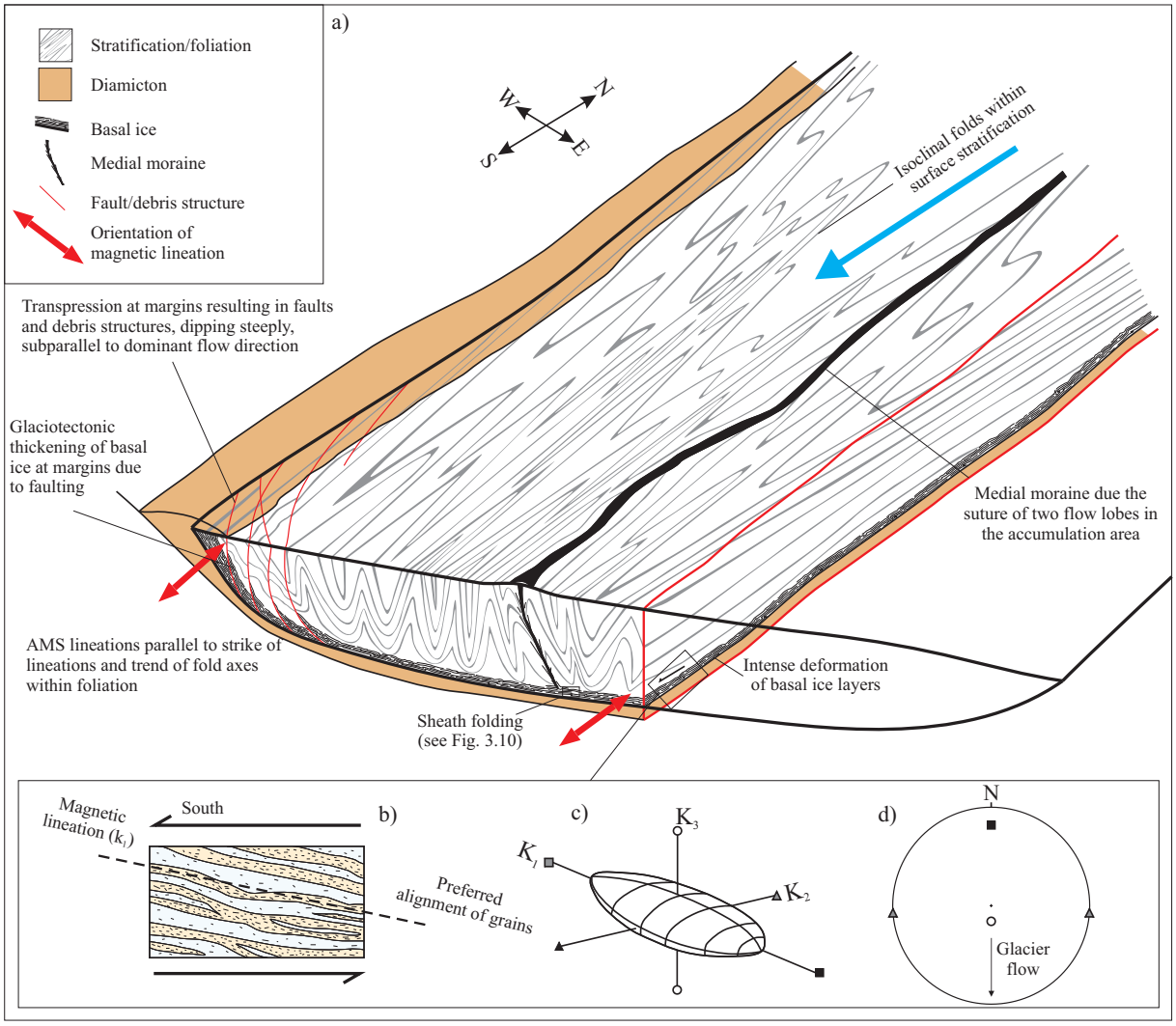

Fig. 3.9 - Schematic diagram illustrating the relationship of structures to AMS fabrics. a) Three dimensional cartoon of Tunabreen (vertical scale exaggerated) showing the structure of the foliation/ stratification, faults and basal ice in relation to the orientation of the AMS lineation.(b) Sketch of banded basal ice showing the preferred alignment of grains. (c) Visualisation of subsequent AMS fabric through the AMS ellipsoid with K_1 (maximum), K_2 (intermediate) and K_3 (minimum) susceptibility axes. (d) Presentation of ellipse through stereonet displaying the mean northerly orientated K_1 parallel to glacier flow direction.

(Fig. 3.10c). Sections perpendicular to the shearing direction are characterised by concentric, eye-shaped folds and doubly-verging fold directions (Fig. 3.10b). Sheath fold noses lie parallel to the orientation of AMS lineations, as fold axes are essentially indistinct from stretching lineations.

Deformation of the ice at Tunabreen has also resulted in the formation of distinct linear features within the basal ice (Fig. 3.7g and h). Clusters of debris are smeared out and aligned about an axis. The smearing of grains in basal ice has been referred to in the past (e.g. Hubbard

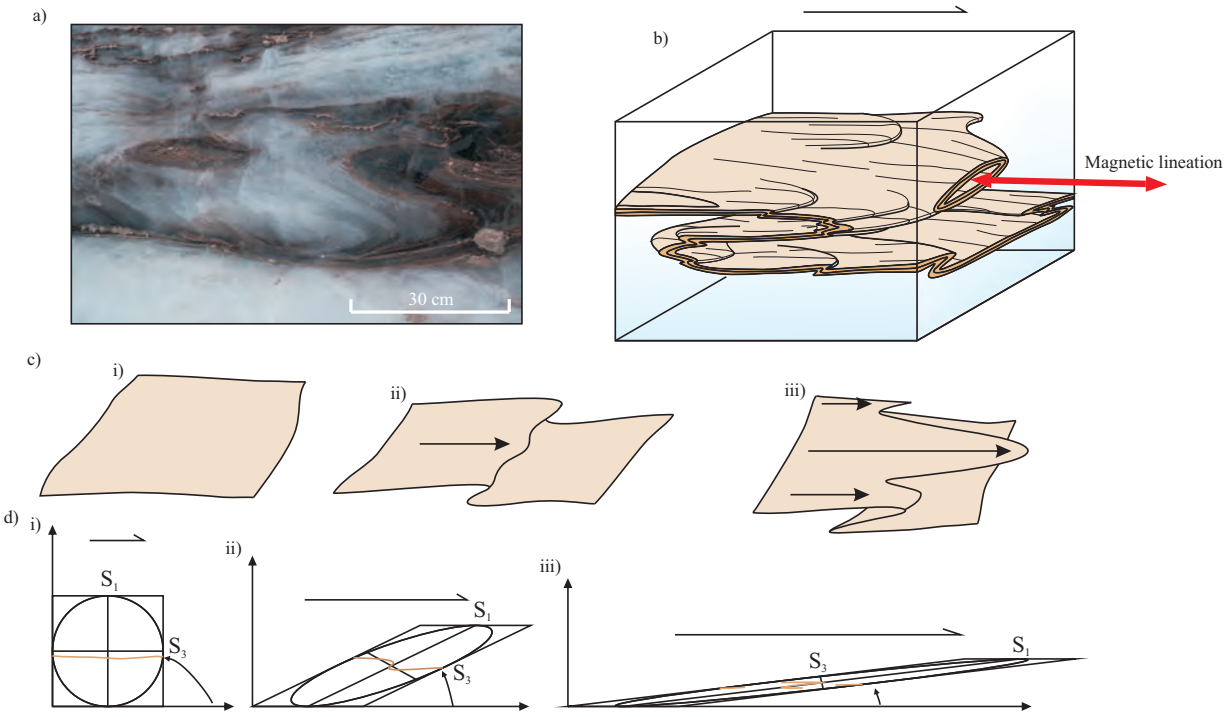

Fig. 3.10 - (a) Photograph of sheath fold within banded ice facies from SE section showing augen pattern with concentric rings and double verging folds. (b) Three-dimensional model of sheath folding observed at SE section. (c) Interpretation of sheath fold development and associated strain ellipse, showing (i) pre-deformation and original configuration, (ii) initial folding and (iii) evolved sheath folding and rotation of fold axes parallel to flow. S_1, S_2 and S_3 refer to the long, intermediate and short axes of the strain ellipse.

and Sharp, 1995; Hubbard et al., 2000), but its relationship to cumulative strain has not. Similar lineations are often seen in structurally deformed metamorphic rocks (Twiss and Moores, 1992; Neves et al., 2005), commonly referred to as stretching lineations. Stretching lineations in deformed rocks form in an orientation parallel to the direction of stretching during ductile deformation (Ramsay and Huber, 1983). Thus, structural analysis of their orientation can provide useful information about the kinematics of deformation and deformational history.

At Tunabreen, these lineations lie at an orientation parallel to the fold axes of sheath folds and the strike of macroscopic surface lineations, and subparallel to the flow direction of the glacier. Also, these lineations lie almost completely parallel to the magnetic lineations, (Fig. 3.8) thus providing independent verification that these form in an orientation parallel to stretching. As such, they are interpreted as stretching lineations. Under high-strain conditions, detrital grains within the ice will rotate into the most stable orientation about an axis parallel to stretching,

subsequently forming the lineations. As these lineations are parallel to the interpreted direction of stretching, they can be used in a similar way to which they are in structural geology and the analysis of tectonically deformed rocks in order to give the kinematics of deformation within the ice.

3.5.3. Kinematics of deformation within the basal ice

The up-glacier dip of K_1 is a feature commonly seen within subglacial sediments under simple shear (Shumway and Iverson, 2009; Thomason and Iverson, 2009). The mean plunge of the K_1 lineation at 20° up glacier (shown in Fig. 3.5 and drawn schematically in Fig. 3.9 b, c and d) may indicate that within the basal ice, as well as pure shear, there is a component of non-coaxial strain and simple shear causing the up-dip rotation of K_1 orientations, matching the S_1 axis of the strain ellipse. Ring-shear experiments of subglacial tills subject to simple shear reveal that steady-state AMS fabrics develop at strains of 7-30. In these experiments, K_1 azimuth lies parallel to shear direction and dips 28° up glacier (Hooyer et al., 2008; Iverson et al., 2008). These experiments produced almost identical fabric characteristics and clustering patterns to those displayed in Figure 3.5. One could argue a similar model for the rotation of grains within basal ice, where slip between the grains and the ice keeps particles from rotating through the shear plane (as suggested by March, (1932)), therefore rejecting Jeffery rotation (Jeffery, 1922) within ice. However, as the magnetic mineralogy of the tills used is different, caution is applied when making direct comparisons. Such conclusions should not be made until further laboratory testing on materials with a similar mineralogy is obtained.

3.5.4. Relationship to surge dynamics

At the NW section (Fig. 3.11a), magnetic lineations lie in an orientation that deviates slightly away from the dominant glacier flow direction in this area. If the fabrics formed purely by stretching and simple-shear because of friction at the bed, one may expect the magnetic lineations to trend parallel to ice flow. However, the flow of the glacier ice is not uniform across the ice

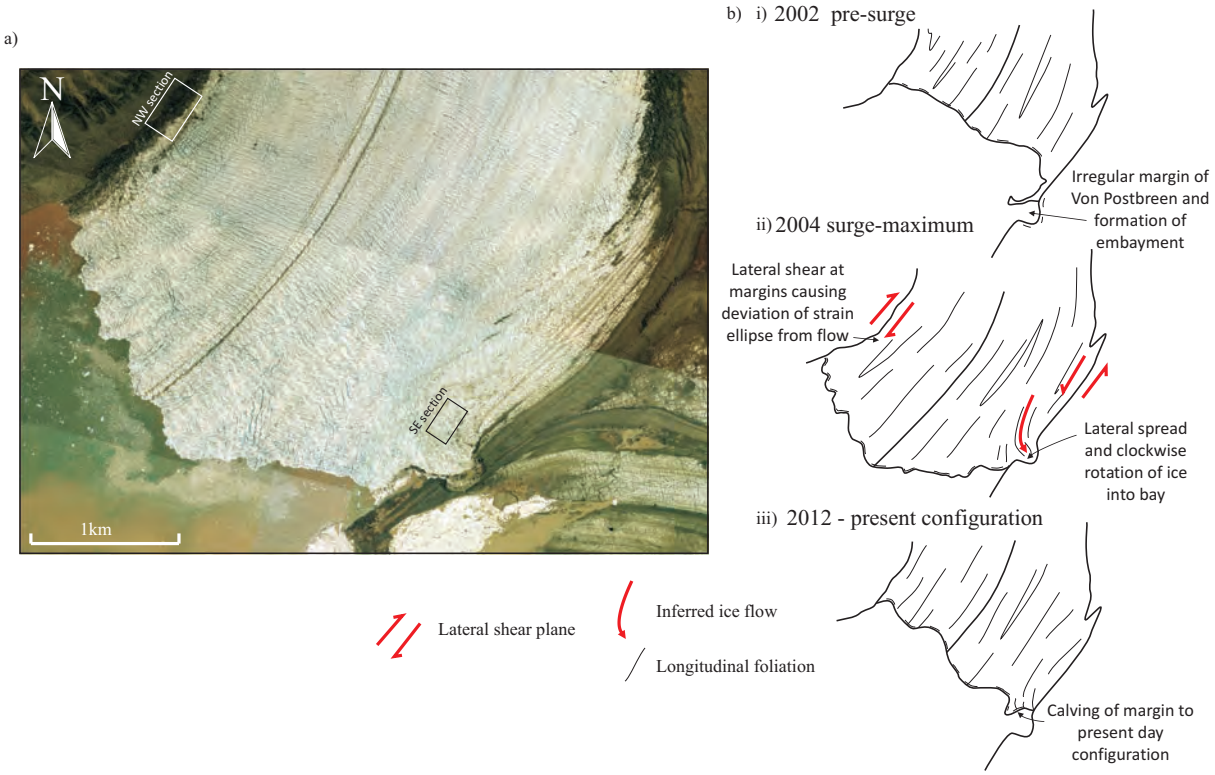

Fig. 3.11- (a) Aerial photograph mosaic of the Tunabreen terminus at surge maximum in 2004 with the mean K_1 orientation and dip direction (blue arrows) and the location of the sections studied. (b) Interpretation of the formation of the magnetic lineations showing (i) 2002 pre-surge configuration and irregular margin of Von Postbreen, (ii) 2004 surge maximum showing the orientations of shear in the NW section and the lateral spreading and clockwise rotation of surface foliation and magnetic lineation at the SE section, and (iii) present configuration of Tunabreen at time of study (2012).

surface. At the margins, lateral drag can result in the development of marginal shear zones such as those recorded after the 1982-83 surge of Variegated Glacier (Sharp et al., 1988; Lawson et al., 1994). At Tunabreen, the deviation of the magnetic lineations from parallel to glacier flow is probably caused by the rotation of the strain ellipse away from glacier flow direction at the margins under non-coaxial strain (Fig. 3.11bi).

At the SE section (Fig. 3.11a), the orientation of the magnetic lineations cannot be explained in the same way, since lateral shear would cause the inclination of lineations in the opposite direction to that observed. However, magnetic lineations lie parallel to longitudinal foliation identified on aerial photographs at that location, indicating that ice flow has been rotated in the opposite direction to that expected. This can be explained by the presence of an irregular pre-surge carving margin (Fig. 3.10bi). During the surge, local splaying of the ice into an embayment

facilitated the rotation in an anticlockwise direction (Fig. 3.10bii). This is interpreted to have caused the slight deviation from overall ice flow direction of both the AMS fabrics and surface foliation (Fig. 3.10biii).

3.5.5. The use of AMS for the analysis of deformation within basal ice

This study has shown that the detrital component of basal ice contains sediment from which an AMS fabric can be measured. This can be used to provide insight into subglacial processes. The magnetic fabric appears to be a direct reflection of the petrofabric of the detrital grains within the ice. A magnetic lineation is recorded which lies parallel to the inferred direction of stretching and simple shear within the ice. This result provides support for the validity of the AMS of subglacial sediment, where magnetic lineations are also seen to form parallel to stretching/shear direction within the sediment (Shumway and Iverson, 2009; Thomason and Iverson, 2009; Fleming et al., 2013). The potential preservation of AMS fabrics from basal ice to sediment during melt-out requires further study. However, as an AMS fabric is seen within basal ice, caution should be taken when interpreting AMS fabrics in subglacial sediments as being formed solely by bed deformation, especially when an origin through melt-out is suspected.

Utilising the methodology described here, the AMS technique can be directly reproduced and applied to other glaciers. AMS has several advantages over other petrofabric techniques (Iverson et al., 2008). The fabric can be determined relatively quickly, accurately and objectively, and the susceptibility ellipsoid can be calculated in three dimensions. AMS represents the volume average of many grains in each subsample and many subsamples make up a site. Being sensitive to minor changes in the state of strain, investigations of the AMS of basal ice has the potential to provide knowledge on the processes occurring at the ice-bed interface, bridging the gap between the analysis of visible structures at the surface of the glacier and deformation within subglacial sediments. AMS, therefore, has the potential to contribute to the highly debated topic of glacier bed deformation.

AMS has been used to calculate shear strains in deformed rocks and sediment (Borradaile,

1988; Borradaile, 1991). The link between the AMS fabric strength (based on the degree of clustering of susceptibility axes) and strain has also been investigated within subglacial sediments through experimental work with ring shear devices (Iverson et al., 2008). This study showed that fabric strength increases with increasing shear strain, up to a point under which steady-state fabrics were reached. In the future, if the magnetic mineralogy of the ice is relatively homogeneous, it may be possible to apply similar experimental tests to the AMS of basal ice and thus investigate the link between fabric strength and strain. Also, in contrast to ice-crystal fabric studies which measure the c-axis orientation of ice crystals (e.g. Bader, 1951; Tison et al., 1994; Wilson and Peternell, 2011), the AMS fabric is dominated by the paramagnetic and ferromagnetic proportion of detrital material in the basal ice. Therefore, the study of AMS in conjunction with ice-crystal fabric analysis allows the detrital portion of the ice to also be analysed which, in contrast to glacier ice, is not subject to recrystallisation under the pressure/temperature ranges encountered in glaciers.

At this study site, although AMS has highlighted interesting variation in the state of strain, the glacier flow direction was never in doubt. The site was chosen intentionally, as visible structures such as the surface longitudinal foliation measured from aerial photographs and the orientations of folds and lineations at the outcrop-scale provide a reference frame for comparison with the AMS results. This has enabled further interpretations to be made and shows that folding style is dominated by sheath folds and lineations which form parallel to stretching within the ice. However, one interesting situation in which AMS could be applied is where the flow direction or past strain history is not known or is poorly understood. For example, on large ice sheets where glacier flow is slow and surface structures are absent or where flow direction is ambiguous (e.g. Conway et al., 2002). AMS of basal ice collected from ice cores could potentially be analysed to provide insight into shear direction at the base of the ice sheet. The AMS technique could also aid research into the subject of massive ground ice, which is thought to originate as the basal portion of pre-existing glaciers, often dating back to the Pleistocene, and is often buried and preserved in permafrost regions (Waller et al., 2009; Fritz et al., 2011). Here, little is known about palaeo-ice flow directions; therefore, AMS could potentially provide considerable palaeo-glaciological

insight.

3.6. Conclusions

The AMS fabrics of basal ice and their relationship to deformation during the most-recent surge of Tunabreen have been investigated and number of conclusions can subsequently be drawn:

- The AMS of basal ice can be measured, and the three components of the susceptibility ellipsoid can be rapidly calculated in the same way that is commonly done for sediment and rock.

- Magnetic fabrics at the sections examined are controlled predominantly by the preferred alignment of inclusions of detrital sediment within the ice. The susceptibility and anisotropy on this sediment is dominated by paramagnetic minerals (presumably phyllosilicate clays). In some samples, a high-coercivity phase (presumably haematite) is also present, possibly contributing to the fabric.

- The folding style within the deformed basal ice is highly non-cylindrical. This is not unusual given the high shear strains expected within the deforming ice and the perturbations in flow that exist across the glacier profile. Within subglacial glaciotectonites, since the deformation of underlying subglacial sediments is largely controlled by the overlying ice motion, non-cylindrical folding should be expected.

- AMS lineations are parallel to, and independently verified by, the macroscopic lineation given by the presence of stretching lineations and the axes of sheath folds. The orientation of stretching lineations in basal ice has the potential to be used as a proxy for stretching direction within the strain ellipse, in the same way that is used in structural geology.

- Magnetic lineations at the NW section have been affected by lateral shear which has

caused a minor amount of deviation of the lineations away from being parallel to the mean trend of the macroscopic foliation, reflecting this non-coaxial deformation. At the SE section, the irregular pre-surge configuration of the contact between Tunabreen and Von Postbreen has affected strain patterns and led to the anti-clockwise rotation of magnetic lineations, stretching lineations and the macroscopic foliation, resulting in a magnetic lineation orientated subparallel to the dominant glacier flow direction.

CHAPTER 4.

NEW INSIGHTS INTO THE DEFORMATION OF A MIDDLE PLEISTOCENE GLACIOTECTONISED SEQUENCE IN NORFOLK, ENGLAND THROUGH MAGNETIC AND STRUCTURAL ANALYSIS

4.1. Introduction

Having described above magnetic fabrics in glacier ice, from which basal sediments are derived, attention is here focused on the actual sedimentary products released from a former ice sheet, in this case the Pleistocene Scandinavian-British Ice Sheet as it impinged on the North Norfolk coast. In this chapter, the power of the anisotropy of magnetic susceptibility (AMS) technique is investigated for determining the fabric of dynamically deposited glacial deposits and the directions of the flows that created them.

The role of deformable materials beneath glaciers is currently one of the most important topics in glaciology, and various authors have suggested that glacier motion is facilitated by shearing of the glacier bed (e.g. Alley et al., 1986; Boulton, 1986; Alley et al., 1987). Sub-sole deformation is considered to be the primary mechanism for sustaining fast flow in ice streams and outlet glaciers and is therefore of great importance for investigations into ice sheet stability (MacAyeal, 1992; Clark, 1994). Deformation of the bed has been successfully measured in several cases (e.g. Boulton and Hindmarsh, 1987; Boulton et al., 2001; Iverson et al., 2003; Hart et al., 2011); however, the study of basal conditions in active glaciers is challenging because of the inaccessibility of the bed and the short length of time over which data can be recorded. Instead, the primary evidence used to infer dynamic processes has been through the properties of the glacigenic sediments and landforms left behind by the large ice sheets that covered much of North America and Europe during the Pleistocene Epoch (Licciardi et al., 1998; Piotrowski et al., 2001).

Glaciotectonism is the structural deformation of the upper horizon of the lithosphere by glacial stresses (Slater, 1926; van der Wateren, 2002). Glacially deformed sediment is often referred to as a glaciotectonite, a term first introduced by Banham (1977) to describe penetrative, subglacially sheared sediments analogous to mylonites in metamorphic rocks. In most studies, a wider definition is used to encompass a body of unlithified or weakly lithified sediment deformed by glacial stresses (van der Wateren, 2002; Benn and Evans, 2010). Within such sediments, distinct structures form such as folds, faults, boudins and fabrics (Hart and Rose, 2001). These structures can be analysed on both macroscopic scales (e.g. Hart, 1990; Hart and Boulton, 1991;

Lee and Phillips, 2008; Benediktsson et al., 2010; Lesemann et al., 2010) and microscopic scales (e.g. van der Meer, 1993; Phillips and Auton, 2000; van der Wateren et al., 2000; Menzies et al., 2006; Phillips et al., 2007; Phillips et al., 2011) and can provide considerable information about the genetic environment and deformational history. For example, in a subglacial environment, deformation is typically dominated by simple shear coupled with extreme extension (Hart and Boulton, 1991; Kluiving et al., 1991), whilst in proglacial settings, glaciotectonic compression may facilitate the formation of structures analogous to fold and thrust belts in an orogenic foreland setting (Huddart and Hambrey, 1996; Hambrey et al., 1997; Bennett, 2001; Phillips et al., 2008).

Similar structures can often be seen in both subglacial and proglacial settings and may not be readily distinguishable (Phillips et al., 2007). Variation in lithology and the dynamic nature of subglacial conditions means that earlier deformation structures can be overprinted (Piotrowski et al., 2004; Evans and Hiemstra, 2005). This can make the interpretation of such structures difficult. Furthermore, fold structures, similar to those found in glaciotectonic environments, are also found in other environments, e.g. slumping on glaciomarine slopes (Kurtz and Anderson, 1979; Eyles and Kocsis, 1988; Arnaud and Eyles, 2002). This makes the interpretation of specific structures ambiguous, and in some stratigraphic sections, the same evidence has been interpreted as being formed by very different processes. For example, the soft sediment deformational structures in the 'North Sea Drifts' of Norfolk, UK are traditionally interpreted as subglacial (Banham, 1975) but have also been reinterpreted as slumping in a glaciomarine setting (Eyles et al., 1989). The objectivity and usefulness of certain techniques used to study subglacial deformation has been doubted (Bennett et al., 1999; Zaniewski and van der Meer, 2005), and it is apparent that there is a clear need for objective and quantitative approaches to the analysis of strain within glacial sediments.

Fabric analysis involving the measurement of the AMS (Tarling and Hrouda, 1993) has provided considerable insight into depositional (e.g. Ellwood and Ledbetter, 1977; Lagroix and Banerjee, 2002; Hooyer et al., 2008) and deformation histories (e.g. Parés et al., 1999; Borradaile

and Jackson, 2004; Cifelli et al., 2009) of rock and sediment. However, the technique has seldom been used in glacial geology until recently (see Chapter 2, Section 2.8).Through comparison of AMS with pebble fabrics, Fuller (1962) was the first to suggest that magnetic fabrics could be a viable technique for petrofabric analysis. Since then, AMS has been applied to several tills, mostly to determine palaeo ice flow directions of Quaternary glaciers and ice-sheets (e.g. Stupavsky et al., 1974a; Stupavsky et al., 1974b; Stupavsky and Gravenor, 1975; Eyles et al., 1987; Stewart et al., 1988; Gentoso et al., 2012).

Recent laboratory work (Thomason and Iverson, 2006; Hooyer et al., 2008) has increased confidence in the reliability of the technique as a quick and objective method of examining strain within subglacial tills. However, as discussed in Chapter 1, Section 1.5, several key questions remain. In particular, no published data exist for the analysis of AMS within glaciotectonites, where pre-existing unconsolidated sediment has been glacially deformed such that relicts of the original structures remain. In addition, previous research has focussed almost exclusively on tills where the AMS signal has been carried by MD magnetite. However, various other magnetic contributors have been identified as controlling the magnetic signal in other sedimentary rocks (Tarling and Hrouda, 1993; Cifelli et al., 2009; Borradaile et al., 2012). The mineralogy of diamict can be highly variable and the AMS fabric of deformed diamict consisting of paramagnetic minerals is not known.

In North Norfolk, England, although exposures provide classic sections from which original work on glaciotectonics emerged (Slater, 1926; Banham and Ranson, 1965; Banham, 1977; Banham, 1988), considerable debate remains over the pattern of lowland glaciation (Eyles et al., 1989; Banham et al., 2001; Hamblin et al., 2005; Gibbard and Clark, 2011). In this chapter, AMS combined with detailed structural analysis is used to reinvestigate sediment genesis and flow vectors in a dynamically-deformed, Mid-Pleistocene diamicton section which has previously interpreted as a glaciotectonite (Lee and Phillips, 2008). As well as addressing the issues described above, the aims of this chapter are to (i) characterise the AMS fabric by determining the orientation, degree of alignment and shape of the susceptibility ellipsoid; (ii) determine the carrier

of the AMS signal through the use of rock magnetic experiments; (iii) examine the relationship of the AMS fabric to deformation structures preserved within the sediment; and finally (iv) construct a model to explain the deformational sequence.

4.2. Geological background

The bedrock geology of North Norfolk consists of gently dipping Cretaceous chalk. Pleistocene aged sediments consisting of pre-glacial fluvial and shallow marine deposits overlie the Cretaceous chalk, which in turn are overlain by a sequence of tills separated by outwash sediments (Banham, 1968). These glacial sediments were previously considered to have been deposited by oscillations at the margins of coexisting British and Scandinavian ice sheets during the Anglian glaciation (478 – 424 Ka, Marine Isotope Stage 12) (Perrin et al., 1979; Bowen et al., 1986; Lunkka, 1994; Fish and Whiteman, 2001). A new glacial lithostratigraphy has been proposed (Hamblin, 2000; Rose et al., 2001; Lee et al., 2004; Hamblin et al., 2005), subdividing the sequence into four formations: the Happisburgh, Lowestoft, Sheringham Cliffs and Briton's Lane. These authors suggested that the deposition of the tills were associated with an entirely British-based, as opposed to Scandinavian, ice sheet (Lee et al., 2002; Hamblin et al., 2005). This interpretation has been disputed (Banham et al., 2001; Preece et al., 2009; Gibbard and Clark, 2011) because of its inability to explain biostratigraphical evidence.

The study site in North Norfolk is located in a cliff section near the village of Bacton (National Grid Reference TG 338345; Fig. 4.1). The lithology consists of a stratified diamicton sequence, previously referred to as the 3rd Cromer Till (Banham, 1968; Lunkka, 1994) but reassigned to the Bacton Green Till Member of the Sheringham Cliffs Formation (Hamblin et al., 2005; Lee and Phillips, 2008) through tectono-stratigraphic relationships and petrological analyses. Although not directly exposed at the section, further along the coastline, the Bacton Green Till Member overlies the Walcott Till Member, previously referred to as the 2nd Cromer Till (Banham, 1968; Lunkka, 1994) and an interglacial, fluviodeltaic, glacial outwash sand, assigned to the Mundesley Sand Member. The top of the Bacton Green Till Member is truncated by the

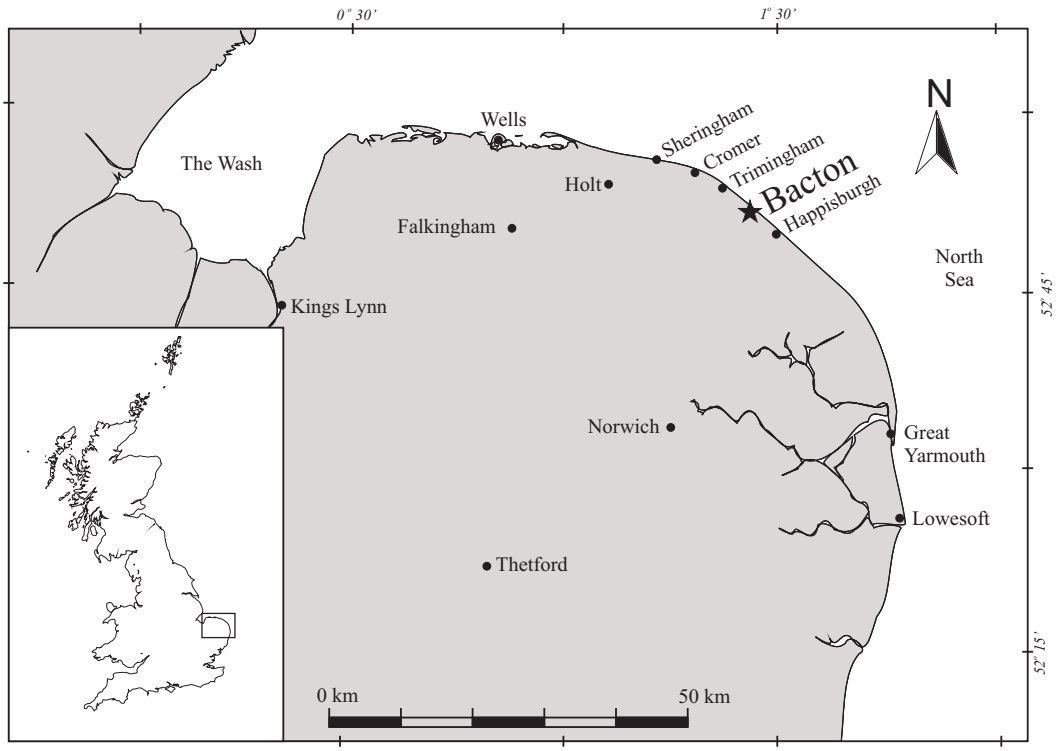

Fig. 4.1 - Map of the Norfolk coastline showing the location of Bacton (black star), National Grid Reference TG 338345.

Stow Hill Sand and Gravel Member of the Britons Lane Formation.

The Bacton Green Till Member consists of a massive to weakly laminated, grey- to brown-coloured sandy diamicton with horizons of sand and gravel (Fig. 4.2), and Bacton is considered the type location for the member (Hamblin et al., 2005). Initial deposition has been suggested to have occurred in a subaqueous setting through processes of mass flow, turbidity currents and rapid rainout, associated with an ice advance from the north (Lunkka, 1994; Lee and Phillips, 2008; Phillips et al., 2008). For simplicity, the terminology previously used at the site have been adopted and continues to refer to the Bacton Green Till Member, whilst acknowledging the subtly different definition of a till *sensu stricto* (cf. Benn and Evans, 2010) as this evokes deposition directly from glacier ice, which is not considered the case for the Bacton Green Till Member (Lunkka, 1994; Hamblin et al., 2005; Lee and Phillips, 2008).

Previous authors have suggested that, after deposition, the Bacton Green Till Member was glaciotectonically deformed creating the structures observed, associated with an ice advance from the west or SW (Lee and Phillips, 2008; Phillips et al., 2008; Scheib et al., 2011). Regional ice

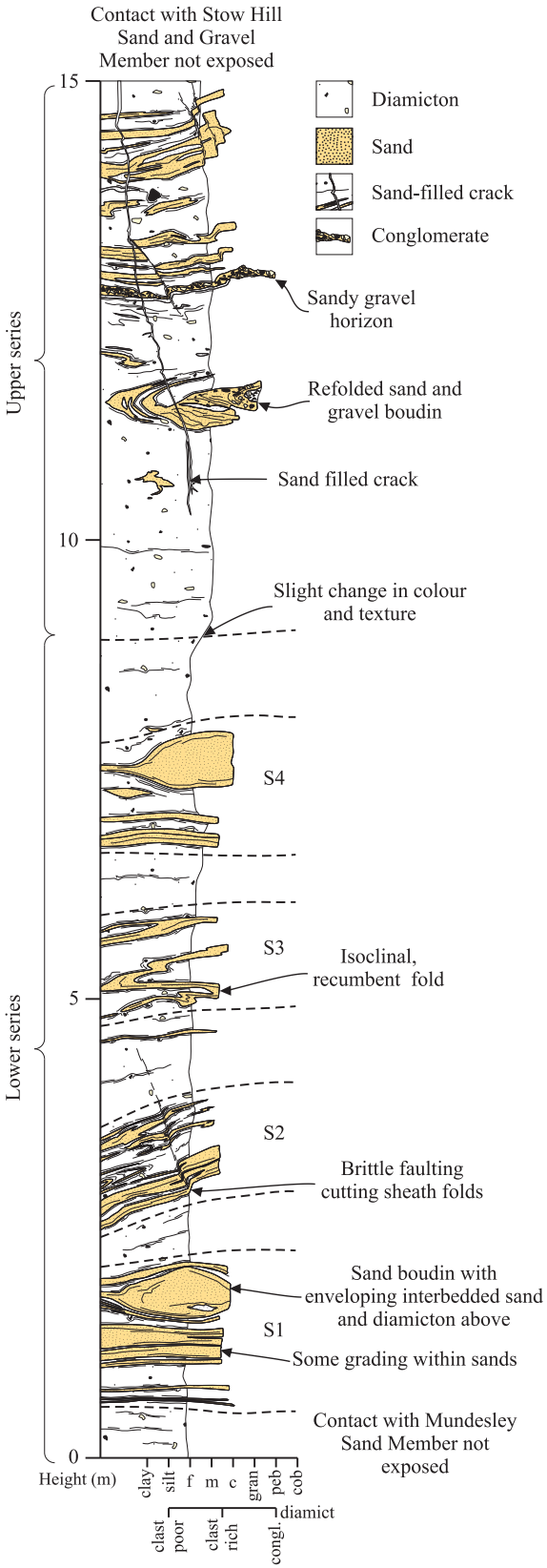

Fig. 4.2 - Sedimentary log through the section at the study site, divided into upper and lower series based on style of deformation structures and distribution of magnetic fabrics. S1 – S4 refers to horizons with sandy layers and sand lenses. A sand-filled crack is shown at the top cutting across deformation structures and bedding.

flow directions across the region, however, are equivocal (cf. Hamblin et al., 2005), and many of the structures seen could arguably have been formed in an entirely subaqueous setting without the need for glaciotectonic deformation (Eyles et al., 1989).

At the Bacton locality, Lee and Phillips (2008) concluded that the sequence had been affected by three phases of glaciotectonic deformation. Phase 1 was characterised by ductile deformation through northward-verging isoclinal recumbent folds. During Phase 2, conditions switched to a non-dilated state, leading to brittle deformation through subhorizontal, north-verging thrusts and Riedel shears. Slices of the underlying Mundesley Sand Member were thrust into the Bacton Green Till Member, forming sand lenses interpreted as augens. Phase 3 deformation resulted in the formation of sand-filled fractures, interpreted as hydrofractures, through water escape from a confined aquifer. It was interpreted that these north-orientated structures were all associated with an ice advance from the SW, loosely fitting in with a regional model which predicted ice flow from the west or SW (West and Donner, 1956; Perrin et al., 1979; Fish and Whiteman, 2001; Scheib et al., 2011). In contrast, investigations of the Bacton Green Till Member from other localities have found that the unit exhibits a phase of deformation from the NW based on geomorphology, pebble fabrics and macroscopic structures (Hart, 2007), and there is clearly still a lack of consensus into the pattern of ice flow across the region.

4.3. Methods

For the analysis of AMS, 21 sample sites were chosen covering both lateral and vertical changes within the succession (location shown on Fig. 4.5). The sampled lithologies were mostly diamicton or sandy diamicton, classified using the Hambrey and Glasser (2003) modification of the Moncrieff (1989) scheme. The till was sampled following the methodology outlined in Appendix A.

In total, 324 cubes were measured with an average of 19 samples per site. AMS samples were measured following the methodology outlined in Chapter 2, Section 2.9. The AMS data

was analysed using standard statistical analysis (see Section 2.4.1), involving the calculation of the mean susceptibility (K_{mean}), corrected anisotropy degree (P_j), lineation (L) and foliation (F) parameters and the shape parameter (T) (Jelínek, 1981).

In order to interpret the magnetic fabrics, the magnetic mineralogy must be identified (discussed in Chapter 2 Section 2.3), as sediment composed of different magnetic minerals can produce very different fabric characteristics. Thermomagnetic experiments were conducted for all 21 samples by investigating the variation of low-field magnetic susceptibility with temperature following the methodology outlined in Section 2.7.1. In addition, the ferromagnetic fraction of six samples was analysed through AF-demagnetisation of the natural remanent magnetisation (NRM) (see Section 2.6.3) and the acquisition of Isothermal Remanent Magnetisation (IRM) (see Section 2.6.4). Thin sections were prepared of samples BG3, BG13, BG16 and BG21. These were impregnated with an epoxy resin, cut and polished using standard procedures and examined under polarised transmitted light.

Structural data was collected in the field. The unconsolidated nature of the diamicton provided access to a three-dimensional view through excavation. Linear data (fold axes and stretching lineations) were measured as plunge and trend, whilst planar data (bedding, faults, fold axial planes and sand-filled cracks) were measured as strike and dip. The contacts around sand lenses were measured and the trends of the lenses were calculated by the fit of great circles to the poles.

4.4. Results

4.4.1. Magnetic Mineralogy

The mean susceptibility (K_{mean}) (Table 1; see Chapter 2, Section 2.4.1 for derivation) of the samples range from 0.05–0.27×10^{-3} (average 0.13 ×10^{-3}) (in the SI system), and the corrected degree of anisotropy (P_j) varies between 1.007 and 1.09 (average 1.033). These values indicate

Site	N	K_m x10^{-3}	K_1	*K_1 95% Error*	K_2	*K_2 95% Error*	K_3	*K_3 95% Error*	L	F	P_j	T	Height (m)
BG1	19	0.135	**171/5**	*42/4*	**79/21**	42/6	**273/68**	7/4	1.036	1.039	1.047	0.878	3.3
BG2	19	0.192	**354/48**	*22/4*	**86/23**	22/4	**253/64**	4/4	1.005	1.025	1.032	0.680	3.6
BG3	19	0.191	**117/1**	*26/5*	**26/20**	26/8	**211/71**	9/5	1.004	1.021	1.027	0.700	3.1
BG4	20	0.113	**333/26**	*52/5*	**243/1**	52/7	**125/87**	7/5	1.002	1.025	1.031	0.856	3.6
BG5	18	0.101	**243/0**	*35/4*	**333/12**	36/6	**151/78**	11/4	1.002	1.009	1.012	0.582	5.4
BG6	18	0.133	**91/20**	*27/4*	**358/8**	27/3	**248/69**	4/3	1.004	1.037	1.046	0.781	2.1
BG7	15	0.267	**335/8**	*15/4*	**245/4**	15/4	**129/82**	4/4	1.008	1.025	1.034	0.517	5.5
BG8	20	0.015	**212/8**	*64/28*	**304/16**	64/19	**94/72**	28/20	1.001	1.006	1.007	0.723	12.6
BG9	20	0.073	**96/2**	*25/14*	**6/4**	25/23	**211/86**	24/12	1.004	1.005	1.009	0.130	13.4
BG10	20	0.119	**281/7**	*32/6*	**191/1**	32/6	**94/83**	7/6	1.004	1.018	1.024	0.599	14.1
BG11	17	0.071	**86/7**	*32/9*	**355/13**	31/12	**202/75**	14/9	1.003	1.011	1.015	0.567	11.0
BG12	16	0.077	**96/2**	*28/9*	**6/4**	28/16	**209/86**	17/9	1.003	1.008	1.012	0.421	9.2
BG13	20	0.166	**355/19**	*28/3*	**94/26**	28/3	**233/57**	4/3	1.004	1.035	1.043	0.798	2.4
BG14	15	0.104	**29/25**	*13/5*	**120/1**	13/4	**212/65**	6/4	1.026	1.060	1.090	0.384	3.0
BG15	20	0.145	**0/2**	*25/5*	**91/31**	25/5	**268/59**	6/5	1.006	1.024	1.032	0.622	2.2
BG16	28	0.166	**35/4**	*41/5*	**126/22**	41/7	**295/68**	7/5	1.002	1.027	1.033	0.833	6.3
BG17	18	0.107	**358/2**	*30/5*	**90/34**	30/9	**265/56**	11/6	1.007	1.036	1.047	0.673	6.2
BG18	20	0.130	**162/7**	*8/4*	**252/1**	11/8	**353/83**	11/4	1.018	1.024	1.043	0.153	6.4
BG19	20	0.055	**68/52**	*24/12*	**335/2**	40/16	**243/38**	37/13	1.019	1.025	1.044	0.134	10.9
BG20	20	0.119	**254/37**	*32/6*	**157/10**	32/6	**54/51**	7/6	1.004	1.018	1.024	0.599	11.9
BG21	19	0.061	**248/5**	*27/15*	**157/4**	24/15	**27/84**	26/5	1.010	1.024	1.035	0.407	14.8

Table 4.1 - Mean site AMS data for the Bacton Green Till Member (see Chapter 2, Section 2.4.1 for calculation): N = number of samples; Km = mean susceptibility; K_1, K_2, K_3 = orientations (declination and inclination) of the principal susceptibility axes with 95% confidence ellipses; L = lineation (L = K_1/K_2); F = foliation (F= K_2/K_3); P_j = anisotropy degree; T = shape parameter; height (m) = stratigraphic height above base at which

that the paramagnetic fraction provides a major contribution to the susceptibility with little contribution by ferromagnetic phases (Rochette, 1987; Borradaile and Henry, 1997).

The variation of low-field susceptibility with temperature was also used to investigate the magnetic mineralogy (Fig. 4.3). Low-temperature susceptibility (Fig. 4.3c) experiments yield a temperature-dependent behaviour on heating from 77–295 K as predicted by the Curie-Weiss law of paramagnetic materials (cf. Fig. 2.9, Chapter 2). Antiferromagnetic, diamagnetic and ferromagnetic (s.s.) materials yield a temperature-independent susceptibility in the range used in the low-temperature experiments (77–295 K). These results indicate that paramagnetic minerals are controlling the susceptibility and the anisotropy of the sediments.

Curie-point estimates and phase transitions of magnetic minerals may be identified from examination of the high temperature susceptibility variation (Fig. 4.3a). Low-field susceptibilities remain constant or decrease smoothly up to 400 °C (following Curie-Weiss behaviour); after

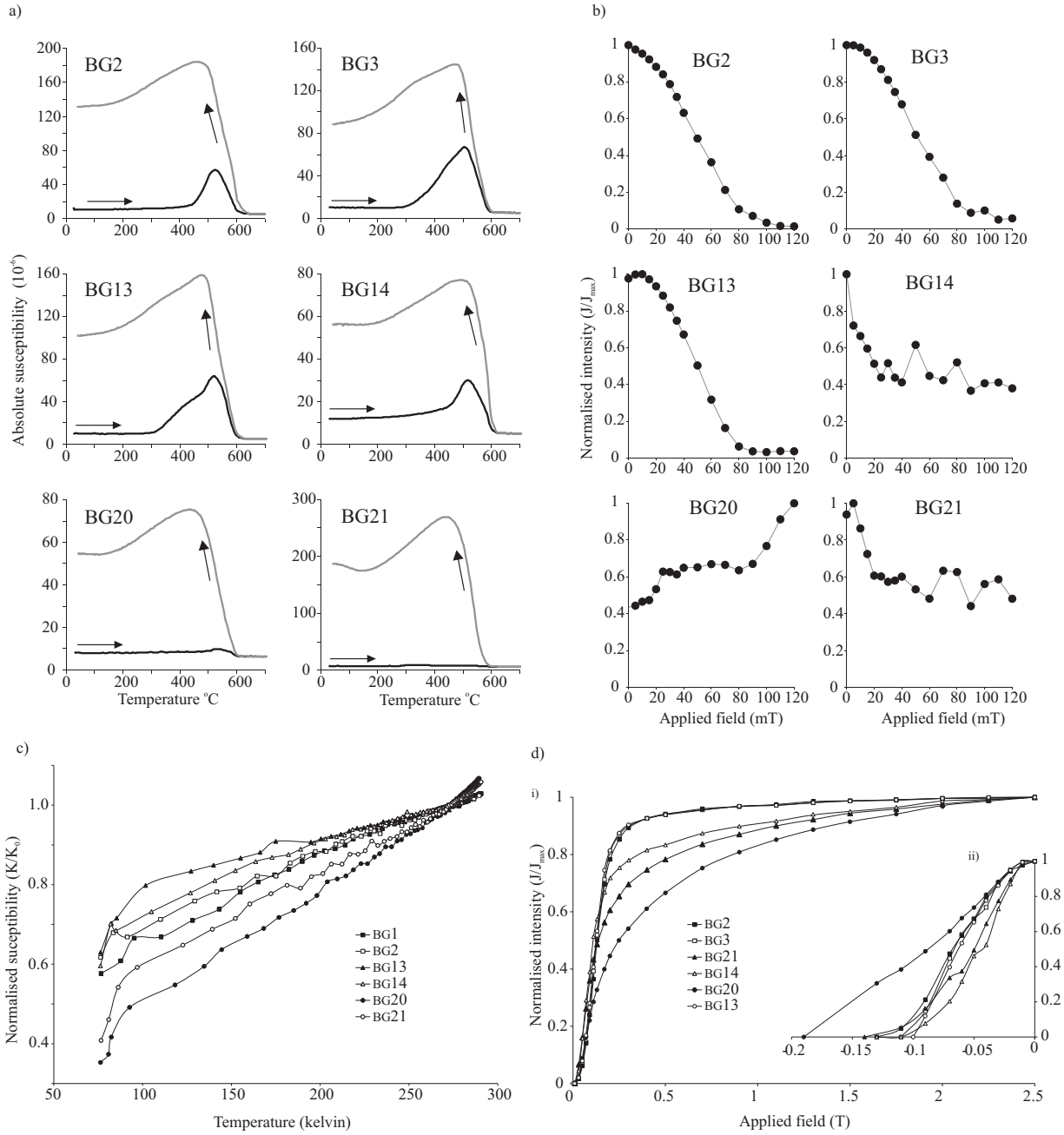

Fig. 4.3 - Rock magnetic experiments. (a) Low-field susceptibility (K) vs. temperature curves. In each case, the heating curve is black and the cooling curve is grey. (b) AF-demagnetisation curves with the normalised magnetisation intensity (J/J_{max}) plotted against the demagnetising field (mT). Samples BG2, BG3 and BG14 reveal a well defined characteristic remanent magnetism that decays to the origin with average medium destructive fields at 50–60 mT. Samples BG14, BG20 and BG21 do not respond to AF-demagnetisation. (c) Temperature vs. the normalised reciprocal (K/K_0) susceptibility. Paramagnetic susceptibility is a function of temperature and follows the Curie-Weiss law ($Kp = C/(T-\theta)$) with C = Curie constant, T is temperature, θ is the paramagnetic Curie temperature. The K/K_0 transforms a paramagnetic curve into a straight line, with an intercept that defines the paramagnetic Curie temperature. Ferromagnetic materials have no susceptibility dependence above the Verwey transition (~120 K) and plots as a straight line of zero slope. (d) Normalised (J/J_{max}) acquisition of isothermal remanent magnetisation (IRM) experiments with (i) IRM acquisition and (ii) Backfield IRM acquisition. See Fig. 4.5 for sample locations.

which, susceptibilities increase before decreasing rapidly above 550 °C. Cooling curves are irreversible and show a strong increase in magnetic susceptibility. This pattern suggests the formation of secondary magnetic phases at temperatures above 400 °C (cf. Fig. 2.10, Chapter 2), but this may also be because of a minor amount of single-domain (SD) magnetite being present within the samples that results in a suppressed Hopkinson Peak near the Curie point of low Ti-titanomagnetite (Hopkinson, 1890; Dunlop and Özdemir, 1997).

To better constrain mineralogy of any ferromagnetic contribution, AF-demagnetisation of the NRM (Fig. 4.3b) and the acquisition of IRM experiments (Fig. 4.3d) were performed (See Chapter 2, Section 2.6.3 for explanation). Of the 6 sites examined, 3 sites, all from the lower series (Fig. 4.5), responded well to AF-demagnetisation and yielded a MDF of 50–60 mT (Fig. 4.3b). This indicates that a low-coercivity phase, probably MD magnetite, is present carrying the remanent magnetism (Dunlop and Özdemir, 1997). Sites BG20 and BG21 from the upper series (Fig. 4.5) and from the sand lens (BG14) did not respond to AF-demagnetisation. Similarly, IRM acquisition curves are typically shallow (Fig. 4.3d), and these samples do not reach saturation until after 2.5 T (Fig. 4.3d). This suggests that in addition to MD magnetite, a very minor high coercivity phase is also present (presumably haematite).

In thin section, the samples are composed of a range of clasts in a clay-silt matrix. Clasts are predominantly quartz with a small proportion of shell fragments and other lithics. They are typically granule- to sand-sized, angular to rounded and have no apparent preferred alignment of long axes. Haematite grains are present, but other opaque minerals are rare. Pigmentary haematite is sometimes observed obscuring a clay-rich matrix. The paramagnetic fraction, largely controlling the AMS, is therefore likely to be within this matrix. This, based on X-ray diffraction (XRD) analysis of the North Norfolk tills (Kazi, 1972), is likely to be a combination of chlorite, kaolinite and illite.

4.4.2. Anisotropy of magnetic susceptibility (AMS)

All samples yield susceptibility ellipsoids where F > L (i.e. dominantly oblate) (Table 1

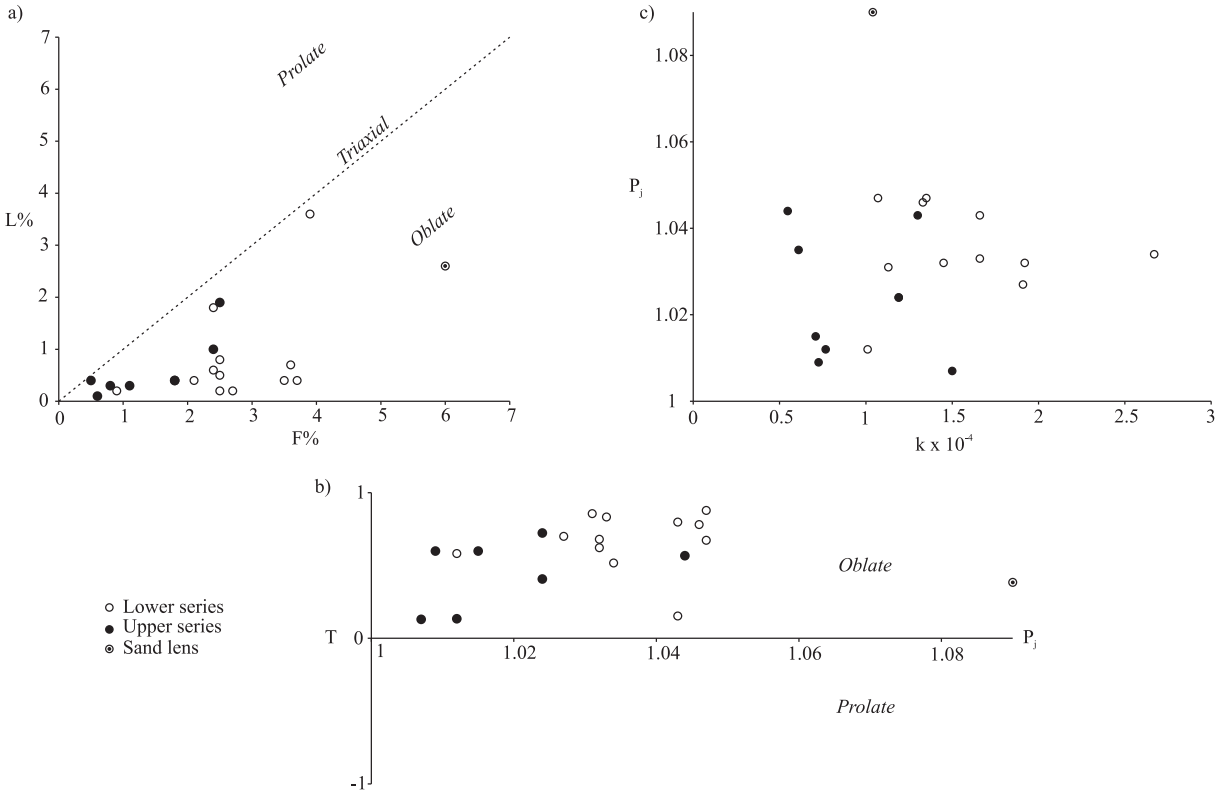

Fig. 4.4 - Variation of AMS parameters for all samples showing upper series (black circles), lower series (white circles) and sand lens (black and white circles). (a) L% vs. F% (magnetic lineation vs. magnetic foliation). (b) Shape parameter (T) vs. anisotropy parameter (P_j). (c) Anisotropy parameter (P_j) vs. susceptibility (K).

and graphically represented in Fig. 4.4a and b). The corrected degree of anisotropy (P_j) versus mean susceptibility (Km) is shown in Figure 4.4c and reveals that the shape of the fabric is not dependent on the strength of susceptibility, which may be the case if different magnetic mineral phases were controlling the susceptibility at different sites. Figure 4.4a shows a graphic display of magnetic lineations (L%) verses magnetic foliation (F%). Strongly prolate ellipsoids lie near the L axis, strongly oblate ellipsoids lie near the F axis, and triaxial fabrics lie near the centre of the diagram. Also shown (Fig. 4.4b) are the conventionally used T/P_j plots which show an alternative, albeit criticised (Borradaile and Jackson, 2004), method of displaying ellipsoid shape. In both plots, ellipsoids are within the oblate to triaxial realm.

Lower hemisphere stereographic projections of the AMS results, with spatial references to the site at which the sample was taken, are shown in Figure 4.5. The minimum susceptibility axes (K_3) are perpendicular to the bedding, defined by the K_1-K_2 plane. These are mostly steeply

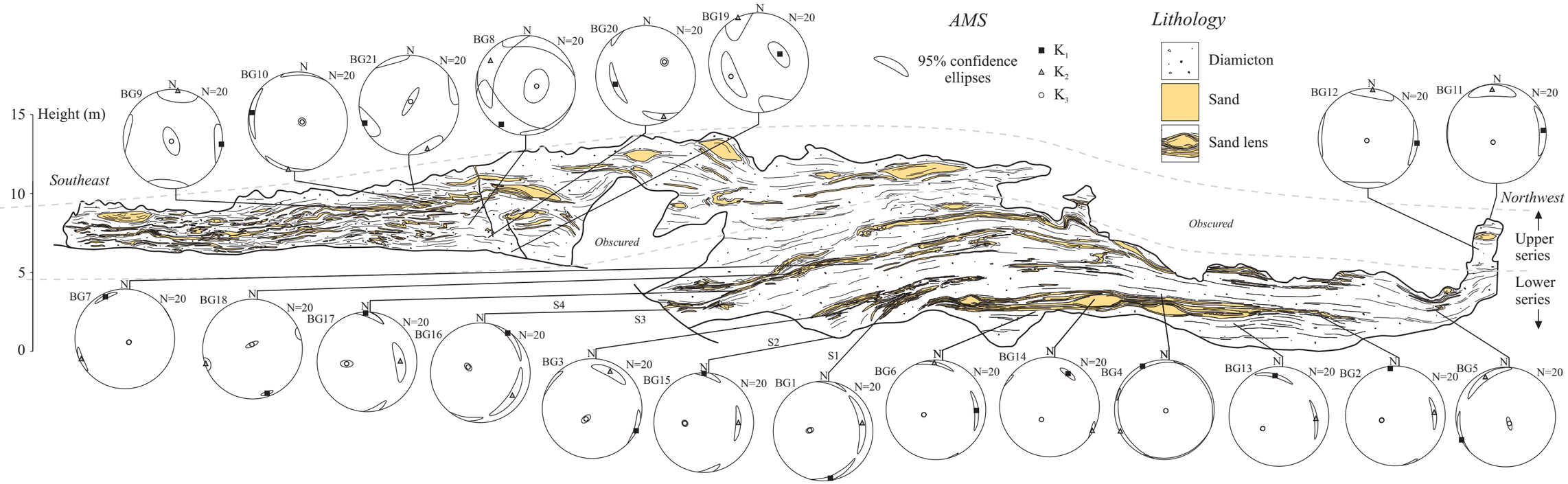

Fig. 4.5 - Sketch of the cliff section at Bacton (no vertical exaggeration) with magnetic fabrics for all sites showing the three mean principal susceptibility axes plotted on to lower hemisphere stereographic projections.

plunging to vertical and show a gently dipping magnetic foliation of variable strike. Magnetic lineations are defined by the K_1 axes, which reveal a clear separation between the upper and lower series. In the lower series, the majority of magnetic lineations trend north-south with mean magnetic lineations clustering at 002° and plunging 6° (Fig. 4.6a), whilst in the upper series there is a switch in trend to east-west and mean magnetic lineations cluster at 267° and plunging 6° (Fig. 4.6b).

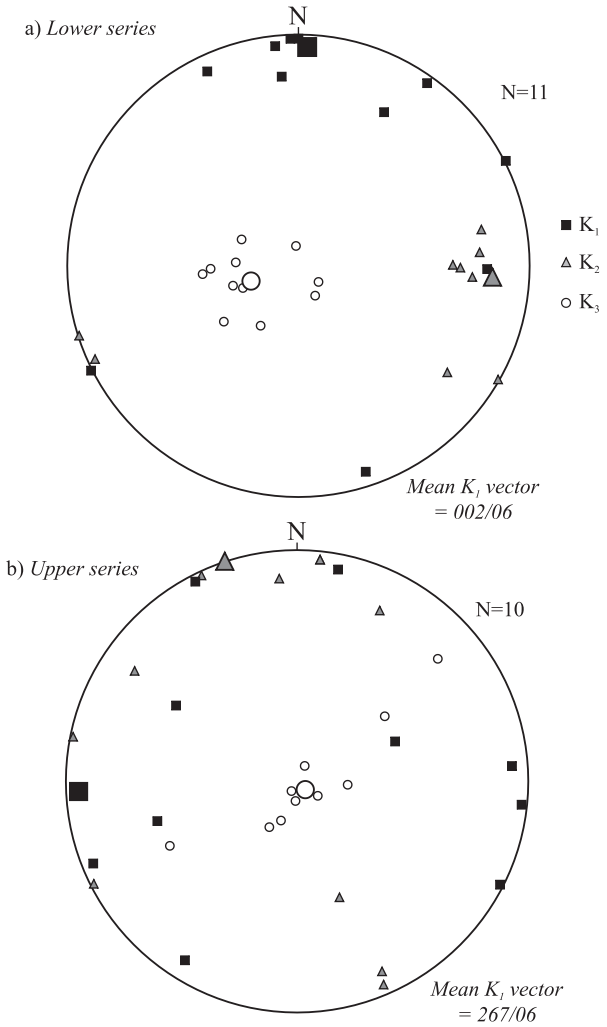

Fig. 4.6 - Stereographic projections of the mean long (K_1), intermediate (K_2) and short (K_3) susceptibility axes of all sites sampled form (a) the upper series and (b) the lower series.

4.4.3. Visible structures

Post-depositional deformation has affected the original sedimentary lamination producing a variety of structures. These can be analysed using standard structural techniques and can be

used to compare strain directions with those calculated from magnetic fabrics. Deformation has taken place in both brittle- and ductile-like manners. There is a vertical change in the styles of deformation as is seen in the magnetic fabrics, and as a result, they are divided into the upper and lower series accordingly.

4.4.3.1. Folding and limb attenuation

Folding and boudinage is common throughout the section (Fig. 4.7, 4.8 and 4.9). Within the lower series, the original sedimentary layering of the stratified diamicton has been strongly attenuated resulting in laterally discontinuous "stringers" of sand (Fig. 4.7b). These stringers typically lie in a north-south orientation and are folded in places (e.g. Fig. 4.7a). Folds are typically steeply inclined to recumbent and asymmetric, with inter-limb angles ranging from tight to isoclinal. Vergence of these folds seems to be in both directions (Fig. 4.7c): a characteristic typical of sheath folding (Kluiving et al., 1991; Alsop and Holdsworth, 2004). The axes of these sheath folds are typically moderately to highly curvilinear with axial planes parallel to subparallel to the stratification. Measurements of fold axes (Fig. 4.9a) show a range of orientations with a distinct clustering plunging 16° to 016°. This orientation is subparallel to the mean lineations of the magnetic fabrics in the lower series (Figs. 4.5a and 4.6).

Within the upper series (Fig. 4.11), the boudinage of more competent sandy horizons has also resulted in sand stringers and folding is common. Folds are typically moderately inclined to recumbent, with interlimb angles ranging from close to isoclinal. Folding styles are more irregular and axial planes cannot be traced throughout the section. The opposing sense of vergence, seen in the two-dimensional cliff face in the lower series, is less common, and an apparent vergence to the SE (on the two-dimensional cliff face) dominates (Fig. 4.11a, b and d). Sheath folding is still prevalent with axes slightly to highly curvilinear, and there is evidence for superimposed folding (Fig. 4.11e). Stereographically, fold axes produce a girdle of orientations in a plane dipping to the west, with a weak clustering in the NE quadrant (Fig. 4.9b). AMS fabrics within the upper series yield lineation data that generally clusters ENE-WSW (Fig. 4.6b). This fits on the girdle of fold

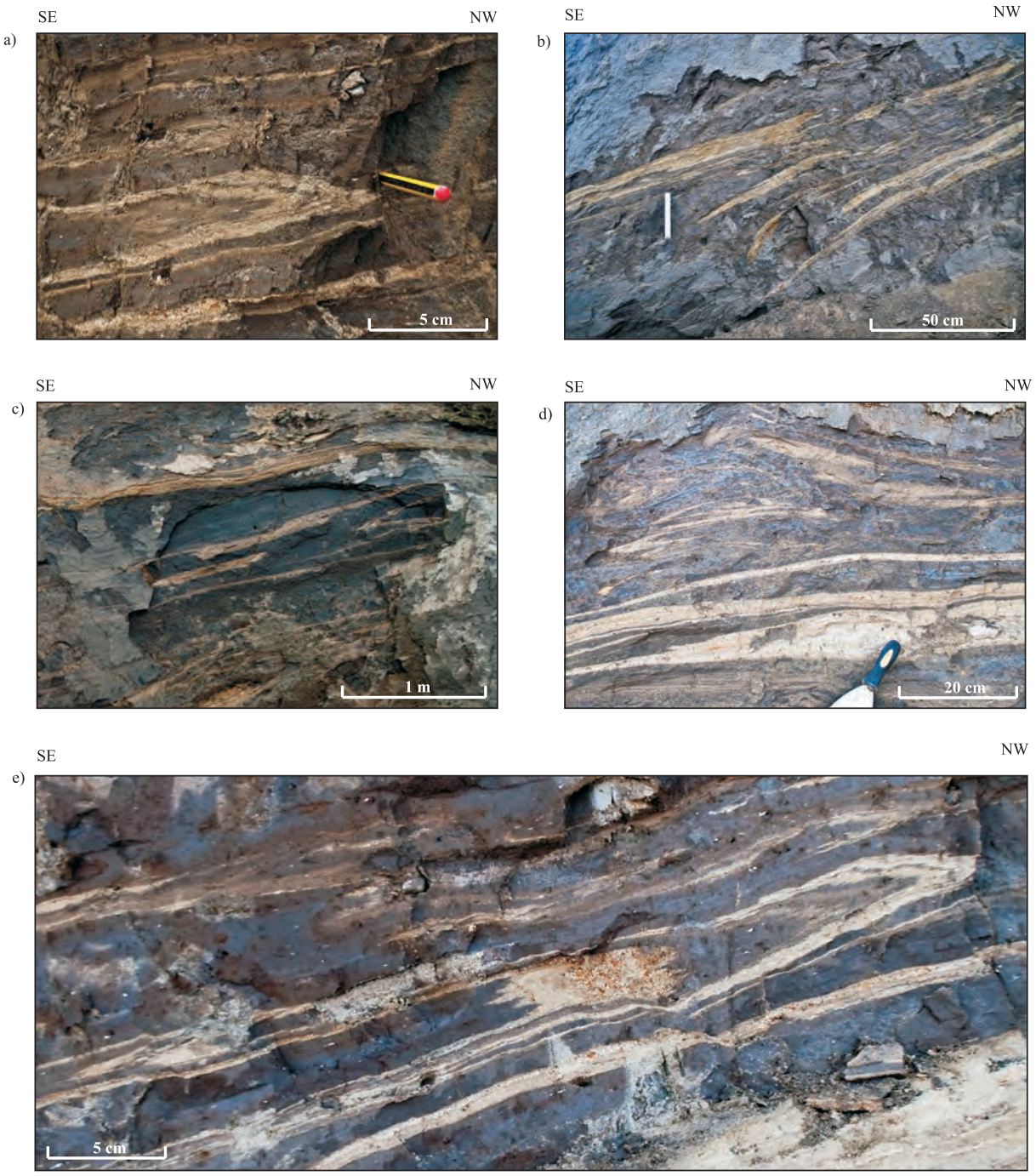

Fig. 4.7 - Photographs of the typical structures associated with the ductile deformation of the lower series. (a) Isoclinal recumbent sheath fold showing parasitic folds around the hinge. Pencil marks the trend of the fold axis. (b) Series of highly curvilinear sheath folds with highly attenuated, boudinaged limbs forming sand "stringers". (c) Sheath folding resulting in a double vergence pattern and "eye" shaped lenses of sand. (d) Subhorizontal bedded sand passing into highly attenuated folds. (e) Cm-scale parasitic fold on a m-scale sheath fold overprinted by Phase 3 steeply brittle faulting.

axes and is generally parallel to the vergence directions observed.

4.4.3.2. Stretching lineations

Within the lower series, stretching lineations are observed on the surfaces of bedding (Fig. 4.10). In some cases, these lineations form a striped pattern, where relief on the bedding surface stays roughly the same (e.g. Fig. 4.10a and b), whilst in other cases they mark steps in the position of the surface (e.g. Fig. 4.10c and d). Stretching lineations, measured from the lower series, form a tight cluster plunging 03° to 016° (Fig. 4.9c). This lies at almost exactly the same orientation as the clustering of the axes of sheath folds (Fig. 4.9a) and the mean direction of the magnetic lineations (Fig. 4.6a).

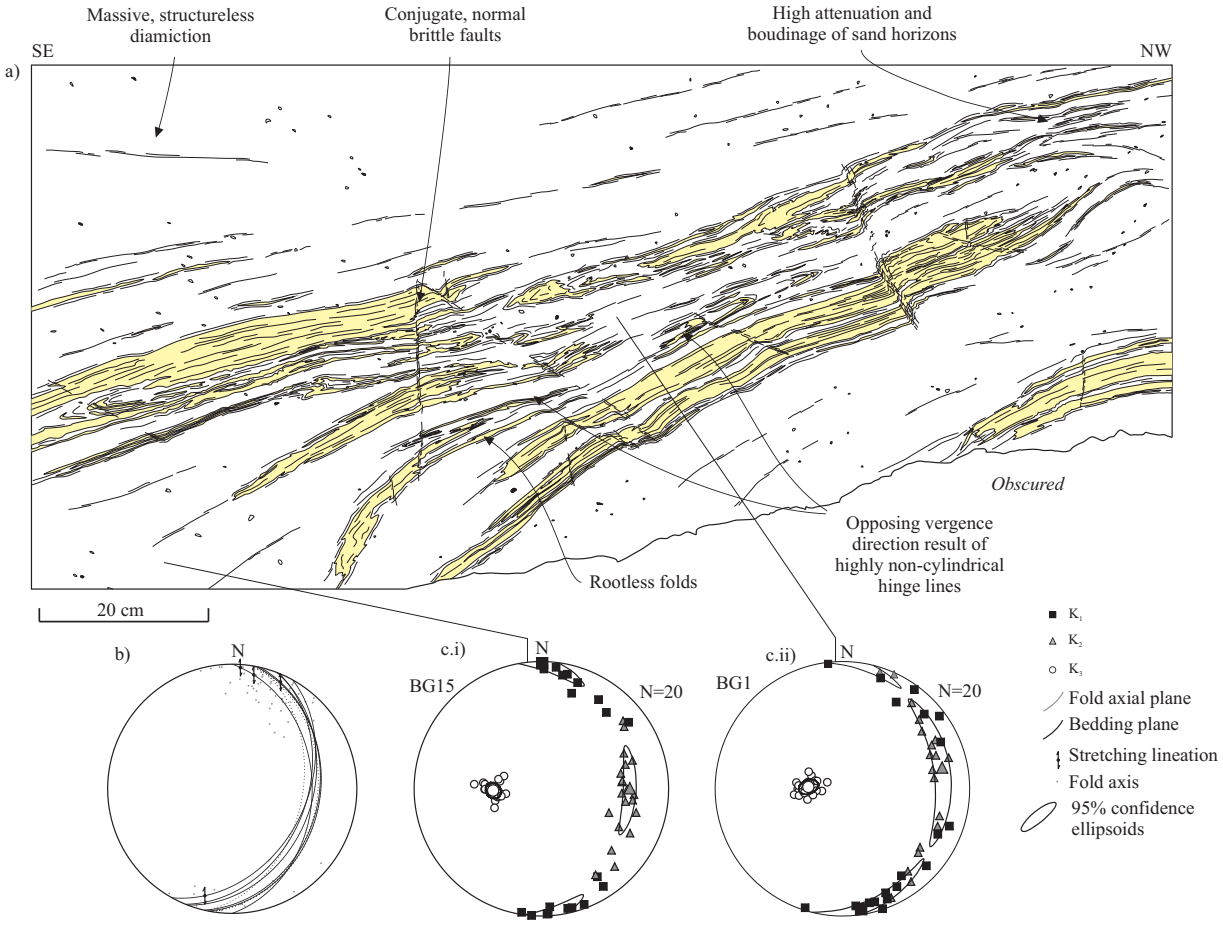

Fig. 4.8 - (a) Field sketch of the styles of deformation within the lower series, with diamicton (white) and sand (yellow). Ductile structures include isoclinal, recumbent sheath folds with highly attenuated and boudinaged limbs. Also seen are the effects of Phase 3 brittle deformation, showing conjugate normal faults under tensile stresses. (b) Stereographic projections of magnetic and structural data taken from location. (c) Stereographic projection of AMS fabric data from (i) BG15 and (ii) BG1.

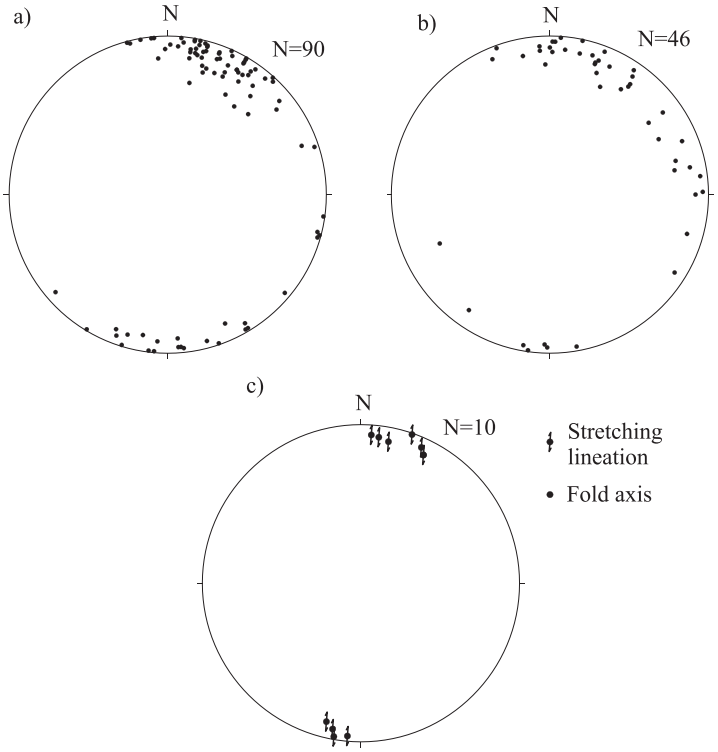

Fig. 4.9 - Stereographic projection of Phase 1 and 2 structural data collected from the lower and upper series. (a) Fold axes from the lower series. (b) Fold axes from the upper series. (c) Stretching lineations from the lower series.

4.4.3.3. Sand lenses

Lenticular bodies of sand exist within both the lower and upper series. Within the lower series, three main lenses are observed, with a maximum height of 80 cm (Fig. 4.12). They are surrounded by sand layering (S1 in Fig. 4.2), which can clearly be seen to wrap around the lens, above and below. The contacts with the sand layering are parallel, and there is no evidence for erosion as would be expected if a subaqueous origin, through channel erosion and fill, was envisaged. Each of the three main lenses originates from separate sand horizons and are formed in progressively lower beds to the NW of the section (Fig. 4.12c). Interbedded diamicton can be seen to pinch out above and below the lenses, and thicken between lenses. Minor folding is evident in the zones on either side of some of the lenses (right of Fig. 4.12a). Partial excavation reveals that long axes are continuous into the exposure and are likely to be linear in form, with azimuths trending roughly NE-SW (Fig. 4.12c).

The sand lenses in the upper series show different characteristics (Fig. 4.13). They typically

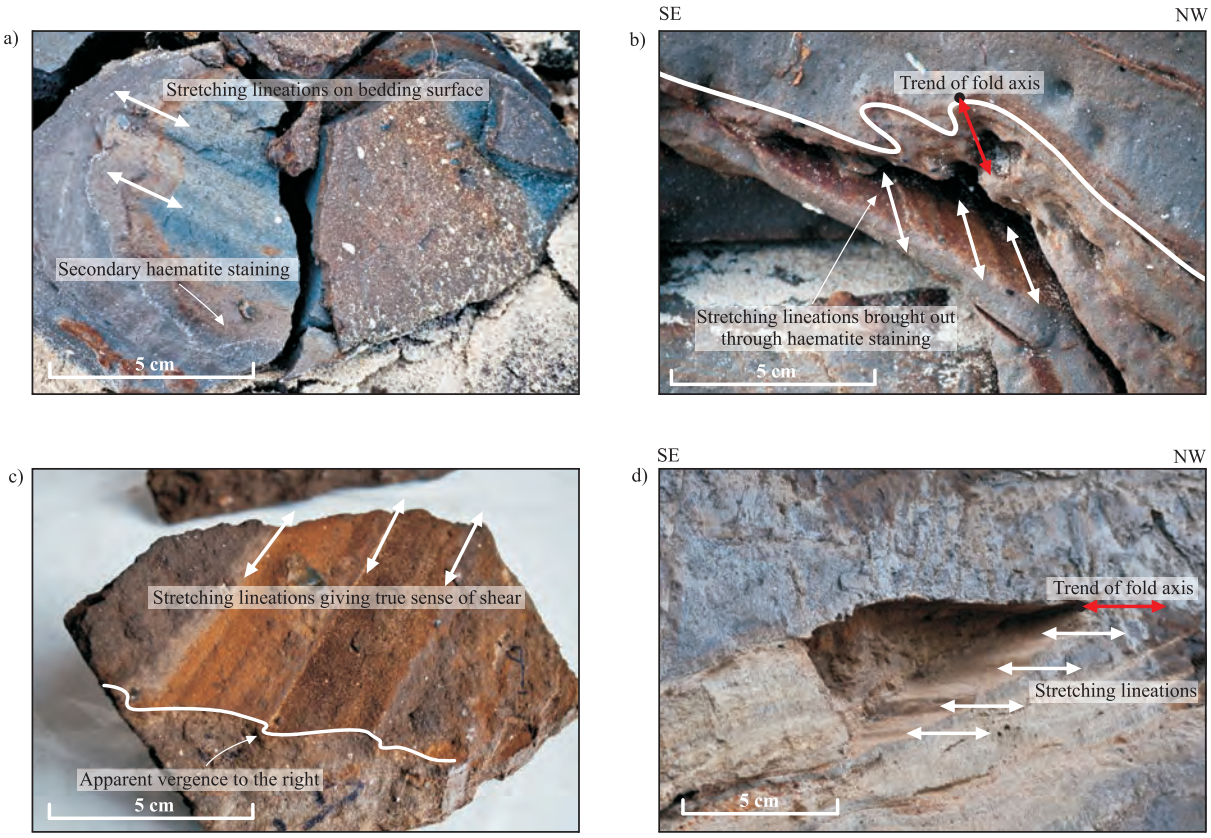

Fig. 4.10 - Photographs of stretching lineations associated with Phase 1 ductile deformation of the lower series. (a) Stretching lineation on the bedding surface of a sand layer within the diamicton. (b) Stretching lineation at the axis of a sheath fold orientated parallel to the axis of the fold, suggesting shear into the exposure in spite of apparent vergence to the left. (c) Impregnated block of diamicton showing stretching lineation on the bedding surface giving an apparent vergence direction to the right. Brown colouration denotes haematite staining. (d) Stretching lineation showing pronounced stepped nature orientated parallel to the axis of the sheath fold.

have a greater degree of asymmetry and do not show the underlying and overlying stratification that characterises sand lenses from the lower series. Sand horizons, at the same stratigraphic level as the lens, are not planar or continuous and form tail-like patterns, which presumably were once connected to bedding and now appear to trail behind the lens (e.g. Fig. 4.13c), indicating movement top to the right and shear kinematics to the east.

AMS fabrics were analysed from the middle sand lens in the lower sequence (sample BG14, Fig. 4.12d). This had a more clay-rich matrix than the others which facilitated sampling and was more suitable for magnetic analysis. A strong clustering of the K_1 axes are observed, plunging 25° to 029°, in an orientation parallel to nearby stretching lineations on bedding surfaces and subparallel or slightly inclined to the axial trend of the lenses.

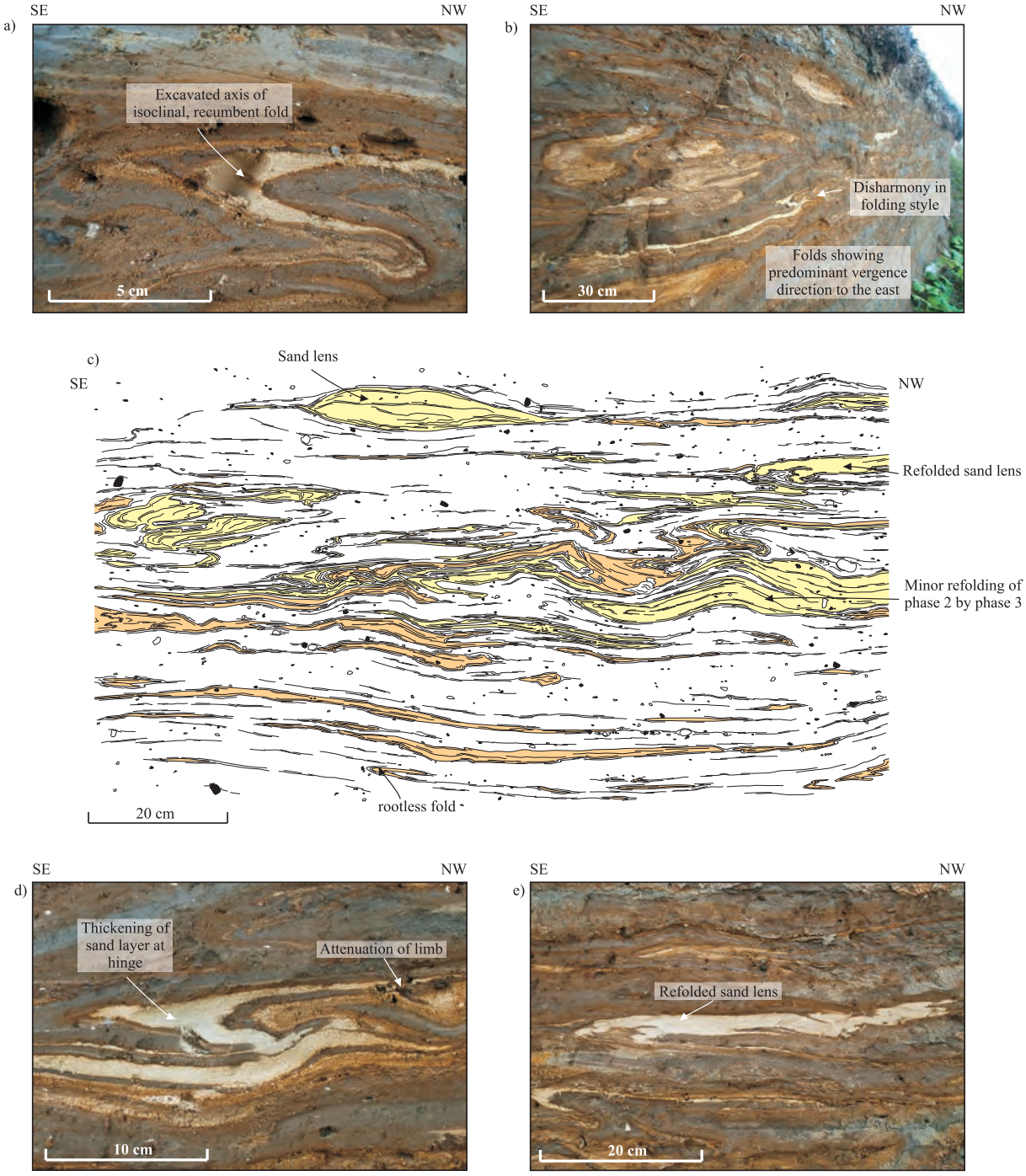

Fig. 4.11 - Photographs and sketch of Phase 2 structures within the upper series. (a) Excavated fold axis of an isoclinal, recumbent fold illustrating how the unconsolidated nature of the sediment facilitates the collection of structural measurements. (b) Cliff section showing disharmonic folds with a dominant vergence direction to the left. (c) Sketch of a typical section of the upper series showing the styles of folding with diamicton (un-shaded) and sand (shaded). (d) Isoclinal, recumbent fold within a sand layer showing pronounced thickening around the hinge and attenuation and thinning of the limbs. (e) Refolding of a sand lens, suggesting a progression of the strain field from extension to compression as a result of the overprinting of deformation events.

4.4.3.4. "Brittle" structures

The term fault is used to describe sediment that has failed in a brittle-like manner with deformation isolated along discrete centimetre-scale shear zones separating blocks of undeformed sediment (or with at least unrelated deformation). Faults are located throughout the section and typically are both extensional (Fig. 4.14a, b and d) and occasionally reverse (Fig. 4.14c). They can clearly be seen to cut the gently dipping isoclinal folding and limb attenuations and, as a result, must post-date the original structures.

Most of the faults are moderately to steeply dipping (>70 °) and, in places, form in two dominant orientations that have an opposite sense of displacement, constituting a conjugate pair (Fig. 4.14d and e). Displacement is low, up to 10 cm in the upper series but typically less than 2 cm in the lower series. Other than the conjugate pairing, the faults show a range of orientations and produce no consistent pattern in terms of shear in any particular direction (Fig. 4.14f). The faults are distributed within the sand lamination and probably continue into the diamicton, but a lack of markers make displacements difficult to discern. Deformation along fault planes takes place in zones ranging from <0.5 mm to >5 cm (Fig. 4.14b). It probably occurs by the means of grain rolling, boundary sliding and the breaking of weak bonding cements that may have formed: a process commonly referred to as granular flow (Twiss and Moores, 1992). This process is probably analogous to the faults produced in sand box models (McClay and Ellis, 1987). In some larger fault zones, displacement occurs along a network of smaller shears rather than distributed evenly across the zone.

As deformation is confined to the faulted zones, the bounding blocks have not been pervasively deformed during this event, which suggests that the AMS fabric has been largely unaffected; however, the deformation associated with the formation of the bands has gently tilted the strata. As such, the orientations of axial planes of folds and foliations have also been somewhat reorientated. Therefore, their imbrications cannot be used as kinematic indicators for direction of shear. Similarly, imbrications of the magnetic lineations cannot be used solely to determine kinematics as has been done in previous AMS studies of sheared till (e.g. Iverson et al., 2008;

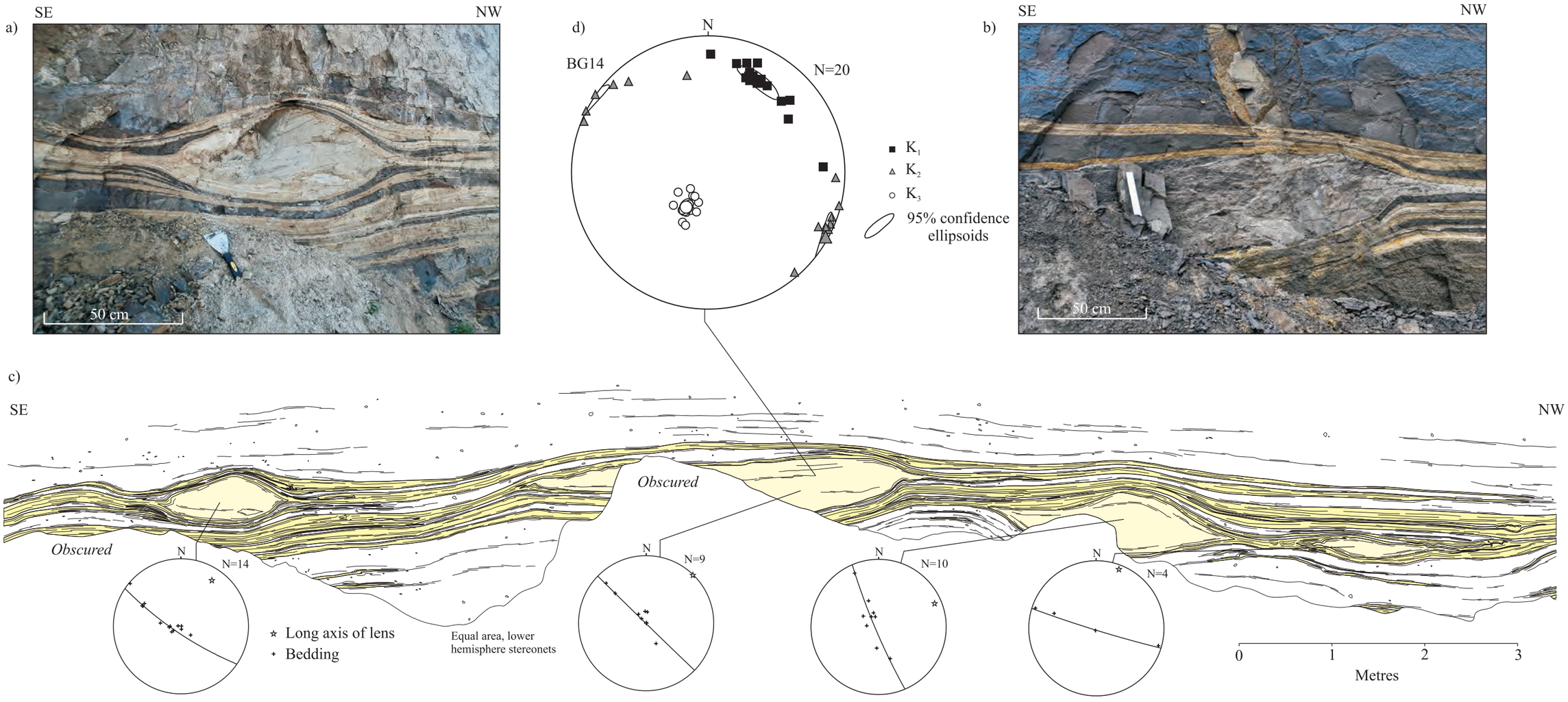

Fig. 4.12 - Photographs and sketches of sand lenses from the lower series with structural and AMS data. (a) Photograph of sand lens from the lower series with asymmetry and parasitic folding, suggesting shear influenced formation to the south. (b) Photograph of sand lens with clay matrix where AMS sample BG14 was collected. (c) Sketch of sand lenses across the lower series. Each lens originates from its own sand horizon at progressively lower intervals to the right of the photo. Attached are stereographic projections with poles to the contacts (black crosses) around the outside of lens with great circle fitted to indicate the axial trend of the lens (stars). (d) Stereographic projection of sample BG14 showing the (K_1), intermediate (K_2) and short (K_3) axes of the susceptibility ellipsoid from all subsamples.

Shumway and Iverson, 2009; Thomason and Iverson, 2009).

4.4.3.5. Sand-filled fractures

Sand-filled structures were observed in the upper series at one location (Fig. 4.15). The largest is 4 metres in height, up to 30 mm in width and extends to the top of the exposure. The sand is fine to medium and is of a similar composition to sand elsewhere within the sequence. The fractures are typically planar in form and dip steeply to the WSW, at the same orientation as nearby faults. They are usually irregular in form and deviate slightly across bed boundaries where they sometimes splay into surrounding diamicton, e.g. the sand "intrusion" in Figure 4.15. The thickness of sand within the fractures varies to up to 30 mm, and there is a general increase in thickness towards the top.

The sand-filled fractures are at the same orientation as faults within the immediate vicinity. They are steeply inclined (>70 °) and have a reverse offset which displaces stratification on either side of the fracture by up to 10 cm. As they overprint previous structures, they must post-date the phases of ductile deformation, and their orientation suggests formation during or after faulting. As with the faults, their orientation bears no relationship to the local stress conditions inferred by previous structures, and as deformation is restricted to a discrete zone, they are not likely to have any major effect on the AMS fabrics other than minor tilting.

4.5. Interpretations

4.5.1. Magnetic mineralogy

Investigations into the magnetic mineralogy reveal that a range of mineral phases are present; however, the strong temperature dependence of susceptibility in accordance with Curie-Weiss behaviour indicate that the AMS signal is controlled by the paramagnetic fraction. AF-demagnetisation and IRM acquisition reveal that high- and low-coercivity ferromagnetic phases are present, presumably low-Ti titanomagnetite and haematite; however, susceptibility

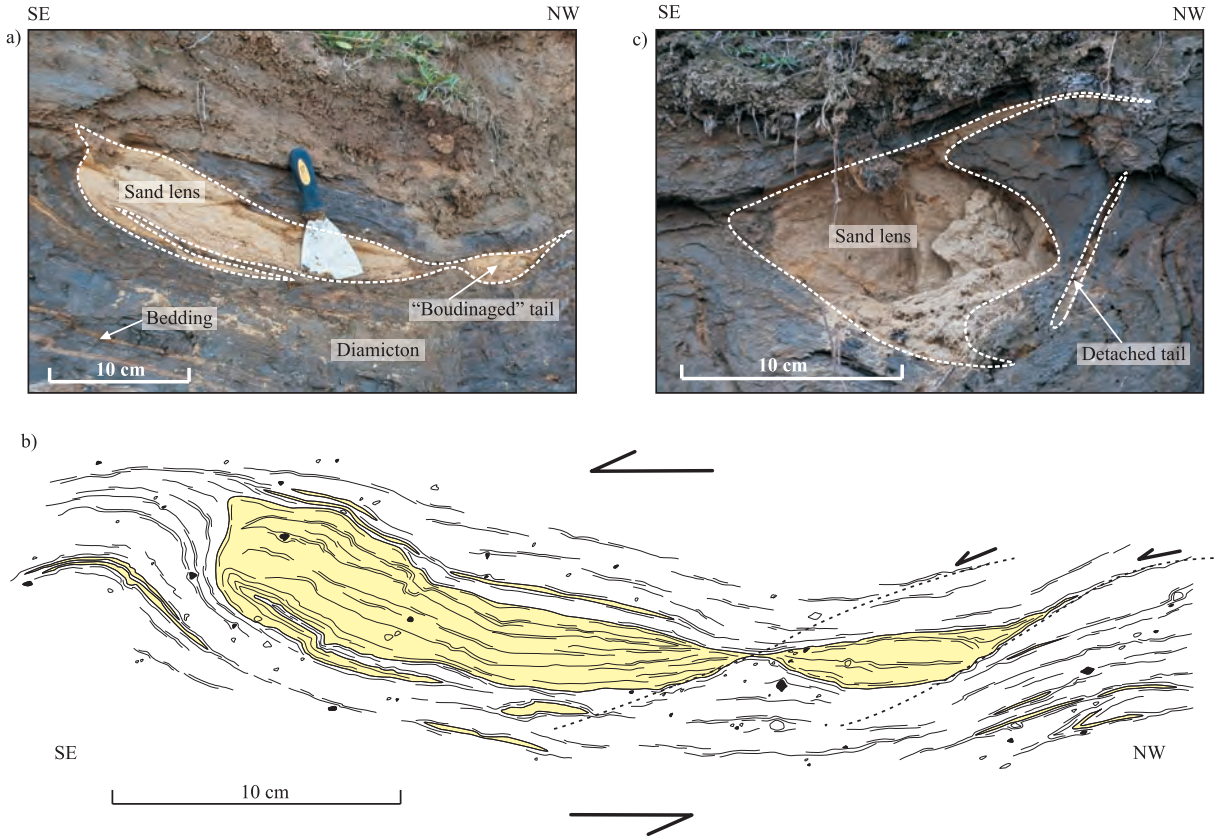

Fig. 4.13 - Photographs and sketch of sand lenses from the upper series. (a) Asymmetric sand lens with tails trailing behind lens to the west with a portion becoming boudinaged. (b) Sketch of the same sand lens showing relationship to stratification. (c) Asymmetric sand lens with tails disconnected from the surrounding horizons.

and thermomagnetic experiments indicate that these are not in sufficient quantities to dominate the AMS signal. The identification of low-Ti titanomagnetite and haematite, whilst they are not controlling susceptibility, do suggest a strong potential for further palaeomagnetic investigations utilising secular variations in the Earth's magnetic field as a relative dating tool (cf. Butler, 1992). Petrological examination reveals that the coarser components are largely diamagnetic quartz and shell fragments which have a negligible susceptibility when other paramagnetic and ferromagnetic phases are present. The paramagnetic carrier must therefore lie within the clay matrix. Previous XRD analysis has revealed that the clay mineralogy of the Norfolk tills is dominated by chlorite, illite and kaolinite; therefore, the AMS signal is likely to be dominated by these phyllosilicate minerals.

Although Iverson et al.'s (2008) AMS fabrics were controlled by magnetite grains, here a paramagnetic phase has been identified, probably chlorite, which is controlling the AMS. During

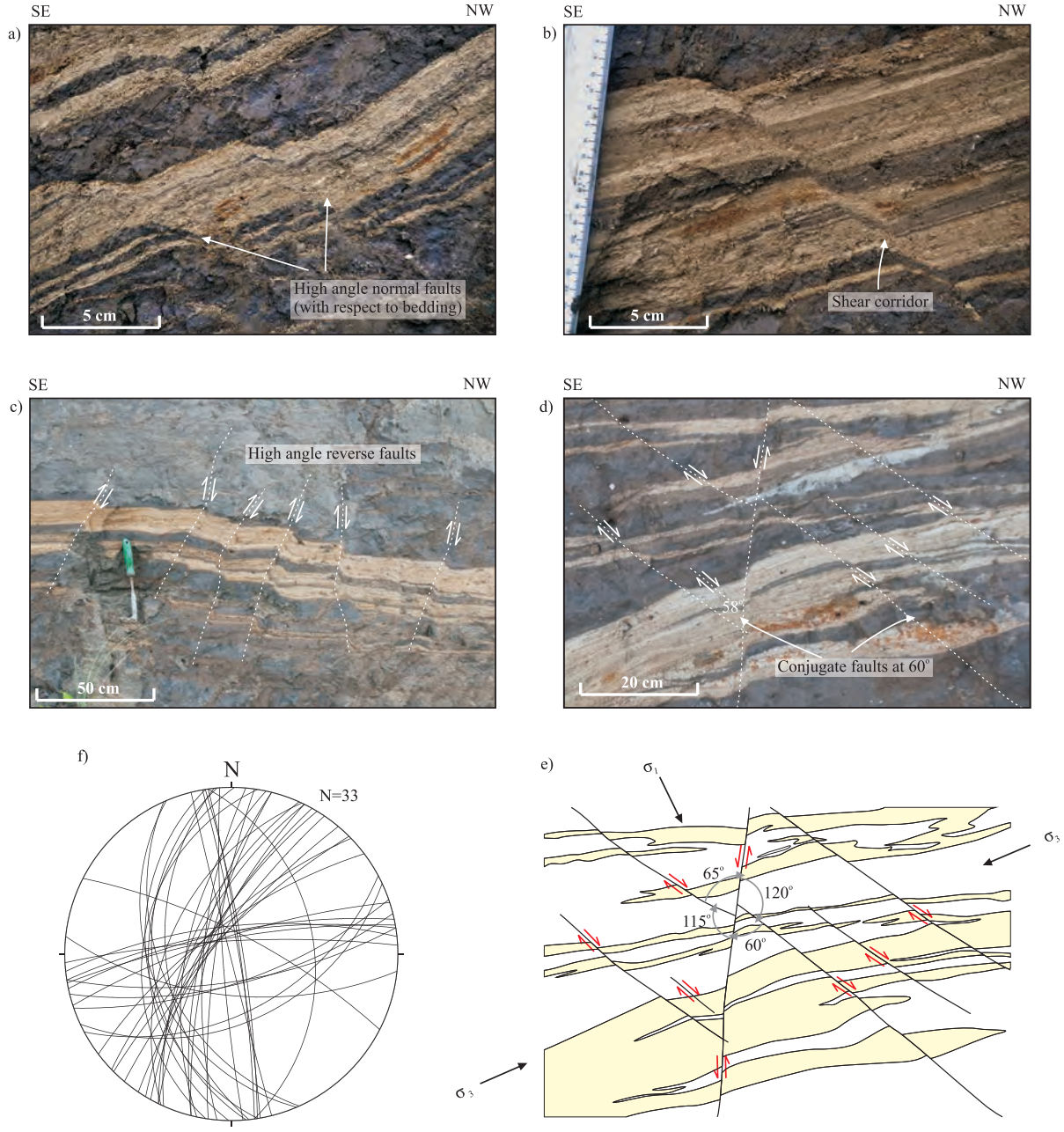

Fig. 4.14 - Brittle structures associated with Phase 3 deformation. (a) Low-angle faults dipping to the north showing normal displacement. (b) Close up of fault showing that movement is accommodated through a 10 mm wide shear zone, presumably through processes of granular flow. (c) Steeply dipping reverse faults showing apparent reverse offset. (d) Photograph and (e) sketch of conjugate faults forming at predictable orientations, revealing formation dominated by subhorizontal tensional stresses. (f) Stereographic projection of planes of faults within both the upper and lower series.

shear, the basal planes of clay minerals will rotate into the most stable orientation. This is parallel to the plane of shearing and therefore will tend to be more sensitive to compressive strain and produce an oblate fabric. Magnetic lineations can be produced by platy clay minerals (Mattei et al., 1997; Parés and van der Pluijm, 2002; Cifelli et al., 2005; Cifelli et al., 2009), where basal planes are disposed about a common axis parallel to stretching (Cifelli et al., 2005). Comparisons with neutron diffraction measurements have shown that AMS of sediments, where a clay fraction is carrying the susceptibility, can successfully be used to quantitatively describe mineral fabrics (Cifelli et al., 2009). At the study site, the correlation between the trend of structures (fold axes and stretching lineations) with the magnetic lineations (e.g. Fig. 4.8b and c) show that this interpretation is also valid. Therefore, the orientations of magnetic lineations, verified through structural measurements, are considered an accurate representative of the stretching direction during progressive simple shear.

4.5.2. Deformational style and genesis

The mechanisms of deformation of the North Norfolk Quaternary glacial sequences have been debated. Most authors agree that glaciotectonic deformation is responsible for most of the structures seen within the Bacton Green Till Member (Banham, 1965; Banham and Ranson, 1965; Banham, 1988; Roberts and Hart, 2005; Phillips et al., 2008), although Eyles et al. (1989) have argued for a subaqueous origin through subaqueous sliding and mass movement. There are similarities between both styles of deformation, but the process driving the deformation is distinct in each case. In a subglacial environment, deformation is controlled by the movement of the glacier, and although perturbations in flow exist, the dominant process of deformation is because of simple shear, and the strain pattern should reflect this (Hart and Roberts, 1994). Within areas affected by slumping and sliding, deformation would be expected to be restricted to local failure planes, and sediments away from these planes are largely undeformed (Hiemstra et al., 2004). At Bacton, except for a switch in orientation within the upper series, magnetic fabrics are generally consistent (Fig. 4.5), indicating that deformation is largely pervasive throughout the section. This, combined with the abundant structures typical of subglacial shear (boudins, sheath folds and

stretching lineations), leads to the interpretation that glaciotectonism is the dominant mechanism for ductile deformation at this location.

Glaciotectonism has resulted in a folding style typical of progressive simple shear. Compressional deformation dominates the initial stages of shear and folding occurs where there are layers with sufficient interlayer contrast in strength. As the shearing progresses, constriction becomes dominant and the strain ellipse migrates to a lower angle to bedding, resulting in attenuation of fold limbs and boudinage. Folds subsequently become highly asymmetrical and attenuated, with axial planes almost parallel to the bedding to the direction of shearing. Under these circumstances, fold axes tend to rotate to an orientation parallel to the direction of shearing creating a highly curvilinear style folding referred to as sheath folding (Alsop and Holdsworth, 2004; Alsop et al., 2007).

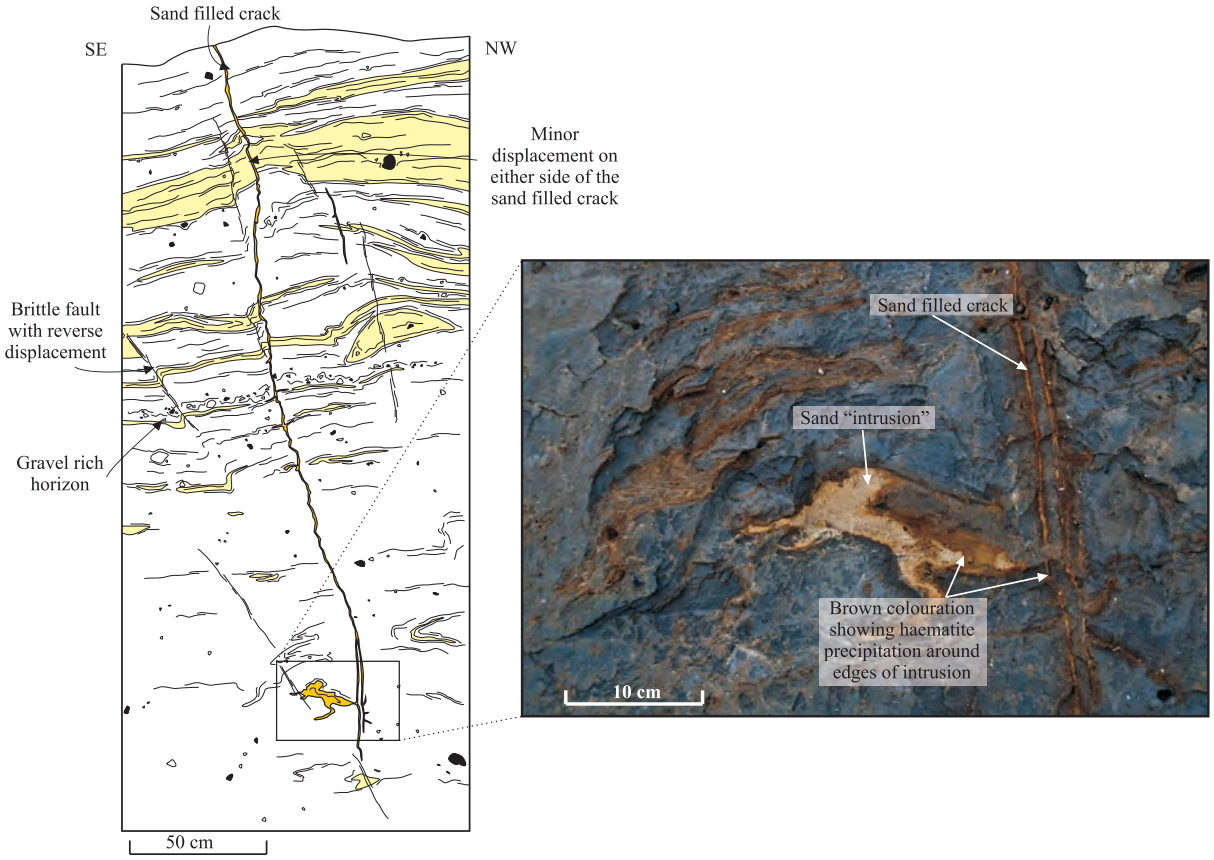

Fig. 4.15 - (a) Sketch of a sand-filled crack and sand intrusion within the upper series of the Bacton Green Till Member with sand within the sand filled crack (yellow), stratification sand (pale yellow) and diamicton (white). (b) Photograph of sand filled crack and sand intrusion into diamicton.

Sheath folding is a phenomenon that is commonly recognised within glaciotectonised sediments (e.g. Kluiving et al., 1991; van der Wateren, 1999; Smith, 2000; Lesemann et al., 2010) and within glacier ice itself (e.g. Hambrey and Huddart, 1995; Goodsell et al., 2002). It was also observed within the basal ice of Tunabreen, described in Chapter 3. The recognition of sheath folding in the Bacton Green Till Member is key to understanding glacial transport directions, as in a two-dimensional section, sheath folding can produce contradictory vergence directions. Only through detailed structural measurements can shear direction be calculated. This could possibly explain discrepancies between the direction of stretching lineations, pebble fabrics and observed vergence directions at other sections, for example, the presence of stretching lineations orientated subparallel to fold axes in Phillips et al. (2008) and contrasting fold directions and pebble fabric orientations in Hart (2007).

4.5.2.1. Stretching lineations

Stretching lineations form either because of the smearing out of subtle variations in mineralogy on the bedding surface or, where they form a stepped nature, as a result of the realignment of linear features e.g. axes of parasitic folds parallel to the direction of stretching. Similar lineations have been noted by Phillips et al. (2008) within the Bacton Green Till Member at a section between West Runton and Sheringham; however, these were attributed to a phase of deformation unrelated to folding. Similar lineations have been observed within pre-quaternary sections (e.g. Le Heron et al., 2005), and they are generally interpreted to form parallel to the direction of shear. Within the section at Bacton, the stretching lineations lie parallel to the orientations of sheath folds and magnetic lineations (e.g. Fig. 4.7b and c). It seems probable, therefore, that they are linked and support a local strain field within the lower series dominated by north-south stretching.

4.5.2.2. Sand lenses

Lenses of sand and chalk have been described in numerous localities along the Norfolk

coast (e.g. Hart and Boulton, 1991; Hart, 2007; Lee and Phillips, 2008; Phillips et al., 2008; Waller et al., 2011), and several interpretations proposed for their origin (cf. Waller et al., 2011). Phillips et al. (2008) suggested, based on heavy mineral compositions, that the sands were derived from the underlying Mundesley Sand Member by thrusting and fragmentation during a brittle phase of subglacial deformation. However, continuous sand layers and diamicton wrap and flow around the lenses (Fig. 4.12a, b and c), consistent with boudinage and inconsistent with thrusting. Magnetic lineations from sample BG14, taken from inside a sand lens (Fig. 4.12d), reveal stretching in a NNE-SSW orientation, consistent with magnetic lineations and structural measurements taken nearby, indicating they formed during the same north-south stretching event.

4.5.2.3. Brittle faults

The faults record a brittle phase of deformation that must have occurred after the initial phase of ductile deformation as pre-existing structures are overprinted. At the study site, Lee and Phillips (2008) recorded low-angle to moderately inclined thrusts and moderately dipping normal faults which may be Riedel shears (Riedel, 1929) associated with a glaciotectonic shearing event to the north. The orientations of structures, however, provide a challenge to this hypothesis. The majority of the faults have a normal offset and form conjugate pairs. They are predominately moderate to steeply dipping and show no relationship to strains predicted, either by magnetic fabrics or from shear in a specific direction. Low-angle thrusts (P shears) and normal faults (R_2 shears), that typically form in association with Riedel shears, were not observed. Instead, all brittle structures were steeply dipping. It is proposed that the simplest explanation for these faults is that they occurred during dewatering and lateral extension associated with loading and compaction during rapid deposition of sands and gravels of the overlying Briton's Lane Formation. Under these circumstances, faults with a reverse offset can form either by the progressive rotation of normal offset faults or through minor flow and remobilisation during loading.

4.5.3. Revised model of the deformation of the Bacton section

The results presented support previous interpretations that indicate the primary mode of deposition was associated with an advancing ice sheet into a glaciolacustrine basin (Lee and Phillips, 2008; Phillips et al., 2008). In this interpretation, diamicton was deposited by underflows and rainout, and sand laid down as turbidites. all of which was subsequently overridden by ice and glaciotectonically deformed. The combined analyses of magnetic fabrics and visible structures has revealed that the sequence has been affected by at least two contrasting directions of simple shear and extension; therefore, the deformation model of Lee and Phillips (2008) can be modified as follows:

Phase 1– Subglacial glaciotectonism and north-south stretching associated with progressive simple shear. Pervasive ductile deformation occurring as a result, producing magnetic lineations through the disposition of clay mineral basal planes about a common axis, sheath folds, the attenuation of fold limbs and the boudinage of sand horizons.

Phase 2 – Subglacial glaciotectonism and east-west orientated stretching restricted to the upper series only. A switch in direction of pervasive ductile deformation occurring as a result, causing the realignment of clay minerals and therefore magnetic lineations, and the refolding of folds and boudins. The reduction in thickness of deformation may be related to a change in the hydrological properties of the sediment or allochthonous thickening of the sedimentary pile.

Phase 3 – Compaction, dewatering and loading of the Briton's Lane Formation, shortly after glacial retreat. Variations in lithology cause inconsistencies in the amount of compaction laterally, and stress is accommodated along brittle faults in a less dilated state, to accommodate strain. Water and fluidized sand is expelled from the sequence through fractures forming the sand filled cracks.

4.6. Discussion

4.6.1. Regional ice flow

Magnetic fabrics, stretching lineations and the trend of sheath folds reveal initial stretching north-south but switching to east-west, as a result of glaciotectonically induced simple shear. Asymmetrical folds and boudins, within the upper series, indicate that this east-west orientated stretching is the result of east-directed shear. If it is assumed that this shear is parallel to glacier flow (which may not necessarily be the case, as in Piotrowski et al., (2004)), then this would indicate east-directed ice flow (Fig. 4.16c). This would support previous work on the Bacton Green Till Member and corresponds well to the regional ice flow that deposited the Weybourne Town and Lowestoft Till Members (e.g. West and Donner, 1956; Fish and Whiteman, 2001; Phillips et al., 2008; Scheib et al., 2011)

More problematic is relating the initial north-south stretching to a particular ice flow direction because of the ambiguities of sheath folding and the presence of bedding-parallel structures, typical of Phase 1 deformation. Furthermore, previous structures have been reorientated during the occurrence of Phase 3. As such, the subtle imbrications of planes and lineations cannot reliably be used as kinematic indicators as has been done previously. Lee and Phillips (2008) and Phillips et al. (2008) suggested that the retreat of the margin of an ice body to the north, allowed ice from the southwest to advance into a temporary basin that was created between the two ice sheets . Under this model, northerly-directed shear associated with local flow from the SE could be envisaged (option 2 in Fig. 4.16b). However, northerly-directed flow seems unlikely given the clast provenance of the glacial deposits of North Norfolk. For example, the Weybourne Town Till, which may have been deposited by the ice that deformed the Bacton Green Till Member elsewhere (Phillips et al., 2008), has a provenance from the North Sea (Hamblin et al., 2005). Other authors suggest that the member was deformed by ice from the north, possibly associated with the same south-flowing ice advance that deposited the member (option 1 in Fig. 4.16b). As such, two possible ice flow vectors are proposed during Phase 1

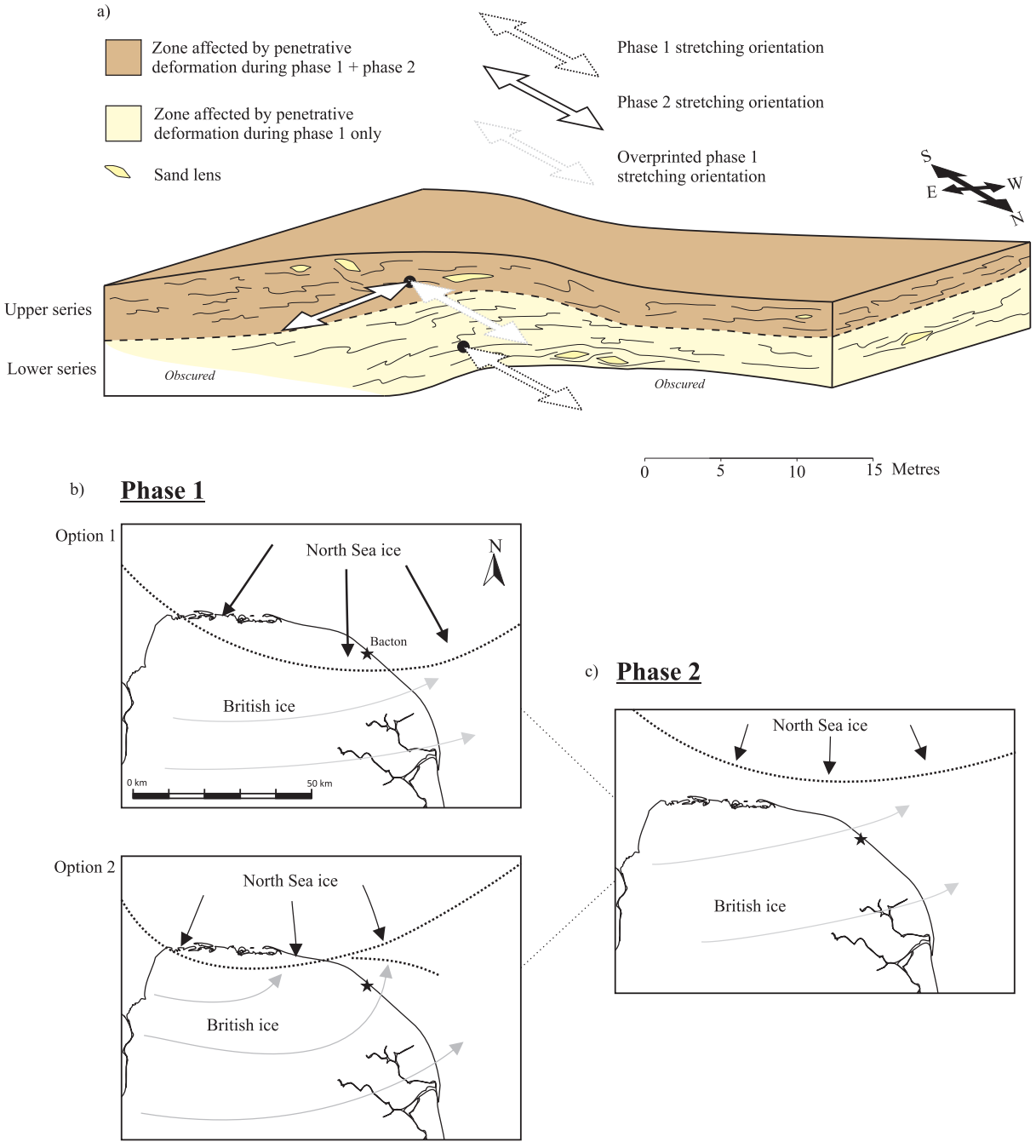

Fig. 4.16 - Revised model for glaciotectonic deformation of the Bacton sequence. a) Stretching directions during shear strain during Phase 1 and Phase 2 deformation. Possible scenarios for ice flow patterns based on previous suggestions (Fish and Whiteman, 2001; Phillips et al., 2008; Scheib et al., 2011; West and Donner, 1956) during (a) Phase 1 and (c) Phase 2 deformation. Scenarios are based on the assumption that ice flow is parallel with direction of simple shear within the sediment which may not necessarily be the case.

which, assuming ice flow is parallel to stretching, could be used to explain the Phase 1 pattern of deformation seen at the locality.

Recent numerical modelling (Boulton and Hagdorn, 2006; Hubbard et al., 2009) has suggested highly dynamic behaviour of the British and Irish Ice Sheet during the last glacial period. Ice was drained largely by a number of transient, switching ice streams, and it is likely that similar concepts could be applied to earlier, Middle Pleistocene ice sheets. Dynamic glaciation within a single ice sheet could be enough to explain the flow vectors and polyphase deformation reported. Moreover, the likely presence of interacting lobes of British ice and Pennine ice provide possible scenarios under which the reported flow vectors and polyphase deformation could occur.

4.6.2. The use of AMS for glaciotectonic studies

This study has shown that AMS fabrics reflect the preferred alignment of minerals within a glaciotectonite. It therefore directly reflects strain acting on the site through glaciotectonic processes. Magnetic lineations are parallel to stretching lineations and the clustering of fold axes, which suggest that they reflect stretching during progressive simple shear as a result of subglacial glaciotectonism. Therefore, the structural data corroborates the AMS results and supports the interpretation that AMS can be used to accurately evaluate strain within glaciotectonites.

The key advantage of AMS over other petrofabric techniques is that strain can accurately and rapidly be determined in three dimensions. Utilising the methodology described, blocks can be impregnated and cut in a few days, and each subsample cam be measured in the Kappabridge in minutes (see Appendix A). As the process is automated, the only potential for error is from the initial measurement of the orientation of the sample. The spatial resolution of the AMS technique is also far better than pebble fabric and structural measurements. Moreover, fabrics from each subsample reflect the volume averaged of many grains within a sample, and an average of 18 subsamples is used to calculate mean fabrics from a site. The technique does not rely on a lithology where structures can be seen, and can thus be used on the many structureless tills. AMS, however, needs to be applied with caution. It is an oversimplification to state that AMS reflects

a preferred alignment of the long axis of mineral grains. In reality, tills can have a highly variable magnetic mineralogy and because of the different properties of different magnetic minerals (e.g. distribution, shape and crystallographic anisotropies) investigating the magnetic mineralogy is a critical step when interpreting magnetic fabrics. For example, if a similar mineralogy to that of Hooyer et al. (2008) was assumed, fabric strengths may be interpreted as being too weak to fit in with the bed deformation model and thus an alternative mode of genesis may have been envisaged. The magnetic mineralogy must therefore be investigated fully before interpretations can be drawn.

This study adds to the work of AMS for glacial sediments and builds on the work of previous authors by showing that AMS can show significant insights into patterns of glaciotectonic deformation, where paramagnetic clays dominate the magnetic susceptibility. This study opens up new possibilities for the investigations of glaciotectonism, and as the technique can be directly repeated and applied to other sections, has potential to add additional constraints on deformation styles and ice flow directions within the Quaternary of North Norfolk and elsewhere.

4.7. Conclusions

The sediment genesis and flow vectors of the Bacton Green section have been reinvestigated using a combined structural and magnetic approach. A number of conclusions can subsequently be drawn that throw light both on the glacial history of North Norfolk and the application of AMS to study glacially deformed sediment.

- Imprinted in the structures and magnetic fabrics of the Bacton Green Till Member are evidence of at least two phases of ductile deformation which formed as a result of oscillations of North Sea-and British-based ice during the glaciations of the Anglian stage. Initially, north-south orientated stretching affected both the upper and the lower series, but was replaced by east-west orientated stretching affecting only the upper series.

- Magnetic fabrics are controlled by the preferred alignment of dominantly iron-bearing paramagnetic clay minerals. Magnetic lineations are formed by the alignment of the basal planes of these clay minerals about a common axis. These lineations are parallel to macroscopic structures (stretching lineations and sheath folds) and are an accurate representative of the stretching direction during progressive simple shear.

- The large amount of stretching within all layers, with no discrete guide planes and a lack of a known significant palaeoslope indicates that glaciotectonic deformation is responsible for ductile deformation during Phases 1 and 2. In contrast, Phase 3 brittle structures are dominated by conjugate faults and are unrelated to shear in any particular direction. These are interpreted to have formed after glaciotectonism during loading, sediment compaction and dewatering.

- AMS, corroborated through structural measurements, has revealed subtle variations in strain direction presumably relating to ice flow and has given new insights in the deformation characteristics not previously possible within a glaciotectonised deposit. In particular, the importance of the realignment of linear features parallel to flow, and as a result, the interpretation of stretching lineations and the clustering of fold axes has been illustrated.

- This study has built on the previous work of the examination of AMS of glacial sediments and shows that the strain field can be accurately measured within a glaciotectonite, where a paramagnetic fraction is controlling the susceptibility. This approach can be directly applied to other glaciotectonised localities and has the potential to provide significant insights into the sometimes complex history of glaciated areas.

CHAPTER 5.

MAGNETIC FABRICS AS A PALAEOFLOW INDICATOR IN LATE CRYOGENIAN GLACIAL DEPOSITS IN NORTHEAST SVALBARD

5.1. Introduction

The previous chapter evaluates anisotropy of magnetic susceptiblilty (AMS) fabrics in a Pleistocene deposit which is well-understood palaeogeographically. This and the following chapter apply the knowledge gained to interpreting Neoproterozoic glacigenic sediments for which the palaeogeography is poorly known, but which are exceptionally well-preserved in NE Svalbard.

In most cases, the AMS studies of glacial sediments have focused on the Quaternary sedimentary record, with the notable exception of Archanjo et al. (2006). However, diamictites are relatively common within the pre-Quaternary geological record (Hambrey and Harland, 1981). These diamictites can show similar evidence of glacial deformation to those observed in post-Quaternary sediments (e.g. Le Heron et al., 2005; Arnaud, 2012; Busfield and Le Heron, 2013). However, as many pre-Quaternary glacial sections have undergone diagenetic and sometimes tectonic changes, the application of AMS can introduce complications. For example, the growth of new diagenetic minerals can disrupt the original fabric (e.g. Schieber and Ellwood, 1993) and, as AMS is highly sensitive to strain, any tectonic deformation can overprint primary fabrics (Averbuch et al., 1992; Parés et al., 1999). However, AMS has been routinely applied to the pre-Quaternary record in non-glacial sediment types (e.g. Schieber and Ellwood, 1993; Dall'olio et al., 2013) and, in the same way as post-Quaternary sediments, has been shown to provide information regarding depositional processes. Therefore, significant potential exists in the application of AMS to glacial sediments in the pre-Quaternary record.

The origin of diamictites within the sedimentary record has been contested (e.g. Harland, 1964; Eyles and Eyles, 1983; Eyles and Januszczak, 2004). Diamictites are often structureless, lacking any diagnostic characteristics, and it is recognised that they can occur in both glacial and non-glacial settings. Diamictites of the Cryogenian Period (850 – 635 Ma) are particularly debated (Fairchild and Kennedy, 2007). Recorded in this period is evidence of widespread low-altitude and low-latitude glaciation. There is a general consensus that ice sheets existed on all continents at all latitudes in a state referred to as pan-glacial (Hoffman, 2009). This represents a climatic scenario that cannot be understood in terms of Quaternary analogues (Halverson

et al., 2004). Several contrasting hypotheses have been proposed for these events (summarised in Fairchild and Kennedy, 2007), the best known being the "Snowball Earth" hypothesis of Hoffman et al. (1998) which postulates an Earth system discontinuity leading to the Earth's surface becoming nearly entirely frozen in one or more global glaciations.

In NE Svalbard, the Cryogenian Polarisbreen Group contains evidence of two separate glacigenic units; an older Petrovbreen Member and a younger Wilsonbreen Formation (Fairchild and Hambrey, 1984). Both are unmetamorphosed and well-preserved. The Wilsonbreen Formation represents the thicker of these deposits and is dominated by diamictites, which commonly form structureless units up to tens of metres in thickness. Little is known regarding the basin palaeogeography, therefore providing an ideal opportunity to use the AMS technique for characterising flow directions in pre-Quaternary sections.

The aims of this chapter are to (i) characterise the AMS fabric in terms of both shape and fabric strength; (ii) interpret the origin of the AMS fabric (sedimentary, diagenetic, or tectonic) through comparisons with other petrofabric techniques (clast fabrics); (iii) determine the dominant basin palaeoflow direction and reconstruct the palaeogeography; and finally (iv) evaluate the potential of the technique for the analysis glacial sediments in the pre-Quaternary rock record.

5.2. AMS for Neoproterozoic diamictites

Glacial sedimentation can occur in a variety of environments, any of which could produce an array of AMS fabric characteristics (see Chapter 2, Section 2.7.1). The AMS fabrics of subaqueous deposition typically produces oblate ellipses, parallel to the bedding plane (Rees and Woodall, 1975). However, AMS is seen to be very sensitive to weak currents acting on the sea floor (Eyles et al., 1987). These can cause the long axis of grains to rotate into a preferred alignment, reflecting current-flow directions. In addition, AMS is sensitive to soft-sediment remobilisation. During these processes, particles may also rotate into a preferential alignment, parallel to the direction of

flow (Gravenor, 1986; Eyles et al., 1987).

In a subglacial environment, the AMS fabrics can be directly related to ice flow. It has been shown in Chapter 3 that AMS fabrics in deformed basal ice form lineations parallel to the direction of flow. In addition, Iverson et al. (2008) showed, through ring-shear experiments, that when an intact till sample was sheared under conditions similar to those expected to be operating at the ice-bed interface, micro-faults develop that facilitate the rotation of the long-axis of particles into the plane of shear, thus giving rise to preferential alignment of grains. This has been shown to be able to be applied to Quaternary tills in North America, to determine former ice flow directions (e.g. Shumway and Iverson, 2009). In Chapter 4, the application of AMS to glaciotectonised sediments was also investigated. This has revealed fabrics largely similar to those seen within subglacial tills. It was discovered that AMS lineations lay parallel to the inferred direction of stretching during shear of the sediment.

Diamictites are common throughout the geological record; however, when applying AMS to pre-Quaternary sediments, additional complications may exist. Post-depositional processes can have a significant impact on fabrics formed during sedimentary processes (e.g. Borradaile and Tarling, 1981; Borradaile and Tarling, 1984; Kissel et al., 1986; Averbuch et al., 1992). Shortly after deposition, gravity can continue to rotate grains towards the horizontal; however, pore space and permeability are reduced as the sediment becomes increasingly compacted and the grains' ability to rotate are restricted. The growth of new minerals during diagenesis can also have an effect, even if those minerals are not strongly magnetic (see Chapter 2, Section 2.7.3). However, the original palaeocurrent can still be extracted in many cases (Schieber and Ellwood, 1988). New magnetic minerals can also form from iron-bearing paramagnetic minerals (e.g., biotite and hornblende). These can fill pre-existing void space within the original mineral and therefore yield similar fabric orientations in many cases (Tarling, 1983).

As well as diagenetic changes, AMS has been shown to be very sensitive to tectonic reorientation, especially if it takes place prior to cementation (Tarling and Hrouda, 1993). Various studies have shown how sedimentary fabrics are affected by tectonic deformation (e.g.

Borradaile and Tarling, 1981; Borradaile and Tarling, 1984; Kissel et al., 1986; Averbuch et al., 1992). Parés et al.(1999) investigated the incipient deformation of mudrocks from the Southern Pyreneen Foreland Basin. This study showed that the progressive development of an overprinting tectonic fabric can be identified in rocks that otherwise showed no mesoscopic evidence of deformation. Starting with an oblate sedimentary fabric (see Fig. 2.13, Chapter 2), the first evidence of tectonic deformation is characterised by the clustering of K_1 axes normal to the tectonic shortening direction. Subsequent tectonic strain results in the deviation of K_1 and K_2 axes away from the bedding plane ultimately forming a great circle girdle parallel to the rock cleavage.

Diagenetic and tectonic changes therefore have the potential to affect primary fabrics, and as such, their impact on the glacial sediments of the Wilsonbreen Formation need to be investigated. In the AMS of glacial sediments, an initial clustering of susceptibility axes is very common and normally forms in response to sedimentary processes (Iverson et al., 2008; Gentoso et al., 2012; Fleming et al., 2013); therefore, the identification of a tectonic overprint may not be straightforward. However, in pre-Quaternary sections with no evidence of macroscopic deformation, a tectonic overprint can readily be discounted by comparisons with other palaeoflow indicators (e.g. clast fabrics, striations) which, because of their large size, are not as prone to tectonic reorientation.

5.3. Geological background

The Polarisbreen Group NE Svalbard (Fig. 5.1 and 5.2) forms part of the relatively undeformed Heckla Hoek succession of the Eastern Tectonic Terrain, which was amalgamated in the Caledonian Orogeny (Halverson, 2011). The group sits near the core of a north-south trending synclinorium, dissected by conjugate NW-SE and SW-NE strike slip faults (Fig. 5.3 and see Appendix E for the full detailed geological map). The rocks are mostly uncleaved and unmetamorphosed, showing excellent preservation of sedimentary structures at all sites visited.

The history of geological research in NE Svalbard is outlined in Halverson (2011). The

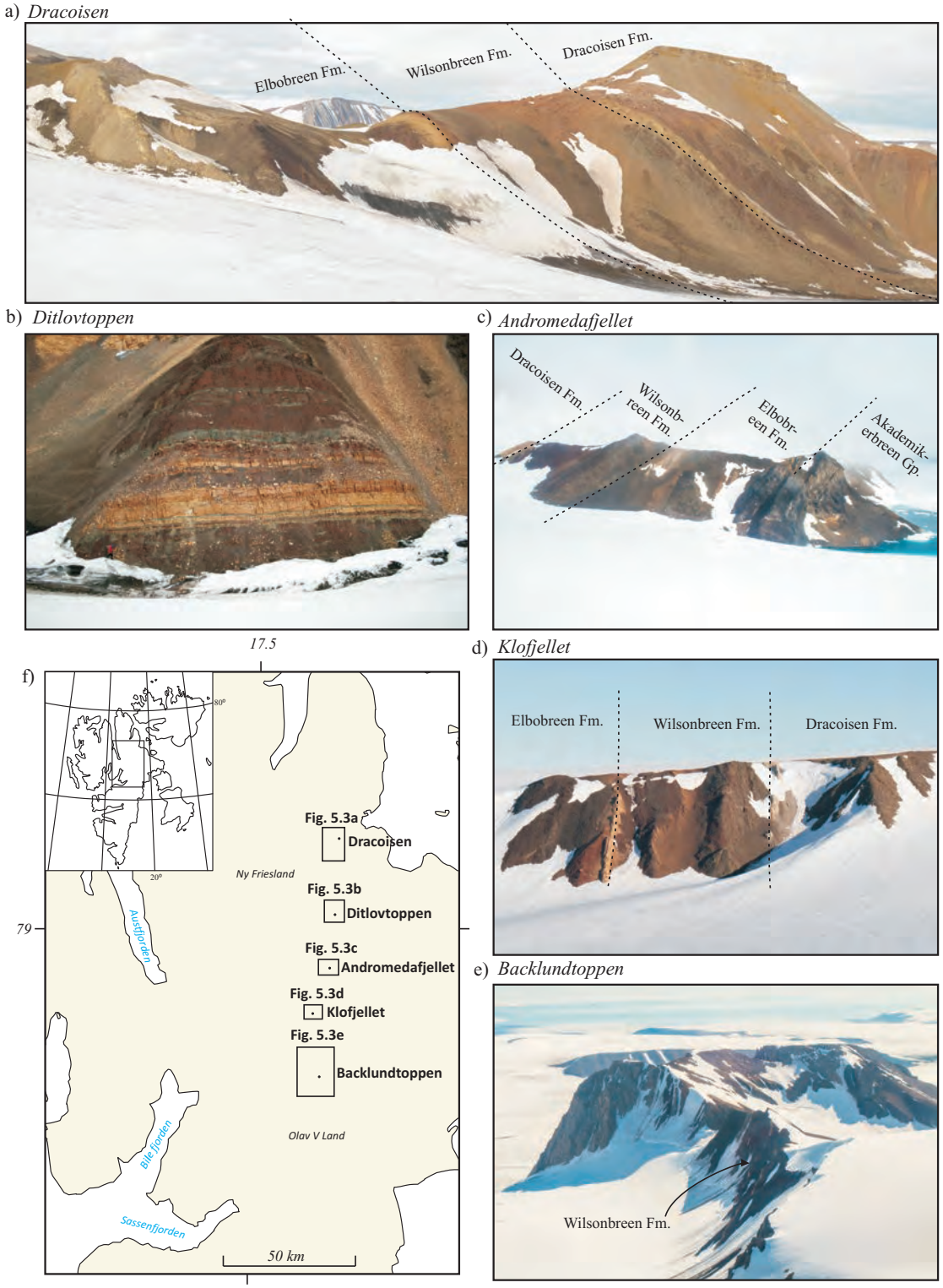

Fig. 5.1 - Field photographs of study sites. (a) Dracoisen showing almost the entire Polarisbreen Group. (b) Ditlovtoppen showing yellow weathering dolomites of the W2 Member surrounded by diamictites of the W1 and W2 Members. (c) Helicopter photograph of Andromedafjellet showing the exposed Polarisbreen Group at Reinsryggen. (d) Klofjellet showing upper Elbobreen, Wilsonbreen and lower Dracoisen Formations exposed on southern cliffs. (e) Backlundtoppen showing upper Wilsonbreen Formation exposure at Pinnsvinfjellet. (f) Simplified map showing study locations referred to in the text; the grey represents area covered by glacier ice.

diamictites were originally studied by Nordenskiöld (1863), but a glacial origin was not proposed until the work of Kulling (1934). Particular attention to the glacigenic rocks was paid by Harland and Wilson (1956) and Wilson and Harland (1964), and their significance in terms of Earth history proposed (Harland, 1964). More detailed sedimentological analyses followed once their global significance was established (Chumakov, 1968; Hambrey, 1982; Fairchild, 1983; Fairchild and Hambrey, 1984; Fairchild et al., 1989). Following the development of the "Snowball Earth" hypothesis (Hoffman et al., 1998), geochemical and stratigraphic analyses of Halverson et al, (2004) were interpreted in this light. The presumption of one glaciation for the whole Polarisbreen Group was later reversed and two separate glacial events were recognised; an older, thinner Petrovbreen Member and younger, thicker Wilsonbreen Formation (Hoffman et al., 2012).

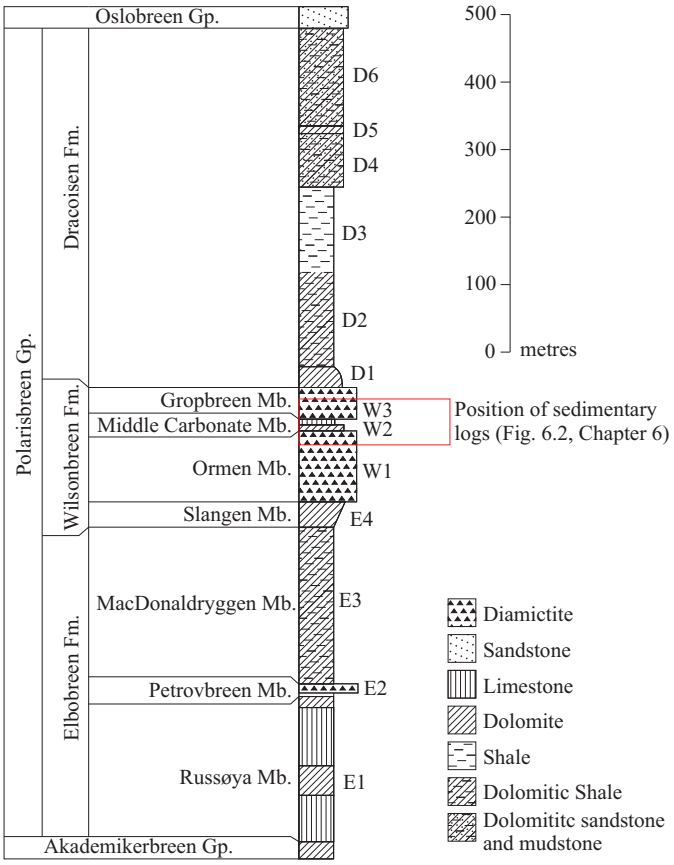

Fig. 5.2 – Summary of the Cryogenian stratigraphy of NE Svalbard with the stratigraphic interval investigated in this chapter shown in red (after Wilson and Harland, 1964; Hambrey, 1982; Fairchild and Hambrey, 1984; Fairchild et al., 1989). Complete logs of the Wilsonbreen Formation in all sections are shown at in Appendix C.

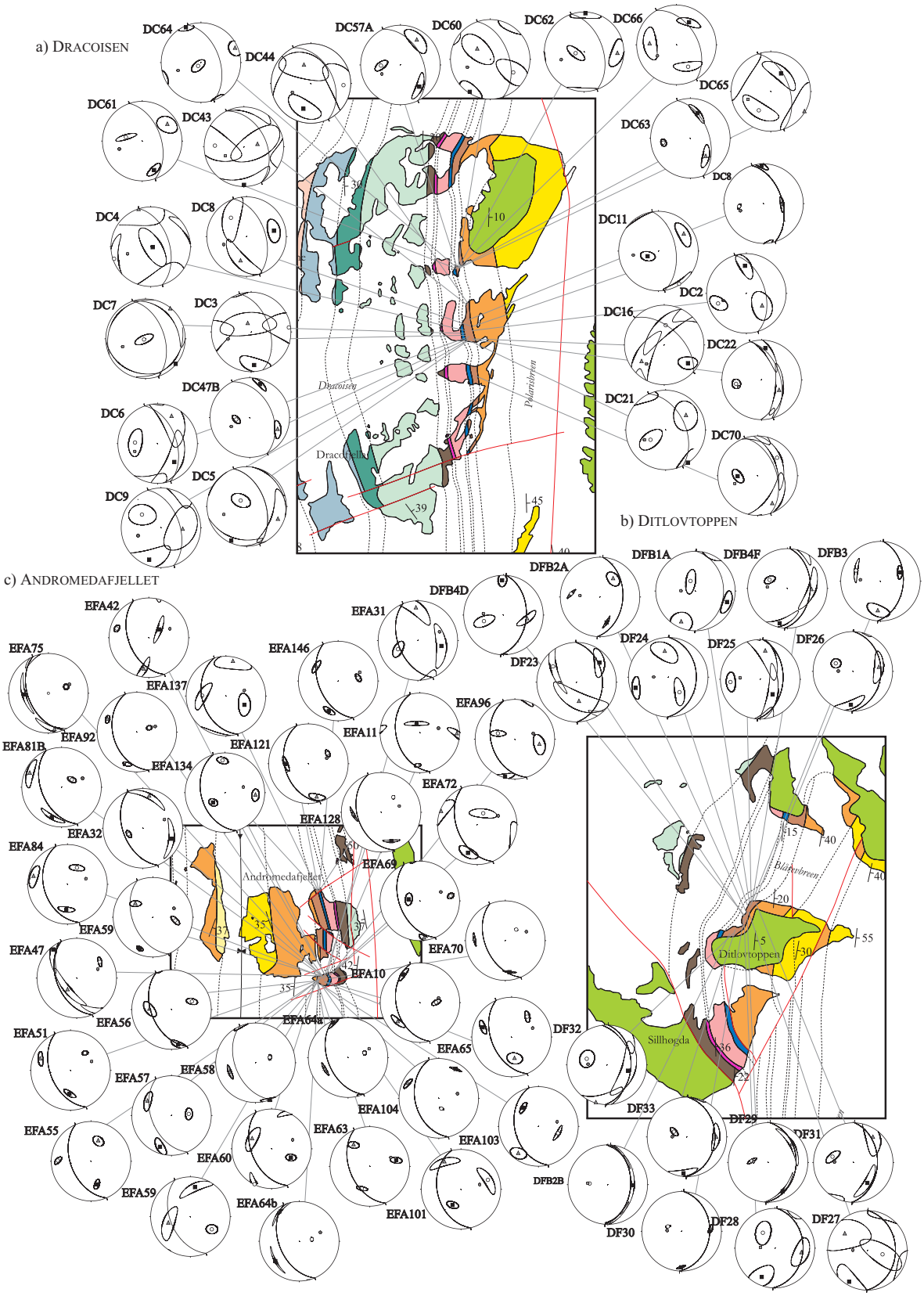

Fig. 5.3 - Geological map with magnetic fabrics for all sites showing K_1 (black squares), K_2 (grey triangles) and K_3 (white circles) with 95% confidence ellipses from (a) Dracoisen, (b) Ditlovtoppen, (c) Andromedafjellet, (d) Klofjellet, (e) Backlundtoppen, displayed on lower-hemisphere, equal-area stereographic projections with bedding (great circles). For the full geological map, see Appendix E.

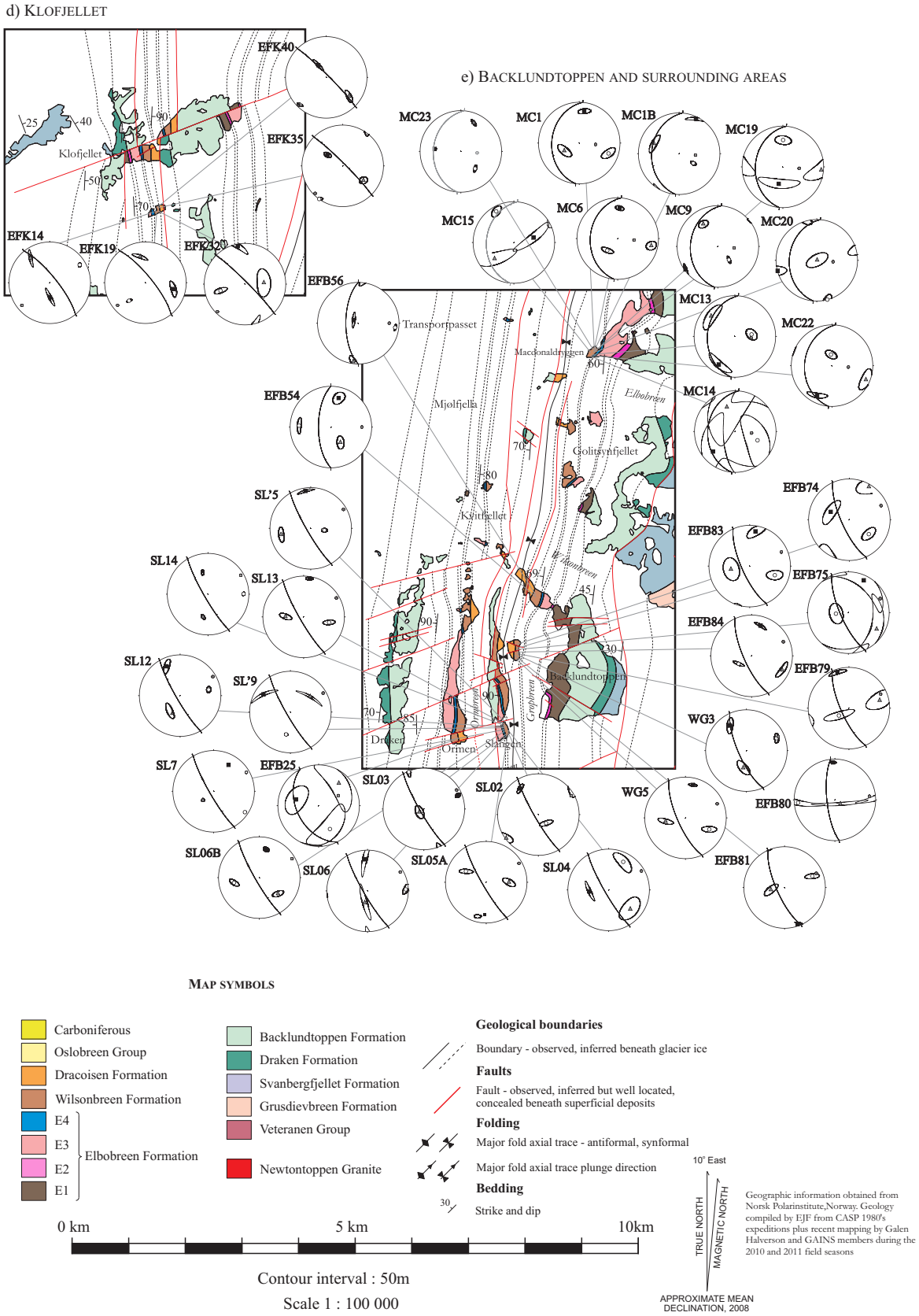

Fig. 5.3 – Continued.

Although no direct radiometric ages have been obtained for the Wilsonbreen Formation, the Dracoisen Formation (overlying the Wilsonbreen Formation) is considered correlative to the Maieberg Formation of northern Namibia, supported by chemostratigraphic and biostratigraphic evidence, which suggests and age of 635 Ma for the end of the Wilsonbreen glaciation (Halverson et al., 2005; Halverson, 2011). The palaeolatitude at deposition is also poorly constrained. The only current (published) palaeomagentic data is from the Akedmeikerbreen Group (underlying the Polarisbreen Group) which gave tropical palaeolatitudes (~15°) during the mid-Neoproterozoic (Maloof et al., 2006).

The Wilsonbreen Formation consists of a 160 - 180 metre, greenish-grey to maroon, massive to poorly bedded diamictite-dominated unit overlying pale dolostones of the Slangen (E4) Member and underlying the Dracoisen Formation (Fig. 5.2). It is divided into three units (see Appendix D): a basal Ormen Member (W1), a Middle Carbonate Member (W2) and an upper Gropbreen Member (W3) (Fairchild and Hambrey, 1984). The Formation is dominated by poorly stratified, greenish-grey to maroon diamictites (Fig. 5.4a and b); although a number of other facies are also seen. These include lenses and interbeds of sandstone and conglomerate (Fig. 5.4e and f), rhythmites, and limestone (Fig. 5.4d). The sediments are typically compositionally and texturally immature. The coarse component is composed of both intrabasinal clasts (including oolitic dolostone, black limestone and chert) and extrabasinal clasts (including quartzite, granite, felsite and gneiss) (Fig. 5.4c). These clasts can normally be easily extracted from weathered, frost-shattered sections for clast-fabric analysis (Fig. 5.4f). The sand-sized fraction is composed of angular to subrounded grains of quartz, feldspar, muscovite, and rock fragments. The fine-grained component grades into a groundmass of dolomicrite with varying proportions of quartz and clay minerals (Wilson and Harland, 1964; Fairchild and Hambrey, 1984)

Deposition of the W1 and W3 Members is interpreted to have occurred in a dominantly subaqueous, ice-marginal land system. Whether this subaqueous deposition is glaciomarine or glaciolacustrine is not clear. Small-scale lakes can produce distinct sequences; however, the depositional architecture of large lakes can be similar to that of marine sedimentation (Wilson

Fig. 5.4 - Typical lithologies sampled. (a) Clast-rich maroon diamictite, Ditlovtoppen (W3). (b) Clast-poor greenish-grey diamictite, with clast-rich zone in centre interpreted as a current-winnowed surface, MacDonaldryggen (W1). (c) Striated boulder pavement within subglacially deposited maroon diamictite indicating ice movement to the NW, Ditlovtoppen (W3). (d) Glaciotectonised rhythmites at the W1/W2 Member boundary showing folding and faulting, Ditlovtoppen. (e) Clast-rich debris flow deposit within greenish-grey diamictites, MacDonaldryggen (W1). (f) Channelised maroon sandstone cutting into maroon diamictite, Andromedafjellet (W3).

and Harland, 1964; Ó Cofaigh and Dowdeswell, 2001). The heavy oxygen isotope values in the dolomitic facies of the W2 Member was used as evidence for strongly evaporative conditions in a lacustrine environment by Fairchild et al. (1989). However, a lack of suitable material in the rest of the sequence mean that such geochemical data is difficult to obtain from other parts of the succession. The construction of the arguments to resolve this issue is beyond the scope of this thesis because it rests on a body of data collected by the team as a whole. As such, for the purposes of this study, the terms subaqueous and glacioaquatic are used where the distinction between lacustrine and marine is ambiguous (as opposed to glaciolacustrine or glaciomarine).

As well as the distinction between glaciomarine and glaciolacustrine, the distinction between subaqueous and subglacial deposition can also be difficult to discern, particularly in massive diamict (Benn and Evans, 2010). Locally, the presence of stratified diamictites with debris-flow deposits suggests a subaqueous origin. However, the presence of possible glaciotectonically deformed sediments (Fig. 5.4d) and striated boulder pavements (Fig. 5.4c) suggests ice-grounding for at least part of the time during the depositional period. The W2 Member is interpreted to have formed during terrestrial and glaciolacustrine conditions in an ice-marginal environment and marks a minor retreat phase during glaciations (Fairchild et al., 1989).

Previous palaeoflow information from the Wilsonbreen Formation is lacking because of limited spatial coverage of exposures and a lack of palaeoflow indicators regionally (Hambrey, 1982). It is widely considered that NE Svalbard was contiguous with NE Greenland during Neoproterozoic time (Fairchild and Hambrey, 1995). Herrington and Fairchild (1989) identified NNE-directed palaeocurrents in turbidites of the early Cryogenian Bed Group 19 of NE Greenland and consequently inferred them to represent axial-basin flow. Moncrieff (1988) and Moncrieff and Hambrey (1990) investigated the glacigenic Storeelv Formation (equivalent of the Wilsonbreen Formation) and concluded dominant ice flow from the SW, based on extensive clast fabric analysis.

In NE Svalbard, previous clast-fabric measurements (Fairchild and Hambrey, 1984; Dowdeswell et al., 1985) and the occurrence of rare cross-beds, slump folds (Hambrey, 1982)

and channel structures suggested that ice may have flowed to the north (Fairchild and Hambrey, 1995). Within the Bråvika Sandstone Member, exposed to the north of the study site and previously considered a lateral equivalent of lowermost Wilsonbreen Formation in the north (Halverson et al., 2004) but now considered more closely related to the Elbobreen Formation (Hoffman et al., 2012), both planar and cross-bedding is observed throughout, which also lead to a tentative interpretation of palaeoflow direction to the north (Halverson et al., 2004). Whilst northerly palaeoflow is therefore suspected, the exact orientations and any the variation between sites or during the depositional period are unknown.

5.4. Methods

Fieldwork was undertaken in NE Svalbard during the summer 2010 (Ny Friesland), spring 2011 and summer 2011 (Olav V land) field seasons. In this region, the Wilsonbreen Formation is exposed in a series of nunataks (Fig. 5.1). Fieldwork involved detailed sedimentological logging (Appendix D), facies analysis, clast-fabric/shape analysis, geological mapping (Appendix E) and sample collection. Samples were typically collected from cliff sections that provided the best exposure (e.g. Fig. 5.1). The majority of the samples collected for AMS analysis were massive, structureless diamictites (Fig. 5.4a and b), but sandstone and siltstone lenses and interbeds were also sampled (Fig. 5.4d and f). The raw field data from the summer 2010 was collected by DB, MJH, CTS and MSP prior to the start of the PhD studentship that this thesis forms part of.

The samples were collected following the methodology outlined in Appendix A. In total, 1295 samples were measured from 113 sites, with an average of 11 subsamples per site. Block samples were also collected for thin section analysis. The AMS of samples was measured following the methodology outlined in Section 2.9. The AMS data was analysed using standard statistical analysis (see Section 2.4.1), involving the calculation of the mean susceptibility (K_{mean}), corrected anisotropy degree (P_j), lineation (L) and foliation (F) parameters and the shape parameter (T) (Jelínek, 1981). The magnetic mineralogy of the samples was investigated utilising the methodology outlined in Chapter 2, Section 2.9. For some analyses, data was corrected for

tectonic tilting by rotation about the bedding strike by the bedding dip. As the plunge of folds was negligible (usually <5°), correction for fold plunge was not necessary.

AMS results were subsequently analysed based on the ellipsoid shape (Fig. 5.5). A 'normal' sedimentary fabric typically produces an AMS ellipsoid where the K_3 axis lies normal to the bedding plane (e.g. Fig. 5.5a). An 'inverse' fabric can be readily identified when the susceptibility axes are seen to have switched, such that K_1 lies perpendicular to bedding and K_3 and K_2 plot in the bedding plane (e.g. Fig. 5.5b). 'Anomalous' fabrics are defined where the K_1/K_2 plane exceeded 25° from the bedding plane (e.g. Fig. 5.5c), such that the fabric displays neither 'normal' nor 'inverse' fabrics characteristics.

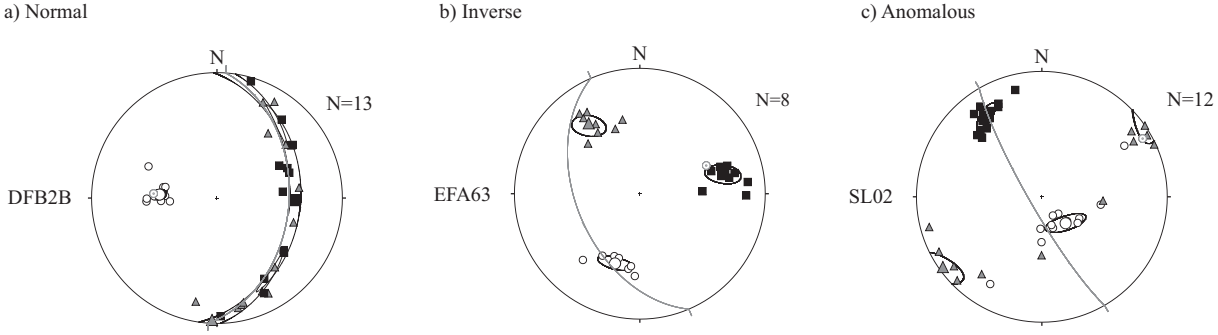

Fig. 5.5 - Styles of AMS fabrics encountered, presented on to showing K_1 (black squares), K_2 (grey triangles) and K_3 (white circles) with 95% confidence ellipses and bedding (grey line). (a) 'Normal' AMS fabric with K_3 perpendicular and K_1/K_2 parallel to the bedding plane. (b) 'Inverse' fabric displaying K_1 perpendicular and K_2/K_3 Parallel to the bedding plane. (c) Anomalous AMS fabric displaying K_2 perpendicular and K_1/K_3 parallel to the bedding plane. Data is displayed on lower-hemisphere, equal-area stereographic projections.

In order to determine the cause of the anomalous AMS fabrics and the reliability of the 'normal' fabrics, the determination of magnetic mineralogy is of importance as different minerals can produce very different fabric characteristics (Tarling and Hrouda, 1993). The rock magnetic experiments used in this chapter are outlined in Chapter 2, Section 2.6. Thermomagnetic experiments were conducted on 71 sites by examining the variation of low-field magnetic susceptibility with temperature (see Section 2.6.1). Demagnetisation of the natural remanent magnetisation (NRM), anhysteretic remanent magnetisation (ARM) and saturation isothermal remanent magnetisation (SIRM) were carried out on 30 samples, following the approach by

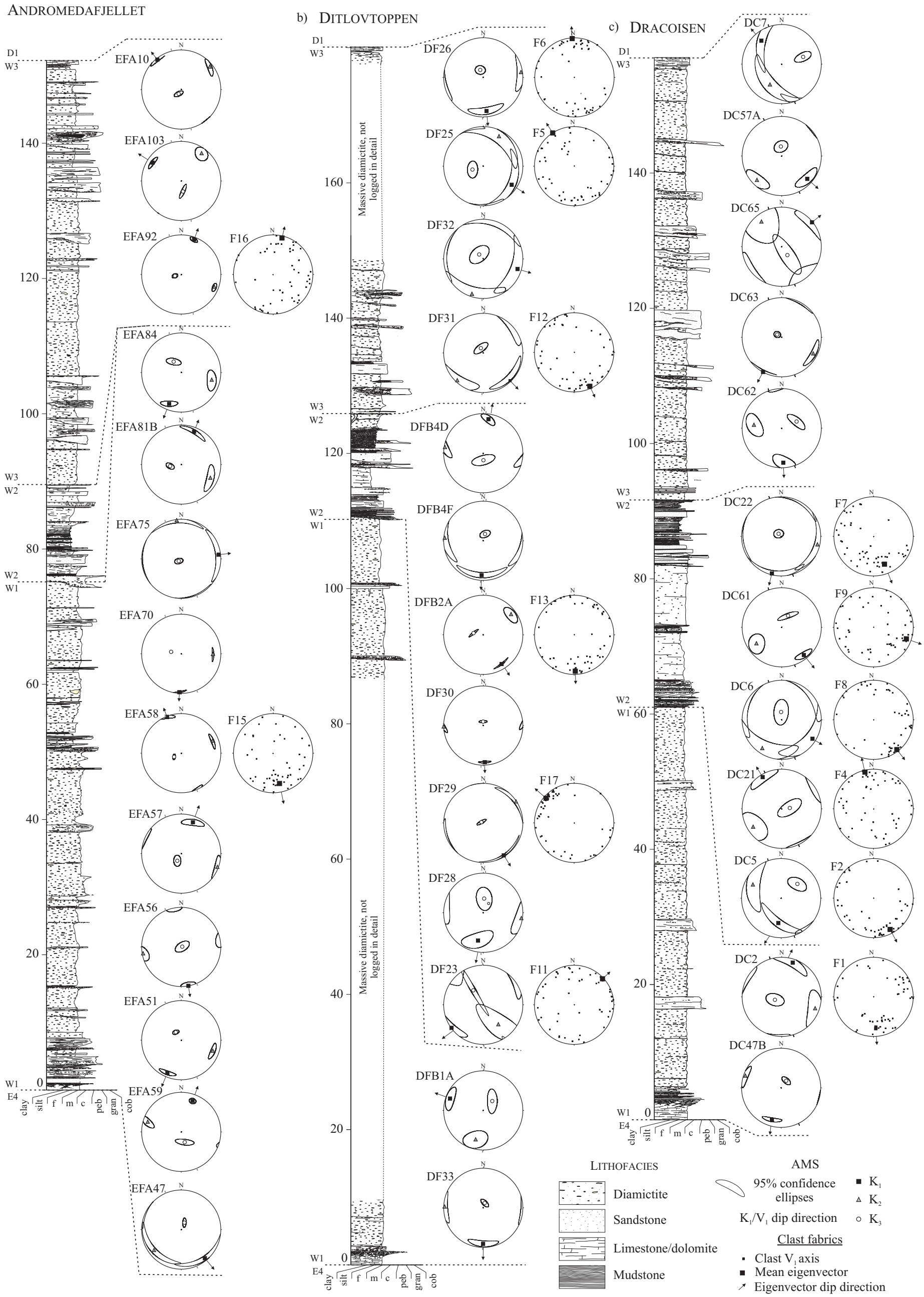

Fig. 5.6 - Sedimentary log through the Wilsonbreen Formation with representative AMS fabrics and clast fabrics, both rotated to palaeohorizontal, at (a) Andromedafjellet, (b) Ditlovtoppen and (c) Dracoisen, displayed on lower-hemisphere, equal-area stereographic projections.

Lowrie (1990) and outlined in Section 2.6.3. Finally, Isothermal remanent magnetism (IRM) and backfield isothermal remanent magnetisation (BIRM) experiments were conducted on 30 samples, following the procedure outlined in Section 2.6.4. In addition to the rock magnetic-experiments, polished thin sections were made of 6 samples for opaque mineral analysis. These were examined under polarised transmitted light and reflected light.

Clast fabrics were measured from Dracoisen, Ditlovtoppen and Andromedafjellet at 16 sites (Fig. 5.6). At each location, the azimuth and plunge of the long (a-) axis was measured using a Brunton compass. Clast fabrics were analysed using the eigenvalue method (Mark, 1973), where the data are resolved into three mutually orthogonal eigenvectors (V_1, V_2 and V_3), where V_3 is normal to the plane of the fabric. The shape of the fabric is represented by the eigenvalue S_1, S_2 and S_3. This is represented by three end-members where the fabric can cluster, girdle or be isotropic (Benn, 1995). In order to obtain clast fabrics, the lithology had to be sufficiently 'shaley' and weathered such that the clasts could be separated from the matrix and extracted. Clast-fabric measurements were not measured in the southern localities (Klofjellet and Backlundtoppen) because of a lack of suitable sites.

5.5. Rock magnetism

Prior to any fabric interpretation, the determination of the magnetic mineralogy is vital as different minerals can produce very different fabric characteristics. The susceptibility of the samples analysed ranges between 5 and 532 $\times 10^{-6}$ (~267 $\times 10^{-6}$) in SI units (Table 5.1). Tarling and Hrouda (1993) suggested that as a general rule of thumb, assuming paramagnetic minerals are common constituents (10%), the anisotropy and susceptibility is controlled by (i) the ferromagnetic fraction if the susceptibility is higher than 5000 $\times 10^{-6}$; (ii) the paramagnetic fraction if susceptibility is lower than 500 $\times 10^{-6}$; and (iii) both the ferromagnetic and paramagnetic fraction, if the susceptibility is between 500 and 5000 $\times 10^{-6}$ (Fig. 2.5, Chapter 2). As the majority of the sites have a susceptibility of less than 500 $\times 10^{-6}$, it is likely that the paramagnetic fraction plays an important role (see Chapter 2, Section 2.6). However, because

Site	Date collected	Lat/long		Lithology	Location	Unit	Bedding	Dip	N	Km (SI)	K_1		K_1 95% Error		K_2		K_2 95% Error		K_3		K_3 95% Error		L	F	P_j	T	Fabric
DC11	26/07/2010	79.2062	18.4092	Diamictite	Dracoisen	W3	351	54	7	108	237	65	15	9	49	24	24	13	141	3	25	7	1.003	1.005	1.008	0.241	Inverse
DC16	29/07/2010	79.2044	18.4142	Diamictite	Dracoisen	W3	313	55	13	326	121	26	23	12	226	30	74	17	357	49	74	17	1.008	1.001	1.009	-0.84	Intermediate
DC2	24/07/2010	79.2055	18.4020	Diamictite	Dracoisen	W1	343	51	18	336	350	31	32	11	122	48	32	20	243	25	21	12	1.003	1.005	1.008	0.273	Normal
DC21	29/07/2010	79.2046	18.4099	Sandstone	Dracoisen	W2	335	49	18	115	139	1	26	14	48	37	30	25	230	53	30	14	1.002	1.001	1.003	-0.078	Normal
DC22	29/07/2010	79.2048	18.4110	Rhythmites	Dracoisen	W2	343	51	15	232	360	21	54	8	114	47	54	9	254	35	10	9	1.001	1.016	1.019	0.874	Normal
DC3	24/07/2010	79.2056	18.4033	Diamictite	Dracoisen	W1	343	51	12	71	168	18	30	16	331	72	61	24	76	5	61	23	1.004	1.001	1.006	-0.53	Intermediate
DC4	24/07/2010	79.2056	18.4048	Diamictite	Dracoisen	W1	343	51	10	216	97	86	46	18	335	2	49	34	225	4	43	10	1.001	1.004	1.005	0.505	Intermediate
DC43	30/07/2010	79.2105	18.4069	Sandstone	Dracoisen	W3	334	43	9	92	173	5	53	15	74	62	61	26	265	28	60	25	1.002	1.002	1.003	-0.129	Normal
DC44	31/07/2010	79.2105	18.4064	Sandstone	Dracoisen	W3	334	43	12	454	190	34	35	19	332	50	54	27	86	19	53	28	1.004	1.002	1.006	-0.467	Inverse
DC47B	01/08/2010	79.2056	18.4051	Diamictite	Dracoisen	W1	334	43	11	284	219	5	17	5	129	3	18	7	12	84	11	6	1.008	1.013	1.022	0.223	Normal
DC5	24/07/2010	79.2057	18.4056	Carbonate	Dracoisen	W2	341	51	6	123	194	6	51	9	106	16	51	17	308	73	21	13	1.001	1.002	1.003	0.09	Normal
DC57	02/08/2010	79.2153	18.3980	Diamictite	Dracoisen	W3	334	43	10	272	132	28	27	7	27	26	27	15	261	50	16	7	1.004	1.006	1.01	0.251	Normal
DC6	24/07/2010	79.2056	18.4073	Rhythmites	Dracoisen	W2	341	51	11	188	131	38	62	17	20	25	62	23	266	43	27	15	1.002	1.024	1.026	-0.844	Normal
DC60	02/08/2010	79.2154	18.3978	Carbonate	Dracoisen	W2	341	51	12	64	205	4	22	18	301	56	43	20	123	34	43	18	1.002	1.001	1.004	-0.337	Intermediate
DC61	02/08/2010	79.2153	18.3979	Diamictite	Dracoisen	W2	341	51	17	198	151	22	16	7	50	25	22	16	277	55	23	5	1.004	1.008	1.013	0.299	Normal
DC62	02/08/2010	79.2153	18.3979	Diamictite	Dracoisen	W3	341	51	10	216	355	4	24	13	86	17	26	15	254	73	22	9	1.004	1.009	1.014	0.448	Normal
DC63	02/08/2010	79.2153	18.3982	Diamictite	Dracoisen	W3	341	51	18	260	9	25	25	6	133	40	24	7	254	32	7	6	1.002	1.011	1.015	0.657	Normal
DC64	02/08/2010	79.2152	18.3991	Diamictite	Dracoisen	W3	341	51	12	232	330	4	13	9	60	8	16	12	213	81	17	9	1.006	1.012	1.018	0.339	Normal
DC65	02/08/2010	79.2151	18.4003	Diamictite	Dracoisen	W3	330	46	18	50	23	47	41	15	114	2	45	35	206	43	40	17	1.003	1.002	1.005	-0.096	Normal
DC66	02/08/2010	79.2151	18.4005	Sandstone	Dracoisen	W3	330	46	9	119	22	35	23	8	265	33	31	15	145	38	28	10	1.005	1.004	1.009	-0.132	Intermediate
DC7	24/07/2010	79.2058	18.4082	Carbonate	Dracoisen	W3	341	51	11	239	123	2	64	9	33	3	64	14	239	87	20	8	1.002	1.009	1.012	0.663	Normal
DC70	03/08/2010	79.1993	18.3890	Diamictite	Dracoisen	W3	341	51	9	430	114	17	20	7	230	54	20	7	14	30	8	7	1.002	1.004	1.006	0.391	Intermediate
DC8	26/07/2010	79.2061	18.4084	Diamictite	Dracoisen	W3	341	51	10	145	71	30	22	15	187	37	49	14	313	38	48	18	1.005	1.003	1.008	-0.183	Intermediate
DC8	24/07/2010	79.2055	18.4020	Diamictite	Dracoisen	W1	343	51	14	191	350	4	15	5	85	52	15	4	257	38	6	2	1.004	1.038	1.047	0.814	Normal
DC9	26/07/2010	79.2061	18.4090	Diamictite	Dracoisen	W3	341	51	18	272	193	16	48	19	87	44	48	30	298	42	30	20	1.002	1.005	1.007	0.402	Normal
DF23	11/08/2010	79.0817	18.4097	Diamictite	Ditlovtoppen	W2	359	35	10	161	42	26	30	11	166	49	63	18	297	29	62	7	1.007	1.004	1.011	-0.28	Normal
DF24	11/08/2010	79.0818	18.4096	Sandstone	Ditlovtoppen	W2	001	30	8	50	245	15	20	10	345	35	31	17	136	51	30	10	1.004	1.002	1.006	-0.255	Intermediate
DF25	11/08/2010	79.0816	18.4104	Diamictite	Ditlovtoppen	W3	004	42	15	357	133	50	62	10	3	29	62	15	258	26	17	11	1.001	1.021	1.025	0.9	Normal
DF26	11/08/2010	79.0815	18.4103	Diamictite	Ditlovtoppen	W3	001	30	9	368	176	17	30	9	75	34	30	10	288	51	10	9	1.004	1.015	1.021	0.557	Normal
DF27	11/08/2010	79.0813	18.4098	Sandstone	Ditlovtoppen	W2	001	30	11	52	203	10	35	19	299	31	54	29	98	58	53	19	1.002	1.001	1.003	-0.58	Intermediate
DF28	11/08/2010	79.0813	18.4098	Sandstone	Ditlovtoppen	W2	003	30	13	5	198	21	33	16	93	32	29	16	315	49	25	15	1.054	1.078	1.137	0.177	Normal
DF29	11/08/2010	79.0809	18.4079	Rhythmites	Ditlovtoppen	W2	003	30	15	197	146	20	39	3	46	26	39	5	269	56	11	3	1.002	1.029	1.035	0.881	Normal
DF30	11/08/2010	79.0809	18.4079	Rhythmites	Ditlovtoppen	W2	003	30	13	147	174	10	8	2	78	28	9	3	282	60	5	2	1.004	1.036	1.045	0.799	Normal
DF31	11/08/2010	79.0807	18.4077	Diamictite	Ditlovtoppen	W3	002	39	16	395	139	38	37	8	31	21	38	15	279	45	17	7	1.004	1.012	1.016	0.536	Normal
DF32	11/08/2010	79.0807	18.4077	Diamictite	Ditlovtoppen	W3	002	39	11	446	98	44	57	16	189	1	57	16	280	46	17	16	1.003	1.009	1.013	0.477	Normal
DF33	11/08/2010	79.0808	18.4034	Diamictite	Ditlovtoppen	W1	001	30	12	200	178	9	25	8	84	27	25	8	285	61	11	5	1.001	1.005	1.007	0.605	Normal
DFB1A	11/08/2010	79.0824	18.4104	Diamictite	Ditlovtoppen	W1	004	42	12	216	103	17	20	11	197	14	26	18	325	68	26	10	1.003	1.002	1.006	-0.203	Normal
DFB2A	11/08/2010	79.0819	18.4093	Diamictite	Ditlovtoppen	W2	004	42	7	186	159	34	15	2	29	43	15	12	269	28	12	2	1.004	1.008	1.012	0.396	Normal
DFB4D	11/08/2010	79.0833	18.4129	Rhythmites	Ditlovtoppen	W2	004	42	12	435	351	14	16	7	92	40	25	7	256	47	25	10	1.007	1.005	1.011	-0.152	Normal
DFB2B	11/08/2010	79.0833	18.4129	Rhythmites	Ditlovtoppen	W2	004	42	13	194	85	38	59	4	175	1	59	3	267	52	4	3	1.001	1.011	1.013	0.873	Normal
DFB3	11/08/2010	79.0837	18.4139	Rhythmites	Ditlovtoppen	W2	004	42	9	150	59	46	13	5	178	26	23	13	287	33	23	4	1.004	1.009	1.013	0.361	Normal
DFB4F	11/08/2010	79.0833	18.4129	Rhythmites	Ditlovtoppen	W2	004	42	8	579	186	11	44	7	86	39	44	9	289	49	12	7	1.004	1.023	1.029	0.676	Normal
EFA121	20/07/2011	78.9528	18.4257	Sandstone	Andromedafjellet E	W2	253	40	12	171	263	42	16	4	160	14	16	7	55	45	7	5	1.005	1.003	1.008	-0.273	Normal
EFA128	20/07/2011	78.9528	18.4257	Diamictite	Andromedafjellet E	W3	251	40	7	409	154	24	16	3	259	30	15	2	32	50	4	2	1.005	1.02	1.027	0.578	Normal
EFA134	20/07/2011	78.9528	18.4257	sandstone	Andromedafjellet E	W1	253	40	10	406	234	58	9	7	88	24	11	9	349	20	11	7	1.005	1.011	1.017	0.376	Intermediate
EFA137	20/07/2011	78.9528	18.4257	Diamictite	Andromedafjellet E	W1	253	40	12	159	108	47	23	13	5	12	31	19	264	40	30	10	1.003	1.004	1.006	0.164	Inverse
EFA146	24/07/2011	78.9528	18.4257	Diamictite	Andromedafjellet E	W3	251	40	11	561	190	22	12	6	296	34	13	6	74	48	9	5	1.008	1.01	1.018	0.108	Normal
EFA10	11/07/2011	78.9383	18.4281	Sandstone	Reinsryggen	W3	256	40	9	496	322	18	14	4	222	27	16	6	82	57	10	5	1.006	1.011	1.018	0.261	Normal
EFA101	19/07/2011	78.9383	18.4325	Diamictite	Reinsryggen	W3	256	40	11	521	201	53	12	7	322	21	28	9	64	29	28	10	1.011	1.005	1.016	-0.325	Normal
EFA103	19/07/2011	78.9383	18.4325	Diamictite	Reinsryggen	W3	256	40	12	533	298	12	12	5	31	13	16	12	165	74	16	4	1.013	1.017	1.031	0.116	Normal
EFA104	19/07/2011	78.9383	18.4325	Diamictite	Reinsryggen	W3	256	40	12	419	23	16	10	2	289	14	10	4	159	68	5	2	1.007	1.033	1.043	0.658	Intermediate
EFA11	11/07/2011	78.9383	18.4281	Diamictite	Reinsryggen	W3	256	40	13	536	334	69	25	5	85	8	25	5	177	19	6	4	1.003	1.028	1.034	0.81	Intermediate
EFA42	16/07/2011	78.9386	18.4400	Sandstone	Reinsryggen	W1	247	48	12	190	45	62	31	5	182	21	31	5	279	17	7	6	1.001	1.003	1.004	0.611	Intermediate

Table 5.1- Mean site AMS data for the Wilsonbreen Formation (see Chapter 2, Section 2.4.1 for calculation): N = number of samples; Km = mean susceptibility; K_1, K_2, K_3 = orientations (declination and inclination) of the principal susceptibility axes with 95% confidence ellipses; L = lineation ($L = K_1/K_2$); F = foliation ($F = K_2/K_3$); P_j = anisotropy degree; T = shape parameter; Fabric = whether the fabric can be classified as 'normal' (K_3 perpendicular, K_1/K_2 parallel to the bedding plane), 'inverse' (K_1 perpendicular and K_2/K_3 Parallel to the bedding plane) or anomalous (K_1/K_2 deviation by >25° from bedding).

EFA47	16/07/2011	78.9386	18.4400	Diamictite	Reinsryggen	W1	247	48	12	254	314	7	50	6	211	59	50	7	48	30	10	4	1.001	1.018	1.021	0.891	Normal
EFA49	17/07/2011	78.9386	18.4400	Sandstone	Reinsryggen	W1	247	48	10	223	196	15	6	5	301	44	12	6	91	43	12	5	1.004	1.005	1.009	0.152	Normal
EFA51A	17/07/2011	78.9386	18.4400	Diamictite	Reinsryggen	W1	247	48	10	264	176	41	14	5	284	20	14	6	33	43	7	4	1.004	1.009	1.013	0.355	Normal
EFA55	17/07/2011	78.9386	18.4400	Diamictite	Reinsryggen	W1	247	48	12	218	159	40	12	4	13	45	12	9	264	18	10	4	1.003	1.006	1.003	0.328	Intermediate
EFA56	17/07/2011	78.9386	18.4400	Diamictite	Reinsryggen	W1	247	48	12	408	162	11	17	6	264	44	19	9	62	44	12	6	1.005	1.003	1.014	0.343	Normal
EFA57	17/07/2011	78.9386	18.4400	Diamictite	Reinsryggen	W1	247	48	12	386	193	17	20	8	294	30	19	8	78	54	12	8	1.003	1.008	1.011	0.472	Normal
EFA58	17/07/2011	78.9386	18.4400	Diamictite	Reinsryggen	W1	247	48	8	460	152	0	14	4	243	32	13	4	62	58	6	3	1.007	1.028	1.037	0.61	Normal
EFA59	17/07/2011	78.9386	18.4400	Diamictite	Reinsryggen	W1	247	48	12	389	2	26	36	9	346	42	36	12	114	37	13	9	1.002	1.014	1.017	0.736	Normal
EFA60	17/07/2011	78.9386	18.4400	Diamictite	Reinsryggen	W1	247	48	12	107	107	48	11	6	290	44	25	11	199	1	25	5	1.006	1.006	1.011	-0.001	Normal
EFA63	17/07/2011	78.9386	18.4400	Siltstone	Reinsryggen	W1	247	48	8	532	70	32	13	5	316	33	12	6	193	41	11	4	1.007	1.032	1.042	0.622	Inverse
EFA64A	17/07/2011	78.9386	18.4400	Diamictite	Reinsryggen	W1	247	48	8	376	330	5	13	4	237	35	13	2	67	55	4	3	1.012	1.033	1.047	0.481	Normal
EFA64B	17/07/2011	78.9386	18.4400	Diamictite	Reinsryggen	W1	247	48	9	262	223	23	27	2	319	12	27	2	74	64	4	2	1.003	1.035	1.042	0.826	Normal
EFA65	17/07/2011	78.9386	18.4400	Diamictite	Reinsryggen	W1	247	48	11	412	282	24	15	5	165	45	15	12	30	36	12	5	1.005	1.015	1.021	0.468	Normal
EFA69	18/07/2011	78.9386	18.4400	Diamictite	Reinsryggen	W1	247	48	10	349	271	67	12	7	166	6	12	5	74	22	8	4	1.007	1.023	1.032	0.553	Normal
EFA70	18/07/2011	78.9386	18.4400	Diamictite	Reinsryggen	W1	247	48	7	641	165	21	12	2	265	23	12	2	38	58	3	1	1.006	1.053	1.065	0.78	Normal
EFA72	18/07/2011	78.9386	18.4400	Diamictite	Reinsryggen	W1	247	48	12	377	191	26	19	11	283	4	30	14	20	64	28	9	1.005	1.008	1.012	0.218	Normal
EFA75	18/07/2011	78.9386	18.4400	Siltstone	Reinsryggen	W1	247	48	12	419	260	38	41	4	163	8	40	5	63	51	6	5	1.004	1.016	1.022	0.573	Normal
EFA81B	18/07/2011	78.9386	18.4400	Diamictite	Reinsryggen	W1	247	48	19	325	191	22	24	5	287	14	24	9	47	64	10	5	1.006	1.017	1.023	0.492	Normal
EFA84	18/07/2011	78.9386	18.4400	Diamictite	Reinsryggen	W1	247	48	10	361	176	37	16	6	276	13	19	11	23	50	16	7	1.004	1.007	1.011	0.215	Normal
EFA92	19/07/2011	78.9383	18.4325	Diamictite	Reinsryggen	W3	253	40	11	227	190	17	7	5	287	20	7	5	64	63	6	4	1.007	1.008	1.015	0.087	Normal
EFA96	19/07/2011	78.9383	18.4325	Sandstone	Reinsryggen	W3	253	40	12	464	188	3	17	6	95	37	20	12	282	53	16	6	1.009	1.006	1.015	-0.212	Intermediate
EFK14	26/08/2011	78.8369	18.1534	Diamictite	Klofjellet South	W3	051	77	10	545	172	61	20	3	315	24	20	3	52	16	4	3	1.005	1.031	1.038	0.731	Normal
EFK19	26/08/2011	78.8369	18.1534	Diamictite	Klofjellet South	W3	051	77	8	491	96	31	16	5	342	35	16	3	215	40	6	2	1.003	1.059	1.071	0.888	Normal
EFK32	27/08/2011	78.8369	18.1534	Sandstone	Klofjellet South	W1	045	85	11	211	342	5	27	5	79	52	27	15	248	38	15	5	1.002	1.004	1.006	0.457	Intermediate
EFK35	27/08/2011	78.8369	18.1534	Diamictite	Klofjellet South	W1	045	85	12	402	299	52	8	4	118	38	9	7	208	0	8	3	1.005	1.019	1.026	0.549	Normal
EFK40	27/08/2011	78.8369	18.1534	Diamictite	Klofjellet South	W1	045	85	12	480	320	61	16	3	123	28	16	4	127	7	5	3	1.007	1.046	1.058	0.736	Normal
MC1	26/04/2011	78.7673	18.2150	Diamictite	Mcdonaldryggen	W1	275	33	11	337	2	33	11	6	235	56	16	8	103	25	16	8	1.004	1.002	1.006	-0.286	Normal
MC13	26/04/2011	78.7673	18.2150	Diamictite	Mcdonaldryggen	W1	275	33	12	277	203	22	25	8	303	25	26	12	76	56	13	9	1.002	1.005	1.007	0.413	Normal
MC14	26/04/2011	78.7673	18.2150	Diamictite	Mcdonaldryggen	W1	275	33	12	92	221	27	77	25	334	37	77	34	104	41	57	24	1.001	1.004	1.006	0.542	Normal
MC15	26/04/2011	78.7673	18.2150	Sandstone	Mcdonaldryggen	W1	275	33	13	39	69	49	49	8	223	38	49	11	323	13	12	8	1.002	1.015	1.018	0.778	Inverse
MC19	26/04/2011	78.7673	18.2150	Sandstone	Mcdonaldryggen	W1	275	33	13	12	187	55	41	10	88	6	42	12	354	35	15	10	1.001	1.032	1.045	0.489	Intermediate
MC1B	26/04/2011	78.7673	18.2150	Diamictite	Mcdonaldryggen	W1	275	33	10	241	19	6	18	3	285	34	18	6	117	56	6	3	1.004	1.011	1.016	0.495	Normal
MC20	26/04/2011	78.7673	18.2150	Diamictite	Mcdonaldryggen	W1	275	33	12	366	248	1	24	7	58	90	24	12	158	0	13	6	1.002	1.007	1.01	0.504	Intermediate
MC22	26/04/2011	78.7673	18.2150	Sandstone	Mcdonaldryggen	W1	275	33	9	126	200	9	18	6	106	11	18	12	348	68	12	7	1.003	1.005	1.008	0.243	Normal
MC23	26/04/2011	78.7673	18.2150	Sandstone	Mcdonaldryggen	W1	275	33	10	323	269	36	3	2	17	24	8	2	133	45	8	2	1.006	1.008	1.015	0.117	Normal
MC6	26/04/2011	78.7673	18.2150	Diamictite	Mcdonaldryggen	W1	275	33	10	239	357	26	8	5	95	17	13	7	214	58	13	5	1.006	1.006	1.012	-0.034	Intermediate
MC9	26/04/2011	78.7673	18.2150	Diamictite	Mcdonaldryggen	W1	275	33	12	208	228	3	10	3	320	35	10	8	133	55	8	2	1.005	1.01	1.016	0.317	Normal
EFB74	05/08/2011	78.7193	18.1642	Sandstone-cc	pinnsvinfjellet	W3	246	74	12	91	286	49	27	11	24	7	27	14	120	40	16	10	1.001	1.007	1.009	0.655	Intermediate
EFB75	05/08/2011	78.7193	18.1642	Sandstone-cc	pinnsvinfjellet	W3	246	74	13	96	18	13	62	18	113	21	62	14	258	65	20	14	1.001	1.004	1.006	0.533	Intermediate
EFB79	05/08/2011	78.7193	18.1642	Sandstone-cc	pinnsvinfjellet	W3	246	74	10	265	335	9	14	5	69	23	33	13	227	65	33	7	1.004	1.003	1.008	-0.085	Intermediate
EFB80	05/08/2011	78.7193	18.1642	Diamictite	pinnsvinfjellet	W3	246	74	11	348	350	9	5	3	120	76	60	3	259	10	60	4.1	1.017	1.001	1.021	-0.885	Tectonic
EFB81	05/08/2011	78.7193	18.1642	Diamictite	pinnsvinfjellet	W3	246	74	12	515	153	5	8	5	253	62	17	6	61	27	17	5	1.01	1.01	1.021	-0.013	Normal
EFB83	05/08/2011	78.7193	18.1642	Diamictite	pinnsvinfjellet	W3	246	74	11	398	2	15	21	8	263	51	22	16	103	35	18	8	1.006	1.009	1.015	0.164	Normal
WG3	27/04/2011	78.7189	18.1661	Diamictite	pinnsvinfjellet	W3	246	74	9	283	320	27	17	5	184	54	17	8	61	21	9	5	1.004	1.01	1.014	0.461	Normal
WG5	27/04/2011	78.7189	18.1661	Diamictite	pinnsvinfjellet	W3	246	74	9	583	5	18	7	3	253	49	17	5	109	35	17	5	1.019	1.016	1.035	-0.078	Normal
EFB84	05/08/2011	78.7193	18.1642	Diamictite	pinnsvinfjellet	W3	246	74	10	301	10	24	12	3	108	18	16	6	232	59	12	3	1.003	1.006	1.01	0.301	Intermediate
SL02	24/04/2011	78.7061	18.1593	Diamictite	Slangen South	W1	240	82	12	336	318	23	10	4	227	2	13	8	131	67	14	5	1.007	1.002	1.01	-0.467	Intermediate
SL03	24/04/2011	78.7061	18.1593	Diamictite	Slangen South	W1	240	82	12	283	61	11	8	3	228	79	14	8	331	2	14	3	1.012	1.008	1.02	-0.222	Inverse
SL04	24/04/2011	78.7061	18.1593	Diamictite	Slangen South	W1	240	82	10	254	259	51	21	3	125	30	23	18	21	23	23	11	1.008	1.004	1.013	-0.317	Intermediate
SL05A	24/04/2011	78.7061	18.1593	Diamictite	Slangen South	W1	240	82	12	213	187	15	6	4	83	44	15	6	291	43	15	4	1.008	1.004	1.012	-0.288	Intermediate
SL06	24/04/2011	78.7061	18.1593	Diamictite	Slangen South	W1	240	82	9	361	348	23	38	4	187	66	39	5	81	7	10	5	1.004	1.011	1.015	0.467	Normal
SL06B	24/04/2011	78.7061	18.1593	Diamictite	Slangen South	W1	240	82	12	281	7	30	6	5	134	39	12	6	252	37	11	5	1.007	1.006	1.013	-0.04	Intermediate
SL12	24/04/2011	78.7061	18.1593	Diamictite	Slangen South	W1	240	82	12	121	330	22	16	5	207	52	16	6	71	29	6	5	1.004	1.008	1.012	0.333	Normal
SL13	24/04/2011	78.7061	18.1593	Diamictite	Slangen South	W1	240	82	12	308	1	5	5	4	264	53	13	5	95	36	13	4	1.009	1.006	1.014	-0.198	Intermediate
SL14	24/04/2011	78.7061	18.1593	Diamictite	Slangen South	W1	240	82	12	240	339	44	5	3	186	42	6	3	83	14	3	2	1.006	1.008	1.014	0.177	Normal
SL'5	24/04/2011	78.7061	18.1593	Diamictite	Slangen South	W1	240	82	12	244	345	8	13	3	251	26	13	6	91	62	58	4	1.004	1.015	1.02	0.549	Intermediate
SL7	24/04/2011	78.7061	18.1593	Diamictite	Slangen South	W1	240	82	12	217	22	26	3	2	223	62	3	3	117	9	3	2	1.006	1.017	1.024	0.467	Intermediate
SL'9	24/04/2011	78.7061	18.1593	Diamictite	Slangen South	W1	240	82	11	253	296	22	28	3	45	39	28	2	184	43	3	3	1.001	1.02	1.021	1.024	Intermediate
EFB25	01/08/2011	78.7040	18.1234	Diamictite	Orman South	W3	243	45	10	150	278	42	30	20	35	27	53	21	147	37	51	20	1.004	1.002	1.006	-0.377	Intermediate
EFB54	02/08/2011	78.7295	18.1706	Sandstone	K-B Ridge	W3	270	65	12	197	8	27	16	9	142	53	14	7	266	23	14	5	1.006	1.015	1.022	0.445	Intermediate
EFB56	02/08/2011	78.7295	18.1706	Diamictite	K-B Ridge	W3	270	65	7	691	297	79	16	2	181	5	16	4	90	10	5	2	1.006	1.018	1.024	0.509	Normal

Table 5.1- Continued.

ferromagnetic minerals can produce contrasting fabric patterns, their influence needs to be determined.

Two dominant rock magnetic characteristics have been identified from the data. The results are grouped into those taken from sediments where the matrix is greenish-grey and those where the matrix is reddened (maroon).

5.5.1. Greenish-grey sediments

Representative examples of the variation of low-field susceptibility versus temperature from the greenish-grey sediments are shown in Figure 5.7. The susceptibility versus temperature in the high temperature range on heating and cooling is shown in Figure 5.7i, whilst the normalised low-temperature (77 K to 295 K) range and the heating curve from the normalised high-temperature susceptibility variation is shown in Figure 5.7ii. All samples reveal strong temperature-dependent susceptibility. In the low-temperature range (Fig. 5.7ii), samples typically show a decrease in susceptibility with increasing temperature, generally following the Curie-Weiss law (cf. Fig. 2.8, Chapter 2). Samples MC14 (Fig. 5.7a) and SL14 (Fig. 5.7b) decrease from a normalised susceptibility of 2.2 and 2.9 K/K_0 respectively whereas EFA60 (Fig. 5.7c) decreases from a lower value of 1.6 K/K_0.

In the high-temperature range, the Curie-Weiss behaviour is less apparent. Samples typically show a decrease in susceptibility up to 200 °C, after which susceptibility increases. A sharp increase is seen in samples SL14 (Fig. 5.7b) and EFA60 (Fig. 5.7c) at 500 °C, followed by a sharp fall representing the Curie point at 570 °C. After this temperature, the susceptibility falls to a value slightly below the susceptibility at room temperature (0.9 K/K_0).

Any ferromagnetic components can be further investigated in BIRM/IRM acquisition experiments and through the demagnetisation of the NRM, ARM and SIRM. IRM acquisition experiments are based on the principle that the coercivity of a mineral varies with composition and grain size (see Chapter 2, Section 2.6.4). The greenish-grey sediments (Fig. 5.9) show

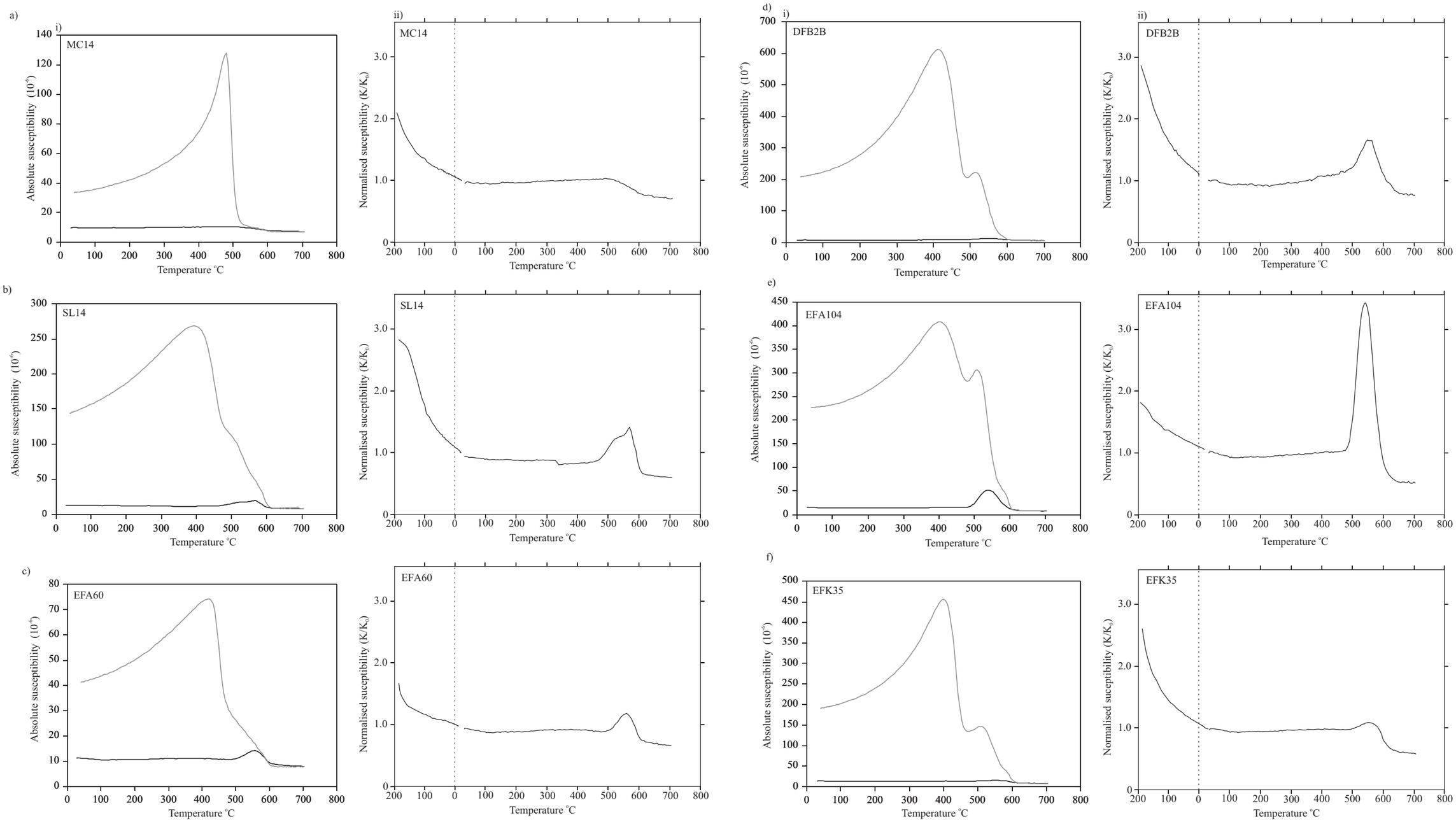

Fig. 5.7 - Susceptibility vs. temperature curves for greenish-grey (a-c) and maroon (d-f) sediments. (i) Low-field absolute susceptibility (K) vs. temperature curves during heating (black line) and cooling (grey line). (ii) Low-field susceptibility (K) normalised to room temperature (20 °C) vs. low-temperature (-196 - 20 °C) and high-temperature (20 - 700 °C) during heating (black line).

complete saturation by 0.5 mT and are demagnetised through the BIRM by -0.08 mT. Demagnetisation of the NRM, ARM and SIRM are shown in Figure 5.8b. All samples show demagnetisation of the SIRM and ARM to 0.2 J/J_{max} by 120 mT peak AF-demagnetisation field. In contrast, the demagnetisation of the NRM reveals sporadic behaviour. The medium destructive field (MDF) of the SIRM and ARM typically varies between 20 mT and 40 mT. The MDF of the SIRM is greater than the MDF of the ARM in all three samples (Fig. 5.8b).

5.5.2. Maroon sediments

Representative examples of the variation of susceptibility with temperature from the maroon sediments are shown in Figure 5.7d, e and f. The normalised low-temperature curves (Fig. 5.7ii) display similar characteristics to the greenish-grey sediments. All samples show temperature-dependent susceptibility and follow Curie-Weiss behaviour (cf. Fig. 2.8, Chapter 2). In the low-temperature segment, Sample DFB2B (Fig. 5.7dii) and EFK35 (Fig. 5.7fii) decrease from 2.9 and 2.6 K/K_0 respectively, whereas sample EFA104 (Fig. 5.7eii) decreases from 1.8 K/K_0.

In the high-temperature range, samples typically show a decrease in susceptibility up to 200 °C, after which, a gradual increase is seen up to 500 °C. After this, a sharp increase occurs and a Curie point can be seen in DFB2B (Fig. 5.7d), EFA104 (Fig. 5.7e) and EFK35 (Fig. 5.7f) at 565 °C, 548 °C and 565 °C, respectively. At higher temperatures, the susceptibility drops to 0.7 to 0.5 K/K_0.

IRM and BIRM acquisition curves of the maroon sediments (Fig. 5.9) reveal incomplete saturation at 2.5 mT. The SIRM reaches zero at far higher BIRM fields than those required for the greenish-grey sediments. Samples EFA104 and EFK35 and DFB2B demagnetise by -0.23, -0.24 and -0.55 mT respectively, requiring much stronger fields than those for the greenish-grey sediments. This indicates the presence of a higher coercivity phase in these samples (cf. Fig. 2.12, Chapter 2).

Demagnetisation behaviour of the maroon sediments (DFB2B, EFA104 and EFK35 in Fig.

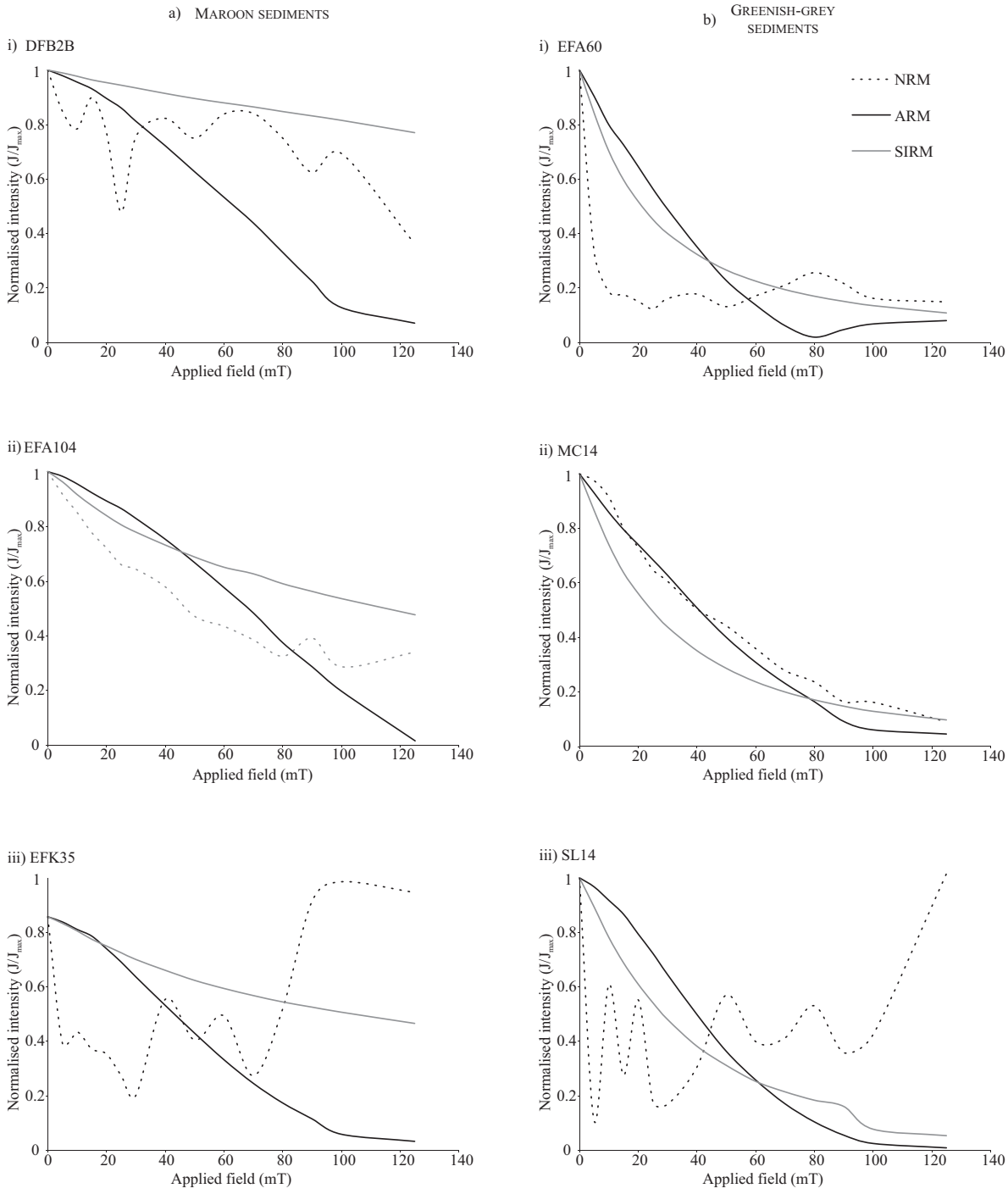

Fig. 5.8 - AF-demagnetisation curves with the normalised magnetisation intensity (J/J_{max}) plotted against the demagnetising field (mT) for the natural remanent magnetisation (dotted), the anhysteretic remanent magnetisation (black) and the saturation isothermal remanent magnetism (grey) for maroon (a) and greenish-grey (b) samples.

5.8a) typically show sporadic behaviour on demagnetisation of the NRM (as with the greenish-grey sediments, cf. Fig. 5.8b). However, a significant difference is seen in the AF-demagnetisation behaviour of the ARM and SIRM. The ARM MDF is 62 mT, 65 mT and 42 mT respectively. These values are far higher value than that for the greenish-grey sediments (20 mT - 40mT). AF-demagnetisation fails to activate grains even at 120 mT, also indicating the presence of a high-coercivity phase(s).

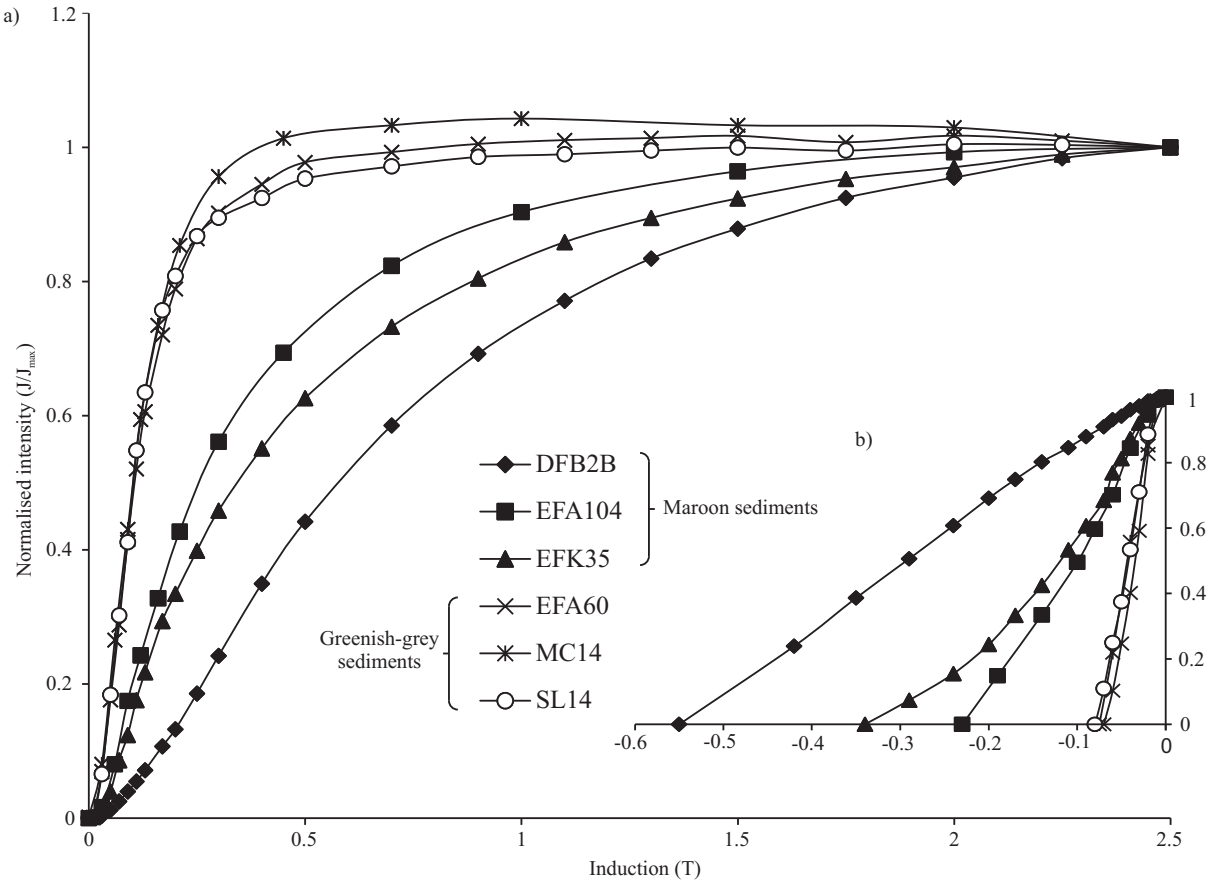

Fig. 5.9 - Normalised (J/J$_{max}$) acquisition of isothermal Remanent Remagnetisation (IRM) experiments with (a) IRM acquisition and (b) Backfield IRM acquisition for greenish-grey samples (un-filled symbols) and maroon samples (filled symbols).

5.6. Anisotropy of magnetic susceptibility

5.6.1. Fabric shape

The majority of the samples yield oblate susceptibility ellipsoids where F>L (Mean F =1.007, Mean L=1.001) (Table 5.1; Fig. 5.10), but some are strongly prolate to strongly oblate (Fig. 5.10b). The mean corrected anisotropy degree (P_j) is 1.008 and varies from 1.004 to 1.137 (Table 5.1). Figure 5.10a shows the variation of P_j with K, revealing no apparent correlation between magnetic susceptibility and anisotropy degree. The exception to this is the two samples that have very low susceptibilities. Here the anisotropy degree is anomalously high (up to 15% anisotropy). This can be explained by the high errors when calculating these parameters at low susceptibilities

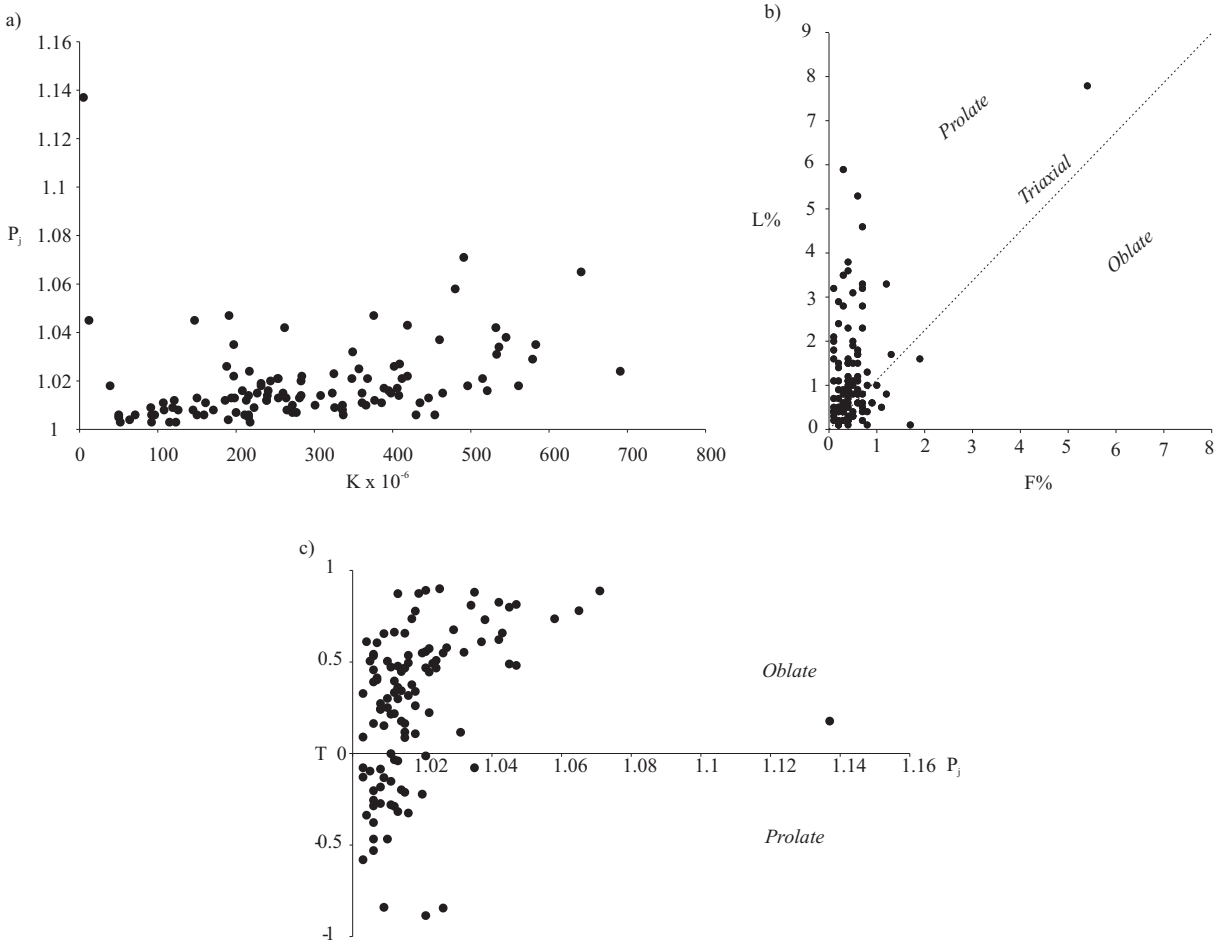

Fig. 5.10 - Variation of mean AMS parameters from all sites. (a) Anisotropy parameter (P_j) vs. susceptibility (K). (b) L% vs. F% (magnetic lineation vs. magnetic foliation). (c) Shape parameter (T) vs. Anisotropy parameter (P_j).

(Hrouda, 2004; Biedermann et al., 2013). Also shown (Fig. 5.10c) are the conventionally used T/P_j plots, which show an alternative method of displaying ellipsoid shape. In both plots, ellipsoids range from the prolate to oblate field; however, the majority lie in the oblate field.

5.6.2. Fabric orientation

Lower hemisphere stereographic projections, with reference to the sites from which the samples were taken, are shown in Figure 5.3. The majority of susceptibility ellipsoids yield a fabric pattern where the K_3 lies perpendicular to bedding and the magnetic foliation (K_1/K_2) plane plots on or close to the bedding plane. However, a broad distribution of fabric patterns can be observed which can be interpreted as 'normal', 'inverse' or 'anomalous' fabrics types (Fig. 5.5).

'Normal' fabrics are those with a predominantly oblate ellipsoid where the K_3 lies perpendicular or almost perpendicular to the bedding plane (e.g. Fig. 5.5a). As such, the magnetic foliation (defined by the K_1/K_2 intersection) lies on or close to the bedding plane. 'Inverse' fabrics (e.g. Fig. 5.5b) are defined as those where the susceptibility axes have switched (cf. Fig. 2.7, Chapter 2). As such, K_1 is normal to the bedding plane and K_3 lies on the bedding plane (defined by K_2-K_3 axes) (Ferré et al., 2004). Anomalous fabrics (e.g. Fig. 5.5c) are defined as those where K_1/K_2 plane deviates from bedding by an angle greater than 25°. An angle greater than this value is considered more than what one would expect to see during depositional processes, through either the deformation of sediment subglacially (Thomason and Iverson, 2009; Fleming et al., 2013), by slumping (Schwehr and Tauxe, 2003) or during mass flow deposition (Eyles et al., 1987).

At Dracoisen, Ditlovtoppen and Andromedafjellet (Fig 5.6a, b and c) in the north, the majority of the fabrics display 'normal' fabric characteristics (i.e. the mean K_3 lies parallel to the pole to bedding). The majority of the fabrics show good apparent correlation with clast fabrics (Fig. 5.6) (see discussion below). However, to the south, the numbers of anomalous fabrics (i.e. those do not conform to 'normal' fabric characteristics) are seen to increase.

5.6.3. Fabric orientation after removal of 'inverse' and anomalous results

In order to fully evaluate the fabrics in terms of their depositional significance, the anomalous fabrics were removed and the fabrics were corrected for the tectonic tilt of the bedding. Focus is paid on the sections to the north for the reasons explained in Section 5.8.2. Figure 5.6 shows representative fabric examples from Dracoisen (Fig. 5.6c), Ditlovtoppen (Fig. 5.6b) and Andromedafjellet (Fig. 5.6a). K_1 shows a range of orientations, but a dominant north-south pattern can be seen. The mean fabric orientations are shown in Figure 5.11a. Andromedafjellet (Fig. 5.11c), Ditlovtoppen (Fig. 5.11b) and Dracoisen (Fig. 5.11a) show mean K_1 values of 04° to 006°, 07° to 178° and 11° to 173° respectively. Confidence ellipses are typically large for K_1 and K_2, and the shape parameter (T) indicates mostly oblate fabric patterns. A weak clustering of K_1 orientation is seen with data plotting in a north-south or NNW-SSE orientation.

5.7. Clast fabrics

14 Clast fabric site measurements were taken from Andromedafjellet, Dracoisen and Ditlovtoppen and the data are summarised in Table 5.2. Clast fabric data are also plotted on to stereonets, corrected for bedding tilt and compared to AMS fabrics and sedimentary logs (Fig. 5.6). Clast a-axis orientations show moderate to strong preferred orientations, typically in north-south orientations. In all cases, the V_1/V_2 plane of the eigenvectors (plane perpendicular to V_3 eigenvector) lies parallel or close to parallel to the bedding plane. In addition, the clast fabrics

									Eignevectors						Eigenvalues			
Fabric	Date collected	Lat/long		Lithology	No	Location	Unit	Bedding	S_1		S_2		S_3		S_1	S_2	S_3	K
1	24/07/2010	79.205486	18.4023	Diamictite	50	Dracoisen	W1	343 51	184	4	86	61	276	29	0.527	0.4161	0.0582	0.1189
2	24/07/2010	79.205502	18.4025	Diamictite	50	Dracoisen	W1	343 51	168	22	60	38	281	44	0.6537	0.2849	0.0614	0.5414
4	02/08/2010	79.214812	18.3997	Diamictite	50	Dracoisen	W2	342 50	343	1	75	55	363	46	0.4676	0.3144	0.218	0.8672
7	26/06/2010	79.205612	18.4047	Diamictite	50	Dracoisen	W2	326 40	174	16	82	8	328	72	0.5393	0.3656	0.095	0.3185
8	28/07/2010	79.204788	18.4111	Diamictite	50	Dracoisen	W1	338 40	151	19	37	48	155	35	0.5885	0.3496	0.0619	0.3009
9	29/07/2010	79.205612	18.4047	Diamictite	50	Dracoisen	W2	320 65	144	40	17	35	264	30	0.4956	0.3337	0.1707	0.5906
11	09/08/2010	79.079457	18.3908	Diamictite	50	Ditlovtoppen	W1	26 32	44	10	139	26	296	62	0.4684	0.4188	0.1128	0.0852
12	09/08/2010	79.083092	18.4135	Diamictite	50	Ditlovtoppen	W3	003 30	162	23	65	17	302	61	0.6081	0.2988	0.0931	0.6094
13	09/08/2010	79.082364	18.4111	Diamictite	50	Ditlovtoppen	W3	003 30	184	14	81	42	289	45	0.6053	0.3256	0.0691	0.4001
17	12/08/2010	79.080193	18.403	Diamictite	50	Ditlovtoppen	W3	004 42	136	30	39	13	289	57	0.6976	0.2658	0.0366	0.4864
5	04/08/2010	79.083643	18.4148	Diamictite	50	Ditlovtoppen	W3	**003 30**	151	20	58	9	305	68	0.5119	0.353	0.1351	0.3393
6	08/04/2010	79.083197	18.4129	Diamictite	50	Ditlovtoppen	W3	003 30	178	5	84	32	276	57	0.7026	0.2179	0.0795	1.4904
15	21/07/2010	78.9386	18.440	Diamictite	50	Andromedafjellet	W1	247 48	150	17	258	46	45	39	0.5717	0.2388	0.1895	3.7718
16	21/07/2010	78.9383	18.433	Diamictite	50	Andromedafjellet	W3	253 40	192	10	285	13	67	74	0.4809	0.3801	0.139	0.2336

Table 5.2 - Clast fabrics data table, analysed using the eigenvalue method (Mark, 1973) where the data is resolved into three mutually orthogonal eigenvectors (V_1, V_2 and V_3). The shape and strength of the fabric is represented by the eigenvalues S_1, S_2 and S_3.

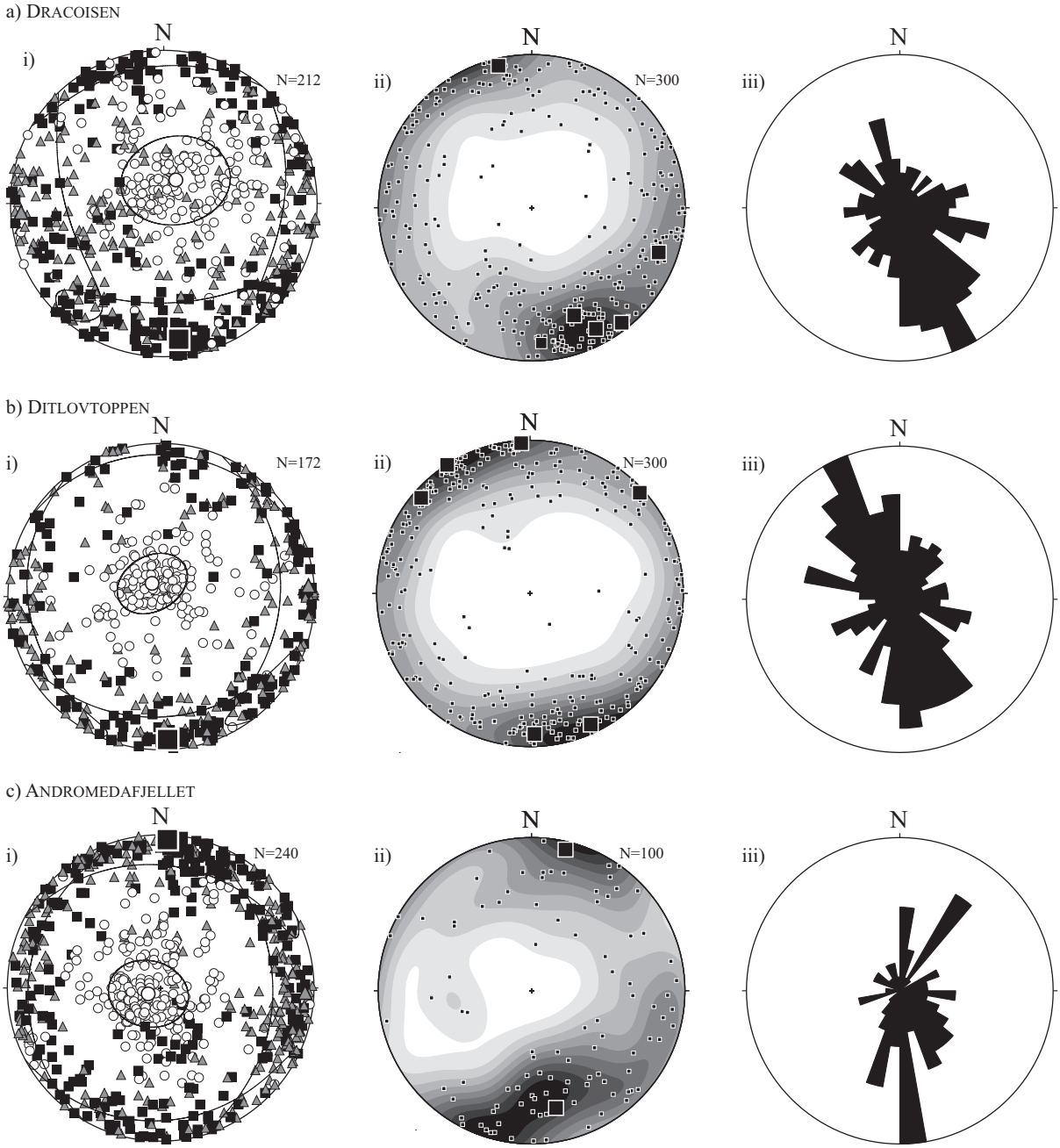

Fig. 5.11 - Comparison of AMS fabrics with clast fabrics for (a) Dracoisen, (b) Ditlovtoppen and (c) Andromedafjellet. (i) AMS fabrics with anomalous fabrics removed, rotated to horizontal showing K_1 (black squares), K_2 (grey triangles), K_3 (white circles) and mean K_1 (large black square) with 95% confidence ellipses. (ii) Clast a-axis orientations from all sites (small black squares) with mean eigenvector (large black square) rotated to horizontal. (iii) Rose diagram showing dip direction of clast a-axis orientations (10° intervals).

often correlate well with the corrected AMS fabrics.

The mean fabric directions from all a-axis measurements at each sample area, compared with the mean AMS fabric directions, are shown in Figure 5.11i and ii. At Dracoisen (Fig. 5.11aii), the mean V_1 vector lies at 11° to 149°. The V_1/V_2 plane lies close to horizontal dipping slightly (02°) to the south (171°). At Ditlovtoppen (Fig. 5.11bii), the mean V_1 vector lies at 01° to 160°. The V_1/V_2 plane dips slightly (03°) to the SW (267°). Finally at Andromedafjellet (Fig. 5.11cii), the mean V_1 vector dips 13° to 172° and the V_1/V_2 plane dips (27°) to the west (110°).

5.8. Interpretation

5.8.1. Magnetic mineralogy

Tarling and Hrouda (1993) suggested that if samples yield susceptibilities less than 500×10^{-6} and have paramagnetic minerals as common constituents (>10%) then the anisotropy is likely to be controlled by paramagnetic mineral phase(s) (see Chapter 2, Section 2.6). However, this is only a general rule as many examples exist where ferromagnetic minerals are interpreted to be predominant if susceptibilities are below this value. The mean susceptibility of the samples in this study is 267×10^{-6} SI, which lies within the paramagnetic realm (cf. Fig 2.5, Chapter 2). However, whilst the majority of samples display 'normal' fabrics, the presence of anomalous and locally 'inverse' fabrics suggests the presence of a different magnetic phase contributing to the fabric in these cases.

Investigations into the variation of susceptibility with temperature (Fig. 5.7) reveal a decrease in susceptibility with increasing temperature. This follows the Curie-Weiss law in the majority of cases, without any indication of a Verwey Transition at 120 K (see Chapter 2, Section 2.6.1). This is commonly interpreted to indicate a major contribution of paramagnetic phases to the anisotropy and susceptibility (Richter and van der Pluijm, 1994; Cifelli et al., 2005; Cifelli et al., 2009). However, at temperatures above 200 °C, Curie-Weiss behaviour ceases and susceptibility

is seen to increase with increasing temperature. A sharp increase is seen in some samples above 500 °C and what could be interpreted as a Hopkinson peak (Section 2.6.1) is displayed. This may have arisen from the growth of new ferromagnetic mineral phases from iron-bearing silicates on heating. However, this does not explain all of the observed behaviours. Therefore, it is apparent that at least in some cases, ferromagnetic minerals are also present within the sample. Curie points for the samples typically range from 550 °C to 570 °C in the majority of cases indicating the presence of a Ti-poor titanomagnetite.

The ferromagnetic component is explored further using BIRM/IRM acquisition and AF-demagnetisation experiments. The results for these vary depending on the colour of the matrix of the sample. IRM acquisition curves for the maroon sediments display very high coercivities, and do not saturate fully until after 120 mT. Similarly on the BIRM, sediment coercivity is often greater than 0.5 mT. The behaviour is fairly typical of a high-coercivity phase, presumably fine maghaemite/haematite (Chapter 2, Section 2.6.4). The AF-demagnetisation curves can also be used to estimate grain size of the ferromagnetic component (Dunlop and Özdemir, 1997). The greenish-grey sediments typically show a MDF of 20 to 40 mT. This is typically within the MD and PSD grain size ranges for titanomagnetite (cf. Fig. 2.11, Chapter 2). The sediments typically display higher MDF of > 50 mT suggesting a predominance of SD grain sizes in the ferromagnetic component.

We can therefore conclude that the majority of the samples displaying 'normal' fabric are predominantly controlled by paramagnetic minerals with only a minor contribution from the ferromagnetic phases (titanomagnetite, maghaemite). A paramagnetic susceptibility in diamictites is usually attributed to clay phyllosilicate minerals (Archanjo et al., 2006; Fleming et al., 2013). Phyllosilicate minerals (e.g. chlorite) display crystalline anisotropy, where the direction of anisotropy depends on the crystalline lattices of the mineral. Such minerals tend to preferentially break into sheets, with K_3 lying perpendicular to the basal plane of the mineral. Lineations can be created in such materials through the intersection of the basal planes (See discussion in Chapter 4, Section 4.5.1).This can occur either through primary sedimentary processes (e.g. shearing

associated glaciotectonism (as discussed in Chapter 4) or through secondary tectonic overprinting (e.g. extension in a rift basin (Mattei et al., 1997)).

5.8.2. Cause of anomalous and 'inverse' fabrics

Whilst the majority of the fabrics yield 'normal' fabric patterns where K_3 lies perpendicular to bedding, both 'inverse' and anomalous fabrics are also present (Fig. 5.5 and Table 5.1). 'Inverse' fabrics can be explained by the presence of SD ferromagnetic grains controlling the anisotropy and susceptibility (Chapter 2, Section 2.5.1). This is because most ferromagnetic minerals have a fabric shape that is strongly dependant on grain size and grain shape. In large MD particles, the K_1 axis is parallel to the long axis of grains (i.e. body diagonal) causing shape anisotropy. However, as SD grains cannot be magnetised along their long axis because of magnetic constriction, they have effectively zero susceptibility along this axis and a maximum susceptibility along their short axis. This can cause susceptibility axes to effectively switch and can lead to erroneous interpretations if not recognised.

As the susceptibility axes are effectively switched, 'Inverse' fabrics can easily be identified (Fig. 5.5b). In a 'normal' fabric, K_3 lies perpendicular to bedding, whereas in an 'inverse' fabrics, K_1 lies perpendicular to bedding and K_2/K_3 lie in the bedding plane (cf. Fig. 2.7, Chapter 2). AF-demagnetisation curves and IRM/BIRM acquisition curves reveal the presence of a high-coercivity phase, presumably SD titanomagnetite or maghaemite in some samples. These fabrics probably arise from the presence of anomalously high proportions of SD titanomagnetite or maghaemite compared with the phyllosilicate clay minerals. Some of the 'inverse' fabrics display anomalously high bulk susceptibilities. For example, DC44 and EFA63 have a bulk susceptibility of 454 $\times 10^{-6}$ and 532 $\times 10^{-6}$ respectively, well above the mean of 267 $\times 10^{-6}$ SI. In these samples, a volumetrically high amount of SD grains can be inferred, which dominates both the anisotropy and susceptibility over the paramagnetic signal, causing the 'inverse' fabric. However, inverse fabrics are not necessarily associated with high susceptibilities. In some sites (e.g. MC15), SD-behaviour can occur even though the mean susceptibility of site is low (39 $\times 10$

$^{-6}$ SI). In thin section, the sample is seen to be composed of a relatively pure quartz arenite, thus lacking a significant amount of clay minerals. This allows any minute ferromagnetic component to dominate susceptibility and anisotropy, in spite of the sample exhibiting a susceptibility that is well within the paramagnetic realm (cf. Fig. 2.5, Chapter 2).

The cause of the anomalous fabrics is difficult to ascertain as they often are characterised by fabric patterns that lie between 'inverse' and 'normal' fabrics. One explanation is that, if both SD and MD magnetite are present in the sample, fabrics will not necessary be either 'normal' or 'inverse'. Instead, intermediate fabrics may form (Rochette et al., 1992; Stephenson, 1994). Ferré (2002) observed that intermediate fabrics can start to form when the 'inverse' component reaches ~20%. Intermediate fabrics normally result in one or more axes switching whilst the others remain constant. As such, several possible fabric patterns can result (cf. Ferré, 2002). This may be an explanation for some of the anomalous fabrics, especially where one axis has switched (e.g. SL02, Fig. 5.5c).

Anomalous fabrics may also be the result of remagnetisation during diagenesis or tectonism. AMS has been shown to be highly sensitive to even weak tectonic strains (e.g. Kissel et al., 1986; Cifelli et al., 2009). Within the study site, there is an increase in the proportion of anomalous fabrics relative to 'normal' fabrics in the south (Fig. 5.3d, e and Table 5.1). This coincides with steeper regional bedding, tighter folding and associated faulting at this location. Tectonic strain may be higher in this zone given its location to the core of the regional Caledonian synclinorium. Whilst there is an absence of evidence for mesoscopic deformation, any increase in tectonic strain within the rock at this location may have overprinted the primary AMS fabrics.

The development of a tectonic AMS fabric has been studied in a variety of cases (e.g. Borradaile and Tarling, 1981; Borradaile and Tarling, 1984; Kissel et al., 1986; Averbuch et al., 1992) and is discussed in Chapter 2, Section 2.7.3. The initial stages of deformation are typically characterised by a clustering of K_1 axes on the bedding plane, in an orientation perpendicular to the plane of shortening (cf. Fig. 2.13). Further strain results in a deviation of K_1 and K_2 axes away from the bedding plane and into a new foliation plane, with K_3 perpendicular to cleavage (Parés

et al., 1999). Fabrics in the south typically display a greater degree of clustering (Fig. 5.6c and d) and, in some cases, K_1 axes appear to deviate away from bedding in a pattern similar to that seen during incipient tectonic deformation.

In the southern locations (Klofjellet and Backlundtoppen, shown in Fig. 5.3d and e) because of (i) an increase in the number of AMS results displaying either anomalous behaviour or evidence of tectonic overprinting; (ii) observations of a greater degree of tectonic deformation; and finally (iii), a lack independent palaeoflow indicators (e.g. clast fabric results), the effect of tectonic deformation cannot be ruled out. As such, these fabrics cannot be reliably interpreted in terms of their depositional significance and are omitted from the following palaeoflow interpretation. Instead, focussed is placed on the northern locations.

5.8.3. Primary sedimentary fabrics

After removal of anomalous and 'inverse' fabrics, the AMS fabrics of the northern localities (Dracoisen, Ditlovtoppen and Andromedafjellet) show strong correlation with clast fabrics (Fig. 5.6). In the majority of cases, the K_1 axes lie close to the mean eigenvector of the clast fabric. The mean AMS fabric and clast fabric from all sites at Dracoisen, Ditlovtoppen and Andromedafjellet are shown in Figure 5.11. The AMS fabrics show a weak clustering of K_1 axes in a north-south orientation at all three locations and displays strong correlation with the mean eigenvalues of the clast fabric. Clast fabrics are considered to be a primary, as any evidence for any meso- or microscopic deformation associated with tectonic reorientation is absent (Dowdeswell et al., 1985). As the size of the clasts are larger (>5 cm), mechanical reorientation is considered very unlikely. The close relationship between AMS fabrics and clast fabrics is common in Quaternary tills (e.g. Fuller, 1962; Gentoso et al., 2012) as both the macro-and microscopic component of till can behave in a similar manner in response to glacial shear. The close correlation of the AMS to clast fabrics, as well the wide spread of AMS vectors that display no apparent relationship with tectonic strain, suggest a primary, depositional origin for the AMS fabric at these sites.

The origin of the fabrics was probably controlled by sedimentary processes occurring during

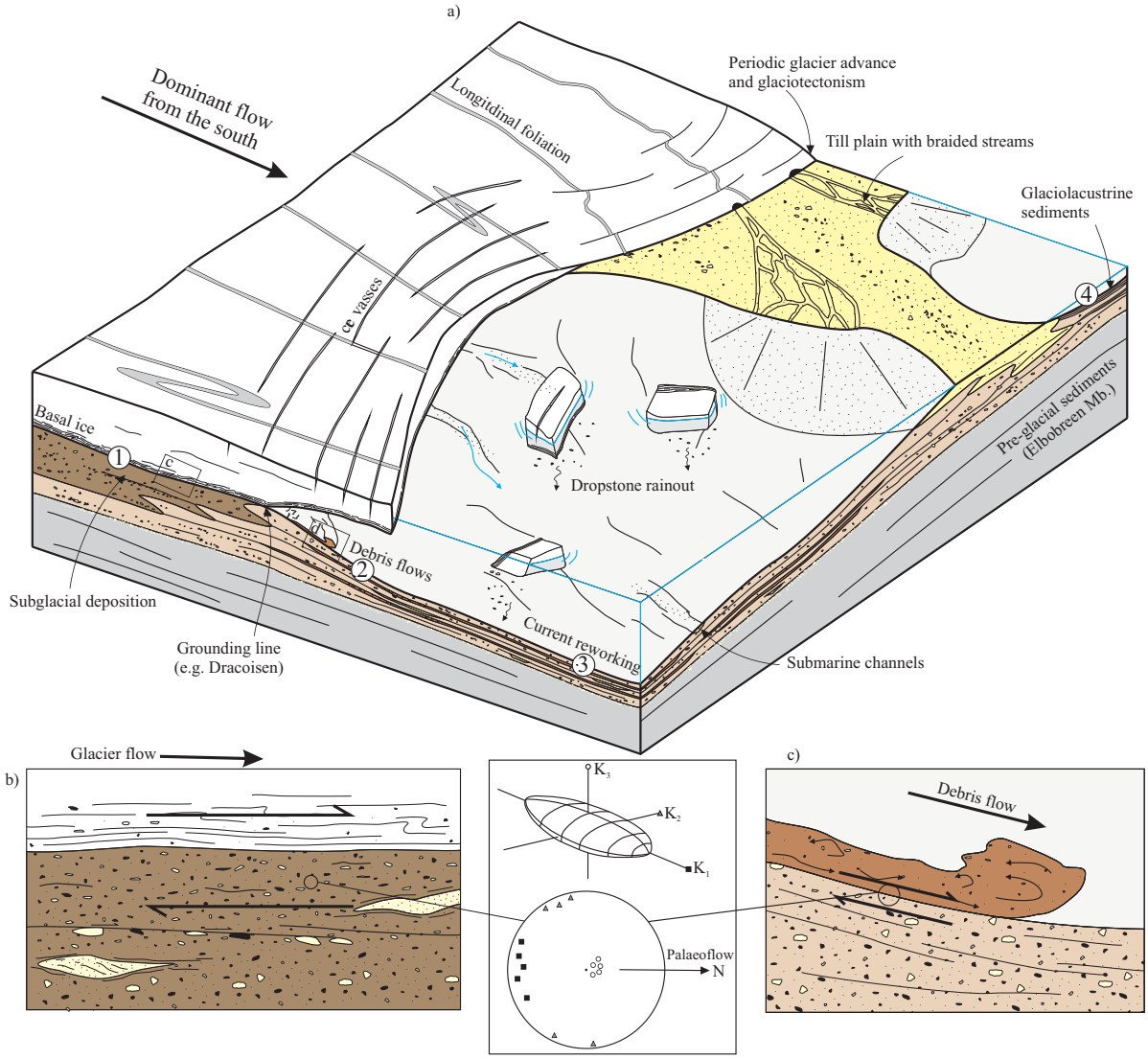

Fig. 5.12 - Depositional model of facies of the Wilsonbreen Formation (a) with interpreted deposition environments of 'normal' AMS fabrics from (b) subglacial environments and (c) glaciomarine environments with debris flows. Numbers 1-4 correspond to locations mentioned in the text.

deposition. Glacial environments, especially ice-marginal environments, of which deposition of the Wilsonbreen Formation is interpreted (Fairchild and Hambrey, 1984; Harland et al., 1993), are typically highly dynamic (see Chapter 1, Section 1.2). Advance/retreat cycles are common within ice-marginal settings, often leading to a large variety of depositional facies that form under different glacio-depositional regimes. A large component of the deposition of the Wilsonbreen Formation can be accounted for by subaqueous deposition (Fairchild and Hambrey, 1984). However, evidence for periodic ice-grounding and the deposition of subglacial sediments is seen in the upper Wilsonbreen Formation (Fig. 5.12, Location 1) by possible glaciotectonised

sediments (Fig. 5.4d) and striated boulder pavements (Fig. 5.4c). These are analysed in detail in the following chapter (Chapter 6).

The AMS fabrics of subglacial sediments are normally interpreted to form in response to the shear imparted by the overriding ice on the sediment (Shumway and Iverson, 2009; Thomason and Iverson, 2009; Gentoso et al., 2012). In a subglacial environment, deformation is typically dominated by shear and a strong extensional regime (Hart and Boulton, 1991; Kluiving et al., 1991). As such, AMS fabrics typically form where the K_1 lies parallel to the direction of shear and K_3 lies perpendicular to the shear plane. This pattern has been seen in both the debris-rich basal ice of active glaciers (Chapter 3) and also within subglacially deformed sediments (Shumway and Iverson, 2009; Thomason and Iverson, 2009; Fleming et al., 2013). Iverson et al. (2008) also demonstrated this experimentally through ring shear experiments. Micro-faults were observed within the till that rotated grains into a preferential alignment under March rotation (March, 1932). K_1 orientations in subglacially deformed sediments are therefore interpreted to represent palaeo-ice flow direction (Fig. 5.12b).

In areas that lack evidence of ice-grounding, subaqueous deposition is interpreted as being the dominant mode of deposition (Locations 2 and 3, Fig. 5.12). Here, evidence for rainout (e.g. Fig. 5.4b) and sediment remobilisation as slumps and debris flows is seen (e.g. Fig. 5.4e). This style of deposition commonly produces diamicton that are difficult to distinguish form subglacial tills (Benn and Evans, 2010). Within subaqueous sediments, AMS fabrics may record the palaeoflow direction of sediment remobilisation events e.g. debris flows (Eyles et al., 1987; Archanjo et al., 2006). In these settings, particles become realigned parallel to the flow direction because of hydrodynamic forcing and shear during flow (Gravenor, 1986), as summarised in Figure 5.12c. The subsequent mean K_1 lineation is typically interpreted as an indication of palaeoflow (Archanjo et al., 2006).

In some areas, diamictites were probably deposited through rain-out from floating ice (Fig. 5.12a). In theory, one may expect the resulting fabric pattern to be largely oblate where grains lie on a girdle about a bedding plane (see Chapter 2, Section 2.7.1). However, AMS fabrics are

shown to be affected by even weak currents (Rees and Woodall, 1975) and purely oblate AMS fabric patterns are rare (Eyles et al., 1987). Current re-working is common in ice-marginal subaqueous environments because of the discharge of large volumes of water through subglacial conduits at the grounding-line. Oblate fabrics with a linear clustering of K_1 axes are commonly produced parallel to the palaeoflow direction of the current (Eyles et al., 1987). It is therefore interpreted that AMS lineations in these settings probably represent the palaeoflow of bottom currents (Location 3, Fig. 5.12).

In summary, after the omission of anomalous data, the AMS fabrics are interpreted to represent palaeoflow associated with primary depositional processes (Fig. 5.12). Where subglacial grounding is suspected, AMS fabrics are interpreted to reflect the glacier shear direction associated with ice flow. Where glaciomarine deposition is suspected, the AMS fabrics are interpreted to represent the palaeoflow of bottom water currents or sediment remobilisation events (e.g. debris flows). A full characterisation of fabrics in relation to different depositional processes is beyond the aims of this chapter. However, in the following chapter (Chapter 6), AMS is combined with facies analysis and structural geology to investigate specific features of the Wilsonbreen Formation.

5.9. Discussion

5.9.1. Implications for palaeogeography

Within the southern localities, the high volume of anomalous fabrics with possible evidence of tectonic influence precludes reliable palaeocurrent determination from these locations. However, in the northern localities (Dracoisen, Ditlovtoppen and Andromedafjellet), the close agreement between clast fabric and AMS fabric indicates that the flow is related to depositional processes (Fig. 5.13). Whilst these fabrics may be caused by different processes (subglacial shear, debris flows), the AMS fabrics of different facies associations are shown to be generally concordant (see Chapter 6, Section 6.5.1). As such, a dominant palaeoflow direction in a north-

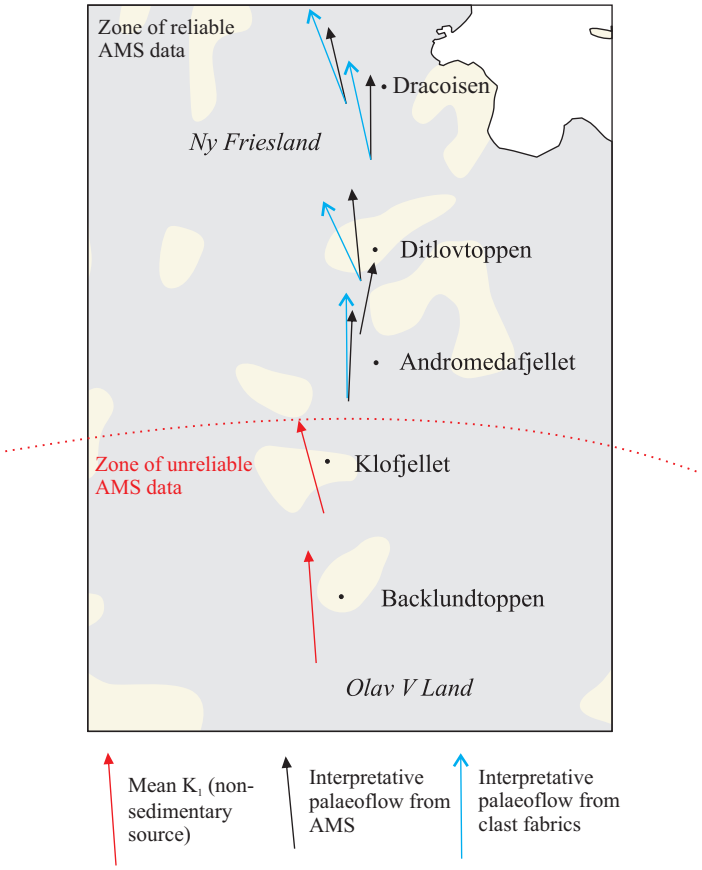

Fig. 5.13 - Interpreted palaeoflow direction across the basin showing the mean azimuth of unreliable AMS at Klofjellet and Backlundtoppen (red arrow) and the mean azimuth of reliable AMS (black arrow) and clast fabric (blue arrow) in at Andromedafjellet, Ditlovtoppen and Dracoisen.

south orientation is interpreted for the basin at these locations.

AMS has accurately determined the fabric throughout the succession at several sites; however, in order to reconstruct basin palaeogeography it is important to determine whether this dominant north-south azimuth denotes flow to the north or flow to the south. One method by which this can be done is through the investigation of minor deviations in the K_1/K_2 planes from bedding. Iverson et al. (2008) noticed, through laboratory experimentation using ring shear devices, that during the subglacial shear of till, an up-glacier dip in the K_1, effectively tilting the magnetic foliation plane away from the direction of shear (cf. Fig. 2.15, Chapter 2). Similar imbrication is also seen in sediment deposited as debris flows or in a current (Rees and Woodall, 1975). Identification of this subtle deviation of the K_1 from the bedding plane could, in theory, be used as an indicator of flow direction (whether north or south). However, this up-glacier dip is not

always observed in applied examples (e.g. Shumway and Iverson, 2009; Fleming et al., 2013) possibly because of minor rotation during compaction and dewatering processes.

In the AMS fabrics of NE Svalbard, a subtle dip of K_1 axes to the south is seen at Dracoisen and Andromedafjellet. This could be interpreted as flow to the north; however, because of the variety of processes that may have formed these fabrics (e.g. subglacial shear, current reorientation, sediment remobilisation), an imbrication alone may not be considered sufficient to warrant this interpretation. However, the previous interpretations of palaeoflow within the basin typically also suggest dominant flow from the south. For example, in the contiguous sediments of NE Greenland, ice flow from the SW was inferred from clast fabrics (Moncrieff, 1988), and basin axial flow to the NNE was interpreted from overlying turbidites (Herrington and Fairchild, 1989). In Svalbard, previous clast fabric measurements, striated surfaces and cross bedding have led authors to suggest movement from the south or SE (Hambrey, 1982; Fairchild and Hambrey, 1984; Halverson et al., 2004). This is supported by the interpretations of the facies architecture presented in Chapter 6. It is therefore suggested that, in keeping with pre-existing research, a dominant palaeoflow from the south is most likely (Fig. 5.13).

5.9.2. Use of AMS as a palaeoflow indictor of glacial sediments in the pre-Quaternary rock record

AMS is a reliable fabric indicator offering several advantages over other fabric techniques (summarised in Iverson et al., 2008). Whereas microscopic optical analysis of grain-fabric normally only measures the fabric in two dimensions, AMS provides a three-dimensional indicator of strain direction and possibly magnitude. Furthermore, in contrast to grain and clast-fabric analysis which documents the orientation of one grain or clast at a time, AMS reflects the volume average of many grains within a sample; therefore the inherent variability that may be seen under single-grain analysis is reduced. AMS is often compared with clast fabrics and microscopic grain-fabric analysis. However, one of the main caveats of direct measurements of particle orientations is the possibility of human bias (Drake, 1977; Benn and Ringrose, 2001).

In contrast, AMS is considered non-subjective; the main uncertainty arises from the orientation process of the sample (Iverson et al., 2008).

In other disciplines, AMS has been used to calculate shear strains in deformed rocks and sediment (Borradaile, 1991). Iverson et al. (2008) identified a link between AMS fabric strength based on the degree of the clustering of the susceptibility axes and strain. With increasing shear strain, AMS fabrics became more asymmetric. K_1 orientations were observed to rotate towards the direction of shear (see Fig. 2.15, Chapter 2). At shear strains above 8, K_1 orientations become tightly clustered and steady-state fabrics were reached, and further increases in shear strength did not result in any further increase in fabric strength. It was suggested that this could be used as a genetic indicator to identify tills that have not been sheared to strains compatible with the bed-deformation model of glacier flow.

This study, however, has highlighted several caveats as to why direct comparison with strain may not be possible. AMS fabrics are observed to be highly dependent on magnetic mineralogy (Tarling and Hrouda, 1993) such that even small variations in sediment composition may result in a different fabric shape, irrespective of shear strain. In this study, the presence of SD titanomagnetite/maghaemite grains has resulted in the formation of 'inverse' and possibly anomalous fabrics in some cases. If the presence of SD ferromagnetic grains are not correctly recognised and interpreted through rock magnetic experiments, erroneous interpretations may subsequently result (Ferré, 2002). With further study, the interpretation of 'inverse' and intermediate fabrics in terms of their primary significance may be possible from remanence-based methods involving the analysis of the anisotropy of anhysteretic remanent magnetisation (AARM) (McCabe et al., 1985) and the anisotropy of isothermal remanent magnetism (Stephenson et al., 1986; Tarling and Hrouda, 1993). However, for the purposes of this study, once identified, anomalous fabrics were removed and are not included in subsequent palaeoflow interpretations.

This chapter has also highlighted additional problems in the interpretation of glacial AMS fabrics in the pre-Quaternary record. As AMS is very sensitive to strain, sedimentary fabrics have the potential to be overprinted by a tectonic fabric, even if minor evidence for meso- or micro-

scale deformation is absent. This is inferred to have to been the case in some sites in the south, where a subtle increase in tectonic strain may have affected sedimentary fabrics such that a reliable palaeocurrent signature cannot be resolved.

In spite of this, in the northern localities, after the identification and removal of anomalous fabrics, AMS fabrics show a strong correlation with clast a-axis orientation and bear no apparent resemblance to regional tectonics structures. The AMS fabrics at these sites are therefore interpreted as primary palaeoflow indicators. As such, this study has shown that the application of AMS to the Neoproterozoic glacial record in Svalbard has provided an independent palaeoflow indicator in an area that is otherwise lacking palaeoflow data from other proxies. From this, a dominant palaeoflow direction to the north has been identified from three locations in Olav IV land (Andromedafjellet, Ditlovtoppen and Dracoisen). To our knowledge, this is the first time AMS has been applied to Neoproterozoic glacigenic sediments for palaeocurrent reconstructions. This technique can be applied to other well-preserved, undeformed Neoproterozoic diamictites and has the potential to increase our understanding of Neoproterozoic glacial palaeogeography.

5.10. Conclusions

The AMS of diamictites from the late-Cryogenian Wilsonbreen Formation have been measured (for the first time) and interpreted for their palaeoflow significance. A number of conclusions have been drawn:

- AMS fabrics of the Wilsonbreen Formation typically reflect the preferential alignment of paramagnetic phyllosilicate clay minerals. In some cases, a minor contribution of titanomagnetite and maghaemite contributes to and may locally control the AMS fabric.
- AMS fabrics show strong correlation with clast fabrics and are therefore considered primary depositional fabrics that reflect the original palaeoflow direction. The mean direction of both data sets from sites at Andromedafjellet, Dracoisen, and

Ditlovtoppen yield northerly orientated vectors.

- Grains have been rotated into a preferential alignment by primary depositional mechanisms and processes. Where subglacial activity is suspected, this resulted through shear of the sediment by the overriding ice producing glacier-flow parallel AMS lineations. In glaciomarine sediments, AMS fabrics reflect down slope remobilisation and re-working by bottom water currents.

- AMS has accurately constrained the fabric throughout the succession from several sites, and has provided a much improved understanding of palaeoflow across the region. The results from the AMS, verified through comparisons with clast fabrics reflect northerly orientated palaeoflow vectors. Based on a subtle dip of K_3 lineations and previous independent palaeoflow indicators from the area and contiguous sediments in NE Greenland, a dominant palaeoflow to the north is interpreted.

CHAPTER 6.

LATE CRYOGENIAN GLACIOTECTONISM AND ICE-GROUNDING DURING THE DEPOSITION OF THE WILSONBREEN FORMATION

6.1. Introduction

Massive diamictites, such as those that dominate the Wilsonbreen Formation, are inherently difficult to interpret (Eyles and Januszczak, 2004). This is in part because they can be associated with various depositional environments: both glacial (glaciomarine, glaciolacustrine, subglacial, proglacial) and non-glacial (Dowdeswell et al., 1985). The extensive research on the Wilsonbreen Formation to date has provided a broad depositional interpretation (e.g. Fairchild and Hambrey, 1984). However, doubts exist over the precise glacio-depositional regimes that occurred and their association with Neoproterozoic climatic conditions.

In the previous chapter (Chapter 5) it was shown how anisotropy of magnetic susceptibility (AMS) can be used to reconstruct basin palaeoflow direction within the formation. In this chapter, a specific example is shown as to how the AMS data can be used, in combination with a range of other techniques including facies analysis and structural geology, to reconstruct the depositional environments of the Wilsonbreen Formation. A full environmental interpretation of the entire sequence is beyond the scope of this chapter as this rests on the body of data collected by the team as a whole. Instead, this chapter focuses on a particular aspect of the stratigraphy: the origin of the soft-sediment deformation features observed at the W2/W3 Member boundary at Andromedafjellet, Reinsryggen, Ditlovtoppen and Dracoisen (Fig. 6.1). However, for the reader's interest, additional sedimentary data is presented in Appendix D that covers the entire succession, including the sections to the south.

The Wilsonbreen Formation has previously been suggested to form in both subglacial and glaciomarine environments (Harland et al., 1993). Glacioaqueous deposition has been suggested through the occurrence of dropstones, mass-flow deposits and turbidites (Fairchild and Hambrey, 1984; Fairchild et al., 1989), whilst terrestrial glaciation and ice-grounding has been interpreted by the presence of striated boulder pavements (Chumakov, 1968; Chumakov, 1978) and a preferred alignment of clasts (Hambrey, 1982; Fairchild and Hambrey, 1984). However, doubt has been cast on the use of clast fabrics alone to distinguish between different depositional facies (e.g. Bennett et al., 1999). This is because similar fabric patterns can be produced during both

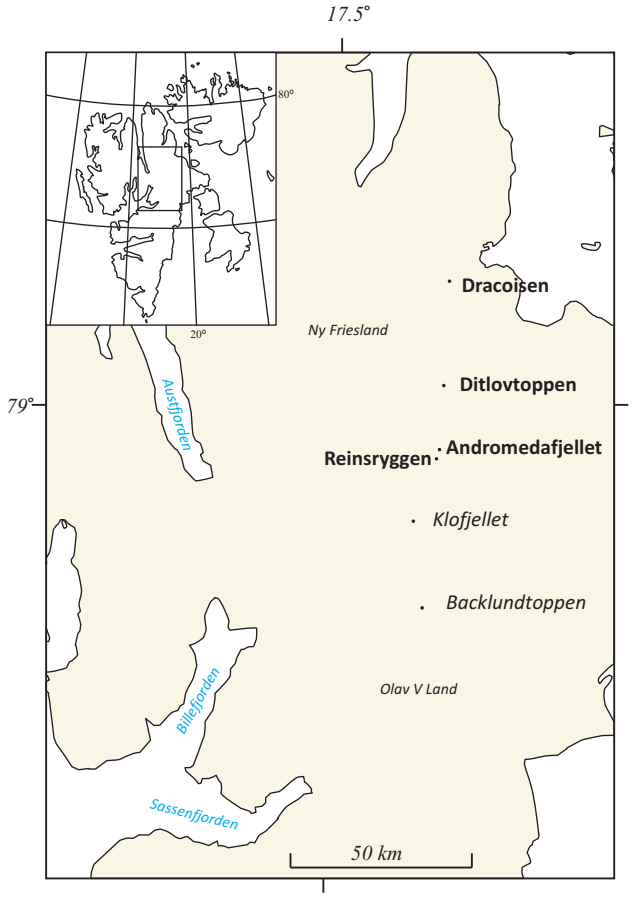

Fig. 6.1 – Location map of the study area with localities detailed in this chapter (Dracoisen, Ditlovtoppen and Andromedafjellet) shown in bold.

sediment remobilisation (e.g. debris flows) and subglacial deformation.

Since the 1980s, when the previous interpretations of the depositional environments of the Wilsonbreen Formation were made, there have been significant new advances and improvements in the understanding of glacial depositional processes. This has partly arisen from the high number of studies on modern glacial environments, which has significantly improved the understanding of the processes leading to the deposition of till (see references in Benn and Evans, 2010). In addition, there is now a greater knowledge of landform assemblages associated with different depositional environments (e.g. Evans, 2005), which enables reliable palaeoenvironmental interpretations to be made from the modern sedimentary record. Furthermore, the application of detailed facies descriptions that emphasise palaeoenvironmental reconstructions has resulted in much improved understanding of terrestrial and marine glacial

processes and their implications for glacier thermal regimes (Hambrey and Glasser, 2012).

There have also been advances in the understanding of the possible modern analogues for Neoproterozoic glaciations. An example is the Antarctic McMurdo Dry Valleys (Atkins and Dickinson, 2007; Hambrey and Fitzsimons, 2010) which have been suggested as analogues for unusual lacustrine carbonates that occur within parts of the Wilsonbreen Formation and display geochemical signatures that are indicative of evaporative regimes (Fairchild et al., 1989; Bao et al., 2009). Whereas in the past many of the modern analogous for glacial sedimentation were restricted to terrestrial settings, access to subsurface data such as sediment cores and geophysical data, is now available and has revealed much information about glacial depositional processes in the marine record (e.g. Powell and Domack, 1995). In particular, there is now a large research archive on the Cenozoic glaciomarine record offshore Antarctica (e.g. Hambrey and Barrett, 1993; Anderson, 1999; Hambrey et al., 2002; Ó Cofaigh et al., 2007; Dowdeswell et al., 2008; Davies et al., 2012), which could potentially be considered an analogue of Neoproterozoic glacioaqueous successions.

The understanding of deformation structures (e.g. glaciotectonites) produced by both cold-based and polythermal glaciers are now also better understood (van der Wateren, 2002; Aber and Ber, 2007). Glaciotectonic structures are common in both modern and Quaternary sediments; however, they have also been observed in many pre-Quaternary sediments (e.g. Le Heron et al., 2005; Benn and Prave, 2006; Busfield and Le Heron, 2013). Analysis of these can provide considerable information about genetic environments and deformational histories.

Utilising this current understanding of depositional environments, combined with the novel application of the AMS technique as developed in this thesis, significant opportunities exist for palaeoenvironments of the Wilsonbreen Formation to be investigated. The aims of this chapter are to (i) categorise the lithofacies observed within the succession in terms of their facies associations; (ii) determine the origin of the soft-sediment deformation features (glaciotectonic or slumping); (iii) using a combination of AMS and clast fabric analysis, identify strain vectors within the sediment so that former ice flow directions can be determined; and finally (iv)

construct a depositional model to explain the deformation and associated deposition of the sequence.

6.2. Methods

Sections through the Wilsonbreen Formation (See Fig. 5.2, Chapter 5 for the stratigraphic location) were examined at Dracoisen, Ditlovtoppen, Andromedafjellet and Reinsryggen in NE Svalbard (Fig. 6.1 and 6.2) during the summer 2010 and 2011 field seasons. Sections were analysed following the lithofacies approach, originally developed for fluvial sediments by Miall (1977) and adapted for glacial sediments by Eyles et al. (1983). Descriptions of diamictites were classified using the scheme developed by Moncrieff (1989) and modified by Hambrey (1994), based on the documentation of the relative proportions of gravel, sand and mud (silt and clay), estimated by eye. In this scheme, diamictites are defined as rocks that contain 1-50% gravel with a matrix comprising greater than 10% of sand, mud or both sand and mud.

The morphology of the clasts were analysed and surface features were identified. This method has previously been shown to provide useful parameters for establishing transport pathways of glacial clasts (Boulton and Hindmarsh, 1987). It involved the measurement of the shape, roundness and texture of 50 randomly selected clasts from 8 sampling sites in diamictites of the W2 and W3 Members. Clast shape was determined by measuring the long (a), intermediate (b) and short (c) axes of individual clasts. This data is displayed on triangular diagrams following the methodology of Sneed and Folk (1958). All clast data were plotted using a modified version of the TriPlot program developed by Graham and Midgley (2000). Clast roundness was measured by assigning clasts to six categories ranging from very angular to well rounded (Krumbein, 1941). The percentages of very angular and angular clasts are used to make the RA-index. Also analysed were the percentages of well-rounded and rounded clasts, which were used to make the RWR-index. Finally, the C_{40} index was analysed which was defined by the percentage of clasts with a c:a ratio of ≤ 0.4.

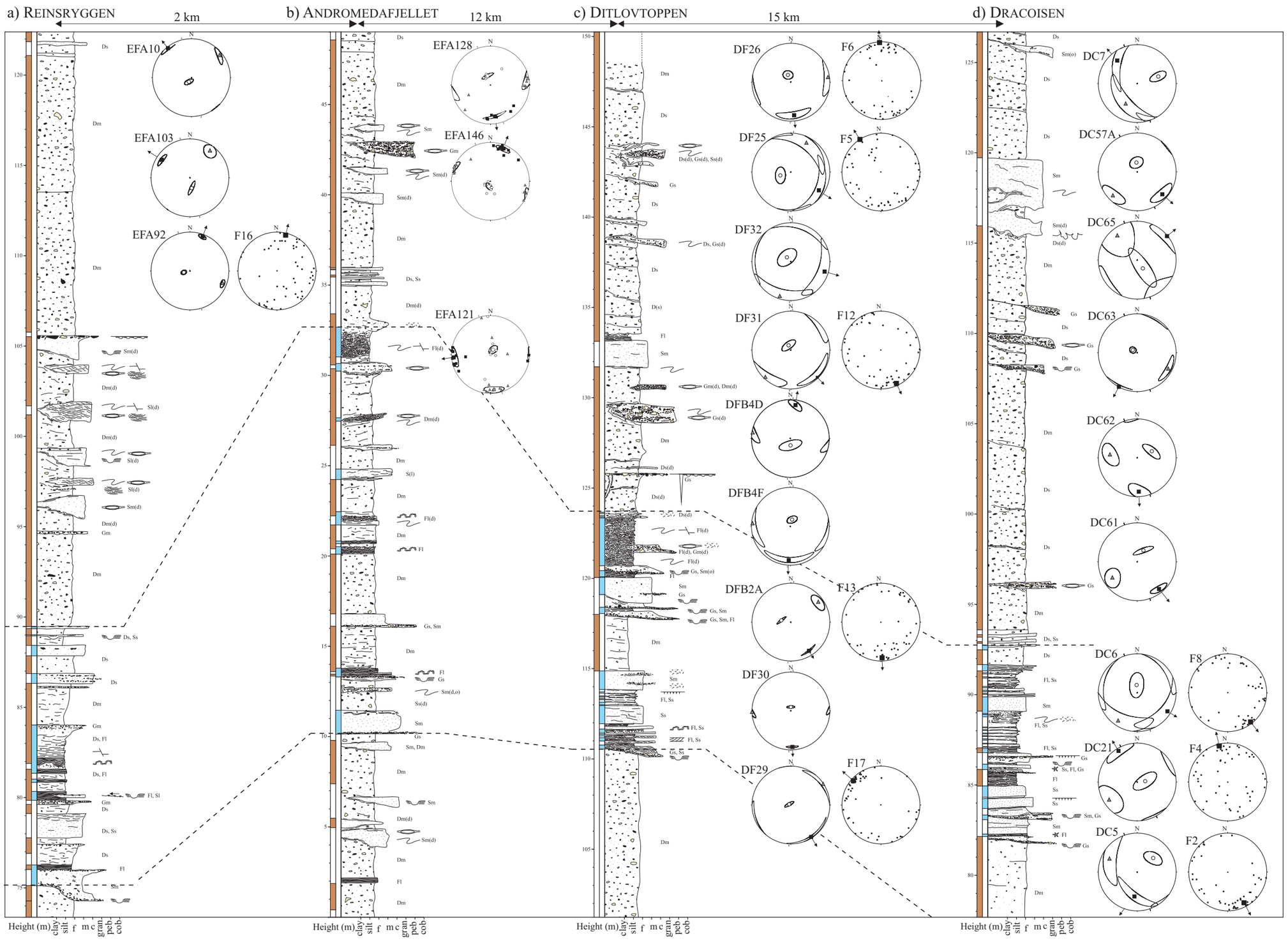
a) REINSRYGGEN
2 km
b) ANDROMEDAFJELLET
12 km
c) DITLOVTOPPEN
15 km
d) DRACOISEN
EFA10
EFA103
EFA92
F16
EFA128
EFA146
EFA121
DF26
F6
DF25
F5
DF32
DF31
F12
DFB4D
DFB4F
DFB2A
F13
DF30
DF29
F17
DC7
DC57A
DC65
DC63
DC62
DC61
DC6
F8
DC21
F4
DC5
F2
Height (m)
clay
silt
f
m
c
gran
peb
cob

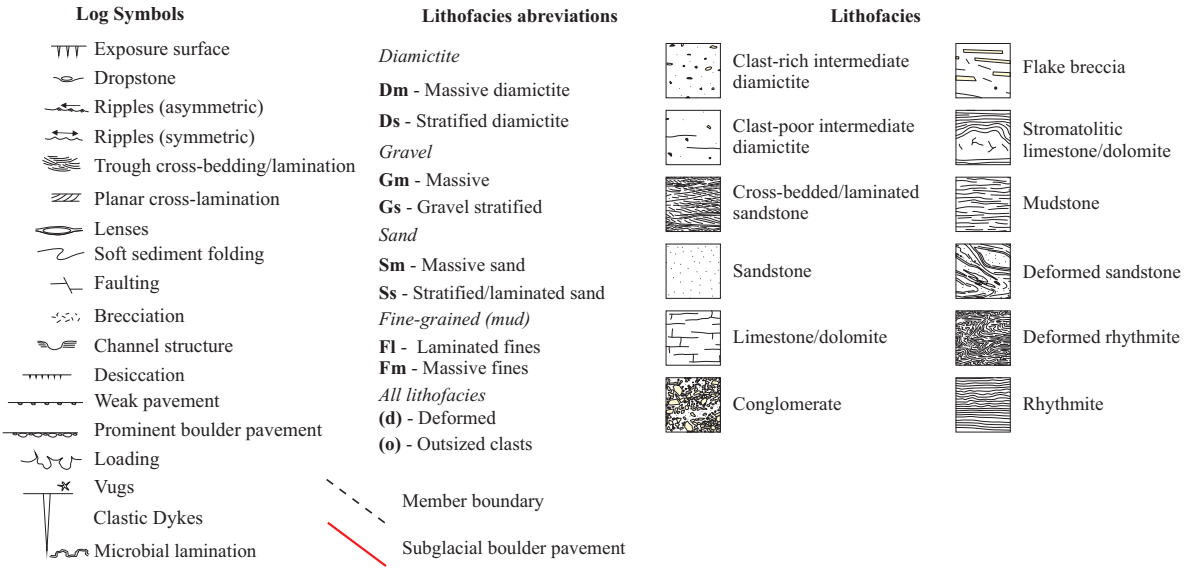

Fig. 6.2 – Detailed composite sedimentary logs of the W1-W2-W3 Member transition, with stereographic projections showing AMS and clast fabric results for (a) Reinsryggen, (b) Andromedafjellet, (c) Ditlovtoppen and (d) Dracoisen. Height refers to stratigraphic distance from the base of the formation. An explanation of the AMS plots is given in Chapter 5.

Co-variant plots, displaying C_{40}-index versus RA-index, have been suggested as a useful method of distinguishing different clast pathways (e.g. Benn and Ballantyne, 1994). The C_{40} RWR-index is also plotted, based on the procedure of Lukas et al. (2013). In order to provide a control for the sample variation, fields from modern glacial regimes of a similar glacial environment were taken from data published in Hambrey and Glasser (2012).

AMS samples were collected using a combination of field-drilling and block sampling (outlined in Appendix A). The samples were measured following the methodology outlined in Chapter 2, Section 2.9. The AMS data were analysed using standard statistical techniques (see Section 2.4.1). This involved the calculation of the mean susceptibility (K_{mean}), corrected anisotropy degree (P_j), lineation (L) and foliation (F) parameters and the shape parameter (T) (Jelínek, 1981). The magnetic mineralogy of the samples has been previously investigated in Chapter 5, utilising the methodology outlined in Chapter 2, Section 2.9. Where possible, three-dimensional clast fabric measurements were taken following the methodology outlined in Chapter 5, Section 5.5.

Structural analysis has been undertaken during both field-based investigations and during

subsequent lab-based microscopic investigations of thin sections. In this chapter, the term *soft-sediment deformation* is used to distinguish rock that has been deformed through primary processes (e.g. slumping and glaciotectonism) from rock that has been deformed tectonically. Although, it is acknowledged that some of this primary deformation is not necessary strictly "soft" as some of the facies were semi-consolidated prior to deformation (Section 6.4.2).

The microscopic analysis of structures has proved useful in characterising and providing insights concerning the processes operating during subglacial deformation (Menzies, 2000). Much of the seminal work in this field has been inspired by soil science concepts, and hence much terminology comes from this field under the term 'micromorphology' (e.g. van der Meer, 1993; Menzies, 2000; Carr, 2001). Others have adopted an approach derived from structural geology and petrology (e.g. Phillips et al., 2002; Busfield and Le Heron, 2013), and the technique is referred to as the analysis of microstructures. Investigations in the field of micromorphology have resulted in a surge of publications; however, the technique can be somewhat subjective, and many of the features identified are not specific to any one environment.

For this chapter, an adapted form of micromorphology is employed for the analysis of the deformed glacial sediments within the study site, where focus is placed on structural analysis and interpretation of the clearly visible features (mostly faults and folds). Polished thin sections of deformed rhythmites were obtained from Andromedafjellet and Ditlovtoppen. These were orientated parallel to the dominant ice flow orientation where possible and were analysed using a standard petrographic microscope at low magnification, under plane- and cross-polarised light.

6.3. Results

Previous facies descriptions and interpretations of the Wilsonbreen Formation have been made in detail by Fairchild and Hambrey (1984) and are summarised in Harland (1993). For the purposes of this thesis, additional facies descriptions and interpretations have been made to build on this previous research. Facies are grouped into those showing evidence of soft-sediment

deformation versus those that are relatively undeformed.

6.3.1. Undeformed and associated facies of the Wilsonbreen Formation

The undeformed facies can be subdivided into those from the W3 Member including: (1a) diamictite and conglomerate facies and (1b) sandstone facies (summarised in Table 6.1) and the W2 Member including: (2a) diamictites and conglomerates, (2b) rhythmites and stromatolite facies sheet, (2c) channelised sandstones and conglomerates and (2d) dolocreted sandstones, mudstones and evaporites (summarised in Table 6.2).

6.3.1.1. Undeformed facies of the W3 Member

6.3.1.1.1. *Diamictite and conglomerate facies (1a)*

Diamictite (Dm, Ds) represents the bulk of the Wilsonbreen Formation. Including the diamictites of the deformational facies (Section 6.3.2), they make up over 80% of the stratigraphy. This facies is dominated by greenish-grey or maroon, clast-poor, sandy diamictites (Fig. 6.3a, b and d); however, clast-rich and sand-poor varieties occur locally. Grains are typically poorly sorted and are rounded to angular (predominantly subrounded).

Clasts make up between 3-10% of the facies, although all proportions up to gravel is present locally. The majority of clast types are considered intrabasinal (60-80%) and can be matched with the underlying strata, particularly the Elbobreen and Backlundtoppen Formations (dolostone, limestone, chert, breccia and siltstone). The remainder are extrabasinal and some have an unknown source area. Of these, coarse-grained pink granites are most common, but other granites, basalts, banded gneisses, quartzites and amphibolites are also seen. A wide range of sizes are encountered and boulders >80 cm are observed locally. A variety of surface textures can also be seen on the clasts. Striations are common on the fine-grained lithologies, affecting up to 28% of the clasts and can be orientated randomly or can form subparallel sets. Facets are common (affecting up to 50% of clasts) and a carbonate crust is seen locally, irrespective of clast lithology.

Facies	Description	Lithofacies codes	Interpretation
Diamictite and conglomerates (1a)	Massive and stratified diamictites, consisting of poorly-sorted, subangular to subrounded, intrabasinal and extrabasinal clasts in a fine-grained sandy matrix, sometimes with a well-pronounced haematite staining. Intercalated with lenses of conglomerate, sometimes displaying channel geometries.	**Dm** **Ds** **Gm** **Gs** *Sm* *Ss*	Subaqueous deposition from either (i) rainout from a high concentration of debris-rich ice bergs or (ii) from sediment-laiden efflux jets at close to the grounding line of a glacier or ice-sheet. Conglomerate facies represent erosional lags or mass flow deposits. In places (e.g. at Dracoisen), the sediment architecture suggests deposition as a grounding-line fan.
Lenticular and tabular sandstones (1b)	Pale yellow to greenish-grey, moderate- to well-sorted sandstones, consisting of quartz with minor feldspar and lithic fragments. Bed thickness is normally 0.1 to 1 metres thick and can display either channel-like and lenticular or tabular geometries. Rare cross-bedding and ripple lamination.	**Sm** **Ss** *Dm* *Ds* *Gm* *Gs*	Proximal subaqueous deposition through the release of debris from subglacial conduits at the grounding-line fan, which can progress into subaqueous channels in a more distal location. Tabular sandstones interpreted as deposition as a subaqueous outwash fan.

Dm = Massive diamictite; **Ds** = Stratified diamictite; **Gm** = Massive conglomerate; **Gs** = Stratified conglomerate; dominant lithofacies (in bold); associated lithofacies (in italics).

Table 6.1 – Summary of the lithofacies that make up the undeformed W3 facies.

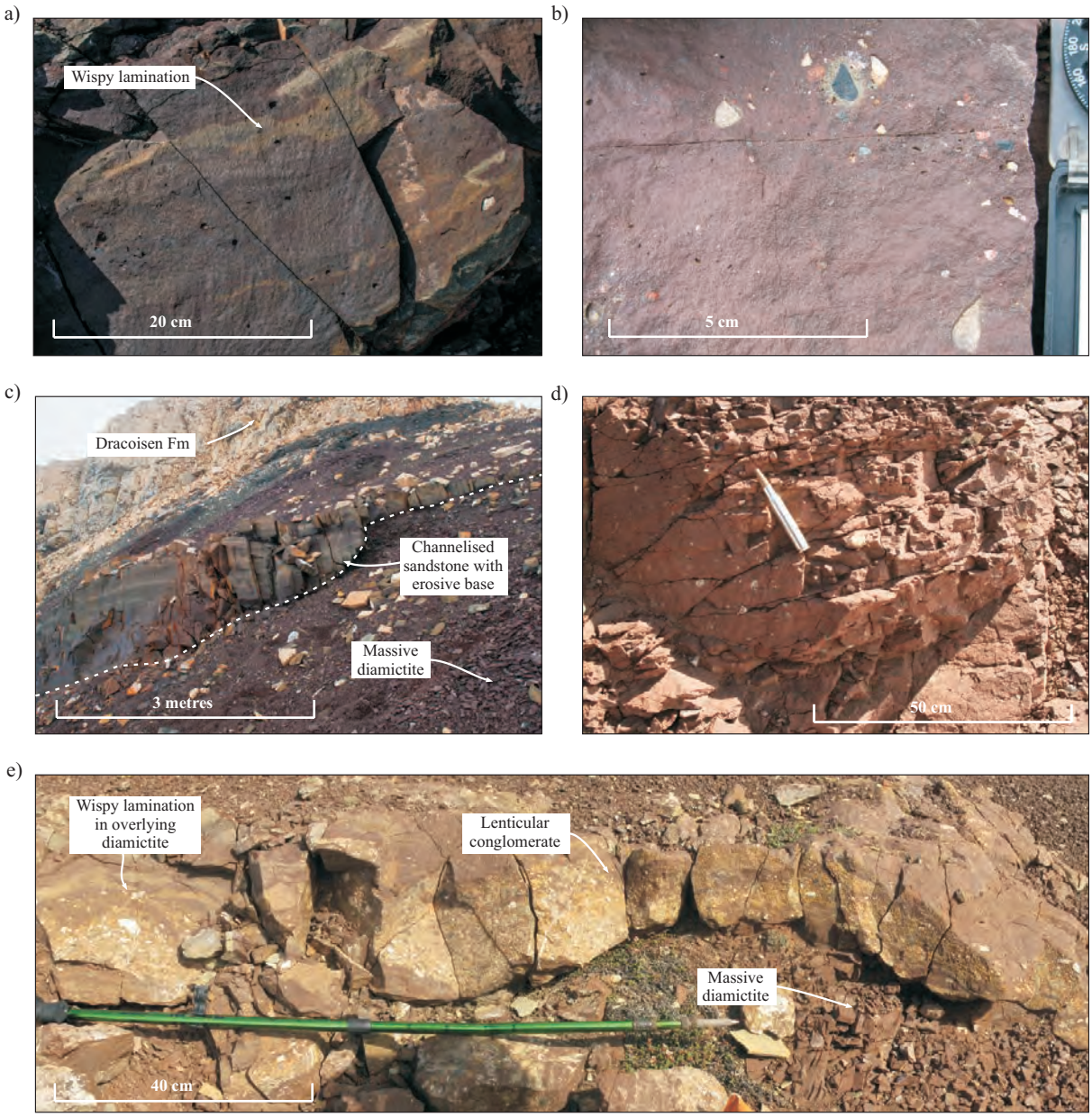

Fig. 6.3 – Field photographs of the typical sediments associated with subaqueous facies associations of the W3 Member. (a) Clast-poor muddy diamictite horizon from Reinsryggen, displaying wispy undulating sand-rich lamination. (b) Massive maroon, clast-poor intermediate diamictite from Dracoisen showing a patch of clast-rich diamicton. (c) Channelised sandstone grey sandstone body cut into massive diamictite from Reinsryggen. (d) Massive friable, maroon, clast-rich sandy diamictite from Dracoisen. (e) Lenticular conglomerate (mass flow deposit) within massive diamictites forming part of the grounding-line fan at Dracoisen.

The sand fraction is composed of predominantly subangular quartz with minor dolostone, mica and other lithic fragments. Heavy minerals are common and are mostly composed of pyrite, haematite or magnetite. They often form separate, subangular to rounded grains which suggest a detrital origin. This is presumably derived from the weathering and erosion of the igneous and metamorphic lithologies; however, secondary growth of haematite and pyrite is seen in places. The silt fraction grades into a dolomicrite groundmass with varying proportions of quartz and clay minerals. This is commonly obscured by a well-developed haematite staining, particularly pronounced in maroon diamictites.

Bedding is poorly developed and can usually only be seen where diamictites are interbedded with associated facies (e.g. conglomerates and sandstones). Where it is seen, bed thickness ranges from 2 to 5 metres. Subtle 'wispy' stratification is seen in some cases (e.g. Fig. 6.3a). This is normally defined by subtle changes in the sand content of the diamictite matrix and is sometimes associated with colour change or mottling.

Conglomerates (Gm, Gs) are commonly associated with the diamictites (e.g. Fig. 6.3e). These form either as isolated lenses or continuous sheets up to 50 cm thick. They can be laterally extensive and remain fairly uniform in thicknesses, or they can be discontinuous and lenticular in form. Some show subtle reverse grading, whilst others have a sharp undulating base with evidence of erosion and channel forms. Normal grading into overlying massive diamictites is seen locally. The clast fraction (50-90%) is composed of similar lithologies to the diamictites. They are angular to rounded (predominantly subrounded), and sorting is poor to medium. The matrix is typically a medium to poorly sorted, fine to coarse sand, and is composed predominantly of angular quartz grains, sometimes surrounded by a muddy dolomicrite.

Both diamictites and conglomerates are easily traced along sections; however, because of a lack of identifiable characteristics, correlation between sections is generally not possible. Where two-dimensional exposure exists, beds can show pronounced thickness variation along strike. For example, a distinct change in dip is seen within diamictite and conglomerate beds of the W3 Member at Dracoisen (Fig. 6.4). Above the W2 Member, the beds are seen to dip 10° steeper

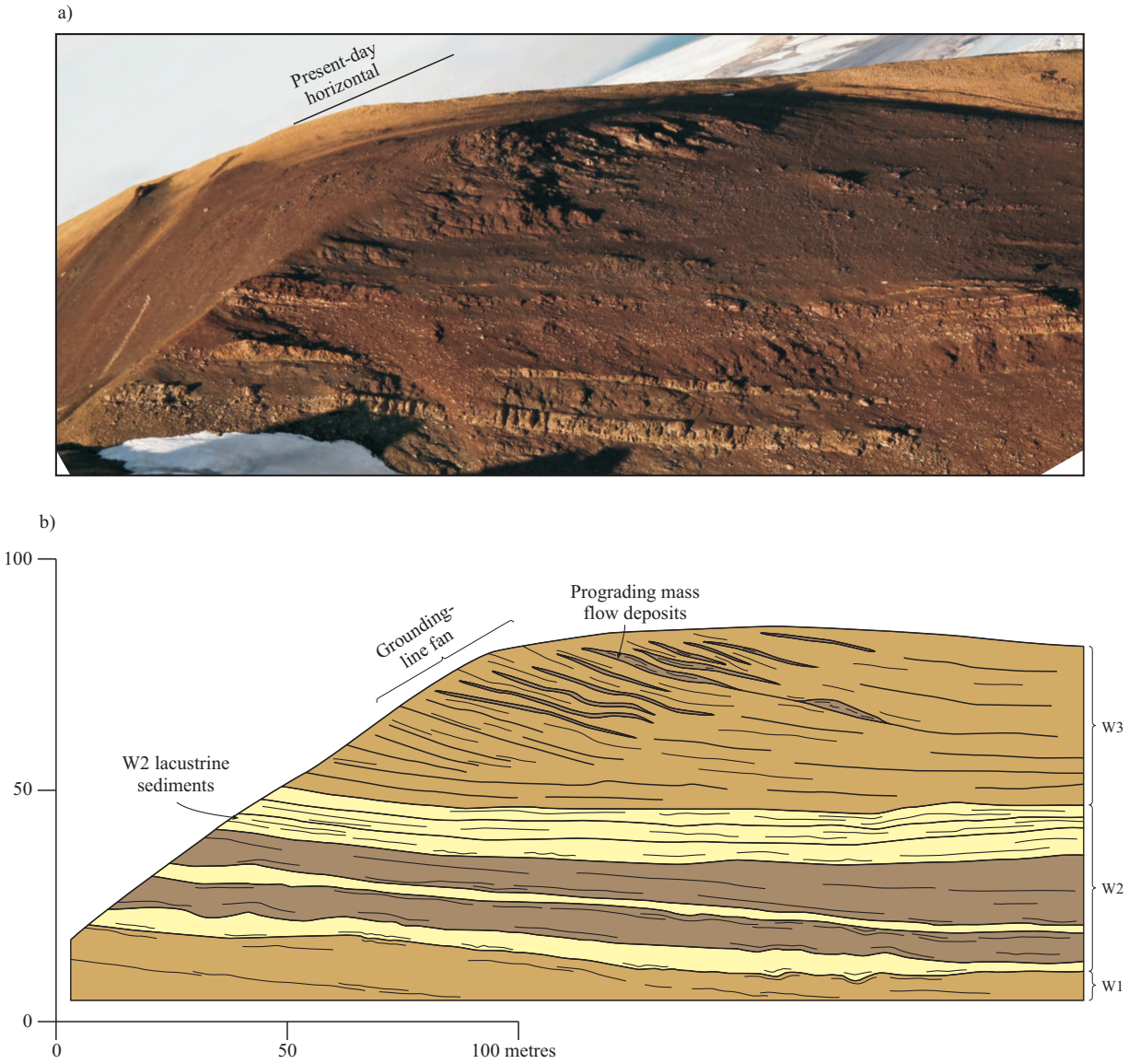

Fig. 6.4 – The grounding-line fan at Dracoisen. (a) Field photograph of grounding-line fan (photo: IJF). (b) Interpretative sketch of grounding-line fan rotated to horizontal showing inclined debris flow and diamictite beds in the W3 Member.

than the regional bedding and show apparent thickening to the east, along the two-dimensional section.

6.3.1.1.2. *Sandstone facies (1b)*

Pale yellow to greenish-grey, moderate- to well-sorted sandstones (Sm, Ss) make up 4-8% of the Wilsonbreen Formation. These are often interbedded with diamictites and form laterally continuous sheets or discontinuous lenses (e.g. Fig. 6.3c). Bed thicknesses varies widely, from thin

(<10 cm) up to several metres.

Grain size is mostly fine to medium but can be highly variable. Quartz predominates the grains in the majority of cases (>95%), defining a quartz arenite, with minor feldspar, dolomite and other lithic fragments. Outsized clasts are common and are composed of the same lithologies as those contained in the surrounding diamictites. Opaque minerals are observed in thin-section and are composed predominantly of subrounded grains of haematite and magnetite with local development of authigenic pyrite. Both silica and carbonate cements are seen and quartz overgrowths are common at grain boundaries. A silty-sand matrix with varying proportions of dolomicrite, clay minerals and quartz, sometimes obscured by a haematite cement is also seen in places. The proportion of this matrix relative to encompassing grains varies considerably from being almost absent up to near greywacke proportions.

Bedding geometry is typically either channel-like and lenticular (e.g. Fig. 6.3c) or laterally extensive and planar. The contacts with overlying and underlying diamictites are mostly sharp. The channel-like sands display erosive bases that cut into underlying diamictites. A wave-rippled top is sometimes developed. Stratification is typically wavy and discontinuous where seen, but can be chaotic in places. In addition, both trough and planar cross-stratification is locally developed, particularly in the sands displaying channel geometries.

6.3.1.2. Lithofacies interpretation

Following the arguments of Hambrey (1982), the presence of laterally extensive diamictites, with evidence of both faceted and striated clasts, suggests unequivocally that the debris was glacially transported. The occurrence of faceted and striated clasts is generally interpreted to represent transportation in the traction zone of a sliding ice mass (e.g. Boulton, 1978). The subtle stratification, close association with facies typical of subaqueous deposition and a lack of associated subglacial facies (boulder pavements, subglacial and glaciofluvial sands and gravels and glaciotectonic deformation) suggest that deposition occurred in a subaqueous glacial environment.

Although stratification occurs locally, the majority of the diamictites are massive with no internal structure: a common problem in the interpretation of diamictites (Eyles and Januszczak, 2004). In a subaqueous interpretation, thick structureless diamictites can be associated with deposition through the release of sediment from a high concentration of debris-rich icebergs (e.g. Dowdeswell et al., 1994; Syvitski et al., 1996), or from sediment-laden efflux jets close to a grounding line. The subtle stratification can be interpreted as the product of minor subaqueous current reworking and subsequent removal of fines during rainout deposition of diamictite from floating ice.

Massive conglomerate can be interpreted either as erosional lags or as debris-flow deposits. Lags can form in subaqueous environments during periods of non-deposition or times of increased bottom water flow. In these situations, finer material can be removed by bottom water currents (e.g. Powell, 1984). Within the subaqueous facies associations, conglomerates displaying reverse grading and sharp contacts with overlying diamictites are interpreted as lags. In contrast, those that have lenticular or channel-like geometries and display grading are interpreted as mass flows. These are common in both glaciomarine and glaciolacustrine environments where deposition occurs on a slope (Laberg and Vorren, 1995; Eyles and Eyles, 2000; Hambrey and McKelvey, 2000). Local slopes can be readily created in such environments, particularly in the proximal zone close to the grounding line (Powell, 1990). Here, the emergence of sediment-laden jets from subglacial tunnels can result in high rates of deposition. As such, local topographic highs and associated slopes can develop at the grounding line. In these settings, sediment remobilisation events, such as debris flows, can occur in tectonically quiescent basins where the bathymetry is otherwise flat.

At Dracoisen, the distinctive architecture consisting of thickening beds of diamictite and conglomerate towards the south suggests the presence of a grounding-line fan (Fig. 6.4). Here, the debris flow deposits can be interpreted as periodic slope failure events that travel down from the grounding line. The Interbedded massive diamictites are interpreted through rainout deposition from sediment-laden efflux jets that emerge from subglacial channels, combined with background

sedimentation from icebergs.

Interbedded sandstones provide further support for a subaqueous interpretation. Channelised sandstones (Fig. 6.3c) are a common feature of glacioaqueous deposition (e.g. Le Heron et al., 2013a) and are particularly associated with the development of grounding-line fans (Powell, 1990). Here, sorted sands are derived from subglacial channels emerging out of the grounding zone. These can build up and develop into a subaqueous outwash fan. Within the sandstone facies, the channelised sandstones are interpreted as representing subaqueous channels emerging from the grounding line. In places where the sands form more extensive sheet-like geometries, deposition as part of a subaqueous outwash fan is interpreted.

6.3.1.3. Palaeoenvironmental interpretation

Therefore, an ice-marginal, subaqueous glacial landsystem is proposed for the deposition of the undeformed W3 Member lithofacies. Deposition is interpreted to have occurred in a location proximal to a grounding line for at least part of the time. In this setting, massive diamictites form through a combination of rainout from a high concentration of debris-rich icebergs and the settling of material from efflux plumes at the grounding line. High rates of sedimentation resulted in the development of local palaeoslopes and the formation of a grounding-line fan (Fig. 6.4). Here, sediment remobilisation events resulted in the emplacement of debris flows deposits. In addition, subaqueous currents, possibly created by emerging subglacial or englacial channels, resulted in the formation of lag deposits and the associated deposition of lenticular and planar sands as subaqueous channel deposits and as part of outwash fans.

6.3.1.4. Undeformed facies of the W2 Member

6.3.1.4.1. *Diamictites and conglomerate facies (2a)*

Diamictite (Dm, Ds) and conglomerate (Gs, Gm) (e.g. Fig. 6.5a) are common within the W2 Member and make up 20 – 60% of the stratigraphy. Diamictite beds can be up to several metres

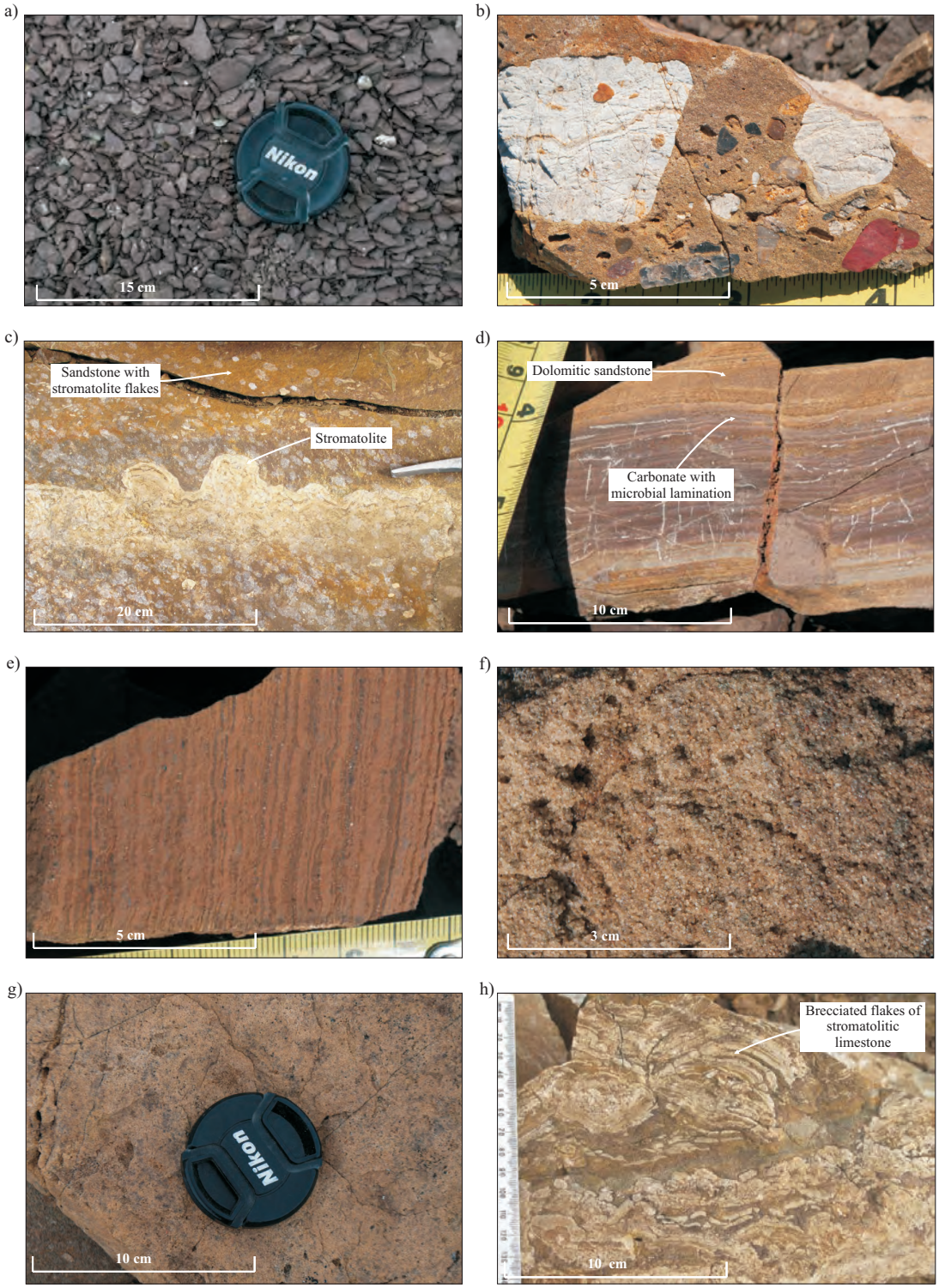

Fig. 6.5 – Field photographs of the typical sediments associated with the W2 Member lithofacies. (a) Massive, clast-poor, muddy diamictite (Andromedafjellet). (b) Conglomerate horizon showing large clasts of oolitic dolostone, black limestone and red granite in a sandy matrix (Reinsryggen). (c) Stromatolite limestone horizon showing domal forms located within a sandstone bed (Dracoisen) (photo: IJF). d) Laminated carbonate horizon showing microbial undulations, cut by a minor tectonic fault. (e) Undisturbed sand/silt – carbonate rhythmite (Reinsryggen). (f) Coarse, poorly cemented sandstone with well-sorted, well-rounded grains. (g) Buff-yellow, dolocreted vuggy sandstone horizon (Andromedafjellet). (h) Brecciated stromatolitic horizon within fluvial sandstones (Dracoisen) (photo: IJF).

thick and are interbedded with several facies that are unique to the W2 Member (described below). The beds typically display tabular geometries and can be traced laterally along strike. They are mostly massive and have sharp contacts with overlying and underlying facies. Conglomerates (Gm, Gs) are uncommon within the diamictites but are more typically associated with the sandstone lithofacies (2c). Where present, they form discontinuous, isolated layers or lenses that are up to 30 cm thick. They are compositionally and texturally similar to the diamictite lithofacies (1a) and display an erosive base.

The diamictite lithofacies of the W2 Member have significantly lower clast-matrix ratios (1-5%) compared with the diamictite lithofacies of the W3 Member (1a). In addition, the proportion of sand in the matrix is less. As such, the diamictite displays a much more friable weathering pattern (Fig. 6.5a). They are almost exclusively maroon, although minor maroon-grey mottling occurs locally, which is particularly pronounced at the contacts with overlying or underlying sand-rich facies. The clasts are up to pebble-sized and larger clasts are virtually absent. Despite this, the diamictites are compositionally and texturally very similar to those of the W3 Member.

6.3.1.4.2. *Rhythmite and stromatolite facies (2b)*

Maroon-brown, rhythmically laminated, sand/silt-carbonate sediments (Fl) are a common feature of the W2 Member at all localities (Fig. 6.5e). In some places (e.g. Andromedafjellet), they occur interbedded with diamictites. In others, they are associated with sandstone, carbonate and stromatolitic facies. At Reinsryggen, a channelised sandstone lens (10 cm) is located within the rhythmites which displays a current-rippled top (Fig. 6.2a). Bed thickness is variable, ranging from 0.1 to 3 metres, and the geometry is typically planar and laterally continuous, although correlation between Reinsryggen and Andromedafjellet (sites 2 km apart) was not possible. Local, small-scale intraformational folding and brecciation is also developed.

The rhythmites are typically characterised by alternating layers of silt/sand and carbonate, although many variants occur in detail. The thickness of each couplet ranges from <1 mm to

Facies	Description	Lithofacies codes	Interpretation
Diamictites and conglomerates (2a)	Massive, poorly-bedded diamictite with occasional conglomerate. Exhibiting distinctly lower clast-matrix ratios than diamictites of the W3 Member. Clasts are poorly-sorted, subangular to subrounded and are both intrabasinal and extrabasinal. Clasts sit in a fine-grained, sandy matrix, sometimes with a well pronounced haematite staining.	**Dm** **Gm** **Gm** **Gs** *Sm* *Ss*	Subaqueous deposition during a glacial advance phase through the rainout of debris from floating ice. Lower clast proportion may suggest smaller, more restricted glaciers than those associated with the deposition of the diamictites of the subaqueous lithofacies (1a). Conglomerates are interpreted as lag deposits and infrequent debris flow deposits.
Rhythmites and stromatolites (2b)	Maroon-brown, rhythmically laminated, sand/silt-carbonate sediments, displaying alternating layers of silt-sand and carbonate <1 mm to 20 mm thick, consisting of medium to poorly sorted, subangular to subrounded quartz in a fine-grained, opaque dolomicrite matrix. Often associated with stromatolitic carbonate displaying distinct domal or bulbous structures.	**Fm** **Fl** *Dm* *Ds* *Sm* *Ss*	Lacustrine deposition during a glacial retreat phase. The lamination reflects daily, meteorological or annual variations in sediment discharge into a lake. Domal laminated carbonates are interpreted as stromatolites, forming in predominantly quiescent shallow water conditions or ephemeral streams when present in cross stratified sands.
Sheet and channelised sandstones and conglomerates (2c)	Pale yellow-grey sandstone and conglomerate bodies displaying either channel-like and lenticular or tabular geometries. Sandstones composed predominately of sub-angular quartz in a silty matrix although well-rounded varieties occur locally. Rare cross bedding and ripple lamination are observed.	**Sm** **Ss** **Gm** **Gs** *Dm* *Ds*	Glaciofluvial deposition in an ice-marginal, predominantly terrestrial setting. The channelised sandstones reflect deposition from braided streams, possibly emerging from the ice margin. Sheet sandstones possibly represent outwash sands. Well-rounded varieties indicate aeolian deposition.
Dolocreted sandstones, mudstones and evaporites (2d)	Typically thin (10 cm) intervals occurring within sandstone and mudstones where a dolomicrite matrix can be readily distinguished. Evaporite pseudomorphs are shown by a cm-dm-scale vuggy texture, with vugs are lined by dolomite crystals.	**Sm** **Ss** **Fl** **Fm** *Dm* *Ds*	Following the interpretation of Fairchild et al. (1989), the dolocretes and evaporate pseudomorphs are interpreted as flooplain deposits. These form during glacial retreat phases during periods of aridity and increased evaporation.

Dm = Massive diamictite; **Ds** = Stratified diamictite; **Gm** = Massive conglomerate; **Gs** = Stratified conglomerate; **Sm** = Massive sandstone; **Ss**= Stratified sandstone **Fm** = Massive mudstone/siltstone; **Fl** = Laminated mudstone/siltstone; dominant lithofacies (in bold); associated lithofacies (in italics).

Table 6.2 – Summary of the lithofacies that make up the undeformed W2 facies.

20 mm and is quite variable over short vertical distances. At the base of each couplet is a sand-silt horizon which sometimes displays evidence of loading and an erosional base. The grains are predominantly composed of medium to poorly sorted, subangular to subrounded quartz with rare lithics and opaque minerals. These sit in a fine-grained, opaque dolomicrite matrix that displays a well-developed haematite staining. At the top is a dolomicrite with rare fine sand and silt. It displays local normal grading and has a prominent haematite staining at the base, but this becomes less prominent towards the top. Lenses of coarse-grained, poorly-sorted sand occur locally. These are composed of quartz, lithics and opaque minerals and have loaded bases which can be associated with minor, small-scale (<2 cm) synsedimentary faulting. Outsized clasts are rare but were observed at several localities. These are seen to puncture the underlying layers but overlying layers on-lap.

Stromatolitic carbonates are seen within the W2 Member at all sites. These form yellowish-grey to maroon, laminated horizons that are typically associated with the dolomitic sandstones (e.g. Fig. 6.5c). The lamination displays distinctive irregular microbial forms (Fig. 6.5d). These can form part of larger domal or bulbous structures (Fig. 6.5c) and were observed up to 5 cm in diameter. Evidence of brecciation is seen through dispersed centimetre-scale stromatolite flakes in overlying cross-bedded sandstones (e.g. Fig. 6.5h). The stromatolites are composed predominantly of micrite with varying proportions of sand grains. This sand fraction is composed primarily of poorly-sorted, subangular to subrounded quartz, which varies in grain size from coarse to very fine. The lamination is formed through the intercalation of layers rich in siliciclastic grains with those of a cleaner micrite. The former are commonly associated with minor haematite staining. This results in a maroon discoloration that is observed within the encompassing micrite matrix.

6.3.1.4.3. *Sheet- and channelised sandstone and conglomerate facies (2c)*

Pale yellow- and grey-weathering sandstone (Sm, Ss) and conglomerates (Gm, Gs) are common within the W2 Member (Fig. 6.5b and f). These display both channelised and sheet-like geometries and are generally between 0.1 and 1 metres thick. Grain size is predominantly

medium to coarse but grades into the associated pebbly sandstones and conglomerates in places (Fig. 6.5b). The grains are composed primarily of subrounded to subangular quartz with minor feldspar and lithic fragments in a fine-grained matrix. In comparison with subaqueous sandstones of the W3 Member, the ratio of grains to matrix is considerably lower. Conglomerates are similar in texture and composition to those seen elsewhere.

In places, these sands form distinct lenses with channel geometries. Here, an erosive base is seen with occasional lags. Trough cross-stratification is common as well as smaller scale uni-directional cross-lamination. Outsized clasts are prevalent, typically constituting <5% of the sediment although this is higher in some areas and can shown normal grading. In places, particularly where sands overlie or are positioned adjacent to stromatolitic lithologies, intraclasts of stromatolitic carbonate are common. A small channelised sandstone body with a current-rippled top was identified within rhythmites at Reinsryggen (Fig. 6.2a). In other areas sandstones are observed to form laterally extensive, sheet-like geometries up to 2 metres thick. The structure can be massive, planar-stratified and cross-stratified. At the Ditlovtoppen section, medium to well-sorted, cross-bedded sheet sandstones were observed that display medium to well-rounded, frosted grains.

6.3.1.4.4. *Dolocreted sandstone, mudstone and evaporite facies (2d)*

Dolocreted sandstones (Sm, Ss) and mudstones (Fm) (e.g. Fig. 6.5g), originally identified and described in detail by Fairchild et al. (1989), can be identified as a separate facies occurring within sandstones or within discrete beds within siltstones. Dolocreted units are typically thin (10 cm) and can form at multiple intervals within a bed. The sand fraction is typically compositionally similar to those associated with facies 1a, but dolocreted sandstones can be readily distinguished by the presence of a dolomite-rich matrix in which skeletal grains can float freely.

Beds of maroon friable mudstone occur locally. These are up to 1 metre thick and are commonly intercalated with thin sandstone units. They are typically composed of a dolomicrite with varying proportions of quartz, clay minerals and lithics and are similar in appearance and

composition to the matrix of the diamictite lithofacies (2a). Discrete dolocreted horizons occur locally where displacive dolomite is observed. These can display a concretionary appearance with a compaction drape of surrounding mudstones. In places, a cm-dm-scale vuggy texture is observed. These vugs are lined by dolomite crystals. A similar vuggy texture is also seen at certain intervals within the rhythmites and sandstones. A distinctive metre-scale unit of stromatolitic dolomite and dolocreted sandstone, that displays a brecciated base, is seen at Dracoisen. This was interpreted by Fairchild et al. (1989) as an evaporite dissolution breccia. It has possibly the heaviest oxygen isotope signatures in the geological record (Bao et al., 2009) and the dolocretes likewise typically have heavier oxygen isotope compositions than non-glacial Neoproterozoic dolomites.

6.3.1.5. Lithofacies interpretation

The diamictites and conglomerate lithofacies seen within the W2 Member are lithologically similar to those associated within the diamictite and conglomerate lithofacies of the W3 Member (1a). These probably formed in a similar way, in a subaqueous environment, through predominantly rainout process. The appearance of such facies suggests that the glacial input into the basin continued during the deposition W2. However, the presence of other facies such as stromatolitic carbonates and rhythmically laminated sediments with no outsized clasts suggest that sustained ice-free periods existed during deposition.

The carbonate bearing lithologies of the W2 Member were extensively investigated by Fairchild et al. (1989) who made detailed comparisons with the hyperarid McMurdo Dry Valleys of Antarctica. The carbonate-siliciclastic couplets were regarded as a diagnostically lacustrine style of sedimentation. The heavy oxygen isotope values in the dolomitic facies were used as evidence for strongly evaporative conditions in a lacustrine environment. The identification of dolocretes and collapse brecciation provide further support for evaporative conditions. Channelised sandstone and conglomerates are consistent with fluvial and glaciofluvial deposition under terrestrial conditions.

6.3.1.6. Palaeoenvironmental interpretation

Therefore, an ice-marginal pro-glacial and glaciolacustrine landsystem is proposed following the interpretations of Fairchild and Hambrey (1984) and Fairchild et al. (1989). In this scenario, diamictites and conglomerates formed during glacial advance phases. The lower clast composition of diamictites could suggest that the contribution of clasts through ice-rafting is lower than that of the W3 Member facies. This may indicate that a lower density of icebergs were present which were possibly related to smaller, more restricted glaciers.

Rhythmites and stromatolites presumably represent glacial retreat phases, but the presence of rare till pellets and outsized clasts, interpreted as dropstones, suggest that glaciers not completely removed from the landsystem. Deposition occurred under predominantly stable, shallow-water conditions which allowed the development of stromatolites and rhythmites. Periodic aridity resulted in the formation of evaporites, dolocretes and floodplain muds. During this, proglacial streams, possible draining from the ice margin, resulted in the deposition of channelised and sheet-like sands and gravels as glaciofluvial deposits. The identification of cross-bedded, medium to well-sorted sands with frosted grains may, in addition, indicate possible aeolian deposition.

The intercalation of these lithofacies associations suggests that the deposition was highly variable. Similar, variability within glacial secessions have been observed in other Cryogenian glacial deposits (e.g. Allen and Etienne, 2008; Le Heron et al., 2011; Le Heron et al., 2013b) and could be interpreted as the waxing and waning of glaciers or ice sheets.

6.3.2. Deformational facies associations

The Deformational Facies Associations (Fig. 6.6 and Table 6.3) are observed immediately above the W2 Member at Reinsryggen, Ditlovtoppen and Andromedafjellet, but are absent from Dracoisen. They can be subdivided into: (3a) deformed rhythmites, (3b) diamictites, (3c) sandstones and conglomerates and (3d) boulder pavements.


a)
Faceted surface
Striations
8 cm
b)
Friable diamictite
Zones of reduced sediment
Faceted surface
Striated boulder pavement
60 cm
c)
Lodged clast
Recumbent folding in reduced horizon
2 m
d)
Shear bands in reduced layers
Friable diamictite
20 cm
e)
Friable diamictite
Deformed rafts of rhythmite
30 cm
f)
Folding of rhythmite horizon
Brittle faulting and brecciation of carbonate layers
20 cm
g)
Glaciotectonic thrust
Lens of diamictite
40 cm
h)
Friable diamictite
W3
W2
Intense folding and brecciation of rhythmites
1 m

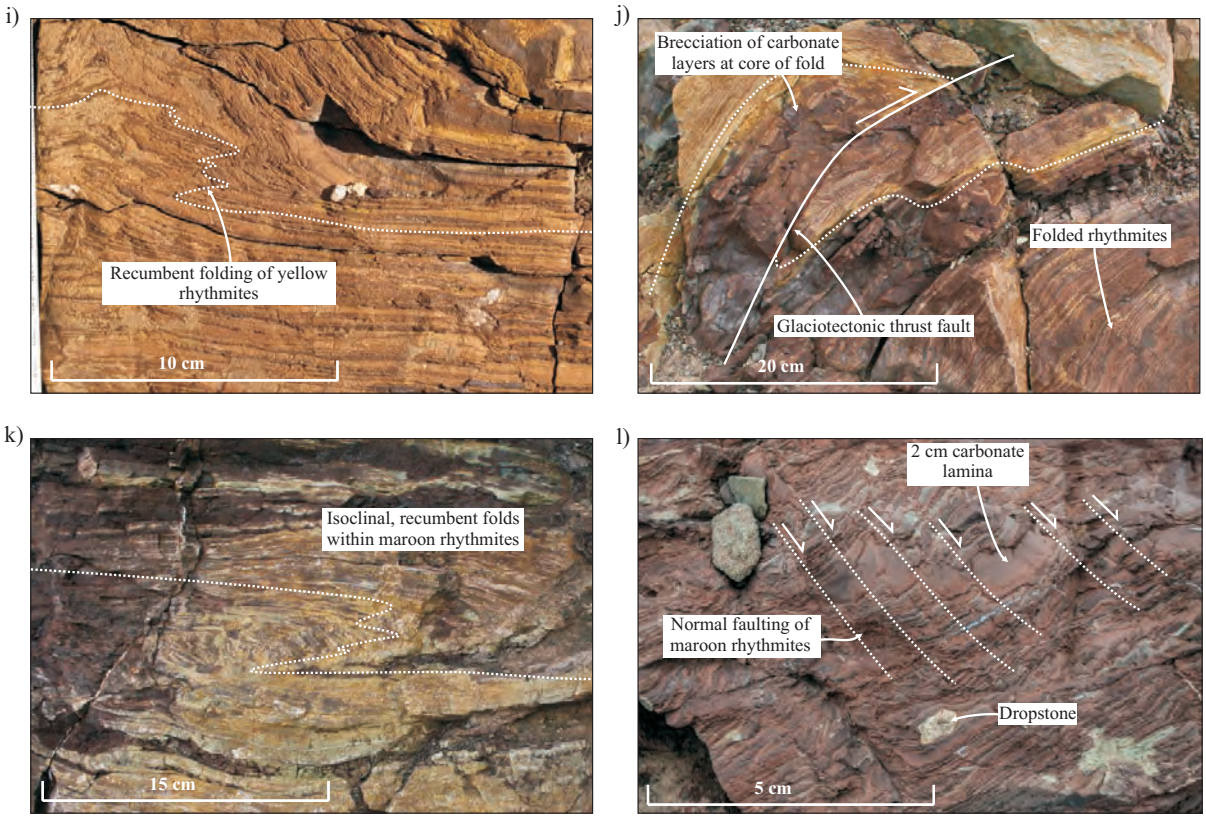

Fig. 6.6 – Field photographs of the typical sediments associated with the deformational facies associations: (a) is from Reinsryggen, (b)-(k) are from Ditlovtoppen and (l) is from Andromedafjellet. (a) Clast of black limestone from a massive diamictite bed showing a faceted, polished surface with several sets of striations. (b) Boulder pavement showing a large faceted granite clast overlain by mottled, friable diamictite (photo: DB). (c) Subglacial diamictite showing large, faceted dolostone clast within a massive diamictite bed with a fold picked out by mottling, overlain by massive diamictite (photo: MJH). (d) Subglacial diamictite beds with horizon displaying mottling in sheared horizons (photo: IJF). (e) Deformed rafts rhythmite from the W2 Member within massive friable diamictite (photo: DB). (f) Inclined fold at the top of deformed rhythmites displaying brecciation of individual carbonate lamina (photo: IJF). (g) Glaciotectonic thrust at the W2/W3 Member transition, showing partial raft formation (photo: MJH). (h) Folded and faulted rhythmite overlain by friable diamictites of the W3 Member (photo: MJH). (i) Recumbent fold with rhythmites with smaller-scale parasitic folds (photo: IJF). (j) Glaciotectonic thrust fault within deformed rhythmites (photo: DB). (k) Isoclinal recumbent folding with maroon rhythmites (photo: DB). (l) Steeply dipping normal faults causing displacement of a 2 cm carbonate lamina within deformed rhythmites.

6.3.2.1. Facies description

6.3.2.1.1. *Deformed rhythmite facies (3a)*

Evidence for extensive disruption and deformation of rhythmites are seen at Ditlovtoppen and Andromedafjellet in the uppermost part of the W2 Member, at the boundary with the W3 Member. The deformed rhythmites display extensive folding and faulting at both micro and

Facies	Description	Lithofacies codes	Interpretation
Deformed rhythmites (3a)	Intercalated silt-sand-carbonate rhythmites exhibiting both ductile (recumbent folds) and brittle (normal and reverse offset faulting and brecciation) deformation. Exhibits an increase in intensity of deformation towards the top. Often overlain by massive diamictite with intraclasts and lenses of the underlying rhythmite.	**Fl(d)** *Dm* *Dm(d)* *Fl*	Quiescent subaqueous sedimentation during an ice retreat phase. Overridden by grounded ice during an ice advance phase and glaciotectonised by an ice advance to the north. The increase in apparent deformation reflects strain profile through the sediment. Rhythmite lenses are interpreted as rafts, dislocated from underlying sediments and emplaced within a subglacial till.
Diamictites (3b)	Massive diamictite, occasionally exhibiting deformed stratification (Fig. 8b) showing strong, consistent clast fabric and AMS fabrics. Predominantly sub-rounded to SA clasts (low Ra-RWR, Fig. 11). Often associated with lenticular sandstone and conglomerate (below).	**Dm** **Dm(d)** *Sm(d)* *Ss(d)* *Fl(d)* *Fm(d)*	Subglacial debris originating through subglacial erosion and transportation. When associated with other subglacial facies, massive diamictites are interpreted as subglacial tills deposited by grounded ice. If associated with glacio-aqueous facies it may also form in subaqueous environment.
Lenticular sandstones and conglomerates (3c)	Lens shaped sandstone and conglomerate bodies (<1 m – 5 m thick) occurring with massive diamictite. Sometimes show internal stratification with cross-stratification and rare climbing ripples. Commonly show visible disruption around margin such as folding and faulting. Surrounding diamictite often envelops the lens.	**Gm(d), Gs(d)** **Sm(d), Ss(d)** *Fl(d)* *Fm(d)* *Dm* *Dm(d)*	Subglacial channel deposits during ice-grounding. Deposits may have initially eroded into underlying sediments as Nye channels. Subsequently deformed and sheared during as part of the subglacial till mosaic.
Boulder pavements (3d)	Prominent surfaces within otherwise massive diamictites containing a high proportion of large (>10 cm diameter) clasts with consistent striations (NW-SE). Clasts commonly display stoss-and-lee forms, often with a facetted upper surface. Strong, consistent AMS and clast fabrics.	**Gm** *Dm* *Dm(d)*	Formed through subglacial deposition and erosion by either (i) a period of erosion at the ice-bed interface and faceting and realignment of clasts because of the overriding ice, or (ii) decoupling within the bed at a décollement surface, within sediment.

Dm = Massive diamictite; **Ds** = Stratified diamictite; **Gm** = Massive conglomerate; **Gs** = Stratified conglomerate; **Sm** = Massive sandstone; **Ss**= Stratified sandstone **Fm** = Massive mudstone/siltstone; **Fl** = laminated mudstone/siltstone; **(d)** =deformed; dominant lithofacies (in bold); associated lithofacies (in italics).

Table 6.3 – Summary of the lithofacies that make up the deformational facies association.

macroscopic scales, but they otherwise compositionally and texturally correspond well to the undisturbed rhythmites of the undeformed W2 Member facies. At Ditlovtoppen, a 2 metre-thick zone of deformed rhythmites are observed which pass into overlying diamictites of the W3 Member (Fig. 6.6h). The deformed zone can be traced 200 metres laterally along strike and is exposed on several buttresses. Deformed rhythmites are also seen at Andromedafjellet in a 1 metre-thick zone that is located beneath massive maroon diamictites of the W3 Member. The rhythmites are composed of 2–10 mm silt/sand – carbonate couplets with a slightly greater sand fraction than those at Ditlovtoppen.

6.3.2.1.2. *Diamictites facies (3b)*

Massive diamictites (Dm) are commonly associated with the deformational facies associations. They are typically located immediately above the W2 Member at Reinsryggen, Andromedafjellet and Ditlovtoppen but are also seen higher in the succession at Reinsryggen and Andromedafjellet. Diamictites of the deformational facies association are similar both compositionally and texturally to the diamictites of a subaqueous origin. They are composed of a poorly sorted mix of clasts (both intrabasinal and extrabasinal) in a matrix dominated by fine-medium quartz, with minor lithics. However, differences can be seen through subtle textures and fabric and by their close association with the other deformational facies associations.

Clast-matrix ratios and composition are variable, but both ratios and the proportion of extrabasinal clasts are typically higher than in the diamictite lithofacies of the undeformed W3 Member. At Ditlovtoppen, for example, a granite-rich horizon is seen in diamictites above the W2 Member with a clast-matrix ratio above 40%. The clasts consist predominantly of granule- to pebble-sized, subangular to subrounded red granites. Immediately overlying deformed rhythmites of the W2 Member at the same section, diamictites contain subangular fragments of rhythmite and carbonate. Diamictites of the deformational facies association commonly display a fissile weathering pattern and are almost exclusively maroon, although mottling occurs locally (e.g. Fig. 6.6c and d); in other cases, the diamictites are massive. Diamictites of the deformational facies are

commonly associated with deformed lenses of sandstone and conglomerate (3c).

6.3.2.1.3. *Sandstone and conglomerate facies (3c)*

Occurring within the diamictites are lenses of maroon and pale yellow-grey sandstone (Sm, Ss) and conglomerate bodies (Gs, Gm). These are generally less than 2 metres in diameter but are locally up to 25 metres (Fig. 6.8). The sandstone is predominantly medium grained; however, the lenses are locally much finer. In addition, conglomerates occur locally, either as isolated lenses or as dispersed clasts within sandstone lenses. Sands are typically poorly sorted and are dominated by subangular to subrounded grains of quartz, lithic fragments and opaque minerals in a fine-grained matrix of varying proportions (5 - 20%).

Contacts with surrounding diamictites are typically sharp, although a 5 cm-thick reduced zone is seen occasionally within the maroon diamictite that envelops the lenses. The structure is either massive or can display subtle stratification (Fig. 6.8c). This is commonly seen to be folded and faulted. Some lenses appear less deformed and display subtle cross lamination with rare climbing ripples (Fig. 6.8d). At Reinsryggen, small (2 - 4 metres wide) deformed sandstone lenses are overlain by a large 10 metre-wide sandstone body (Fig. 6.8). This has a distinctive erosive base and truncated top at the boundary with a nascent boulder pavement (Fig. 6.8a).

6.3.2.1.4. *Boulder pavements (3d)*

Boulder pavements occur at two localities within the Wilsonbreen Formation. At Ditlovtoppen (Fig. 6.7), a distinct boulder pavement is seen 2 metres above the contact with deformed rhythmites of the W2 Member. It is composed of a boulder conglomerate with clasts predominantly 10-20 cm, but up to 50 cm in diameter. Clast lithologies are mostly dolostone, but other intrabasinals and extrabasinals are present. They are clast-supported but sit in maroon sandy matrix that is composed of fine-grained, subangular quartz and lithics in a silty-sand matrix. Clasts at the top surface of the pavement show a faceted top. On which, unidirectional striations are present that are orientated parallel to the bedding plane and trend at 130° to 72°.

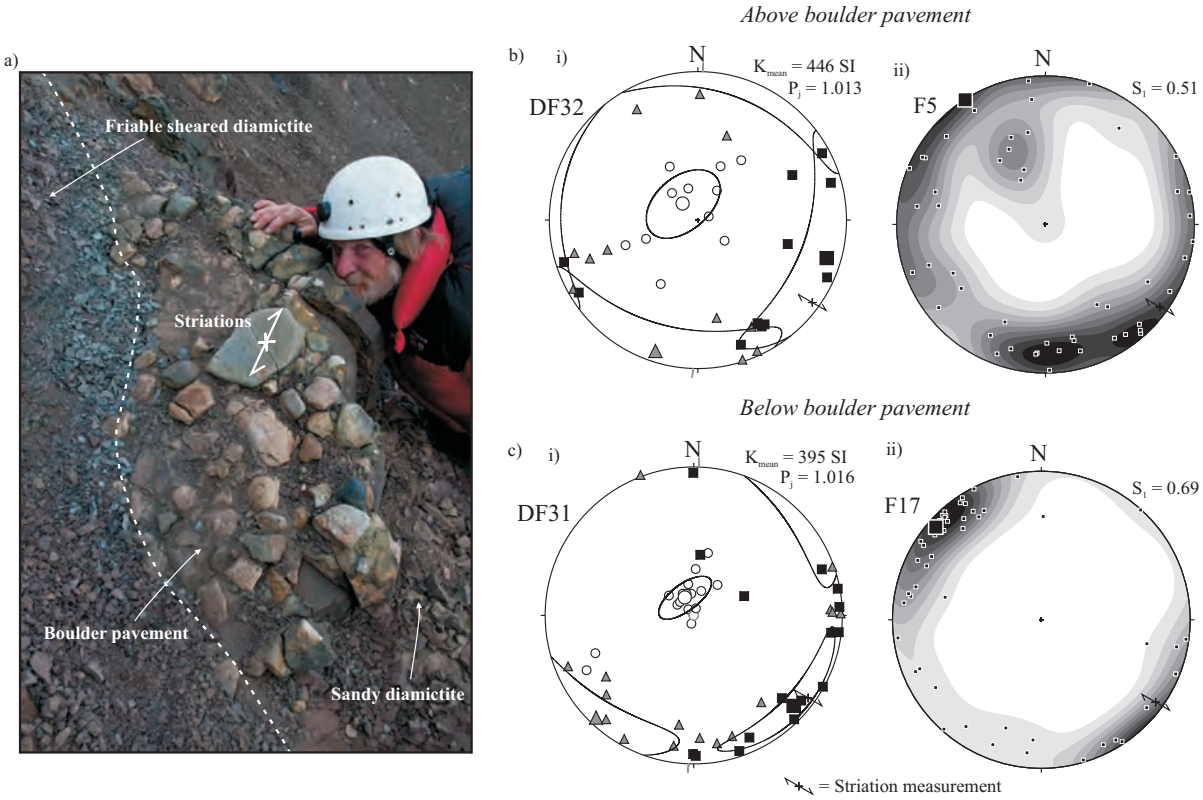

Fig. 6.7 – The boulder pavement at Ditlovtoppen. (a) Field photograph of the boulder pavement showing faceted, striated clasts overlain by friable diamictite (photo: MJH). Equal-area, lower-hemisphere stereonets from (b) above the boulder pavement and (c) below the boulder pavement showing (i) AMS results and (ii) clast fabric orientations.

Overlying the boulder pavement is a massive, maroon diamictite which has similar compositional and textural characteristics to the diamictites of the deformational facies association (3b). 25 metres along strike, the boulder pavement changes to a granite-rich horizon that contains clasts concentrations of over 30%.

A similar boulder pavement is seen at Reinsryggen (Fig. 6.8), occurring 30 metres above the contact with the W2 Member. In contrast to the boulder pavement at Ditlovtoppen, the clasts are matrix-supported and concentrations are distinctly lower (10%). The clasts sit in a maroon sandy diamictite with a silty-sand matrix which has the same composition as that from diamictites of the deformational facies association (3b). 40 metres along-strike to the north, the boulder pavement lies at the top of a 30 metres wide channelised maroon sandstone body composed of poorly-sorted, fine-grained subangular quartz. Clasts show a faceted top surface (Fig. 6.8b), but striations were not observed at this locality.

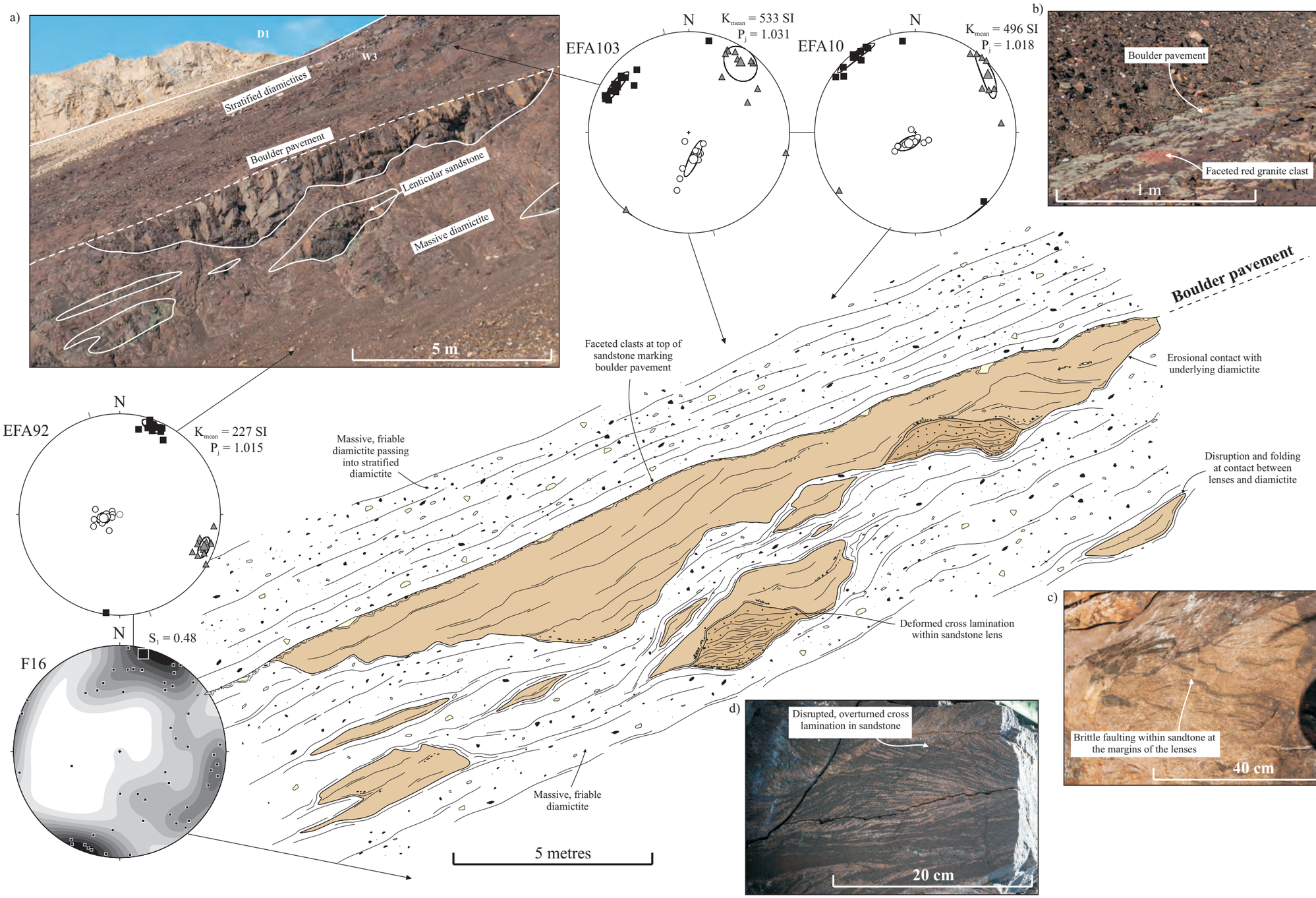

Fig. 6.8 – Interpretative sketch and photographs of deformational facies associations at Andromedafjellet. (a) Field photograph and subsequent interpretative sketch displaying a boulder pavement overlying a subglacial diamictite with lenticular sands and channel structures. (b) Faceted granite clast at the top of a clast-poor boulder pavement, overlain by massive maroon diamictite. (c) Conjugate faulting and folding of wispy lamination surrounding a sandstone lens. (d) Sandstone lens with displaying disrupted, overturned cross-stratification.

6.3.2.2. Clast shape analysis of diamictites

Figure 6.9 shows the results from systematic clast shape analysis of massive diamictites from the Wilsonbreen Formation. Ternary shape diagrams and roundness histograms for the massive diamictites of the W2 and W3 Members are shown in Figure 6.9b. The C_{40} index, defined by the percentage of clasts with c:a ratios ≤ 0.4, is seen to be relatively low, ranging from 28% to 60%. This therefore indicates that a large proportion of the clasts are can be defined as 'blocky' as opposed to platy or elongate. In all sites, the majority of the clasts sit in the subangular to subrounded realm. Very angular and well-rounded clasts are rare or absent in all cases. The clast shape results of massive diamictite of the deformational facies associations (Fig. 6.9bii, iv, vi and viii) do not show any distinct difference in clast shape when compared to massive diamictites from the undeformed facies of the W3 Member (Fig. 6.9bi, iii, v and vi).

Covariance plots of RWR-C_{40} and RA-C_{40} for massive diamictites are shown in Figure 6.9c. A close spread of data is seen in both plots which reflect the consistent low to medium C_{40} values and very low RA and RWR values at all sites. Figure 6.9d shows the results from modern control sites at polythermal Svalbard glaciers (Fig. 6.9di) and cold Antarctic glaciers (Fig. 6.9dii) (Hambrey and Glasser, 2012). As a general rule, in warm and polythermal glaciers, clasts that have been derived through supraglacial transport paths typically display high C_{40} and RA, but low RWR values. In contrast, clasts derived through subglacial transport paths typically display low C_{40} and RA values and low RWR values. Finally clasts, derived through fluvial transport pathways typically display medium C_{40}, low RA and medium RWR values. Within the Wilsonbreen Formation, the clasts plot within the subglacial realm. This suggests that the clasts have been derived through subglacial pathways.

6.3.2.3. Macrostructural analysis

The rhythmites of the deformation facies association (3a) display a variety of soft-sediment deformation features at the macroscopic (outcrop) scale through the occurrence of folding and faulting (Fig. 6.10). An increase in intensity of deformation is seen towards the top, and the

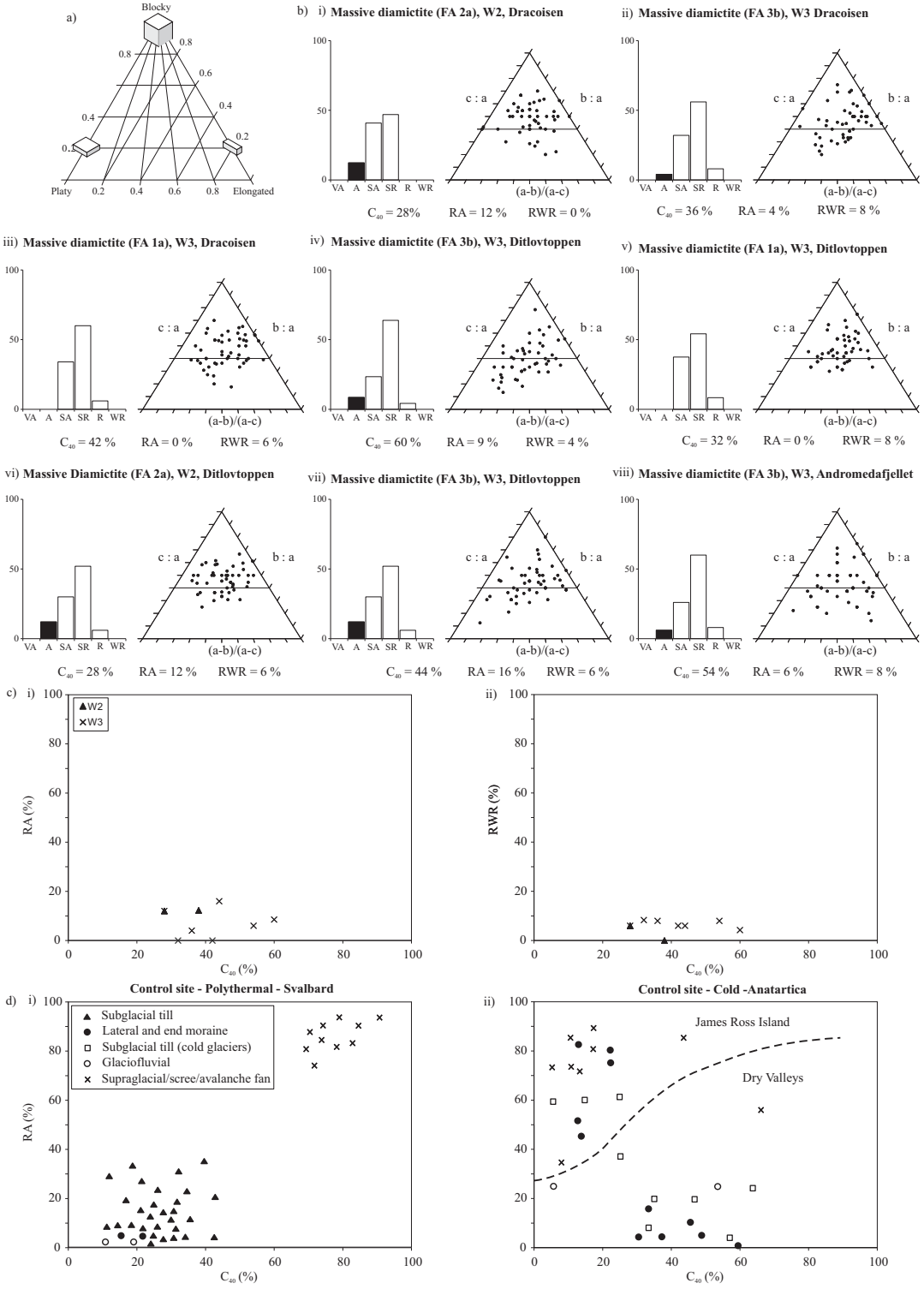

Fig. 6.9 – Clast morphological data. (a) Visual representation of triangular diagrams showing blocky, platy and elongate end members (after Benn and Ballantyne, 1993). (b) Clast shape (triangular diagrams) and roundness (histograms) data for massive diamictites from the Wilsonbreen Formation. (c) Covariance plots for all data from the Wilsonbreen Formation and (d) Modern control sites for comparison (after Hambrey and Glasser, 2012) showing variation in RA vs. C_{40}-index from (i) polythermal glaciers in Svalbard (Midre Lovénbreen, Austre Lovénbreen and Austre Brøggerbreen) (ii) cold glaciers in Antarctica (Antarctic Dry Valleys and James Ross Island).

rhythmites pass into massive diamictites (3b). At the base of the facies, deformation is typically small-scale and is characterised by the occurrence of conjugate faults, showing both low-angle and high-angle reverse offset. Some display possible Riedel shear geometries (Riedel, 1929) (e.g. Fig. 6.11b). The offset along faults is typically low (up to several cm). In addition, small-scale thrust-faults and augen-like structures are seen.

The offset along conjugate brittle faults and thrusts increases upwards in the section towards the boundary with the diamictite. Larger-scale recumbent folds are seen on the 0.2-1 metre scale (Fig. 6.6f, i and k). Smaller-scale parasitic folding is sometimes seen on fold limbs. Fold vergence is typically to the north, although precise measurement is typically not possible because of a lack of three-dimensional exposure. Larger-scale thrusts are also observed showing displacement of 50 cm and over (Fig. 6.6g and j), and southerly dips prevail.

The boundary with the overlying diamictites is typically transitional. At the top of the deformed rhythmites, north-verging, low-angle reverse faults are observed (Fig. 6.6g and j), some showing displacement over 1 metre. At Ditlovtoppen (Fig. 6.10a and b), dolomite rafts occur at the boundary between the diamictites and the rhythmites, showing internal folding and faulting and brecciation e.g. (Fig. 6.10b). In places, overlying diamictites are seen to envelop 0.5–2 metre lenses of deformed rhythmite (Fig. 6.6e).

Diamictites of the deformational facies association are typically similar in structure to those of a subaqueous origin (1a). The key difference is the close relationship of other deformed facies within the deformed facies association and the presences of rafts of underlying units and deformed lenses. For examples, at Reinsryggen (Fig. 6.8) the diamictites beneath the boulder pavement contain deformed lenses of sandstone and conglomerate bodies (e.g. Fig. 6.8 c and d). The surrounding diamictite displays a weak fabric that appears to envelope the lens structure. Wispy lamination is sometimes seen immediately surrounding the lenses, showing evidence for small-scale folding and faulting (Fig. 6.8c). The sandstone lenses themselves are massive or stratified. If present, the stratification is commonly undulating and folded and faulting is common, especially at the margins of the lenses.

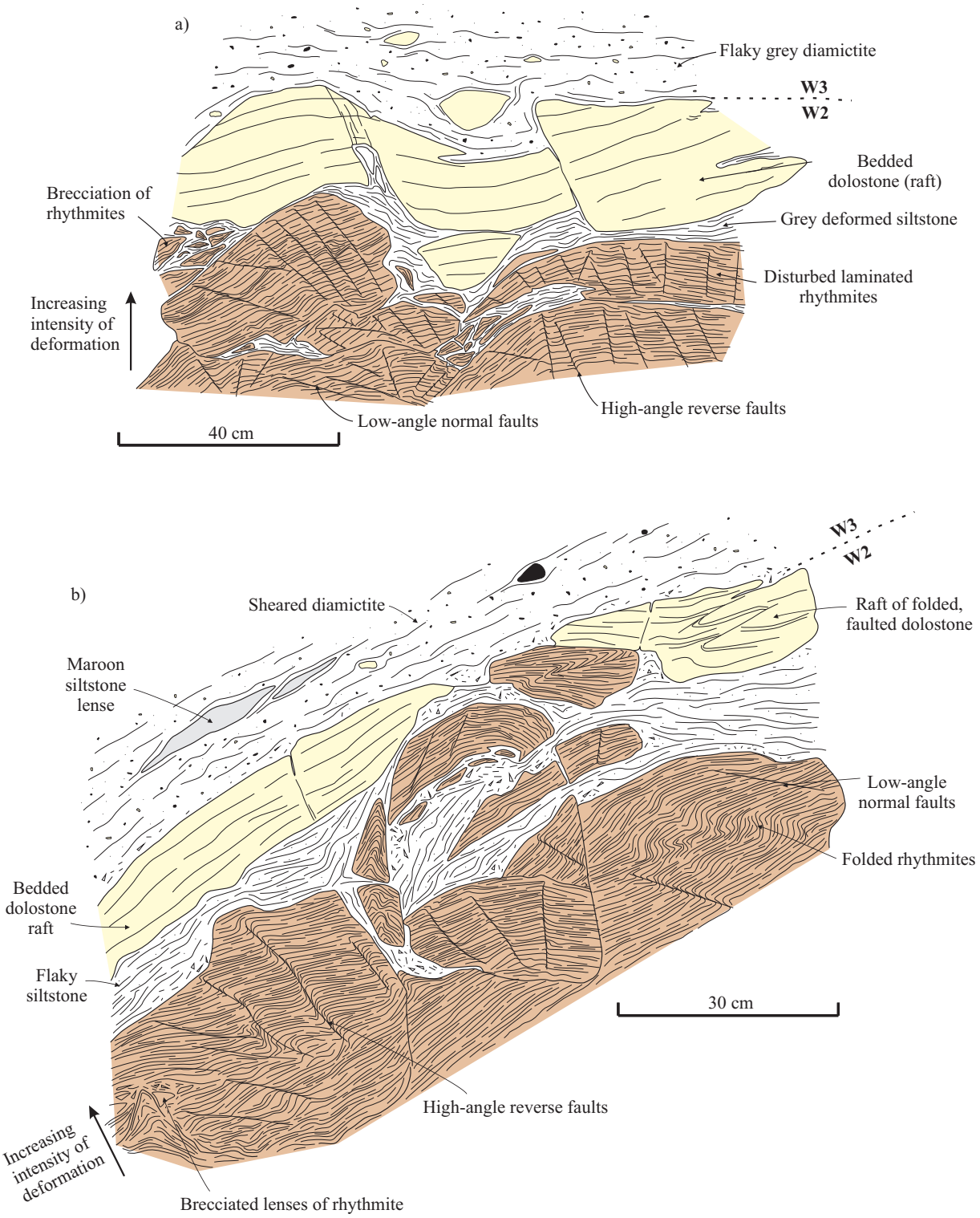

Fig. 6.10 – Interpretative sketches of deformational structures at the W2-W3 Member transition at Ditlovtoppen. (a) Deformed rhythmite showing conjugate, brittle faulting becoming progressively brecciated and disrupted towards the top. Overlain by a deformed dolostone raft with internal faulting and brecciation that passes into a subglacial diamictite. (b) Deformed rhythmites with rafts becoming detached and becoming incorporated into the overlying subglacial diamictite with sheared lenses of siltstone and sandstone.

6.3.2.4. Microstructural analysis

Evidence of intense folding and faulting in the deformed rhythmite facies is also seen microscopically (Fig. 6.12). Deformation has taken place in both brittle and ductile manners. This is determined in part by the composition. Rhythmite couplets composed of carbonate display brittle deformation, often breaking into fragments separated by faults (Fig. 6.12a and b). In contrast, the silt-sand component of the rhythmite is seen to behave in a ductile manor and is commonly folded and fills in the space between the carbonate layers. This is clearly seen in Figure 6.12b where the rhythmite displays a close monocline structure. At a large scale, the bed appears to be folded; however, microscopic analysis reveals that the folding is partially facilitated through faulting. Brittle deformation has occurred within the carbonate lamella which produces tabular fragments, whilst the silt-sand fraction has undergone predominantly ductile deformation.

Faulting within the deformed rhythmites can appear chaotic in places (e.g. Fig. 6.12a) and the analysis of fault kinematics can be difficult; however, high-angle reverse faults and low-angle normal faults (Fig. 6.12d) dipping to the south are common. These could be interpreted as R_1 and R_2 Riedel shear geometries, associated with shear to the north. Low-angle thrusts are also present typically dipping to the south (Fig. 6.12a). In places at the boundaries between faulted carbonate laminae, a network of sand-filled veins can be observed microscopically (e.g. Fig. 6.12b). Sand within these veins has the same composition as the silt-sand component of the rhythmite couplet, but typically contains less of the silt fraction.

An increase in the amount of folding and faulting is seen up to the boundary with the overlying diamictite. Figure 6.12d shows a highly deformed rhythmite taken from close to this boundary at Andromedafjellet. Sand within the rhythmites displays an augen-like geometry with asymmetric tails suggesting shear to the north. On either side of this augen structure, a low-angle shear zone dipping to the north separates the augen from the surrounding sandy lamination.

Site	Lat/long		Lithology	Location	Unit	Bedding	Dip	No	Km (SI)	K_1		*K_1 95% Error*		K_2		*K_2 95% Error*		K_3		*K_3 95% Error*		L	F	P_j	T
DC2	79.2055	18.4020	**Diamictite**	Dracoisen	**W1**	343	51	18	336	**350**	**31**	*32*	*11*	**122**	**48**	*32*	*20*	**243**	**25**	*21*	*12*	1.003	1.005	1.008	0.273
DC5	79.2057	18.4056	**Carbonate**	Dracoisen	**W2**	341	51	6	123	**194**	**6**	*51*	*9*	**106**	**16**	*51*	*17*	**308**	**73**	*21*	*13*	1.001	1.002	1.003	0.09
DC57	79.2153	18.3980	**Diamictite**	Dracoisen	**W3**	334	43	10	272	**132**	**28**	*27*	*7*	**27**	**26**	*27*	*15*	**261**	**50**	*16*	*7*	1.004	1.006	1.01	0.251
DC6	79.2056	18.4073	**Rhythmites**	Dracoisen	**W2**	341	51	11	188	**131**	**38**	*62*	*17*	**20**	**25**	*62*	*23*	**266**	**43**	*27*	*15*	1.002	1.024	1.026	-0.844
DC61	79.2153	18.3979	**Diamictite**	Dracoisen	**W2**	341	51	17	198	**151**	**22**	*16*	*7*	**50**	**25**	*22*	*16*	**277**	**55**	*23*	*5*	1.004	1.008	1.013	0.299
DC62	79.2153	18.3979	**Diamictite**	Dracoisen	**W3**	341	51	10	216	**355**	**4**	*24*	*13*	**86**	**17**	*26*	*15*	**254**	**73**	*22*	*9*	1.004	1.009	1.014	0.448
DC63	79.2153	18.3982	**Diamictite**	Dracoisen	**W3**	341	51	18	260	**9**	**25**	*25*	*6*	**133**	**40**	*24*	*7*	**254**	**32**	*7*	*6*	1.002	1.011	1.015	0.657
DC65	79.2151	18.4003	**Diamictite**	Dracoisen	**W3**	330	46	18	50	**23**	**47**	*41*	*15*	**114**	**2**	*45*	*35*	**206**	**43**	*40*	*17*	1.003	1.002	1.005	-0.096
DC7	79.2058	18.4082	**Carbonate**	Dracoisen	**W3**	341	51	11	239	**123**	**2**	*64*	*9*	**33**	**3**	*64*	*14*	**239**	**87**	*20*	*8*	1.002	1.009	1.012	0.663
DF25	79.0816	18.4104	**Diamictite**	Ditlovtoppen	**W3**	004	42	15	357	**133**	**50**	*62*	*10*	**3**	**29**	*62*	*15*	**258**	**26**	*17*	*11*	1.001	1.021	1.025	0.9
DF26	79.0815	18.4103	**Diamictite**	Ditlovtoppen	**W3**	001	30	9	368	**176**	**17**	*30*	*9*	**75**	**34**	*30*	*10*	**288**	**51**	*10*	*9*	1.004	1.015	1.021	0.557
DF29	79.0809	18.4079	**Rhythmites**	Ditlovtoppen	**W2**	003	30	15	197	**146**	**20**	*39*	*3*	**46**	**26**	*39*	*5*	**269**	**56**	*11*	*3*	1.002	1.029	1.035	0.881
DF30	79.0809	18.4079	**Rhythmites**	Ditlovtoppen	**W2**	003	30	13	147	**174**	**10**	*8*	*2*	**78**	**28**	*9*	*3*	**282**	**60**	*5*	*2*	1.004	1.036	1.045	0.799
DF31	79.0807	18.4077	**Diamictite**	Ditlovtoppen	**W3**	002	39	16	395	**139**	**38**	*37*	*8*	**31**	**21**	*38*	*15*	**279**	**45**	*17*	*7*	1.004	1.012	1.016	0.536
DF32	79.0807	18.4077	**Diamictite**	Ditlovtoppen	**W3**	002	39	11	446	**98**	**44**	*57*	*16*	**189**	**1**	*57*	*16*	**280**	**46**	*17*	*16*	1.003	1.009	1.013	0.477
DFB2A	79.0819	18.4093	**Diamictite**	Ditlovtoppen	**W2**	004	42	7	186	**159**	**34**	*15*	*2*	**29**	**43**	*15*	*12*	**269**	**28**	*12*	*2*	1.004	1.008	1.012	0.396
DFB4D	79.0833	18.4129	**Rhythmites**	Ditlovtoppen	**W2**	004	42	12	435	**351**	**14**	*16*	*7*	**92**	**40**	*25*	*7*	**256**	**47**	*25*	*10*	1.007	1.005	1.011	-0.152
DFB4F	79.0833	18.4129	**Rhythmites**	Ditlovtoppen	**W2**	004	42	8	579	**186**	**11**	*44*	*7*	**86**	**39**	*44*	*9*	**289**	**49**	*12*	*7*	1.004	1.023	10.29	0.676
EFA121	78.9528	18.4257	**Sandstone**	Andromedafjelle	**W2**	253	40	12	171	**263**	**42**	*16*	*4*	**160**	**14**	*16*	*7*	**55**	**45**	*7*	*5*	1.005	1.003	1.008	-0.273
EFA128	78.9528	18.4257	**Diamictite**	Andromedafjelle	**W3**	251	40	7	409	**154**	**24**	*16*	*3*	**259**	**30**	*15*	*2*	**32**	**50**	*4*	*2*	1.005	1.02	1.027	0.578
EFA146	78.9528	18.4257	**Diamictite**	Andromedafjelle	**W3**	251	40	11	561	**190**	**22**	*12*	*6*	**296**	**34**	*13*	*6*	**74**	**48**	*9*	*5*	1.008	1.01	1.018	0.108
EFA10	78.9383	18.4281	**Sandstone**	Reinsryggen	**W3**	256	40	9	496	**322**	**18**	*14*	*4*	**222**	**27**	*16*	*6*	**82**	**57**	*10*	*5*	1.006	1.011	1.018	0.261
EFA103	78.9383	18.4325	**Diamictite**	Reinsryggen	**W3**	256	40	12	533	**298**	**12**	*12*	*5*	**31**	**13**	*16*	*12*	**165**	**74**	*16*	*4*	1.013	1.017	1.031	0.116
EFA92	78.9383	18.4325	**Diamictite**	Reinsryggen	**W3**	253	40	11	227	**190**	**17**	*7*	*5*	**287**	**20**	*7*	*5*	**64**	**63**	*6*	*4*	1.007	1.008	1.015	0.087

Table 6.4 - Mean site AMS data. No = number of samples; Km = mean susceptibility; K_1, K_2, K_3 = orientations (declination and inclination) of the principal susceptibility axes with 95% confidence ellipses; L = lineation ($L = K_1/K_2$); F = foliation ($F= k_2/k_3$); P_j = anisotropy degree; T = shape parameter; Fabric = whether the fabric can be classified as 'normal' (K_3 perpendicular, K_1/K_2 parallel to the bedding plane), 'inverse' (K_1 perpendicular and K_2/K_3 parallel to the bedding plane) or anomalous (K_1/K_2 deviation by >25° from bedding).

6.3.2.5. AMS and clast fabric analysis

6.3.2.5.1. *AMS fabric*

AMS results (Table 6.4) are shown on lower-hemisphere, equal-area stereographic projections (Fig. 6.2) linked to the corresponding locations on the log from where the samples were taken. In Chapter 5, it was shown that, in most samples, the AMS was controlled by paramagnetic minerals. A minor anomalous SD ferromagnetic source was identified in some samples (Chapter 5, Section 5.8.2) and were omitted from subsequent analysis. Samples are typically oblate to triaxial with a mean corrected anisotropy degree (P_j) of 1.011 (Table 6.4). The mean AMS orientations from samples within the study area at all sites are shown in Figure 6.13a. The mean (K_1) plunges gently (5°) to the SSE at a mean azimuth of 158°, and the mean minimum susceptibility axis (K_3) is subvertical (85° to 325°), defining the pole to the magnetic foliation (K_1-K_2 plane), whilst the mean intermediate susceptibility axis (k_2) plunges gently to the NNE (01° to 068°).

Variation in azimuth of the mean K_1 axes is seen within the stratigraphic section at some sites. For example, at Ditlovtoppen (Fig. 6.2c) a possible shift in fabric orientation is seen. AMS fabrics at the top of the W2 Member typically lie in a north-south orientation, whilst higher in the sequence a shift is seen to predominantly NW-SE orientated K_1 azimuths. In spite of this local variation, the dominant fabric trend lies in a north-south orientation at all sections.

In addition, the AMS fabric is shown from diamictites associated with the boulder pavements (Fig. 6.7 and 6.8). Figure 6.8 shows the AMS fabric from above and below the boulder pavement at Dracoisen. Here, the AMS K_1 lineations is completely parallel to both the c-axis clast fabric orientation and the trend of striations (mean K_1 = 10°/122°). Sample DF31, from below the boulder pavement, has a slightly stronger anisotropy (P_j = 1.016) and degree of clustering than sample DF32 from above the boulder pavement (P_j = 1.013). The AMS fabrics associated with the boulder pavement at Reinsryggen are shown in Figure 6.8. Here, the AMS lineation trends 07° to 020° beneath the pavement but switches to 12° to 307° above the pavement.

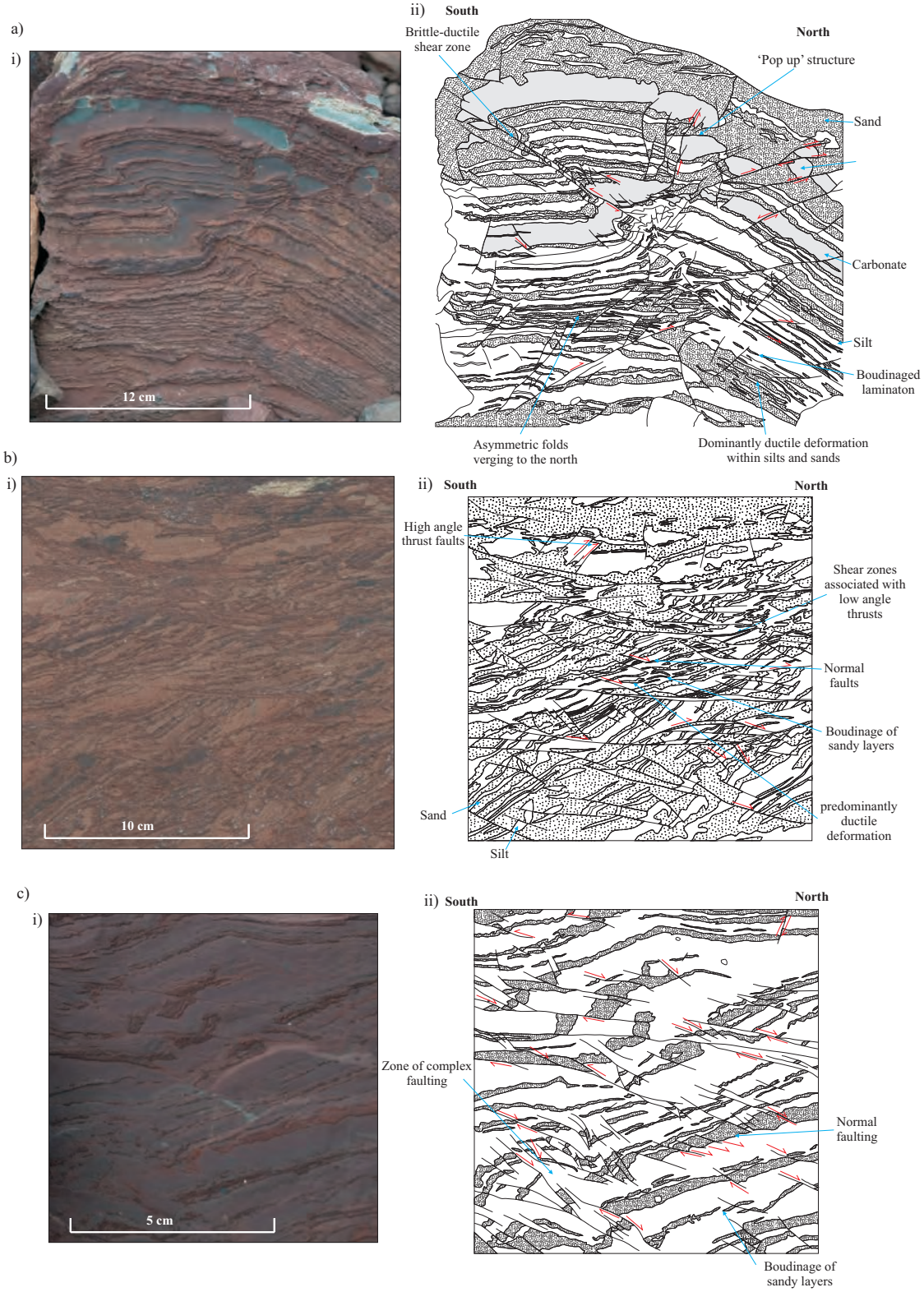

Fig. 6.11 – Interpretative sketches of hand specimens from the deformed rhythmites at Andromedafjellet. (a) South-verging thrust fault with pop-up structures within a mottled silt/sand – carbonate rhythmite. (b) Predominantly ductile deformation in low-carbonate rhythmites, showing inclined boudinaged lamination cut by low-angle normal faults and shear zones dipping to the north, and high-angle reverse faults dipping to the south. (c) Extensive brittle and ductile deformation of rhythmites dominated by north-dipping, low-angle normal faults.

The mean AMS for samples taken from subaqueous facies and deformational facies associations are shown in Figure 6.14. In the AMS fabrics taken from the subaqueous facies associations (Fig. 6.14b), K_1 trends at 10° to 160° and k_3 trends 80° to 342°. The corrective anisotropy degree (P_j) is 1.011, but considerable variation occurs between sites. The mean trend of the deformational facies association (Fig. 6.14a) is almost parallel. Here, K_1 trends at 01° to 157° and K_3 trends 88° to 273°, and the mean anisotropy degree is slightly higher (P_j=1.014), but the overall fabric patterns are very similar and show consistent orientations (Fig. 6.2).

6.3.2.5.2. *Clast fabric*

Clast fabric data, corrected for regional tilt, are shown in Figure 6.2 with reference to the location on the log from which the sample was taken. The mean directions are shown in Figure 6.13. In all cases, the V_1/V_2 plane lies parallel or almost parallel to the bedding plane. In the majority of cases, the clast fabrics show good correlation with the AMS fabrics. At Ditlovtoppen for example (Fig. 6.2c), the same shift in trend is seen from predominantly north-south to NW-SE upwards in the sequence. Here, the mean long-axis clast vector (V_1) trends at 03° to 158° at almost the exact same orientation as the mean K_1 AMS vector (Fig. 6.13). Eigenvalues are typically high, ranging from 0.5 to 0.7 (Table 6.5).

6.4. Interpretation of deformational lithofacies

6.4.1. Origin of the deformational structures

The facies that show evidence for deformation can be grouped into a deformational facies association (summarised in Fig. 6.15 and Table 6.3). The style of deformation within the Wilsonbreen Formation shows strong evidence for being primary; however, tectonic deformation can result in the production of sometimes similar structures. The interpretation of such structures can be difficult in situations where both tectonic and soft-sediment deformation has occurred (e.g. Williams et al., 1969). As such, the possibility of tectonic deformation must first be

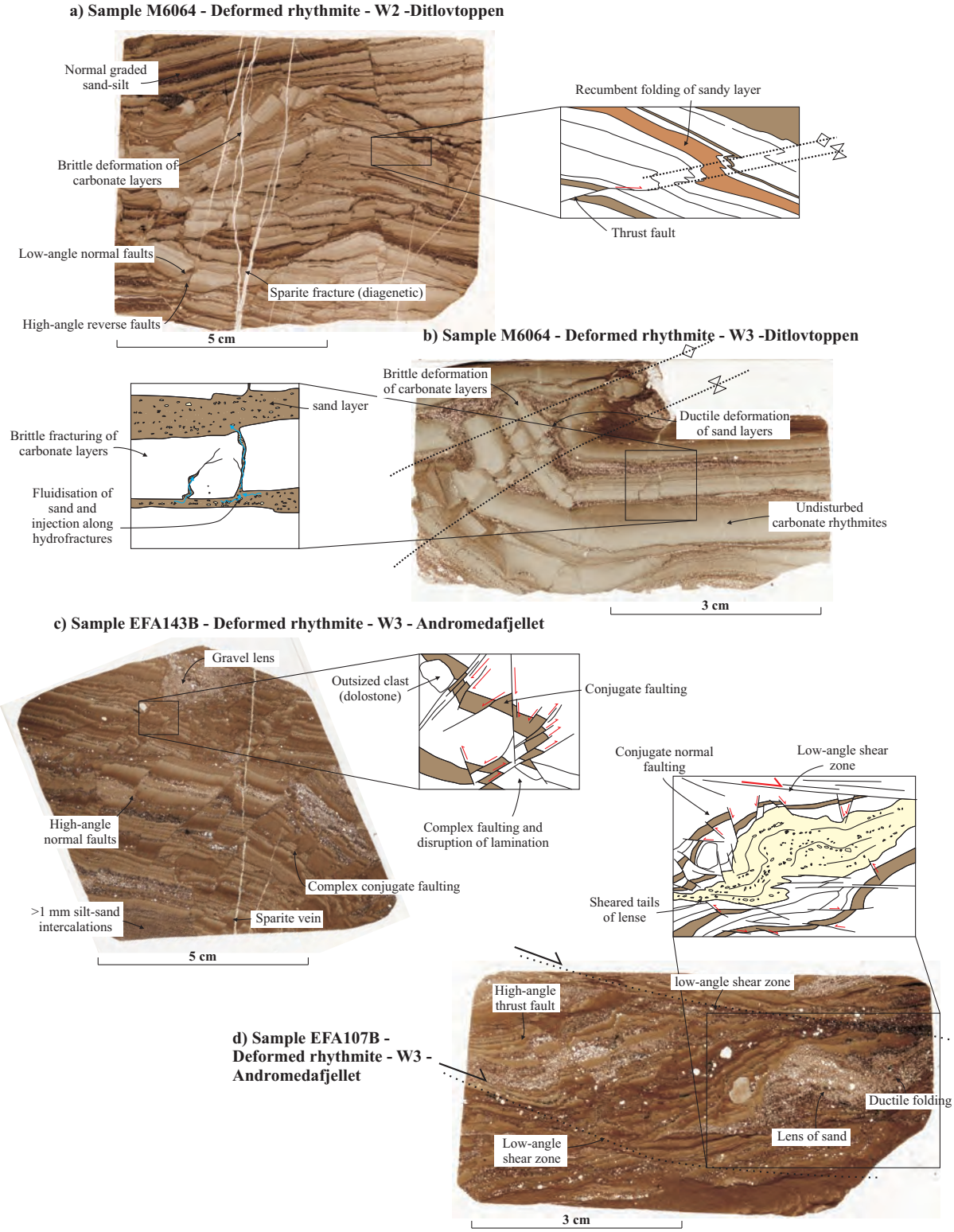

Fig. 6.12 – Microstructural analysis of deformed rhythmites. (a) Recumbent fold structure in faulted rhythmites, Ditlovtoppen. (b) Recumbent fold within deformed rhythmite at Ditlovtoppen showing brittle deformation and brecciation of carbonate horizons and ductile flow of sand-silt horizons, with sand-filled veins interpreted as hydrofractures cutting brecciated carbonate horizons. (c) Conjugate faulting in deformed rhythmites from Andromedafjellet. (d) Intense deformation from rhythmites at the boundary with overlying diamictite from Andromedafjellet displaying augen-like silty sand lens cut by low-angle shear zones.

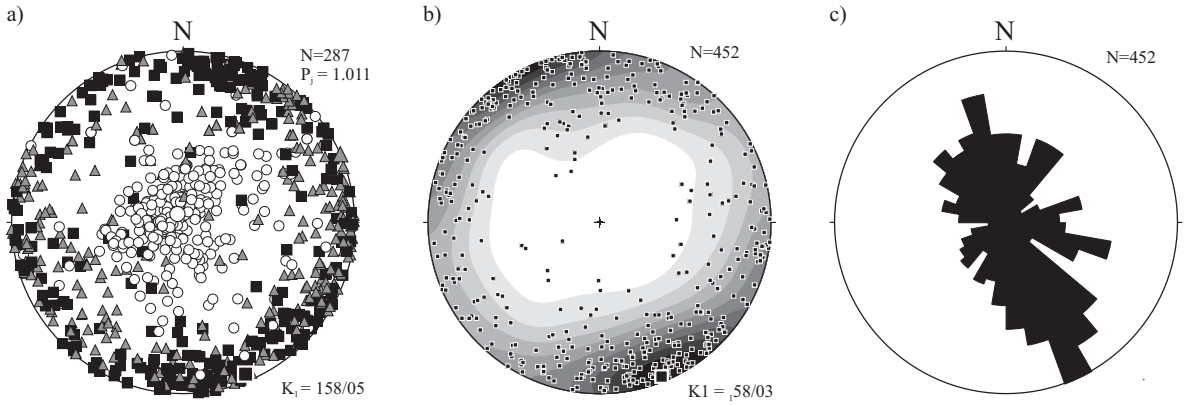

Fig. 6.13 – Fabric comparisons from all sites within the studied section. (a) AMS fabrics rotated to horizontal showing K_1 (black squares), K_2 (grey triangles), K_3 (white circles) and mean K_1 (large black square) with 95% confidence ellipses. (b) Clast a-axis orientations from all sites (small black squares) with mean eigenvector (large black square) rotated to horizontal. (c) Rose diagram showing dip direction of clast a-axis orientations (10° intervals).

discounted.

Within the Wilsonbreen Formation, a tectonic origin can be ruled out for several reasons. The deformation is localised and does not cross-cut beds. It occurs within distinct horizons where, based on sedimentary structures, a relationship to depositional processes can be demonstrated. Furthermore, the deformation is not dependent on lithology but varies stratigraphically through the section. For example, both deformed and undeformed rhythmite varieties are seen at different stratigraphic levels. Finally, although the rocks have been folded into a syncline during the Caledonian Orogeny, pervasive tectonic deformation is absent and there is no associated cleavage formation. The folding pattern is not consistent with the Caledonian trend. Instead, the folds are either chaotic or show dominant vergence to the north.

Primary deformation in glacial environments can occur in a number of ways (see Chapter 1, Section 1.2). In a subglacial environment, sediments typically undergo simple shear processes associated with glacier flow (Hart and Boulton, 1991; Kluiving et al., 1991). Although minor deviation in shear direction can occur (Piotrowski et al., 2004), this shear is normally parallel to the flow of the glacier. Within a proglacial environment, in contrast, glaciotectonic compression may facilitate the formation of structures analogous to fold and thrust belts in a compressive setting (Huddart and Hambrey, 1996; Hambrey et al., 1997; van der Wateren, 1999; Bennett,

								Eigenevectors						Eigenvalues			
Fabric	**Lat/long**		**Lithology**	**No**	**Location**	**Unit**	**Bedding**	**V_1**		**V_2**		**V_3**		**S_1**	**S_2**	**S_3**	**K**
2	79.205502	18.4025	Diamictite	50	Dracoisen	W1	343 51	168	22	60	38	281	44	0.6537	0.2849	0.0614	0.5414
8	79.204788	18.4111	Diamictite	50	Dracoisen	W1	338 40	151	19	37	48	155	35	0.589	0.3496	0.0619	0.3009
12	79.083092	18.4135	Diamictite	50	Ditlovtoppen	W3	003 30	162	23	65	17	302	61	0.6081	0.2988	0.0931	0.6094
13	79.082364	18.4111	Diamictite	50	Ditlovtoppen	W3	003 30	184	14	81	42	289	45	0.6053	0.3256	0.0691	0.4001
17	79.080193	18.403	Diamictite	50	Ditlovtoppen	W3	004 42	136	30	39	13	289	57	0.6976	0.2658	0.0366	0.4864
5	79.083643	18.4148	Diamictite	50	Ditlovtoppen	W3	003 30	151	20	58	9	305	68	0.5119	0.353	0.1351	0.3393
6	79.083197	18.4129	Diamictite	50	Ditlovtoppen	W3	003 30	178	5	84	32	276	57	0.7026	0.32179	0.0795	1.4904
16	78.9383	18.433	Diamictite	50	Andromedafjellet	W3	253 40	192	10	285	13	67	74	0.4809	0.3801	0.139	0.2336

Table 6.5 – Data table of clast fabrics analysed using the eigenvalue method (Mark, 1973) where the data is resolved into three mutually orthogonal eigenvectors (V_1, V_2 and V_3). The shape and strength of the fabric is represented by the Eigenvalues S_1, S_2 and S_3.

2001; Phillips et al., 2008).

Primary deformation in glacial environments is not necessary a direct result of the deformation by ice. It is also common in both glaciolacustrine and glaciomarine settings and is normally associated with sediment remobilisation events, such as slide, slumps or mass flows. Because of high rates of sediment deposition and rapid changes in depositional environments, local palaeoslopes can develop even in basins with no regional palaeoslope. For example, grounding-line fans can readily develop in front of grounded ice. Here, rapid deposition of sediment can occur at efflux points where subglacial melt-waters exit the glacier and experience a sudden drop in flow velocity (Powell, 1990; Bennett et al., 2002). In such environments, slope failure can occur, resulting in sediment remobilisation through slides or slumps. These can evolve into mass flows and produce debris flow deposits.

Both subglacial deformation and sediment remobilisation can result in similar structures; therefore, interpretation can be ambiguous (Arnaud and Eyles, 2002). However, as deformation processes in each case are different, analysis of the strain profile can reveal deformational

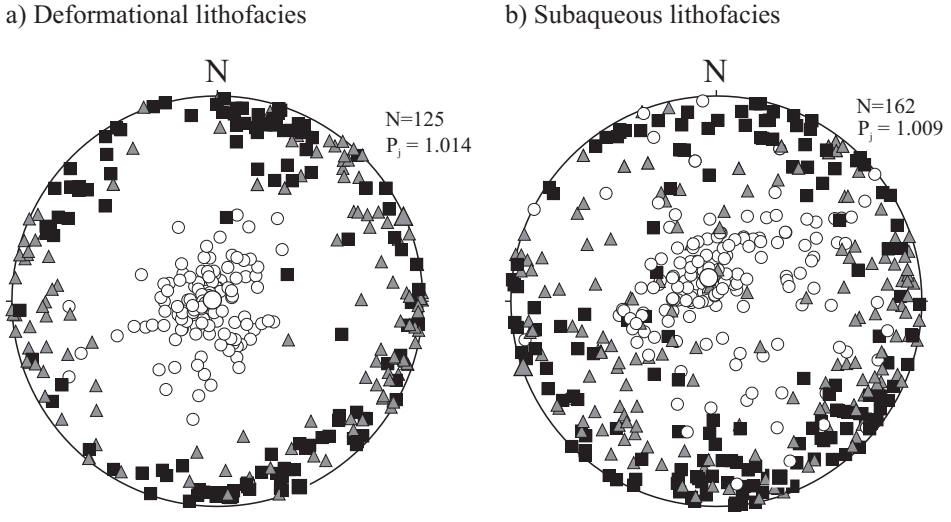

Fig. 6.14 – Comparisons of AMS fabrics rotated to horizontal showing K_1 (black squares), K_2 (grey triangles), K_3 (white circles) and mean K_1 (large black square) with 95% confidence ellipses. (a) All AMS subsamples from the deformation facies. (b) All AMS fabrics from the subaqueous facies. The deformational facies show a very slightly stronger anisotropy degree (P_j = 1.014) than the subaqueous facies P_j = 1.009. However, this is not considered significant.

mechanisms (e.g. Busfield and Le Heron, 2013). Glaciotectonic deformation typically results in an upwards increase in intensity of deformation towards the ice-bed interface (e.g. Boulton and Hindmarsh, 1987; Hart and Roberts, 1994; Evans et al., 2006) as shown in Figure 1.2a, Chapter 1. In contrast, slide and slump deposits typically display a decrease in deformation intensity away from a failure horizon, and the highest cumulative strains are recorded at the base (Hart and Roberts, 1994; Hiemstra et al., 2004), as shown in Figure 1.2b, Chapter 1.

Deformation of the sediments within the Wilsonbreen Formation shows an upwards increase in intensity in most cases. This is particularly well seen in the deformed rhythmites (e.g. Fig. 6.10). At the base of the deformed sequence, the rhythmites are characterised by small-scale conjugate faulting. Upwards in the section, the degree of disruption increases. At the top, the rhythmites pass into a massive diamictite which contains isolated lenses of the underlying rhythmite (e.g. Fig. 6.6e). In addition, there is a close relationship of deformation with other structures typical of subglacial deposition and deformation (e.g. subglacial channels and boulder pavements). As such, the structures associated with the deformational facies association are interpreted to be have been produced by glacially induced shear.

6.4.2. Origin of the deformed rhythmites

The deformed rhythmites of the deformational facies association can therefore be interpreted as a glaciotectonite. Prior to deformation, these rhythmites were originally both structurally and compositionally the same as the rhythmites of the undeformed W2 Member (see Section 6.3.1.4.2). Therefore, the original deposition of the unit is interpreted to have occurred in a glaciolacustrine environment with the lamination reflecting daily, meteorological or annual variations in sediment discharge into a lake. The deformation of the rhythmite can be associated with a glacier advance. During which, the sediments were glaciotectonically deformed through simple shear associated with the motion of the overriding ice.

Deformation has occurred in both ductile and brittle manners. The style of which appears to, at least in part, be controlled by composition. The carbonate fraction displays brittle deformation,

whilst the silt-sand matrix deforms in a ductile manner (e.g. Fig. 6.12a and b). This can be explained by early cementation of the carbonate horizon, prior to glaciotectonism. This is also consistent with the occurrence of carbonate intraclasts in undeformed sediments. The brittle faults typically form conjugate pairs or can appear chaotic and show no uniform pattern in shear in any particular direction. However, high-angle normal faults and low-angle reverse faults are identified in places. These display possible Riedel shears geometries which may highlight simple shear processes. In addition, the presence of sand veins in-between the faulted carbonate lamella suggests that the sand fraction was subject to liquefaction and remobilisation during folding, possibly as hydrofractures: a common feature of subglacially deformed sediments (Phillips et al., 2013).

The diamictites of the deformational facies associations that overlie these deformed rhythmites are interpreted to have formed in a subglacial environment. These would have formed as a subglacial traction till through a variety of processes, such as lodgement, frictional retardation and melt-out (Benn and Evans, 2010). The transitional contacts and consistent fabric orientations (see W2-W3 boundary on Fig. 6.2d) between the rhythmites and the overlying diamictites suggests the deposition of both deposits occurred during the same glacial advance.

6.4.3. Origin of sandstone and conglomerate lenses within diamictites

Lenses of sand and gravel within massive diamicton are a common feature of subglacial traction tills (e.g. Hart and Roberts, 1994; Evans and Campbell, 1995). A variety of mechanisms have been proposed for their formation (see review in Waller et al., 2011), which generally involve either the entrainment of the sand through thrusting or folding from an underlying layer (e.g. Hart and Boulton, 1991) or the melt-out of sand from the overlying basal ice (e.g. Hoffmann and Piotrowski, 2001). A thrust origin is considered unlikely, as a cohesionless block under high pour-water pressures and shear stress (as typical of subglacial regimes) would quickly disaggregate (Waller et al., 2011). This problem can be overcome if the sediment is frozen prior to entrainment (Menzies, 1990; Waller et al., 2011) as may be the case if it was affected by permafrost. If this

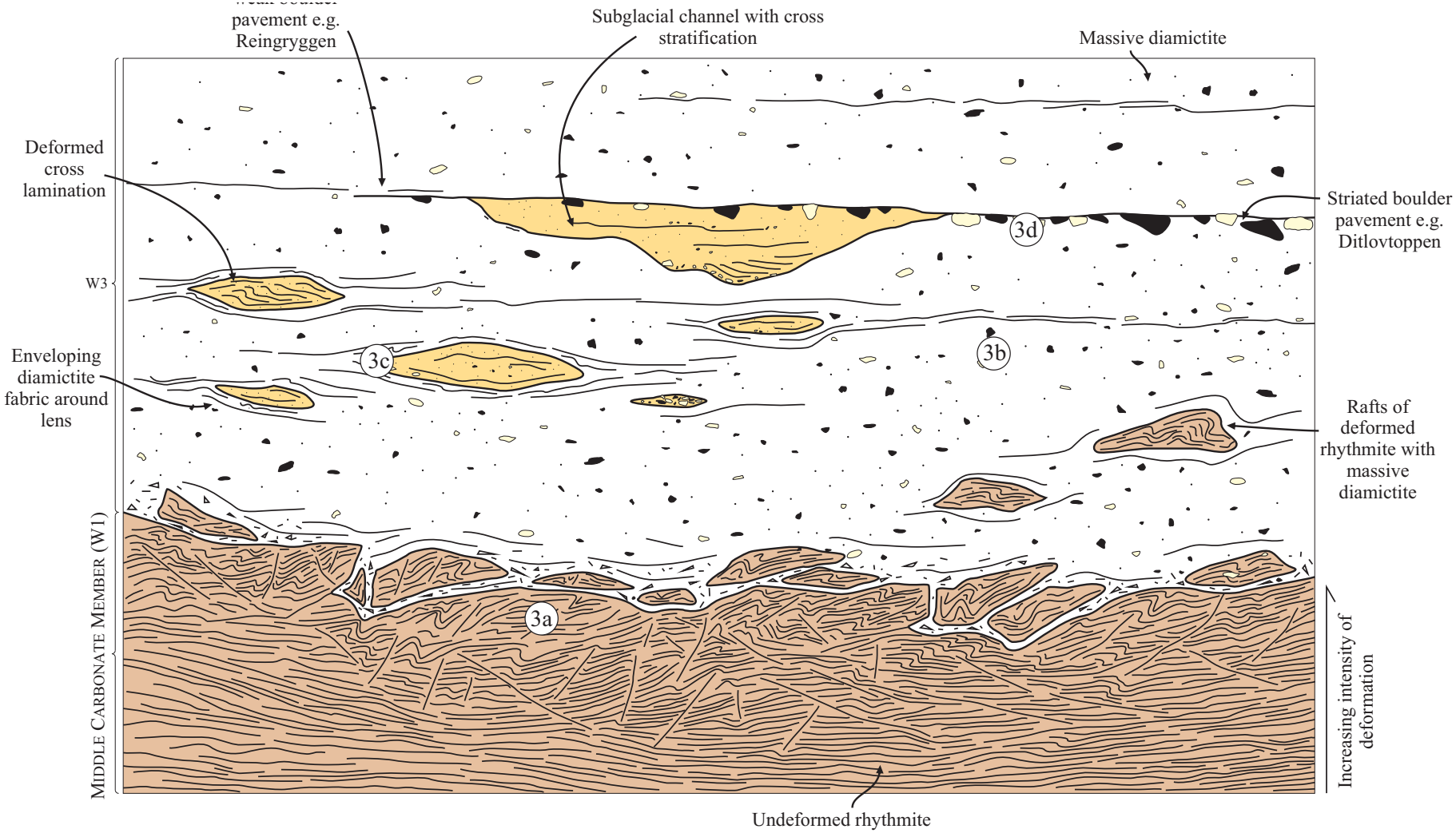

Fig. 6.15 – Summary diagram showing the deformational facies association referred to in Table 6.3: (3a) glaciotectonised rhythmites, (3b) subglacial diamictite with rhythmite rafts, (3c) subglacial diamictite with deformed lenses of sandstone and conglomerate (subglacial channel deposits) and (3d) a striated boulder pavement.

permafrost was relatively warm (close to but slightly below the pressure-melting point), the lens may be able to actively deform whilst maintaining cohesion. Alternatively, sands and gravels can be produced subglacially by the deposition of sorted sediments flowing within subglacial channels at the ice-bed interface (Alley, 1991; Clark and Walder, 1994). Although being originally fluvial in origin, these deposits can be cannibalised and deformed by the array of processes associated with the formation of a subglacial traction till (Hart, 1998; Evans et al., 2006; Benn and Evans, 2010), and they can subsequently become incorporated as deformed lenses in otherwise massive diamicton.

Within the sandstone lenses of the deformed facies association, a mechanism through thrusting of pre-existing sands is unlikely owing to the lack of similar sands lower down in the sequence. Furthermore, the identification of channel-like geometries on some of the lenses with deformed cross-bedding is consistent with a glaciofluvial origin (Fig. 6.8). For example, the large channelised sandstone body occurring immediately below the boulder pavement at Reinsryggen (Fig. 6.8a) has geometry typical of a subglacial channel. Therefore, the sandstone and conglomerate lenses of the deformational facies associations are interpreted as subglacial channels, some of which have been deformed and incorporated into a subglacial traction till, whilst others remain undeformed such that their depositional geometries are preserved.

6.4.4. Development of the boulder pavements

Boulder pavements are a feature commonly associated with subglacial environments (e.g. Boyce and Eyles, 2000) and are generally considered diagnostic. Different mechanisms have been proposed for their formation. The most straightforward is that they represent the former position of the ice-bed interface (Benn and Evans, 2010). Here, the combined effects of subglacial meltwater and glacier sliding may be responsible for the removal of fines leading to a concentration of larger clasts (Boyce and Eyles, 2000). However, Clark (1991) and Boulton (1996) suggested that pavements could also form within the deforming bed itself, as a result of excavation at the base of the deforming layer.

At Ditlovtoppen, the boulder pavement is characterised by a prominent surface on which sits a high concentration of large clasts (>10cm) with facetted tops and uni-directional striations. In the diamictite beneath the surface, clast fabrics are relatively strong (S_1 eigenvalue = 0.69) (Fig. 6.7c), and have a mean V_1 eigenvector parallel to the striations on the pavement surface. AMS fabrics are also relatively strong (P_j = 1.016) and the mean K_1 vector lies exactly parallel to the both V_1 and the striations. This suggests that the underlying diamictite was subglacially deformed either before or during the formation of the pavement by ice flowing in the same direction. In the overlying diamictite, the clast fabric and AMS fabrics have similar strengths (S_1 = 0.51 and P_j = 1.013), and the direction is consistent with the mean V_1 eigenvectors from the diamictite from below the boulder pavement.

This switch in fabric strength along with the presence of the striated pavement may arise from simple variation in the relative contributions of the processes operating to form a subglacial traction till (e.g. lodgement, meltout and frictional retardation). However, as the surface is very prominent and can be traced for several hundred metres along strike, it could be interpreted as being more significant. The boulder pavement possibly marks a period of non-deposition where erosional and deformational processes dominate over depositional ones within the deforming bed mosaic. As such, the diamictite beneath the boulder pavement sits in the deforming zone for a longer period of time resulting in the higher fabric strengths observed.

The boulder pavement at Reinsryggen occurs at a similar height to the one at Ditlovtoppen; however, it is not clear whether they represent the same event. At Andromedafjellet (2 km from Reinsryggen) the boulder pavement is not seen, instead at the same stratigraphic level are the rhythmites of the deformational facies association (3b). The boulder pavement is similar in appearance, but the boulder concentration of the surface is lower and striations were not observed. At the top of the boulder pavement, a large sand-filled subglacial channel cuts into the diamictite. This presumably formed by meltwater at the ice-bed interface.

Boulder pavements are common in subglacial sediments and highlight the wide variety of processes that are simultaneous occurring during the formation of a subglacial traction till.

Importantly for Neoproterozoic palaeoclimatic interpretations, its occurrence and the associated subglacial channel deposits could have significant implications for the interpretation of the thermal regime of the glacier. This is because the occurrence of these features indicates the presence of water at the ice-bed interface, suggesting that warm-based conditions were present for at least part of deposition.

6.5. Discussion

6.5.1. Palaeoflow and depositional architecture

AMS fabrics are interpreted to represent palaeoflow associated with primary depositional processes. This is based on the close relationship to clast fabrics and the lack of penetrative deformation (discussed in detail in Chapter 5, Section 5.8.3). Where subglacial grounding is suspected, AMS fabrics are interpreted to reflect the preferential alignment of grains resulting from simple shear of the sediment occurring parallel to ice flow. Where glaciomarine deposition is suspected, the AMS fabrics are interpreted to represent the palaeoflow of bottom water currents or sediment remobilisation events (e.g. debris flows). Clast fabrics reveal orientations that closely match that of the AMS fabrics and can be interpreted in the same way.

The mean fabric orientation lies predominantly in a north–south azimuth in both the deformational facies association and subaqueous facies association. However, whether the associated flow was to the north or south is often difficult to determine (see Chapter 5, Section 5.9.1). The dip of the K_1 axes from subglacially deformed till has been used in previous studies (e.g. Hooyer et al., 2008; Thomason and Iverson, 2009). Iverson et al. (2008) showed that during subglacial shear of till, an up-glacier dip in the K_1 develops. As such, the dip direction could potentially be used to estimate shear direction. The 5° dip of K_1 could indicate flow to the south; however, in the light of the typical variation in the data and the possible errors during measurement and rotation, this is not considered reliable in its own right.

The sediment architecture supports the interpretation of flow to the north. The deformational facies are thickest at Reinsryggen and thin to the north. These are absent at Dracoisen; instead, a grounding-line fan is observed (Fig. 6.4). This is supportive of previous interpretations of palaeoflow (Fairchild and Hambrey, 1984; Halverson et al., 2004) and from the contiguous sediments of NE Greenland (Moncrieff and Hambrey, 1988; Herrington and Fairchild, 1989). Flow can therefore be interpreted to be predominantly to the north. The consistent north trending fabric data and consistent sediment thickness (see Appendix D) may indicate that the exposed sections lie along the axis of a northerly flowing ice stream within a larger ice-mass, possible of ice-sheet proportions.

6.5.2. Depositional model

The close association of subaqueous, subglacial, and glaciofluvial conditions suggests that deposition occurred in an ice-marginal environment, although significant variation occurs throughout the succession. The widespread coverage of the Wilsonbreen Formation (with contiguous deposits in NE Greenland) and the large range of both intrabasinal and extrabasinal clasts suggests that deposition occurred predominantly from a large, widespread, possibly continental-scale ice sheet. Evidence of subglacial deformation through glaciotectonism and deformed subglacial facies, suggests the presence of a deformable bed for at least some periods during deposition. Deformable beds are traditionally associated with wet-based ice sheets and glaciers where the basal conditions are at or above the pressure melting point. However, recent evidence from the Antarctic Dry Valleys of glaciotectonised substrate at cold-based glaciers has challenged this view (Atkins and Dickinson, 2007; Hambrey and Fitzsimons, 2010). Nevertheless, the presence of widespread striated and polished clasts, low RA and C_{40} values (Fig. 6.9c), striated boulder pavements and the intercalation of subglacial channel deposits suggest meltwater at the base. Furthermore, the presence of thick, massive rainout diamictites suggests deposition from ice with a relatively high bed-load, more akin to warm-based polythermal conditions. Therefore, whilst it is difficult to fully determine thermal conditions, it is likely that the ice was warm-based for significant periods during deposition.

Modern analogues, illustrating the range of conditions seen within the Wilsonbreen Formation, are not well known. Indeed, because of the range of lithofacies present and subsequent palaeoenvironmental interpretations that can be made, it is unlikely that any one single analogue can be used solely. The deposition of thick, massive diamictites such as those associated with the Wilsonbreen Formation and many other Neoproterozoic glacial successions were traditionally thought to be rare. However, recent sedimentological investigations from boreholes and geophysical data in marine environment have suggested several locations where thick sequences of glacial sediments are currently forming. Possible modern analogues exist in the fjordal deposits of East Greenland. Here, thick deposits of massive diamictites are formed under a sikkusak model (Dowdeswell et al., 1994; Syvitski et al., 1996), where the rapid influx of icebergs in a topographically constrained fjordal system results in a high density of icebergs with residency times of 2-years. However, within the Wilsonbreen Formation, the widespread coverage of deposits and lack of supraglacial material, points to deposition in a lowland basin.

The Cenozoic glacial record of the Antarctic Ice Shelf displays similar sequences to those displayed in the Wilsonbreen Formation and despite being pre-Quaternary, they are well-constrained. Although previously thought to be largely cold-based, it is now thought that a significant subglacial drainage network exists beneath the present-day Antarctic ice sheet (Siegert et al., 2005; Wingham et al., 2006; Fricker et al., 2007) and there is significant evidence of direct deposition by a warm-based ice sheet during the Cenozoic (Hambrey et al., 2002; McKay et al., 2009). The Antarctic Dry Valleys region could also provide an explanation for the unusual carbonate-diamictite facies interactions seen in the W2 Member, interpreted to be associated with widespread glacial retreat and subsequent aridity. Comparisons between the Antarctic Dry Valleys and the W2 Member carbonates are discussed in Fairchild et al. (1989).

Based, on lithofacies interpretations, analysis of the sequence architecture (Fig. 6.16) and through comparisons with modern glaciological settings, a three-stage depositional model can be constructed to explain the sedimentation associated with the deformational facies of the Wilsonbreen Formation and is summarised in Figure 6.17.

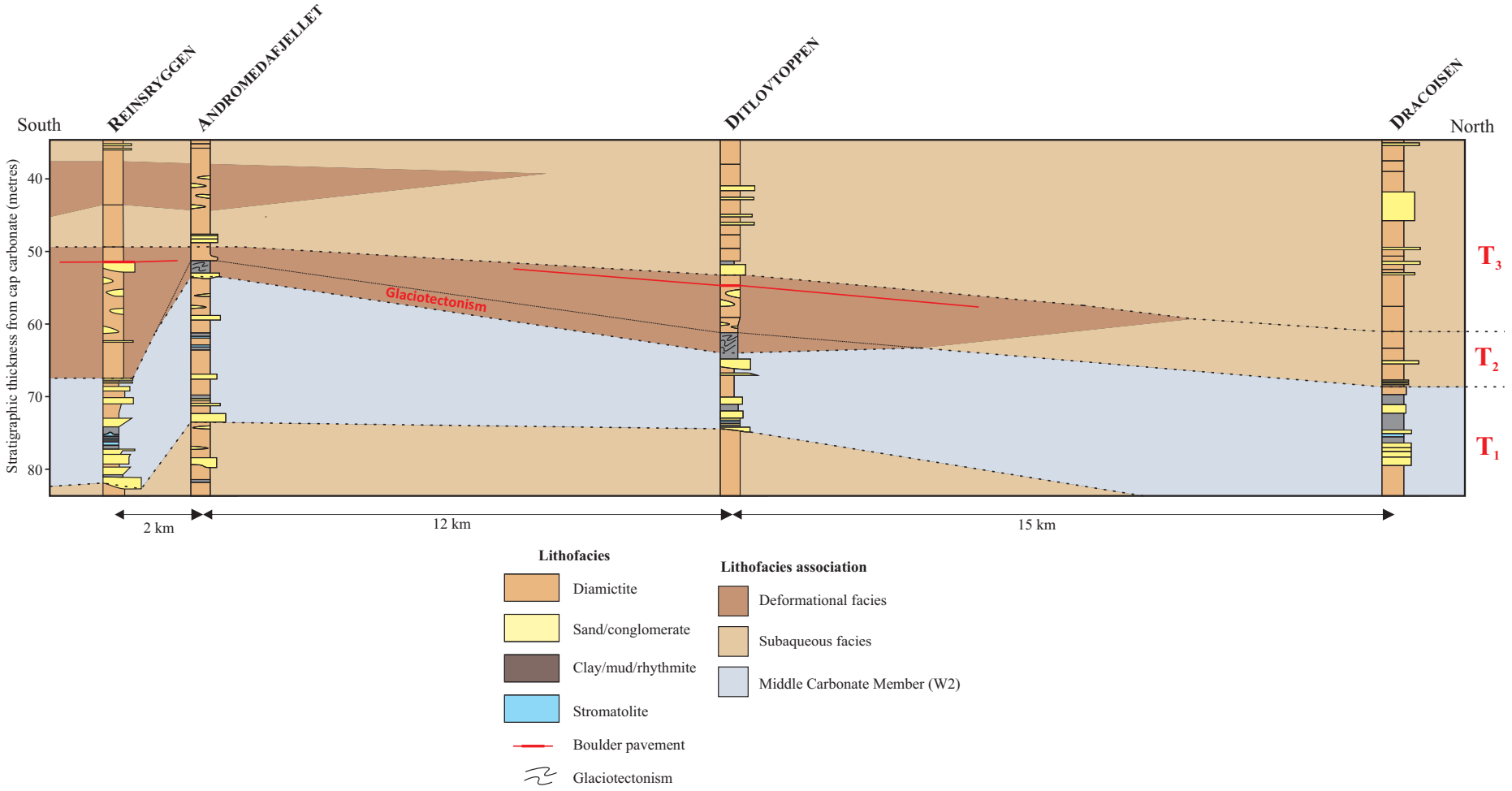

Fig. 6.16 – Summary sedimentary logs with facies correlations between sites. Subglacial facies at the top of the W2 Member, seen at Reinsryggen, Andromedafjellet and Ditlovtoppen but do not occur at Dracoisen are associated with an ice advance from the south resulting in glaciotectonism at Andromedafjellet and Ditlovtoppen at the top of the W2 Member. Deformational facies higher up in the W3 Member at Reinsryggen and Andromedafjellet are interpreted as a minor re-advance phase.

Stage 1 (T_1) Following on from the glacioaqueous sedimentation of the W1 Member, the W2 Member is characterised by ice-marginal terrestrial and proglacial sedimentation associated with a period of aridity and/or sea level fall, following the interpretation of Fairchild et al. (1989). This resulted in the deposition of rhythmites and stromatolites in proglacial lakes during glacial retreat phases and diamictites and conglomerates during glacial advance stages. Periods of aridity resulted in evaporative conditions and the precipitation of evaporites and dolocretes. Meltwater from the ice-margin resulted in the formation glaciofluvial river systems and ephemeral streams, depositing the sandstone and conglomerate bodies.

Stage 2 (T_2) – A major advance of an ice sheet from the south, presumably triggered by changes in climatic conditions (e.g. reduced aridity), caused widespread glaciotectonism of the upper W2 Member rhythmites. Continued deposition of debris in a subglacial environment led to the formation of subglacial tills at Reinsryggen, Andromedafjellet and Ditlovtoppen. Meltwater from warm-based ice resulted in the deposition of subglacial channel sands and gravels, which were subsequently deformed and incorporated into the subglacial deposits as part of a subglacial traction till. Periodic décollement between the ice-sheet and the bed resulted in the formation of striated bolder pavements. In front of the grounding line, high rates of deposition as a result of efflux at the glacier margin led to the development of a grounding-line fan, with associated sediment remobilisation through mass-flow deposits interbedded with rainout diamictites.

Stage 3 (T_3) - A retreat of the grounding line to the south resulted in predominantly subaqueous glacial deposition to the north. Massive, subaqueous diamictites were deposited through a combination of debris settling from sediment plumes originating from subglacial conduits at the grounding line and the rainout of debris from a high density of debris-rich ice bergs. Subglacial meltwater resulted in the formation of subaqueous channels and fans which emerged from the grounding line and flowed into the basin. This resulted in the deposition of submarine channel and outwash sand deposits. Periodic ice-sheet grounding events, possibly triggered by external orbital forcing or internal dynamics, resulted in the deposition of subglacial tills at Reinsryggen and Ditlovtoppen.

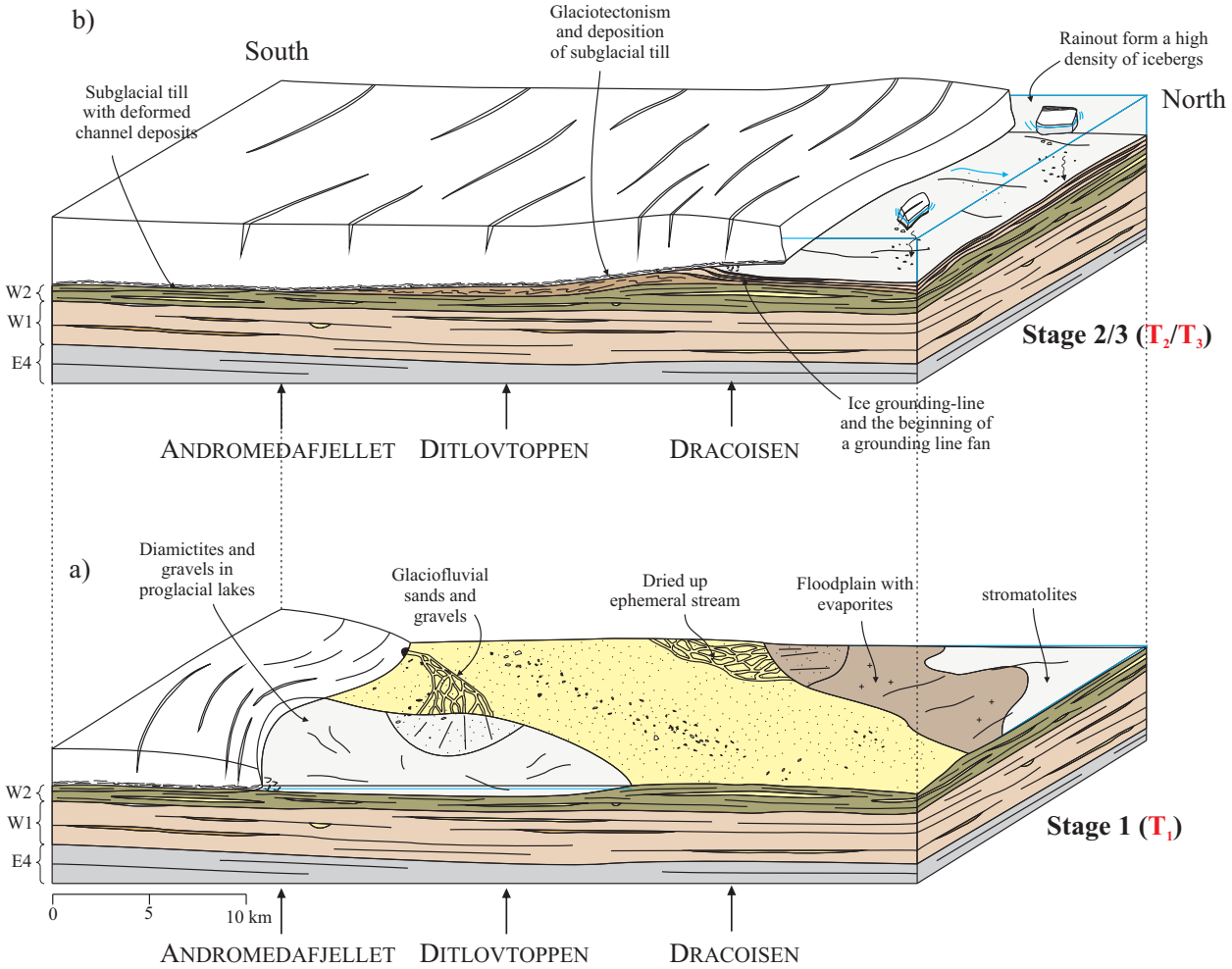

Fig . 6.17 – Three-stage depositional model of the formation of the deformational facies of the Wilsonbreen Formation (see Fig. 6.16 for location of sequences on stratigraphic log). (a) ice-marginal terrestrial and proglacial sedimentation during the formation of the W2 Member (T_1). (b) Glacial advance and glaciotectonism of the W2 Member rhythmites (T_2) and the deposition of subglacial till behind the grounding-line and the development of a grounding-line fan in front of the grounding zone (T_3).

6.5.3. The use of AMS for the investigation of Neoproterozoic glaciotectonism

After the removal of anomalous sites (as discussed in Chapter 5, Section 5.8.2), AMS has been identified as a reliable tool for the identification of fabric within Neoproterozoic diamictites and deformed sediments. In this chapter, an example has been provided as to how these data can be used in combination with more traditional sedimentology techniques to reconstruct the deformational environments within the Wilsonbreen Formation.

AMS is shown to give very similar fabric patterns to those produced through the measurement of clast fabrics. However, AMS has several advantages over traditional methods of identifying fabric. In contrast to grain and clast fabrics, which typically measure only one clast or grain at a time, AMS reflects the volume average of many grains within a subsample, and each site is made up of several subsamples, thereby reducing the inherent variability that is seen under single-grain analysis. Finally, as the measurement of AMS is automated, the only associated errors that can arise occur during sample collection.

This result from this chapter corroborates the findings of the previous chapters and supports the interpretations that AMS is a reliable method in the determination of palaeoflow (e.g. Fuller, 1962; Thomason and Iverson, 2009; Gentoso et al., 2012). However, other authors have suggested the use of AMS as a tool to identify genetic criteria from otherwise massive diamictites (e.g. Eyles et al., 1987; Hooyer et al., 2008; Iverson et al., 2008). Iverson et al. (2008) investigated AMS development in subglacial sediments through ring-shear experiments. When till was sheared under the same conditions expected at the bed of glaciers or ice sheets, AMS fabric strength increased with increasing shear strain up to a threshold where steady-state fabrics were reached. However, as discussed in Chapter 5, Section 5.9.2, the inherent variability of magnetic mineralogy makes direct comparison to this experiment unlikely to be possible.

This problem is illustrated in Eyles et al. (1987) who identified that the strongest AMS fabrics in glacial diamictons formed under glaciomarine conditions as a result of reorientation through current activity or during sediment remobilisation. The AMS fabrics of subglacial sediments were actually seen to be weakly related to ice flow. Importantly, these interpretations were made on

tills from different sections and the magnetic mineralogy from these studies was not investigated. Subglacial tills were sampled from modern glacial environments (Breidamerkurjokull, Iceland) whilst glaciomarine examples were taken from Pleistocene tills (around lake Ontario, USA). As variability resulting from changes in magnetic mineralogy was not investigated, significant doubts are cast on the reliability of such interpretations.

Within the AMS results of the Wilsonbreen Formation, comparisons between fabrics from the deformational facies association with fabrics from subaqueous facies associations show no significant difference in strength or direction. Therefore, the use of AMS as a genetic indicator in the Wilsonbreen Formation has not been possible. A similar pattern is seen in the analysis of clast fabrics of the Wilsonbreen Formation. No significant difference is observed between those interpreted as subglacial and those interpreted as glaciomarine. Clast fabrics, traditionally used as a diagnostic criterion for subglacial deformation or deposition has similarly been shown to be not as reliable as was previously thought and remains controversial (Bennett et al., 1999).

Although casting doubt on the use of AMS as a genetic indicator, this study does indicate that AMS can provide useful constraints on palaeoflow directions across the basin. Through the analysis of AMS fabrics, independently verified and compared with clast fabrics, a dominant ice flow direction towards the north can be interpreted across the basin. This has enabled accurate palaeoenvironment reconstructions to be made in an area that is otherwise lacking palaeoflow indicators.

6.6. Conclusions

Detailed investigations of the deformational facies of the Wilsonbreen Formation have been undertaken utilising facies analysis, structural geology and fabric analyses. In summary, from the interpretations made above, the following conclusions can be drawn:

- A range of soft-sediment, deformational structures are seen within the Wilsonbreen Formation. Through detailed sedimentological and structural analysis, these are

shown to be primary in origin, relating to deformation and deposition in a subglacial environment.

- Although diamictites are difficult to interpret on their own, based on the analysis and interpretation of associated facies, a deformational facies association has been developed that can aid interpreting depositional environments from Neoproterozoic glacial sections.
- AMS and clast fabrics can be effectively analysed and interpreted from the Wilsonbreen Formation. Although the ability of AMS and clast fabrics to elucidate depositional environments has previously been suggested, no significant difference is seen in fabric shape or strength between diamictites associated with subglacial deformation and diamictites associated remobilisation or current reworking. In spite of this, AMS can be used as an effective palaeoflow indicator. A dominant northerly alignment is seen in both AMS and clast fabrics, which based on analysis of the sediment architecture and comparisons with pre-existing work, is interpreted to represent flow to the north.
- Deposition of the Wilsonbreen Formation occurred in a low-relief, sedimentary basin affected by ice-sheet scale glaciation. Deposition occurred dominantly in subaqueous, subglacial and terrestrial settings in an ice-marginal environment, possibly associated with a north flowing ice stream. The top of the W2 Member marks major glacier advance across the basin associated with the glaciotectonic deformation of lacustrine rhythmites. Subglacial sediments were subsequently deposited in a dominantly subglacial environment in the south and a subaqueous environment in the north.

CHAPTER 7.

SYNTHESES AND CONCLUSIONS

Photo by MJH

7.1. Introduction

This thesis presents the findings of a study into the potential use of the anisotropy of magnetic susceptibility (AMS) technique in assisting in the analysis of the formation and deformation of glacial sediments. AMS and other magnetic characterisation techniques have been combined with sedimentological and structural approaches in order to provide a comparative basis to support the results of the analysis. This approach has been applied to a representative range of different environments including modern (Chapter 3), Quaternary (Chapter 4) and Neoproterozoic examples (Chapter 5 and 6). Each chapter has addressed a different aspect of glacial sedimentology, each connected by the use of the AMS technique. The key outcome is that there is a strong correlation between AMS and traditional techniques (e.g. structural features, clast fabric analysis) in each of the areas of study. These corroborate the validity of the technique and suggest that there is sufficient potential to warrant further studies. The new contributions made in this study will serve to increase both the understanding of the AMS technique and the processes that go into the formation and subsequent deformation of glacial sediments.

7.2. Empirical findings

The research questions posed in Chapter 1 have been answered in the following chapters. In addition, each chapter has included its own specific aims and objectives that not only relate to the technique, but attempt to elucidate a particular area of glacial sedimentology. The empirical findings from each chapter can be summarised as follows.

7.2.1. Chapter 3 - AMS of basal ice

AMS has been applied (for the first time ever) to debris-rich basal ice to examine deformation associated with surge behaviour of a tidewater glacier in Svalbard. Previous attempts to measure small-scale deformation in ice normally involve optical techniques such as measurement of the crystallographic c-axis of ice crystals. However, ice-crystals are known to be particularly prone

to recrystallisation. Therefore, rather than representing deformation during flow, the fabric may represent a recent recrystallisation event . In contrast, AMS measures only the detrital grains. As ice is diamagnetic, its contribution to the AMS fabric is negligible. It is therefore thought that the AMS of basal ice has significant potential to be used as a tool to measure fabrics, without the recrystallisation problems associated with standard optical analysis.

Through the analysis of AMS and visible the structures (faults, sheath folds and stretching lineations), the basal ice at Tunabreen is interpreted to be highly deformed. Under the shear associated with the movement of the glacier, detrital paramagnetic mineral grains rotate into a preferential orientation creating a magnetic lineation (K_1) parallel to the direction of maximum extension within the ice. This direction is independently supported by the known overall flow direction of the glacier and the presence of pre-existing structures (stretching lineations, folds and faults). It can therefore be concluded that an AMS fabric can be measured in basal ice.

The analysis of AMS of the basal ice at Tunabreen has provided interesting new insights into the processes associated with the surge of the glacier. The K_1 axes are observed to have an up-glacier plunge (20°), similar to that of deformed subglacial sediments (e.g. Shumway and Iverson, 2009; Thomason and Iverson, 2009).This suggests that strain within the basal ice was non-coaxial and involved a large component of simple shear. In addition, the AMS samples taken from the NW margins have K_1 axes that deviate slightly away from the mean ice-flow direction. This is interpreted to have occurred because of resistance at the glacier margin, resulting in a deflection of the magnetic lineations in response to change in orientation of the strain ellipse.

At the SE section, similar deviation in K_1 orientations are observed; however, these are interpreted to have arisen because of flow perturbations associated with an irregular fjord margin. An embayment in the lateral moraine of the neighbouring glacier (Von Postbreen) is observed in the pre-surge aerial imagery. This is interpreted to have resulted in local clockwise rotation of ice-flow at the margins during the surge which subsequently caused the rotation of the magnetic lineations.

Although seminal, this study has shown that the application of AMS to basal ice has excellent potential. In addition, the study has provided interesting insights into the behaviour of the glacier during surges and has increased the knowledge of how fabrics within subglacial sediments can be inherited from glacier ice. Finally, it has revealed a new research area where the AMS technique can be applied. Significant opportunity exists for the use of this technique at other glaciers and various key glaciological issues could be investigated (See section 7.5.1).

7.2.2. Chapter 4 - AMS of a glaciotectonite

AMS has been applied (for the first time) to study deformation within a glaciotectonite. The sequence, exposed by coastal erosion at Bacton in Norfolk, England, can be divided into an upper and lower series. In both series, analysis of the AMS reveals that K_3 axes form perpendicular to bedding, which is subhorizontal, whilst K_1 and K_2 axes are parallel to bedding. K_1 axes lie parallel to macroscopic structural indicators such as folds, faults and stretching lineations. It was concluded that the AMS fabric resulted from the preferential alignment of predominantly iron-bearing paramagnetic clay minerals, which had rotated under conditions of progressive simple shear.

The large amounts of visible deformation in all layers, coupled with a lack of failure horizons within the sediment, led to a glaciotectonic interpretation, in line with previous interpretations of the area (e.g. Banham, 1988; Hart, 1990; Lee and Phillips, 2008). However, the presence of both ductile and brittle structures, refolded folds and switching AMS fabric orientations, suggested that the deformation was complex. The ductile folding and dominantly north-south magnetic lineations in the lower series are interpreted to have arisen from north-south orientated stretching. In contrast, dominantly east-west magnetic lineations and refolded folds in the upper series are interpreted to represent east-west stretching in response to a switch in the ice flow direction.

It was concluded that the sequence has undergone at least two phases of glaciotectonic deformation as a result of oscillations of North Sea-and British-based ice during the glaciations of the Anglian Stage. Initially, north-south orientated stretching affected both the upper and

the lower series. Assuming, stretching was parallel to ice-flow, and bearing in mind wider palaeogeographic constraints, this is interpreted to represent to an ice advance from the north. This was subsequently was replaced by east-west orientated stretching affecting only the upper series in response to an ice advance from the west.

This study has built on the previous work on the investigation of AMS of glacial sediments and shows that the strain field can be accurately measured within a glaciotectonite, in which a paramagnetic mineralogy is controlling the susceptibility. The study has also revealed important conclusions in regards to deformation styles in glaciotectonites. Detailed analysis of structures has revealed sheath folding is prevalent, which was previously unrecognised in north-Norfolk sections. The approach adopted in this chapter can be directly applied to other glaciotectonised localities, both in Norfolk and elsewhere. In this way, the technique has the potential to provide significant insights into the sometimes complex history of glaciated areas (for future recommendations, see Section 7.5.2).

7.2.3. Chapter 5 - Deciphering AMS fabrics in diamictites

AMS has been applied to Neoproterozoic diamictites (for the first time) to investigate depositional processes and palaeoflow directions from the Wilsonbreen Formation, in NE Svalbard. A wide range of fabric characteristics were observed. As well as normal sedimentary fabrics, inverse and anomalous behaviour was also identified locally. To determine the cause of this behaviour, detailed rock magnetic investigations were undertaken. In most cases, a paramagnetic mineralogy dominated the AMS, but a minor contribution of fine grained SD magnetite is observed in some samples resulting in the anomalous fabrics. Additional anomalous fabrics were found in the southern localities as a result of increased tectonic deformation in this region. In spite of this, primary AMS fabrics can still be distinguished as the anomalous fabrics are easily identified and omitted.

The remaining AMS fabrics show excellent correlation with clast fabrics and are therefore considered to be primary and reflect depositional processes. Where subglacial activity is suspected,

the AMS fabrics are interpreted to have formed because of subglacial shear as a result of the flow of the over-riding ice. These fabrics are therefore interpreted to represent the palaeo-ice flow direction. In other areas, subaqueous deposition is suspected and the fabric is interpreted to have been created either through downslope resedimentation processes or through current reworking. Consequently, the susceptibility axes can be used to reconstruct the palaeoflow directions across the region. The results from both the AMS and clast fabrics reflect north-south palaeoflow vectors. Based on previous independent palaeoflow indicators (e.g. cross-bedding, fold vergence, grounding-line fan architecture) and published data on contiguous sediments in NE Greenland, a dominant palaeoflow to the north is interpreted.

This study has shown that, although additional complications can be present when investigating AMS in Neoproterozoic diamictites (e.g. the effects of SD magnetite and tectonic remagnetisation), after detailed rock magnetic analysis and careful interpretation, primary AMS fabrics can successfully be delineated. This technique can be applied to other well-preserved, undeformed Neoproterozoic successions and has the potential to increase our understanding of Neoproterozoic palaeogeography.

7.2.4. Chapter 6 - Neoproterozoic glaciotectonism

An example is presented as to how AMS, in combination with facies analysis, structural geology, and clast fabric analysis, can be used to investigate the origin and significance of deformational structures within the Wilsonbreen Formation. Although difficult to interpret on their own because of their often massive nature, glacial diamictites and associated facies were categorised into facies associations (deformed and undeformed). Of this, a deformational facies association was established which was subdivided into: (1) Deformed rhythmites displaying both brittle faulting and ductile folding, interpreted to have resulted from glaciotectonic disruption and simple shear associated with an ice advance; (2) Massive diamictites, interpreted as a subglacial traction till; (3) Interbedded sand and gravel lenses, interpreted as subglacial channel deposits, incorporated into a subglacial traction till; and (4) Boulder pavements, interpreted to

represent a former ice-bed interface, associated with periodic décollement at the ice-bed interface of a warm-based ice-sheet.

Investigations of the AMS fabric within these facies reveal that K_1 axes lie predominantly in a northerly orientation, parallel to pebble fabric orientation. This matches the overall palaeoflow directions concluded in Chapter 5 and it is interpreted to reflect dominantly northerly orientated shear associated with a dominant ice flow direction to the north. Because of inevitable variations in the proportions of magnetic minerals in the diamictites, accurate characterisation of depositional processes through AMS fabric alone is not possible. However, once a subglacial origin has been identified, AMS can easily, quickly and accurately be used to establish fabric orientations related to the deforming ice.

Through the use of facies, structural, and clast fabric analyses in combination with AMS analysis, it is concluded that deposition of the Wilsonbreen Formation occurred in an ice-marginal environment under predominantly subaqueous, subglacial and terrestrial settings. Glaciotectonic deformation at the top of the W2 Member (see Chapter 6, Section 6.5.2) marks a major glacial advance across the basin. Spatial variation is identified in the depositional architecture. In the south, diamictite deposition occurred in a predominantly subglacial environment. In contrast, the north was dominated by more distal deposition in a predominantly subaqueous environment.

This study has provided an example of how AMS, in conjunction with traditional sedimentological techniques, can be used to investigate particular issues in Neoproterozoic research such as the interpretation of deformed lithofacies. Through this study, a greater understanding of both the depositional environments and the palaeogeography of a Neoproterozoic sedimentary basin have been gained.

7.3. Key findings for the use of AMS in glacial sediments

In addition to the empirical findings of each chapter presented above, the following

conclusions can be drawn with respect to the use of AMS for glacial sediments, in answer to the particular issues raised in Chapter 1, Section 1.5.

7.3.1. The relationship between AMS and deformation within glacier ice

The relationship between AMS and glacier ice was explored in Chapter 3. It was shown that AMS could successfully be measured in basal ice and the results could be used to show insight into ice deformation. The AMS fabric of the basal ice at Tunabreen revealed an up-glacier dip of the K_1 lineations at 20° in an orientation parallel to the direction of ice flow. This pattern is almost exactly the same as that observed and in laboratory experiments of sheared till (Hooyer et al., 2008; Iverson et al., 2008) and within subsequent analysis of Quaternary subglacial tills (e.g. Shumway and Iverson, 2009; Thomason and Iverson, 2009). As such, it is interpreted to reflect the strain ellipse of the deforming basal ice. Within subglacial sediments, AMS fabrics are interpreted to reflect the long axes of grains, rotated into preferential alignment as a result of simple shear processes in response to the flow of the glacier. In Chapter 3, it was determined that a similar pattern is developed in basal ice, suggesting that deformation processes that are occurring within the sediment are similar to those occurring within the overlying basal ice.

7.3.2. The AMS response of paramagnetic mineralogies to subglacial shear

Until this thesis, all of the AMS investigations of subglacial deformation within diamicts has either been on tills with a mineralogy dominated by ferromagnetic minerals, or the magnetic mineralogy has not been identified (See Chapter 2, Tab.2.1). However, the magnetic mineralogy is likely to vary considerably depending on the source material being eroded. The resulting diamict can have a highly variable mineralogy accordingly. In this thesis, a paramagnetic mineralogy has been identified in subglacial tills and the response of the fabric in relation to shear has been investigated.

It was stated in Chapter 4, that the paramagnetic Bacton Green Till, Norfolk produced predominantly oblate fabric patterns. However, distinct clustering of the K_1 axes were observed

defining a magnetic lineation parallel to the direction of shear within the sediment. A similar pattern is seen in the Neoproterozoic diamictites of NE Svalbard. In most cases paramagnetic phyllosilicate clays (Chapter 5 and 6) also dominated the AMS. Here, a similar clustering of K_1 axes was seen which lies in an orientation parallel to the clast fabric orientation.

In contrast to ferromagnetic grains, where the AMS is directly controlled by the shape of the grain, the AMS of paramagnetic minerals is controlled by the arrangement of the crystal lattice. In spite of this, the fabrics produced in each are often compatible. This is because phyllosilicate minerals (e.g. chlorite, illite) tend to preferentially break along crystallographic axes. In rocks dominated by extensional tectonics (e.g. Parés and van der Pluijm, 2002; Cifelli et al., 2005; Cifelli et al., 2009), these grains are observed to girdle about an axis parallel to the direction of maximum stretching. A similar process is interpreted to occur in subglacial deformed sediments under shear. A lineation results from the girdling of the basal planes of phyllosilicate minerals about an axis parallel to maximum stretching (i.e. the long axis of the strain ellipsoid). This thesis has shown that AMS can be used as a reliable indicator of deformation in subglacial sediments where a paramagnetic mineralogy is controlling the AMS fabric.

7.3.3. The use of AMS in the study of glaciotectonites

Prior to this study, no published data exists for the application of AMS to glaciotectonites, where pre-existing unconsolidated sediment has been glacially deformed such that relics of the original structure remain. As discussed in Section 7.2.2, at Bacton, Norfolk, the AMS fabrics reflect the preferred alignment of minerals within a glaciotectonite. It is interpreted to directly reflect the strain imparted on the site through glaciotectonic processes. Magnetic lineations are parallel to stretching lineations and the clustering of fold axes, which suggest that they reflect stretching during progressive simple shear as a result of subglacial glaciotectonism. Therefore, the structural data corroborates the AMS results and supports the interpretation that AMS can be used to accurately evaluate strain within glaciotectonites.

7.3.4. The preservation of primary fabrics in pre-Quaternary glacial sediments

Most of the previous literature on the analysis of subglacial sediments has focussed on the Quaternary geological record. In this thesis, it has been demonstrated that AMS can readily be applied to pre-Quaternary successions. However, this thesis has also highlighted that additional complications can be introduced, specifically relating to diagenetic processes or remagnetisation during subsequent tectonic deformation. Despite this, AMS is routinely used in other areas of sedimentology to the determine palaeoflow directions in pre-Quaternary deposits (e.g. Schieber and Ellwood, 1988), and in most cases, primary AMS fabrics can be readily determined (Tarling and Hrouda, 1993).

Within the Neoproterozoic diamictites of NE Svalbard, primary AMS fabrics can be identified at the northern localities. However, tectonic overprinting is recognised in some areas to the south. Here, some sampled sites displayed AMS fabrics where the K_1 axes deviated away from the bedding plane, onto a plane parallel to the regional fold trend. This fabric is interpreted to represent an intermediate tectonic fabric where the original sedimentary fabric has been affected by tectonic overprinting (see Fig. 2.13, Chapter 2). This interpretation matches the observation of greater evidence of macroscopic tectonic deformation in these areas through steeper fold limbs, and evidence of tectonic faulting.

In contrast, the northern localities (Reinsryggen, Andromedafjellet, Ditlovtoppen and Dracoisen) reveal primary fabrics and evidence of tectonic deformation is mostly absent. Here, the AMS fabrics show a strong correlation with clast a-axis orientation and bear no apparent resemblance to regional tectonic deformation. Therefore, the AMS fabrics from these sites can be interpreted as being related to depositional processes. This suggests that the application of AMS to the Neoproterozoic glacial record in Svalbard, as presented in this thesis, provides an independent palaeoflow indicator in an area that is otherwise lacking. From this, a dominant palaeoflow direction to the north has been established.

It can therefore be concluded that AMS can successfully be applied to Neoproterozoic diamictites. As such, excellent opportunities exist for the technique to be applied to other similar

sequences where tectonic deformation is minor and information on primary palaeoflow can be established. However, detailed rock magnetic investigation and comparison with other proxies are needed before full interpretations can be made.

7.3.5. Distinguishing depositional processes based on AMS characteristics

It has been suggested that the AMS could be used as a genetic indicator of depositional or deformational processes (Eyles et al., 1987; Iverson et al., 2008). Clast fabrics have been used by some in a similar way (e.g. Dowdeswell et al., 1985; Benn, 1995). This typically involves the analysis of the degree of clustering of a-axis clast fabric measurements. Some have doubted the ability of the use of clast fabrics as genetic fingerprinting alone (e.g. Bennett et al., 1999); however, it is generally considered that in combination with other proxies, clast fabrics have the ability to provide considerable constraint over depositional processes.

In some cases, a correlation between fabric strength with strain and therefore depositional environment has been identified (e.g. Benn, 1994). It may be tempting to think that AMS can be used to measure similar correlations. However, this thesis has highlighted important reasons why this may not be possible. Whilst clast fabrics anisotropy relies on the direct analysis of the a-axis of clasts, the magnetic anisotropy can be highly variable depending on both the magnetic mineralogy and size of the constituting grains. Different magnetic minerals can produce different fabric characteristics (see Chapter 2.3). Thus, the relative proportions of these minerals will produce distinctly different AMS fabric characteristics that may not necessarily be linked to strain. Whilst this thesis has shown that AMS can provide constraints on deformational processes, because of the large variation in the composition of glacial diamicts, the ability of AMS to quantitatively determine strain magnitude is unlikely (see section 7.4).

7.4. Implications of research

Glacial sediments, particularly diamicts, are inherently difficult to interpret because of their

massive, non-diagnostic character. For this reason, significant controversy and debate surrounds many diamict sequences in the literature. The AMS technique has been previously been shown to have significant potential in determining subtle fabrics from massive diamicts and providing insight into depositional processes. However, several important research questions still remained. In this thesis, through the application of the technique to a variety of different settings from the modern, Quaternary and Neoproterozoic, some of these questions have been answered and understanding of the technique has been furthered.

It has been shown that AMS has several advantages over other petrofabric techniques. It can readily be used in a variety of glacial materials from debris rich basal glacier ice to unlithified sediments and rock. AMS can also be used where other fabric indicators are lacking or are not possible to measure. For example, it can be used in cemented diamictites, where traditional clast fabric analysis is not possible. In addition, it could prove to be particularly useful in the study of basal glacier ice as it targets only the paramagnetic and ferromagnetic contributions to the fabric. Therefore, the diamagnetic ice, which is prone to recrystallisation in ambient strains and may give erroneous results, is not measured.

Certain limitations are also highlighted. Comparisons of fabric strength between studies and even between sites in the same region can be problematic because of the inherent variability in the mineralogy of glacial sediments. A reoccurring theme throughout this thesis has been the importance of accurate determination of the magnetic mineralogy. This is because a subtle different mineralogy can affect fabric shape and strength without necessarily being linked to strain. Hooyer et al. (2008) had suggested the use of the technique as a tool to identify tills not deformed to sufficient strengths to fit in with the bed deformation model. However, because of the mineralogical variability identified in different tills, direct comparison to this should be avoided. The same is true for the identification of genetic criteria based on AMS (Eyles et al., 1987). In addition, the effect of post-depositional processes can also significantly influence both fabric strength and direction. Tectonic deformation can alter fabric patterns resulting in the creation of anomalous fabrics that can no longer be linked to depositional processes.

These limitations are not new to AMS studies (Borradaile and Jackson, 2010) and can be largely overcome by detailed investigations into the cause of the magnetic signal and comparison of the AMS fabric with independent fabric indicators. Because of the different response of different magnetic minerals, it is important that the magnetic mineralogy is investigated as part of the AMS study. Through this, the cause of the AMS can be determined and anomalous fabrics identified and omitted. In addition, the relationship of the fabric to strain or flow should be independently verified through comparisons with other techniques (e.g. clast fabrics, fold analysis) where possible.

Once this has been undertaken, this study has shown that AMS can be a particularly effective petrofabric tool. AMS represents a quick, accurate and objective method of characterising grain fabric. In conjunction with other techniques (facies analysis, structural geology), it can provide significant information on several current issues in glacial geology.

7.5. Recommendations for future research

This thesis has built on pre-existing research and has furthered the knowledge of the AMS of glacial sediments. However, it has also brought attention to areas where further study is required. In addition, potential new research areas in which AMS could be applied have been highlighted. These could provide significant information for current problems in glacial sedimentology and glaciology.

7.5.1. Debris rich basal ice

The identification of an AMS fabric related to strain in basal glacier ice (Chapter 3) is a significant discovery. Basal ice is observed at the base of almost all glaciers and ice sheets on Earth. It forms at the critical zone between the ice bed and the bulk of the glacier ice and is shown to be strongly affected by glacial motion. The traditional optical techniques of fabric analysis can be problematic because of the recrystallisation processes that can occur in ice. Therefore, AMS has

significant potential to be used, in addition to crystallographic optical measurements, as a tool to measure strain within basal ice.

It is critical to note, whilst significant advances have been made, in order to fully test the ability of AMS to measure deformation within basal ice, further detailed study is required which is beyond the scope of this study. In particular, investigation of the effects of variation in the relative proportions of ice and sediment is needed. In addition, an investigation into the effects of sediments with a different mineralogy is also required. These will both help determine additional variables, other than strain, that may affect AMS fabric development in basal ice. Finally, laboratory verification similar to that of Iverson et al. (2008) for till could be applied to basal ice. This would facilitate more accurate comparisons with strain and would significantly strengthen the reliability of the results.

Once these variables have been established, the AMS technique could be useful in assessing a wide range of glaciological issues. An interesting study would be to test whether fabric strength can be quantified with strain and whether vertical changes in fabric strength can be measured. One would assume that strain would be greatest at the ice-bed interface and decrease upwards away from the bed. However, one possible mechanism of basal ice formation involves progressive accretion of new ice to the base of the glacier (e.g. Hubbard, 1991; Goodwin, 1993; Hubbard et al., 2009). In this model, the newest basal ice would be at the ice-bed interface. Therefore, cumulative strain would in fact be low in the newly accreted basal ice and increase upwards as older basal ice is met that has spent longer in the deforming zone. If the relationship between AMS and strain could be identified, which may be possible if the magnetic mineralogy of the basal ice remains consistent, AMS could help determine the importance of this mechanism in basal ice formation.

AMS may also be able to help in the recognition of past surges in glaciers. Surge-type behaviour is common in many Arctic glaciers. They are easily recognised whilst they are taking place, yet the recognition of past surges can be difficult. The number of surge type glaciers is currently debated. For example, in Svalbard, some authors have suggested as little as 13% (Jiskoot

et al., 2000) whilst other suggest as many as 90% (Lefauconnier and Hagen, 1991) of glaciers could be surge-type. AMS, combined with use of structural geology and other studies (e.g. water stable isotopes), could provide information on the deformation styles within the basal ice of surge-type glaciers. Through this, it may be possible to develop a set of diagnostic criteria which can be used for the recognition of past surges imprinted in the basal ice.

AMS could also prove to be particularly useful in the investigation of strain in ice where other information on flow direction is lacking. For example, the study of massive ground ice in permafrost regions (e.g. Waller et al., 2009; Fritz et al., 2011). Much of this ice is thought to have originated from the basal portion of pre-existing glaciers and ice sheets dating back to the Pleistocene. The study of the AMS of this ice could provide an indication of its origin, and the palaeoflow directions of the ice that it was associated with, enabling more accurate palaeogeographical reconstructions.

7.5.2. Glaciotectonism and Quaternary glacial deposits

The results from Chapter 4 highlight the ability of the AMS technique to accurately evaluate strain within glaciotectonites. This approach can be adapted to other glaciotectonites along the north Norfolk coast and has the ability to provide constraints on palaeoflow directions across the region. Glaciotectonites are not only common in north Norfolk. They have been identified in many other glaciated regions, and there is significant opportunity for AMS to be applied globally.

As well as indentifying past ice flow directions, the application of AMS, in the manner presented in this thesis, has the potential to increase our understanding of how sediment deforms during glaciotectonism. One interesting area where this could be applied is in the identification of proglacial versus subglacial glaciotectonism (compare and contrast subglacial and proglacial environments in Fig. 3, Chapter 1). Subglacial glaciotectonism occurs when the ice is directly overlying the sediment. Consequently, deformation within the sediment is dominated by simple shear processes. In contrast, proglacial glaciotectonism occurs when sediment is bulldozed in front of a glacier and the structures produced are often considered analogous to those in fold and

thrust belts. Here, compressional deformation dominates and distinctly different AMS fabrics in each environment are expected. In a subglacial environment, one may expect the K_1 axes to be sub-horizontal, parallel to the direction of ice flow. In contrast, proglacial glaciotectonism may result in k_1 orientations perpendicular to glacier flow, with the magnetic foliation dipping steeply reflecting the horizontal shortening associated with compressional deformation.

7.5.3. Neoproterozoic diamictites

The potential of AMS analysis for the study of Neoproterozoic diamictites has been highlighted in Chapters 5 and 6. Diamictites from the Neoproterozoic period have been a source of controversy since they were first identified. With the advocacy of the Snowball Earth Hypothesis, their importance in terms of extreme climatic perturbations in the Earth's history is now widely recognised. Many Neoproterozoic glacial deposits have attracted intense geological research (see reviews in Fairchild and Kennedy, 2007). Despite this, considerable debate exists around the origin and significance of many of these diamictites. This thesis has identified that AMS could be used alongside the various other techniques currently used to study these deposits and may provide considerable palaeogeographic information.

The Tillite Group of NE Greenland (Hambrey and Spencer, 1987) is considered to be very similar to the Polarisbreen Group of NE Svalbard. The two formations are generally thought to have originally been contiguous and formed in the same sedimentary basin (Fairchild and Hambrey, 1995). Being similarly undeformed and possibly representing a different part of the basin, the depositional sequence here is of particular interest. A study, similar to that presented in Chapter 5 and 6 which utilises the AMS technique, combined with a modern understanding of glacial depositional environments, could provide significant information on palaeoflow. This would enable a better understanding on the basin palaeogeography and palaeoenvironments.

Neoproterozoic diamictites are not only restricted are very widespread and have been discovered on 23 palaeocontinents (see articles in Copons et al., 1997). In many cases, these diamictites are similarly well-preserved and are also relatively undeformed. In many of these

locations, significant opportunity exists for the use of AMS to unravel palaeoflow information from these deposits.

APPENDICIES

APPENDIX A –AMS SAMPLING AND MEASUREMENT

A.1. Introduction

AMS can be measured in a wide range of materials, both consolidated and unconsolidated. The sampling techniques are typically similar to those in used in palaeomagnetic analysis, and the same samples can normally be used for both applications. Ideally, samples would be sphere-shaped to remove any effects of the shape of the samples; however, spheres are difficult to manufacture and orientate. Instead, cylinders or cubes are normally used (Fig. A.1). These cylinders normally have a diameter of 2.5 cm and a height of 2.1 cm, whilst the cubic samples normally have sides of 2 cm.

Lithified rock is usually sampled by two main methods: by drilling directly in the field or by collecting and orientating a block of rock in the field and drilling later in the lab (Section 4.1). However, unconsolidated sediment is soft, and it normally cannot be drilled, therefore alternative methods needed to be developed to sample unconsolidated diamicton. In addition, as the application of the AMS technique to basal ice is completely new, a sampling strategy had to be devised. In the following, the sampling procedure in each study is outlined.

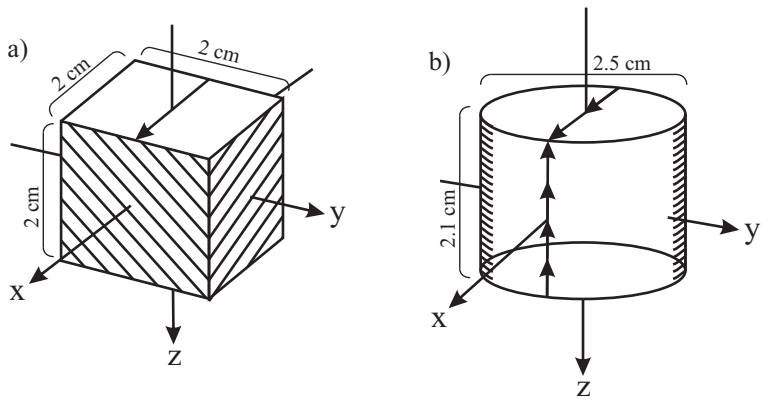

Fig. A.1 – The standard-sized subsamples used in AMS analysis. The Kappabridge is designed to measure either (a) cubes with sides of 2 cm or (b) cylinders with a 2.5 cm diameter x 2.1 cm height. The axes x, y and z represent the specimen frame axes at which the AMS results are initially presented prior to reorientation to geographic coordinates (after Collinson, 1983).

A.2. Basal-ice sampling

To measure the AMS of basal ice (Chapter 3), suitable samples had to first be collected. These samples needed to be the correct size and shape (either cylinders or cubes). They need to be accurately orientated so that their geographical vectors can be re-established after measurement. In addition, they needed to be transported back to the University of Birmingham's Rock Magnetic Laboratory, and measured in a Kappabridge at room temperature. Both of these need to be done without the sample melting or the sample markings being lost. Meeting these requirements posed a significant challenge.

A.2.1. Sample collection

It was decided that the easiest way to collect samples was to use a petrol-powered portable rock drill (Fig. A.2b). This could easily be transported to the site (Fig. A.2a) by snowmobile and could be used remotely, without the need for an external power source, down to the low temperatures (-20°C) that were encountered. Sampling sites were selected where the detrital sediment concentration exceeded 10% (Fig. A.2c). This was to maximise the chance of obtaining reliable AMS fabrics which are dominated by either ferromagnetic (s.l.) or paramagnetic minerals. Suitable areas of basal ice were selected and the portable rock drill was used to obtain a core of basal ice. In contrast to drilling lithified rock, drilling fluids were not needed for cooling. This is because, the material being drilled was dominantly ice, and as such, any heat created resulted in melt of the ice and the creation of self-cooling fluids. Normally, core length was restricted to <5 cm, since if this was exceeded the core became prone to fracturing and becoming lodged in the drill barrel prior to orientating. This would have resulted in a loss of the original orientation. The cores were orientated using a Pomeroy Orienting Fixture with attached Brunton compass (Fig. A.2d). A fiducial mark was placed on the core using non-magnetic wire. As temperatures were well below freezing, samples could be subsequently transported back to the laboratories at UNIS, Svalbard (Fig. A.2e) and stored in a cold room at -20 °C, ready for sample processing.

a)

b)

c)

d)

e)

f)

Fig. A.2 - Photographs of the field sampling procedure for basal ice. a) The study site at Tunabreen showing the location at which the samples were collected. (b) Drilling into the basal ice using a portable petrol-powered rock drill. (c) Drill hole within the debris-rich basal ice. (d) The author measuring the orientation of a drill core using a Pomeroy Orienting Fixture. (e) Basal ice cylinders, stored in a cold room at -20 °C. (f) An example of a basal ice AMS subsample, showing a foliated fabric with several larger clasts on the top surface.

A.2.2. Sample processing

In a cold room, the sample orientation was extrapolated along the length of the core using a permanent marker. The samples were then cut into cylinders of 2.1 cm length (Fig. A.2f), using a non-magnetic, diamond-tipped circular rock saw. As with field drilling, cooling fluids were not required. The samples were subsequently transported back to the University of Birmingham's Rock Magnetic Laboratory. Samples were packed in an insulated container, cooled to –78.5 °C with dry ice. 2.5 kg of dry ice was used, which was sufficient to keep the samples below freezing for the duration of the flight. On arrival at the University of Birmingham, the samples were placed in a freezer at -20 °C ready for AMS analysis.

A.2.3. Diamicton sampling

As with the sampling of basal ice, the sampling of unlithified diamicton (Chapter 4) required the development of a sampling strategy. Unlithified diamicton cannot be drilled because it is too soft and readily disaggregates. Previous attempts at sampling unlithified diamicton have involved the use of cylindrical sample holders (e.g. Shumway and Iverson, 2009; Thomason and Iverson, 2009) These are directly pushed into the sediment by hand and subsequently orientated (Fig. A.3a). This method was initially adopted; however, it was soon found that because of the high compaction of the sediment, a sampling-induced anisotropy was created, as has previously been encountered (e.g. Copons et al., 1997; Gravenor et al., 1984); therefore, an alternative methodology was developed.

A.2.4. Sample collection

Whilst the sediment was unconsolidated, it was sufficiently compacted for a block to be

a)

b)

c)

d)

e)

f)

g)

Fig. A.3 – Photographs of the field sampling procedure for diamicton. (a) The initial sampling methodology adopted involved pushing a cylindrical sampling holder directly into the diamicton, Note: this technique was abandoned when a sampling induced anisotropy was detected. (b) The adopted sampling technique showing the excavation of a block of diamicton close to the hinge of an isoclinal recumbent fold. (c) Orientating the sample with a fiducial mark. (d) Samples wrapped in cling film ready to be air-dried. (e) A diamicton sample after sodium silicate impregnation and coating in epoxy resin, showing the engravings of the fiducial mark. (f) Fingers of sediment being re-impregnated with resin, partway through the cutting process. (g) Final cubic specimen of 20 × 20 × 20 cm ready for subsequent measurement in the Kappabridge.

excavated without disaggregation. A 20 cm excavation was made into the cliff face to remove any till which may have been affected by surface processes (Fig. A.3b). A block of sediment (approximately 20 cm × 10 cm × 10 cm), was isolated from the surrounding till. A flat surface was made on the frontal face and measurement of the orientation of that surface made with a Brunton compass through a fiducial mark drawn with a non-magnetic blade (Fig. A.3c). The block was subsequently separated from the surrounding till and wrapped in plastic wrap, and transported back to the University of Birmingham's Rock Magnetic Laboratory (Fig. A.3d).

A.2.5. Sample processing

Once in the laboratory, blocks were left to air dry over a period of 1 week. As the blocks were still unconsolidated, subsequent hardening was needed before sample suitable for AMS analysis could be made. Samples were hardened initially using a sodium silicate solution. As it is non-magnetic, mixes ready with water and the cementation process does not affect grain alignment, sodium silicate routinely used to harden samples in palaeomagnetic analyses (e.g. Théveniaut and Freyssinet, 1999). The sample was soaked in a diluted solution consisting of one part sodium silicate solution to 2 parts water and left to air dry. After this, a final layer of epoxy resin was added to the outside of the sample (Fig. A.3e). This did not penetrate more than 5 mm into the block, but it created a waterproof membrane and added integrity to the sample during water drilling. Markings on the block were extrapolated around the sample so that the geographic orientation could be reconstructed after measurement. The blocks were subsequently wet cut on a circular saw into 20 cm slices (Fig. A.3f). After this, a further layer of concentrated sodium silicate was added to the newly created surfaces. The slices where subsequently dry cut into cubes

Fig. A.4 – Photographs of the field sampling procedure for diamictite. (a) Field photograph of geologist collecting AMS samples through field drilling. (b) AMS block sample with fiducial mark. (c) Block sample attached to the drilling table ready for field drilling. Note the drilled surface is not horizontal and hence requires an additional rotation stage during reorientation. (d) Example drill cores from a site ready to be cut into 2.1 cm cylinders. (e) Final cylinders ready for subsequent measurement in the Kappabridge.

(20 cm × 20 cm × 20 cm), ready for AMS measurement (Fig. A.3g).

A.3. Diamictite Sampling

The Diamictites were generally well lithified, and as such, standard sampling procedures could be used, involving both field drilling and the collection of block samples for subsequent lab drilling (Chapter 5 and 6). Field drilling (Fig. A.4a) is generally more labour-intensive whilst in the field, but sample transport is facilitated and there is a time-saving later in the laboratory Therefore, field-drilling was used over block sampling where possible. However, field drilling requires a reliable source of running water, and because of the weight of the drill, is not suitable where long distances have to be walked. In addition, not all lithologies were suitable for field drilling. Some samples were partially friable and shattered during drilling. Hence, a combination of field drilling and block sampling (Fig. A.4b) was used for the diamictites in this thesis.

A.3.1. Sample collection

Field-drilled samples were obtained through the use of a portable petrol-powered rock drill fitted with a non-magnetic diamond tipped drill bit (Fig. A.4a). A continued stream of water, collected from snow melt, was flushed through the drill bit to facilitate cutting and minimize heat. The cores of rock obtained measured up to 6 cm in length (Fig. A.4c). These were subsequently orientated using a Pomeroy Orienting Fixture with attached Brunton compass by scratching a fiducial mark along one side of the core. The cores were separated from the outcrop and transported back to the laboratory.

Where field drilling was not possible, block samples were also collected for later drilling under laboratory conditions. These were collected by identifying an in-situ rock sample, ideally (20 cm × 10 cm × 10 cm) or big enough to obtain at least 8 subsamples (Fig. A.4b). A flat surface was identified and the sample was orientated using a Brunton compass by the drawing of a fiducial mark. The block was subsequently separated from the outcrop using a combination of hammers

and chisels and transported back to the laboratory for subsequent analysis. Collection was facilitated by the frost-shattered nature of most lithologies in the area.

A.3.2. Sample processing

To obtain subsamples, block samples first had to be drilled in the laboratory. This was undertaken using a 24.5 mm-diameter, diamond tipped drill bit. Prior to drilling, the fiducial mark drawn on to the specimen was extrapolated along the top surface of the sample. The block was subsequently secured to a mounting surface and drilled from above (Fig. A.4c).Hence, the top surface of the block is not necessary horizontal, and the drilling effectively takes place at an angle. This means that an additional reorientation step needs to be added to correct for this tilt (Section 5). The axis and degree of this rotation is calculated by the measurement of the new strike and pitch of the surface, following the procedure of Owens (1994). After drilling, cores were subsequently extracted and the orientation arrows on the top surface (Fig. A.4d), extrapolated down the entire length of the core. Both the field- and laboratory-drilled cylinders were subsequently cut into 2.1 cm-long cylindrical subsamples with a non-magnetic diamond-tipped circular saw, ready for AMS analysis (Fig. A.4e).

A.4. AMS measurement procedure

The AMS was normally measured using an AGICO KLY-3 Kappabridge operating at 875 Hz with a 300 A/m applied field at the University of Birmingham and an AGICO MFK-1A Kappabridge operating at 976 Hz with a 200 A/m applied field at New Mexico Highlands University. Each subsample was placed into the Kappabridge sample holder and measured in three orthogonal orientations. In each orientation, the sample was lowered into the Kappabridge and rotated through 360° about an axis. During this, the variation in magnetic susceptibility was measured, enabling the determination of the AMS. In addition, a single measurement of the bulk susceptibility was undertaken. This process was repeated for all subsamples making up a site.

Particular care and attention had to be taken for the measurement of the basal ice samples (Chapter 3). The AMS samples were stored at -20°C in a container adjacent to the Kappabridge, but the AMS measurement was undertaken at room temperature. This can be done without the sample melting as the measurement of each axis takes less than a minute. Particular care and attention was taken to careful cleaning and calibration between each measurement. As the susceptibility of the basal was very low, any dust left behind from previous analyses containing ferromagnetic (s.l.) grains could potential affect the AMS.

One the AMS has been measured, the subsequent data were analysed in the Anisoft42 program (obtained from http://www.agico.com/software/winsoft/anisoft/). Here, the data can be rotated into the specimen frame based on the strike and dip data collected in the field. The data can subsequently be analysed and interpretations made. Samples collected through block sampling required an additional step in the rotation process. As laboratory drilling was not necessarily perpendicular to the orientated surface, the data had to be corrected prior to the geographic coordinates being assigned. This process is outlined in Owens (1994) and involves rotating the principal susceptibility axes about the drill table strike, into the original specimen frame. Once these steps have been undertaken, the AMS data can subsequent be analysed and interpreted.

To characterise the shape and strength of the fabric, the parameters K_{mean}, P_j, L, F, and T were also calculated. Because of the reasons discussed in Section 2.9, the eigenvalue method was not used to calculate fabric strength. AMS parameters were compiled both on Microsoft Excel and through the Agico Anisoft 4.2 software. AMS data is presented onto lower hemisphere, equal-area stereographic projections.

APPENDIX B – AMS RESULTS OF THE WILSONBREEN FORMATION, SVALBARD

AMS results of the Wilsonbreen Formation at Dracoisen, Ditlovtoppen, Andromedafjellet, Klofjellet and Backlundtoppen. The long (K_1), intermediate (K_2) and short (K_3) susceptibility axes are plotted as black squares, grey triangles and white circles respectively, displayed on lower hemisphere, equal area stereographic projections. Left-hand column represents data uncorrected for bedding with the bedding plane shown as a great circled (grey) and pole to bedding (grey circle). Right-hand column shows data after rotation about the bedding orientation to horizontal.

UNCORRECTED CORRECTED

DC2 - Diamictite - W1

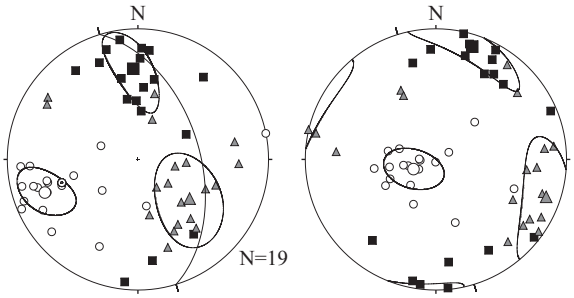

UNCORRECTED CORRECTED

DC3 - Diamictite - W1

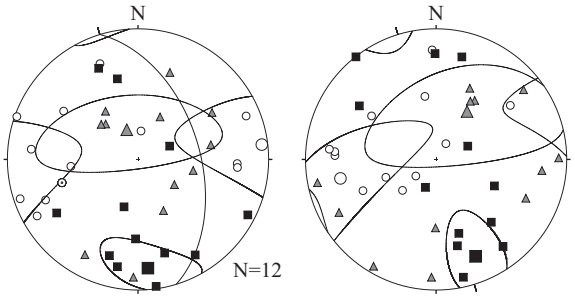

DC4 - Diamictite - W1

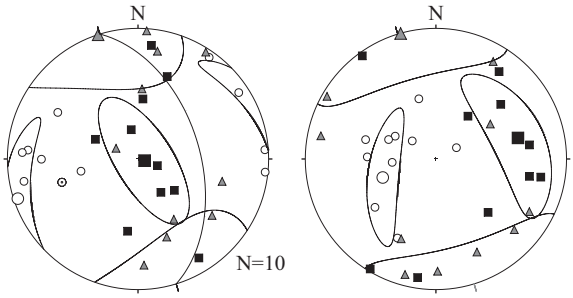

DC5 - Limestone - W2

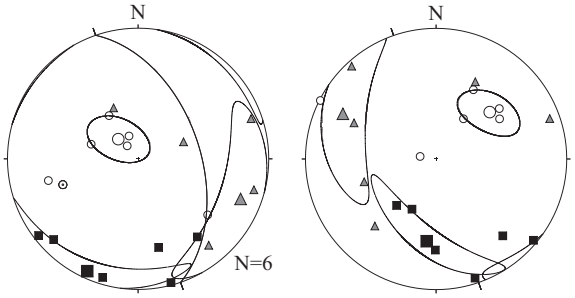

DC6 - Rhythmite - W2

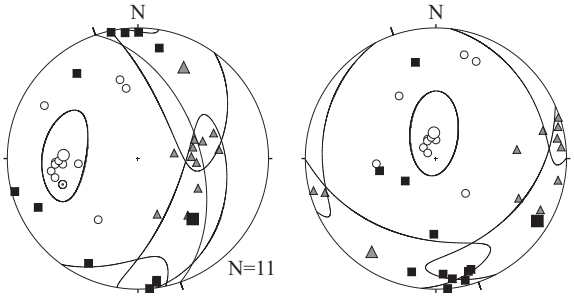

DC7 - Limestone - W2

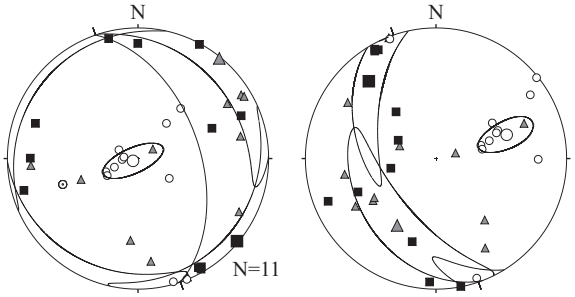

DC8 - Diamictite - W1

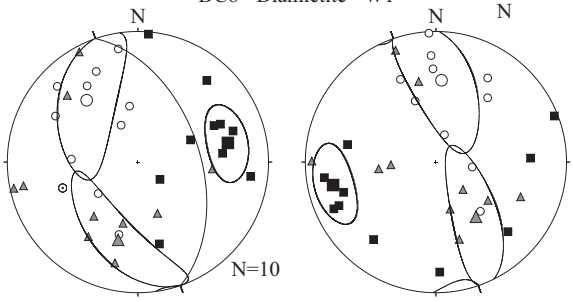

DC9 - Diamictite - W3

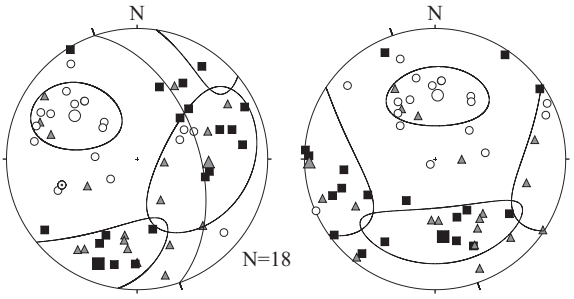

DC11 - Diamictite - W3

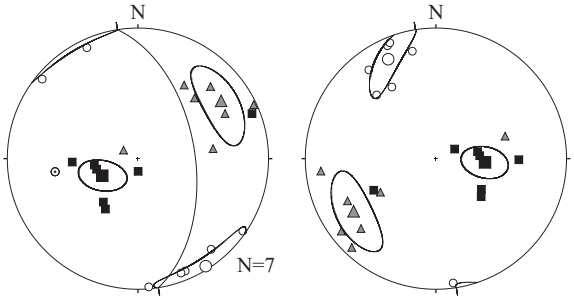

DC16 - Diamictite - W3

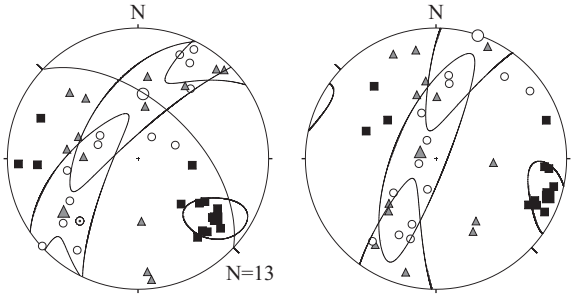

UNCORRECTED CORRECTED

DC21 - Sandstone - W2

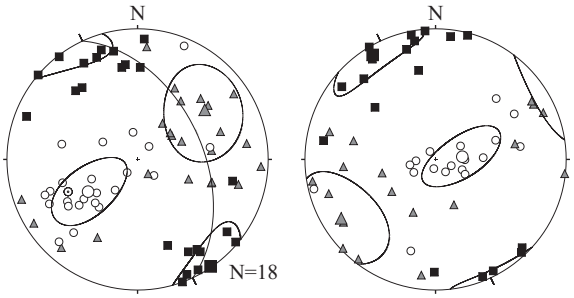

UNCORRECTED CORRECTED

DC22 - Rhythmite - W2

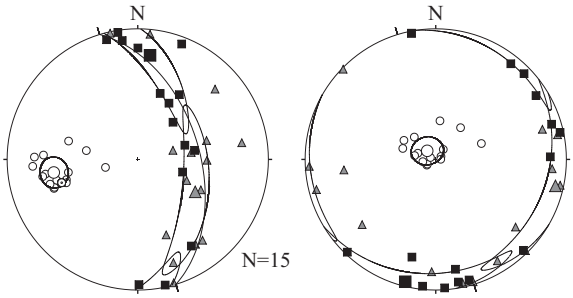

DC43 - Sandstone - W3

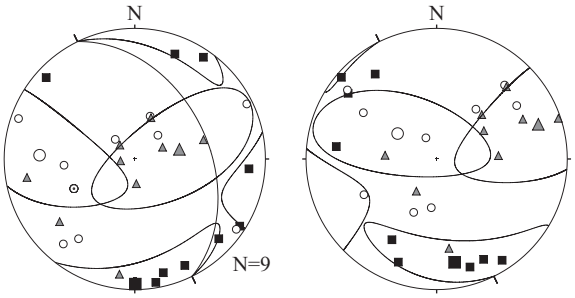

DC44 - Sandstone - W3

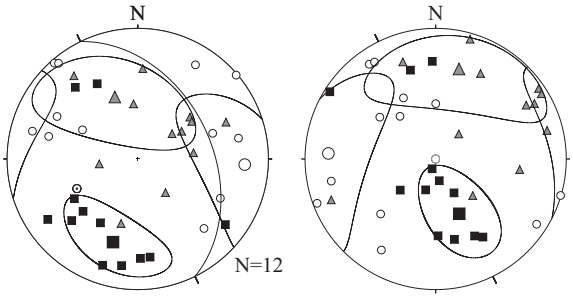

DC47b - Diamictite - W1

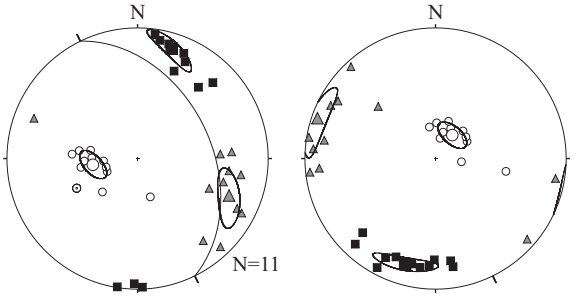

DC57 - Diamictite - W3

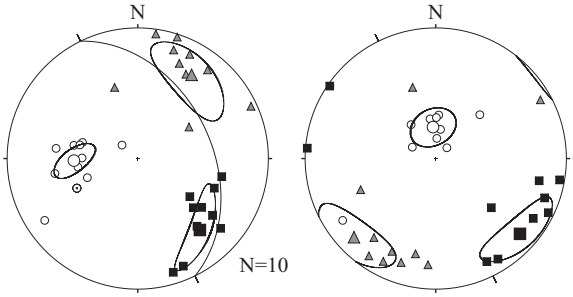

DC60 - Limestone - W2

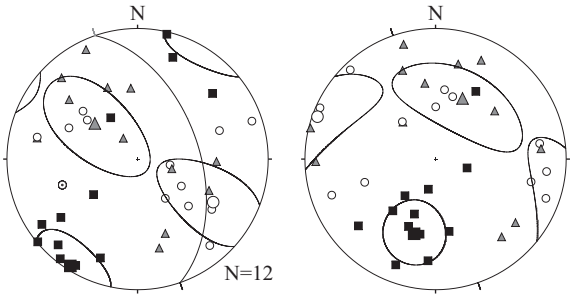

DC61 - Diamictite - W2

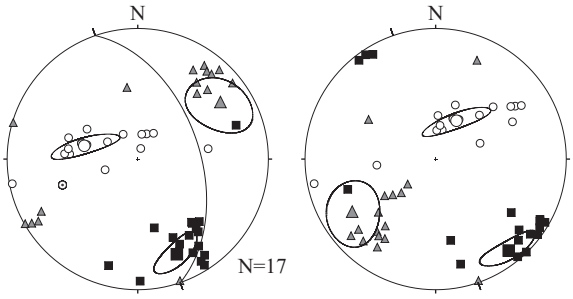

DC62 - Diamictite - W3

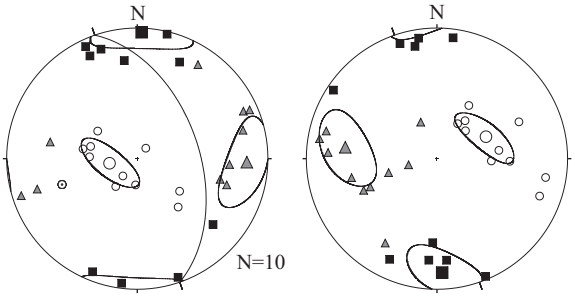

DC63 - Diamictite - W3

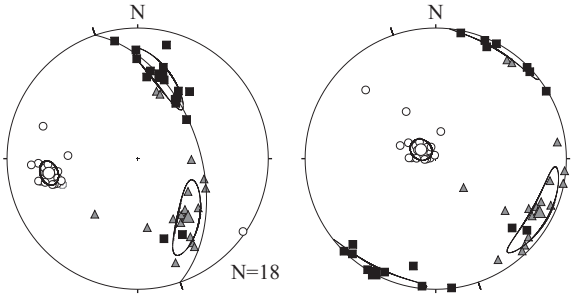

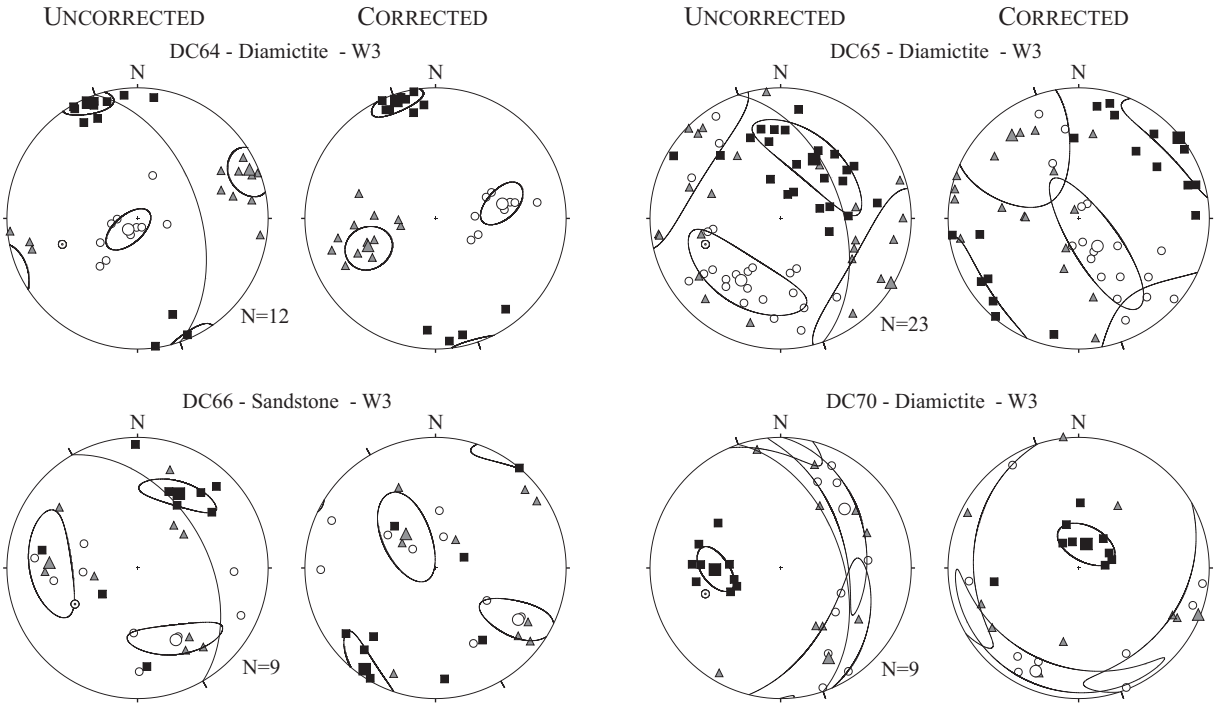
UNCORRECTED
CORRECTED
DC64 - Diamictite - W3
N
N
N=12
UNCORRECTED
CORRECTED
DC65 - Diamictite - W3
N
N
N=23
DC66 - Sandstone - W3
N
N
N=9
DC70 - Diamictite - W3
N
N
N=9

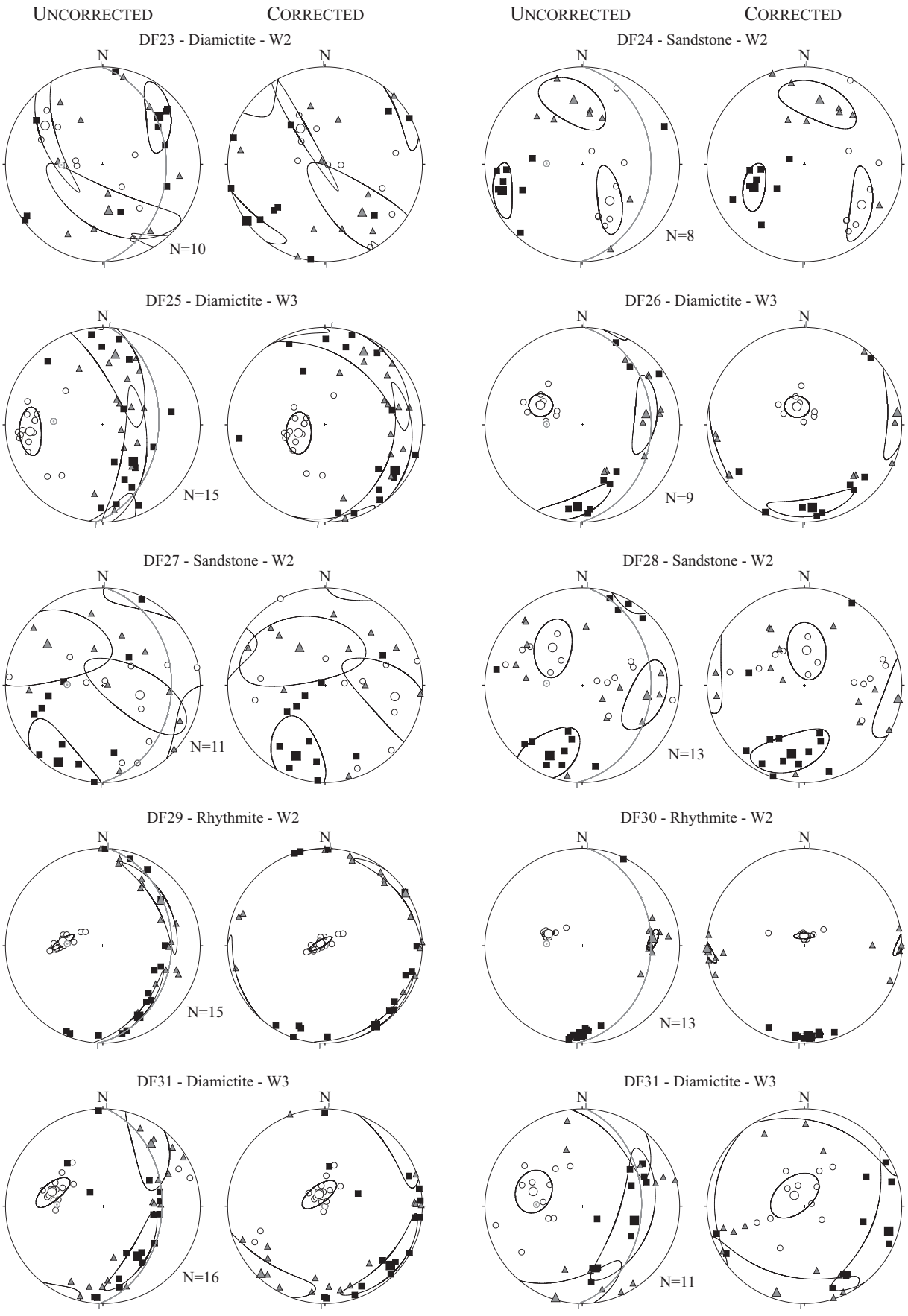
UNCORRECTED
CORRECTED
DF23 - Diamictite - W2
N
N=10
DF24 - Sandstone - W2
N=8
DF25 - Diamictite - W3
N=15
DF26 - Diamictite - W3
N=9
DF27 - Sandstone - W2
N=11
DF28 - Sandstone - W2
N=13
DF29 - Rhythmite - W2
N=15
DF30 - Rhythmite - W2
N=13
DF31 - Diamictite - W3
N=16
DF31 - Diamictite - W3
N=11

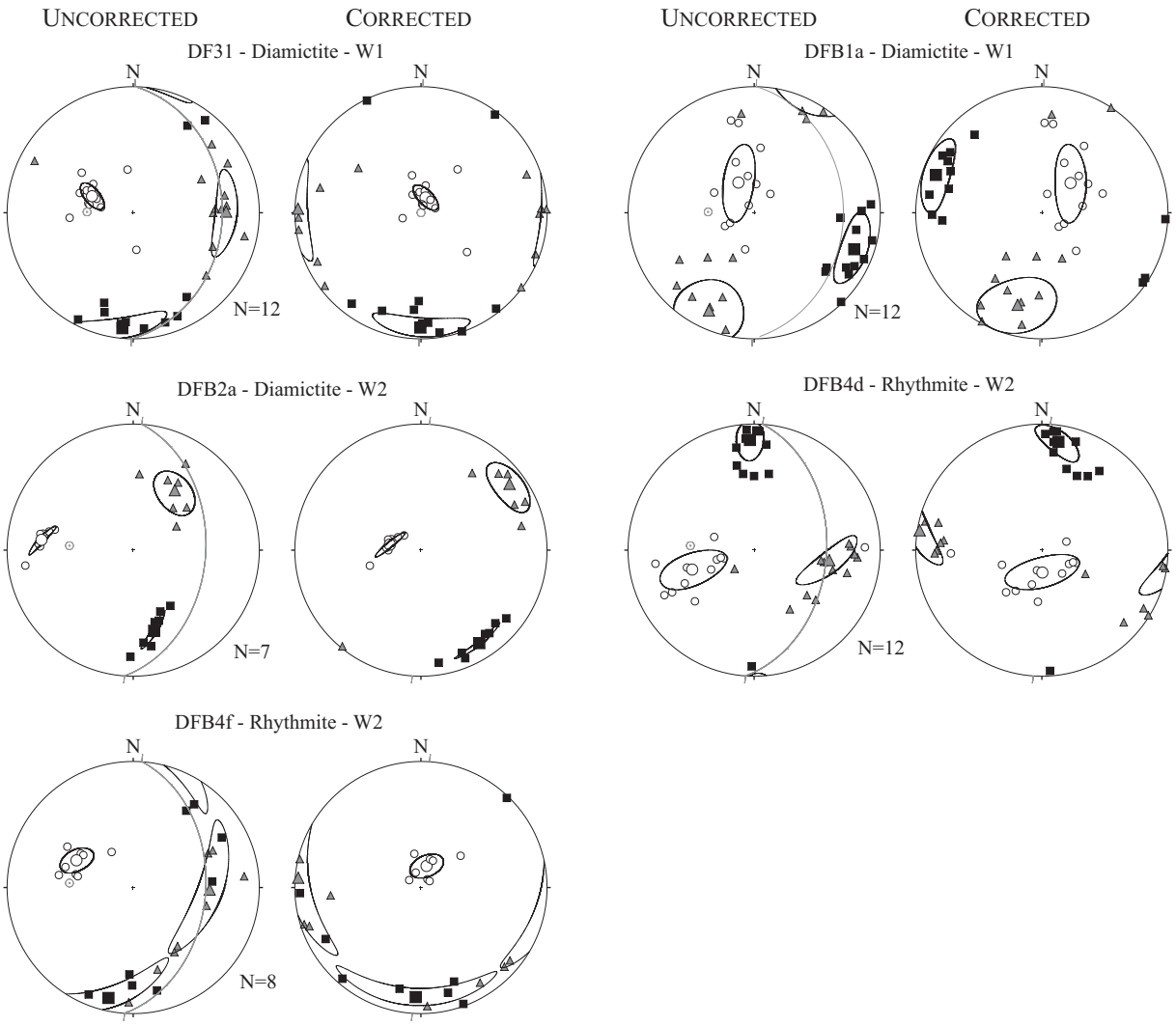
UNCORRECTED
CORRECTED
DF31 - Diamictite - W1
N
N
N=12
DFB1a - Diamictite - W1
N
N
N=12
DFB2a - Diamictite - W2
N
N
N=7
DFB4d - Rhythmite - W2
N
N
N=12
DFB4f - Rhythmite - W2
N
N
N=8

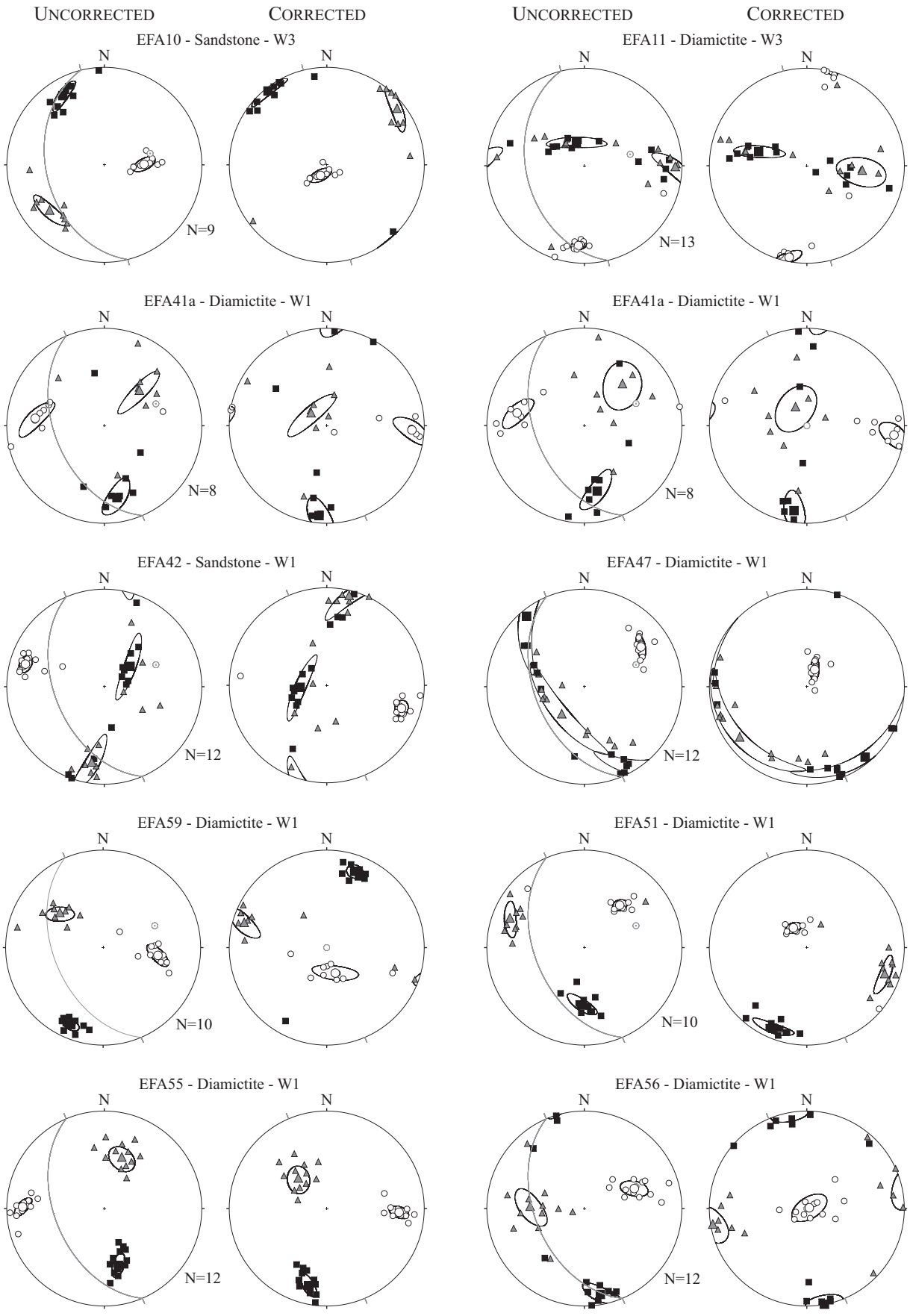
UNCORRECTED
CORRECTED
EFA10 - Sandstone - W3
N
N=9
UNCORRECTED
CORRECTED
EFA11 - Diamictite - W3
N
N=13
EFA41a - Diamictite - W1
N
N=8
EFA41a - Diamictite - W1
N
N=8
EFA42 - Sandstone - W1
N
N=12
EFA47 - Diamictite - W1
N
N=12
EFA59 - Diamictite - W1
N
N=10
EFA51 - Diamictite - W1
N
N=10
EFA55 - Diamictite - W1
N
N=12
EFA56 - Diamictite - W1
N
N=12

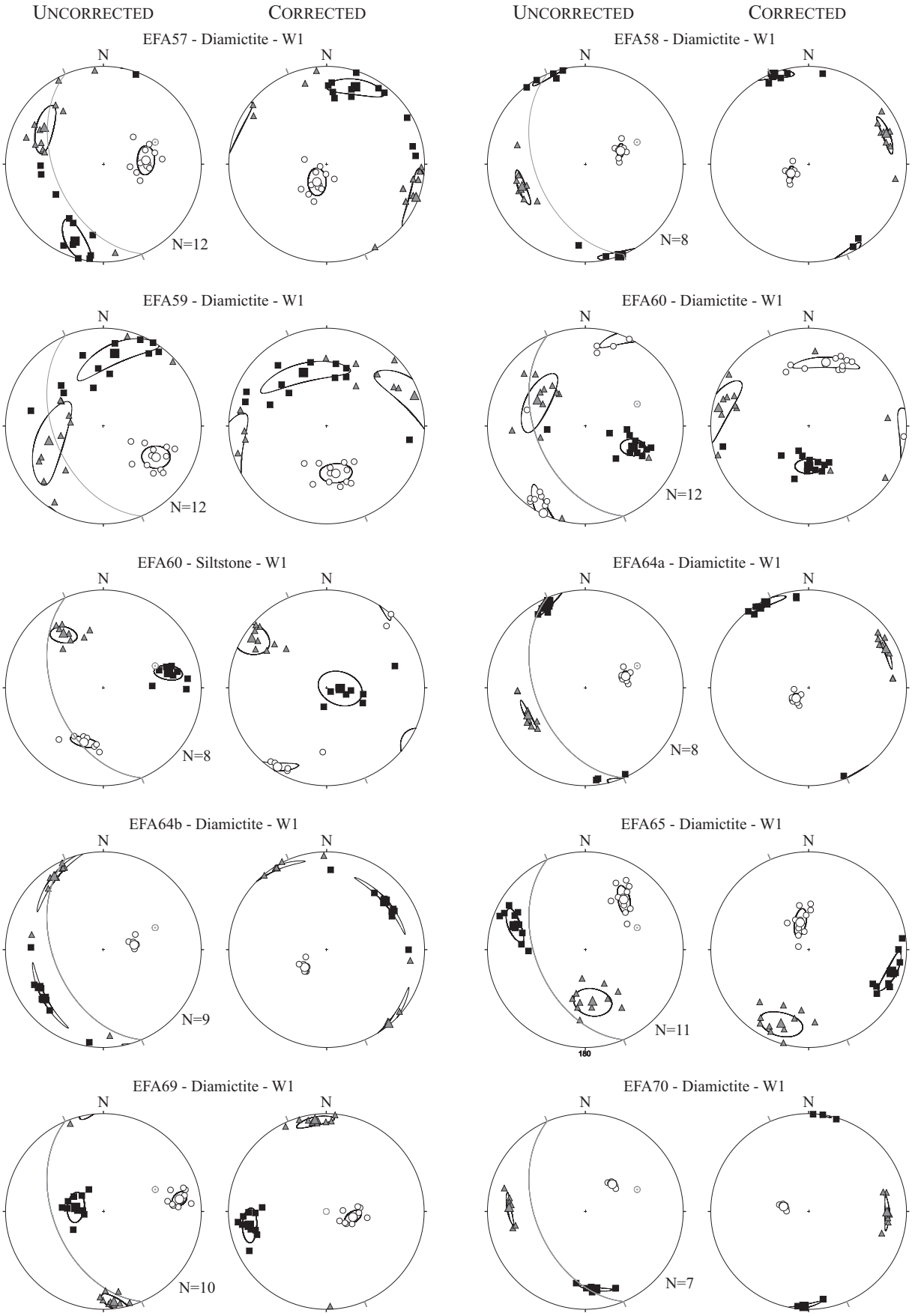
UNCORRECTED
CORRECTED
EFA57 - Diamictite - W1
N
N=12
EFA58 - Diamictite - W1
N=8
EFA59 - Diamictite - W1
N=12
EFA60 - Diamictite - W1
N=12
EFA60 - Siltstone - W1
N=8
EFA64a - Diamictite - W1
N=8
EFA64b - Diamictite - W1
N=9
EFA65 - Diamictite - W1
N=11
180
EFA69 - Diamictite - W1
N=10
EFA70 - Diamictite - W1
N=7

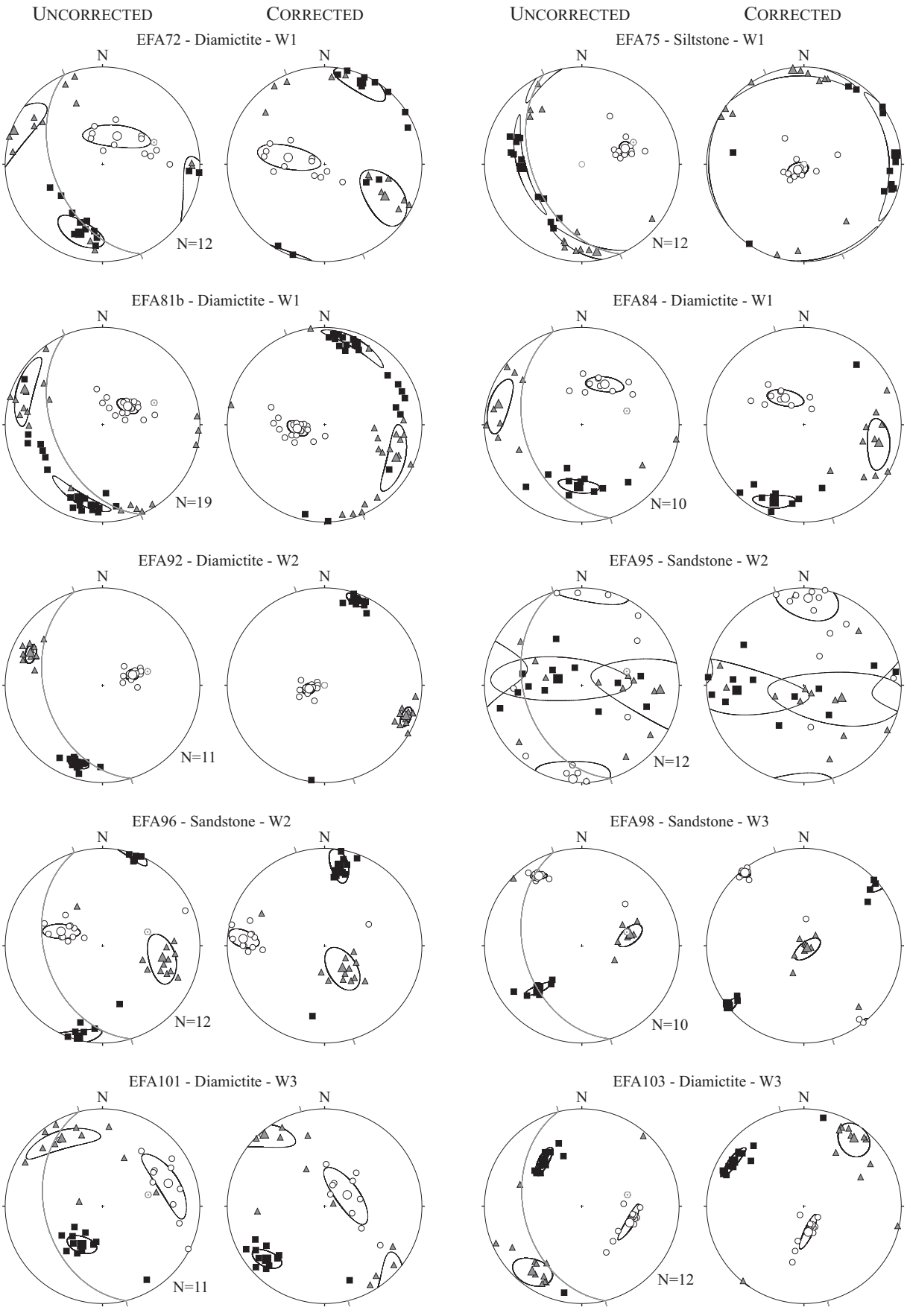
UNCORRECTED
CORRECTED
EFA72 - Diamictite - W1
N
N=12
EFA75 - Siltstone - W1
N=12
EFA81b - Diamictite - W1
N=19
EFA84 - Diamictite - W1
N=10
EFA92 - Diamictite - W2
N=11
EFA95 - Sandstone - W2
N=12
EFA96 - Sandstone - W2
N=12
EFA98 - Sandstone - W3
N=10
EFA101 - Diamictite - W3
N=11
EFA103 - Diamictite - W3
N=12

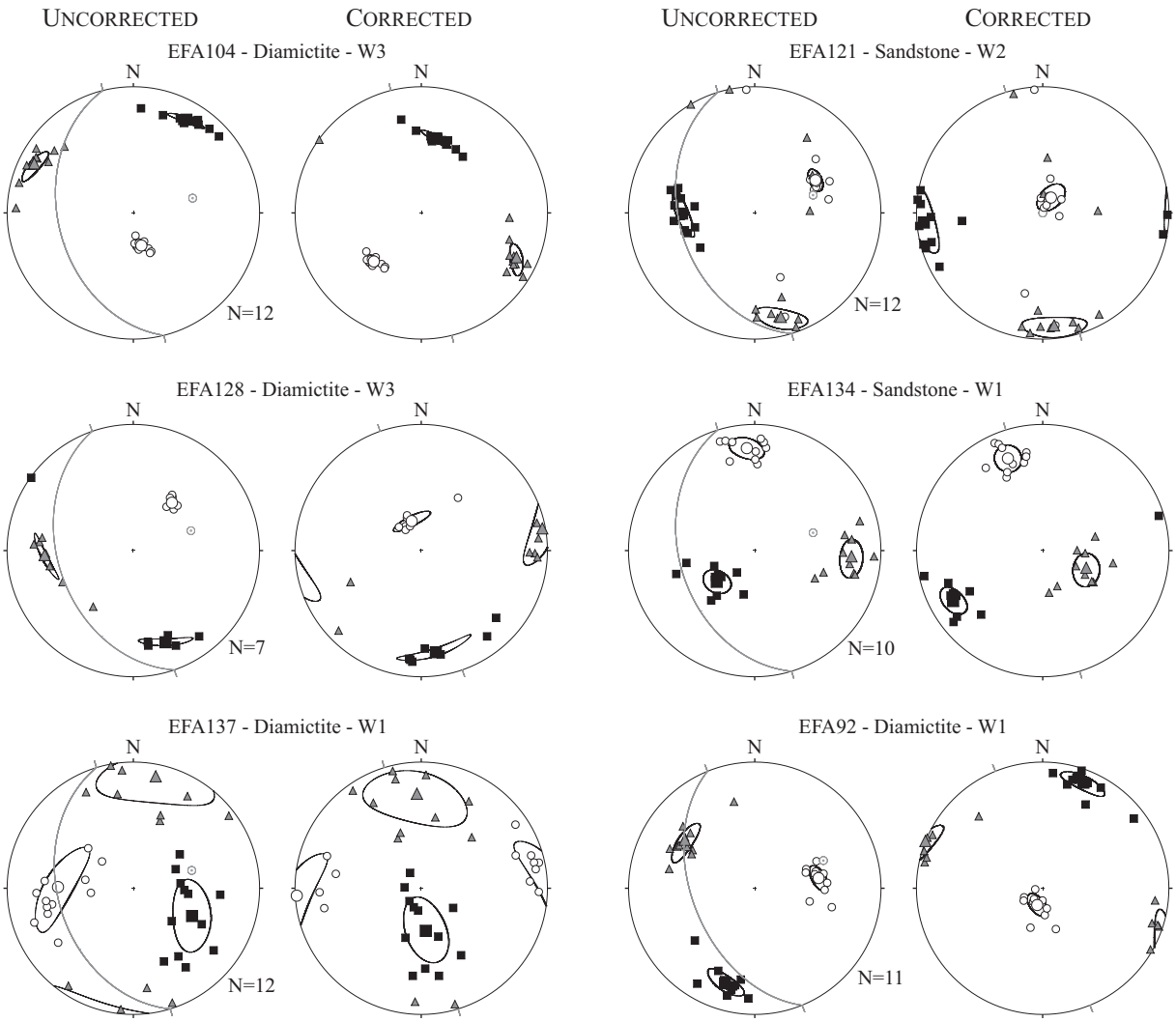
UNCORRECTED
CORRECTED
EFA104 - Diamictite - W3
N
N=12
EFA121 - Sandstone - W2
N=12
EFA128 - Diamictite - W3
N=7
EFA134 - Sandstone - W1
N=10
EFA137 - Diamictite - W1
N=12
EFA92 - Diamictite - W1
N=11

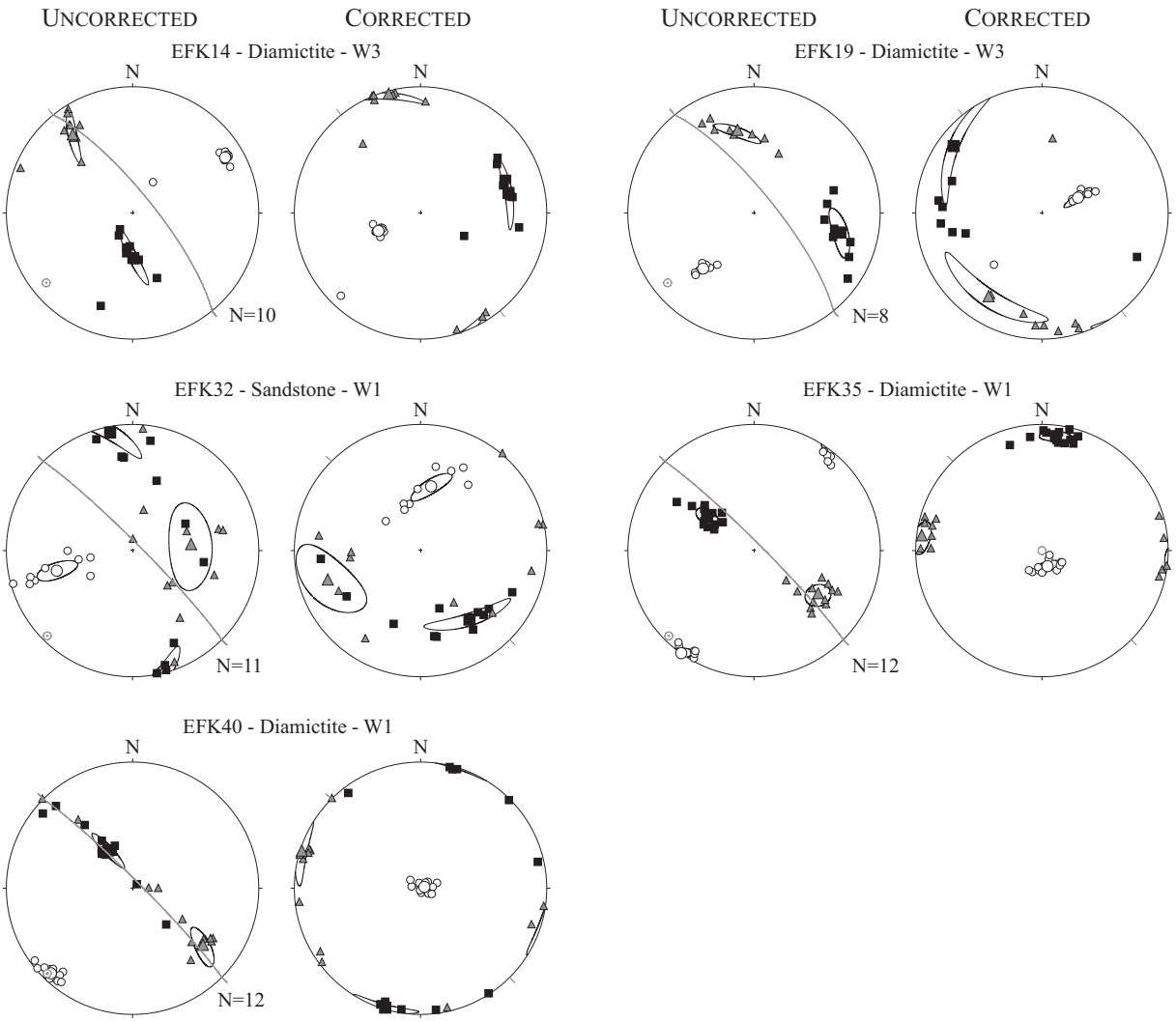
UNCORRECTED
CORRECTED
EFK14 - Diamictite - W3
N
N=10
EFK19 - Diamictite - W3
N=8
EFK32 - Sandstone - W1
N=11
EFK35 - Diamictite - W1
N=12
EFK40 - Diamictite - W1
N=12

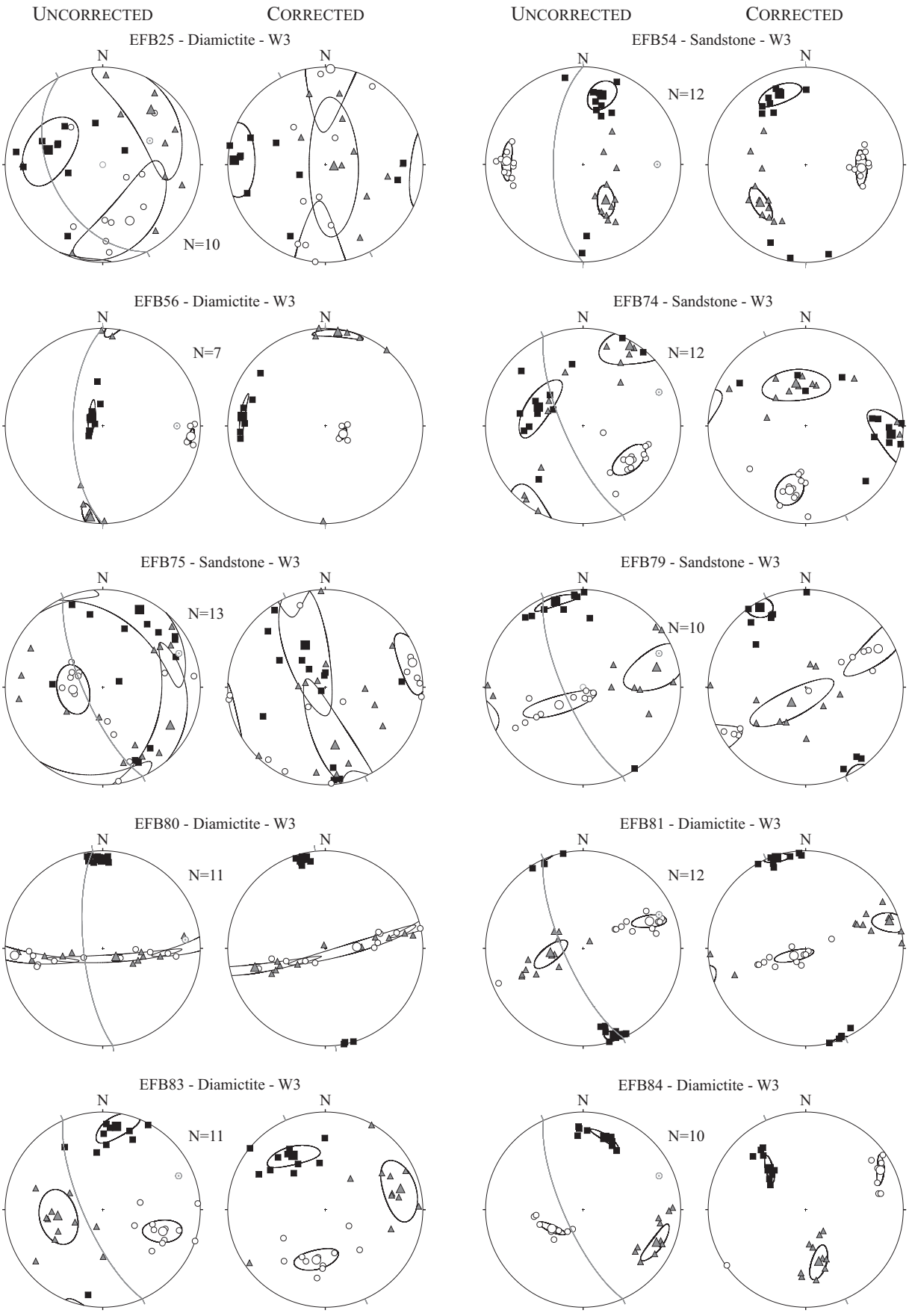
UNCORRECTED
CORRECTED
EFB25 - Diamictite - W3
N
N=10
EFB54 - Sandstone - W3
N=12
EFB56 - Diamictite - W3
N=7
EFB74 - Sandstone - W3
N=12
EFB75 - Sandstone - W3
N=13
EFB79 - Sandstone - W3
N=10
EFB80 - Diamictite - W3
N=11
EFB81 - Diamictite - W3
N=12
EFB83 - Diamictite - W3
N=11
EFB84 - Diamictite - W3
N=10

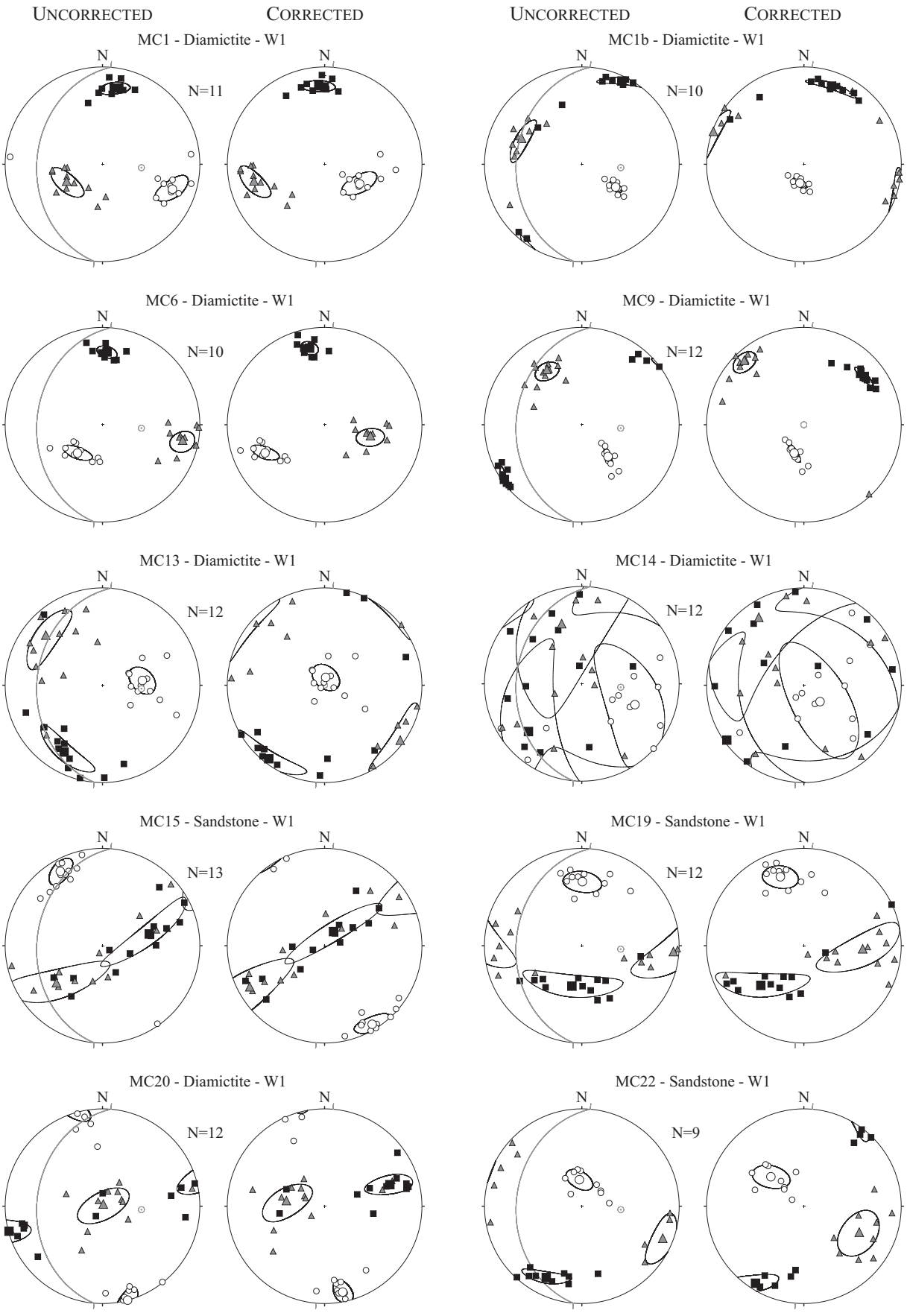
UNCORRECTED
CORRECTED
MC1 - Diamictite - W1
N=11
MC1b - Diamictite - W1
N=10
MC6 - Diamictite - W1
N=10
MC9 - Diamictite - W1
N=12
MC13 - Diamictite - W1
N=12
MC14 - Diamictite - W1
N=12
MC15 - Sandstone - W1
N=13
MC19 - Sandstone - W1
N=12
MC20 - Diamictite - W1
N=12
MC22 - Sandstone - W1
N=9
N

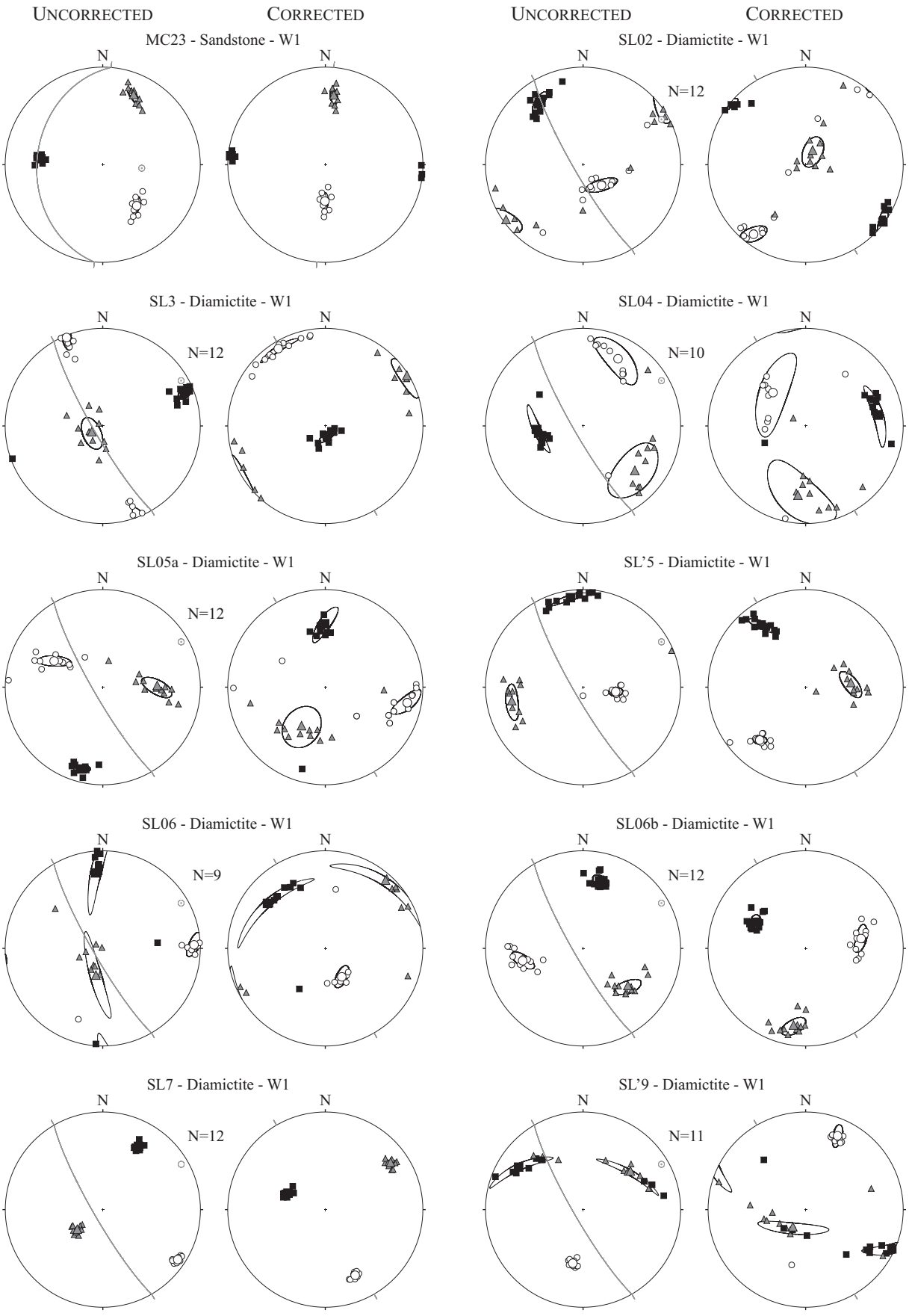
UNCORRECTED
CORRECTED
MC23 - Sandstone - W1
SL02 - Diamictite - W1
N=12
SL3 - Diamictite - W1
N=12
SL04 - Diamictite - W1
N=10
SL05a - Diamictite - W1
N=12
SL'5 - Diamictite - W1
SL06 - Diamictite - W1
N=9
SL06b - Diamictite - W1
N=12
SL7 - Diamictite - W1
N=12
SL'9 - Diamictite - W1
N=11

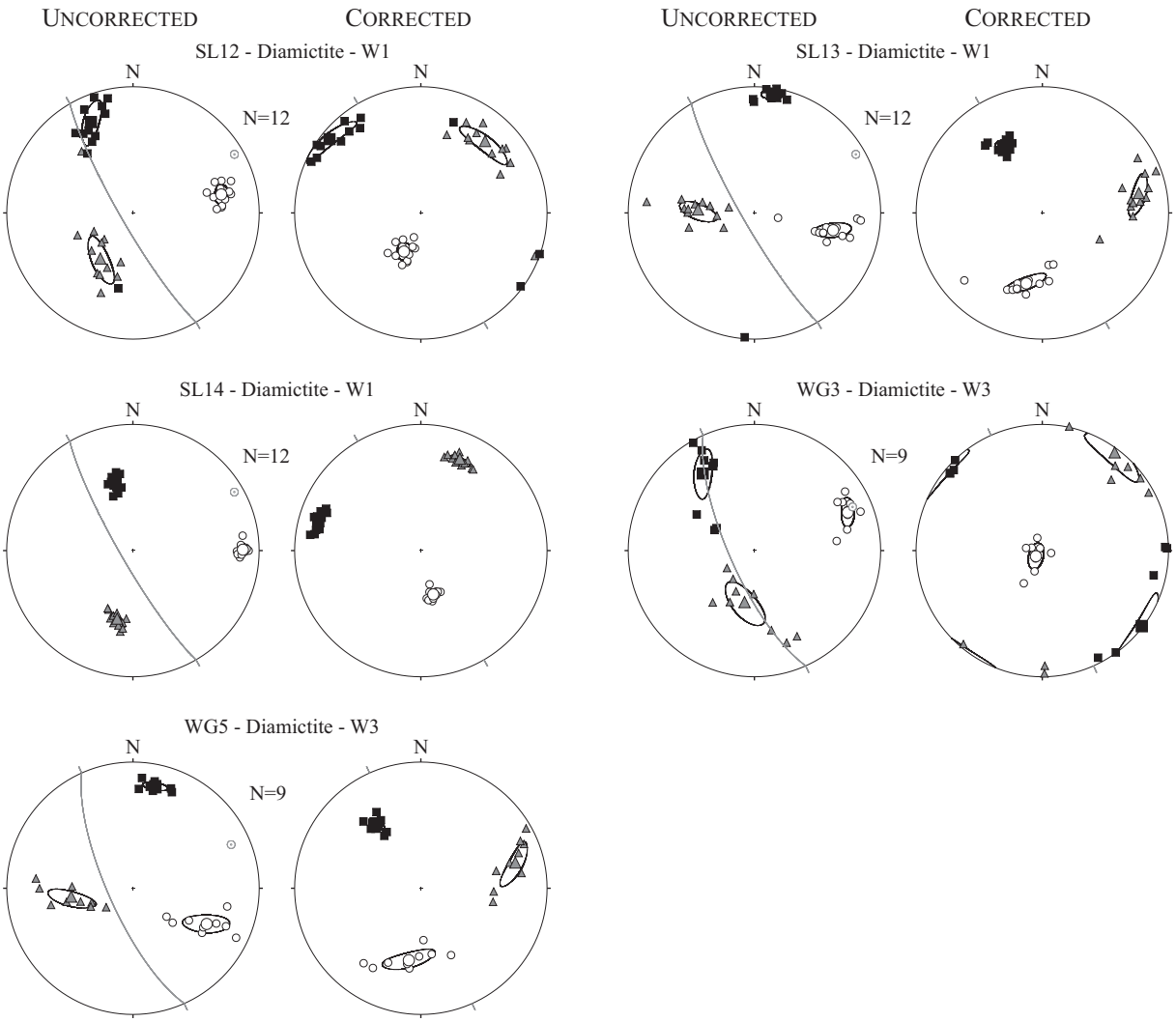
UNCORRECTED
CORRECTED
SL12 - Diamictite - W1
N
N=12
N
UNCORRECTED
CORRECTED
SL13 - Diamictite - W1
N
N=12
N
SL14 - Diamictite - W1
N
N=12
N
WG3 - Diamictite - W3
N
N=9
N
WG5 - Diamictite - W3
N
N=9
N

APPENDIX C – CLAST MACROFABRIC RESULTS OF THE WILSONBREEN FORMATION, SVALBARD

Clast fabric results of the Wilsonbreen Formation at Dracoisen, Ditlovtoppen and Andromedafjellet, displayed on lower hemisphere, equal-area stereographic projections. (a) Long axis clast fabric data (black squares) with bedding plane (black great circle). (b) Long axis clast fabric data (black squares) rotated about the bedding plane to horizontal. (c) Contour plot of long axis clast fabric data (contour interval = 10). (d) Rose of long axis clast fabric data.

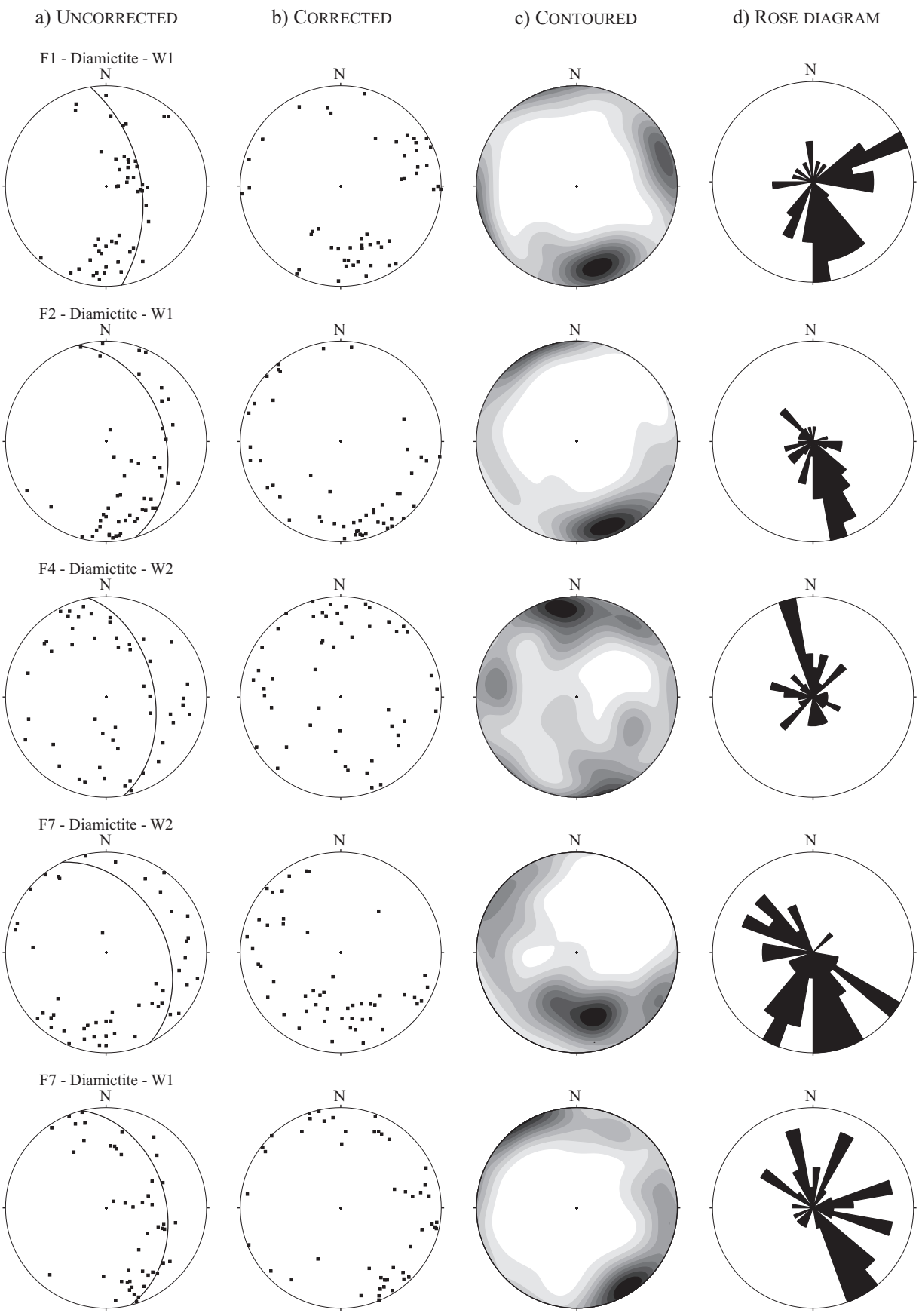
a) UNCORRECTED
b) CORRECTED
c) CONTOURED
d) ROSE DIAGRAM
F1 - Diamictite - W1
F2 - Diamictite - W1
F4 - Diamictite - W2
F7 - Diamictite - W2
F7 - Diamictite - W1
N

a) UNCORRECTED b) CORRECTED c) CONTOURED d) ROSE DIAGRAM

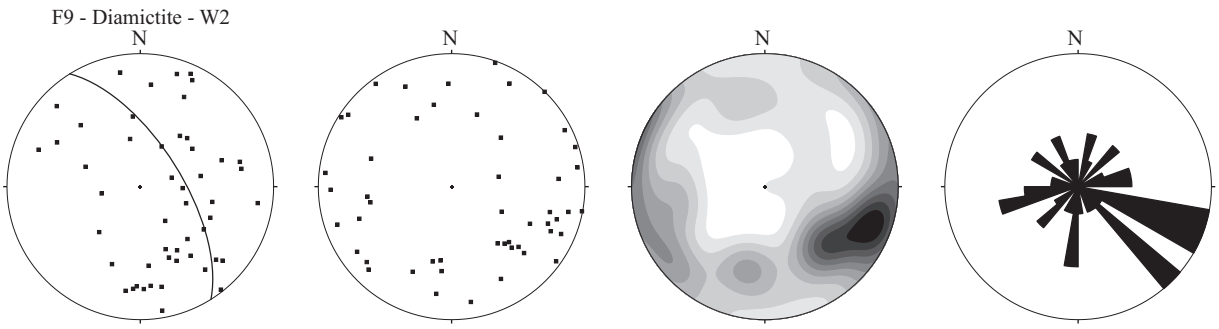

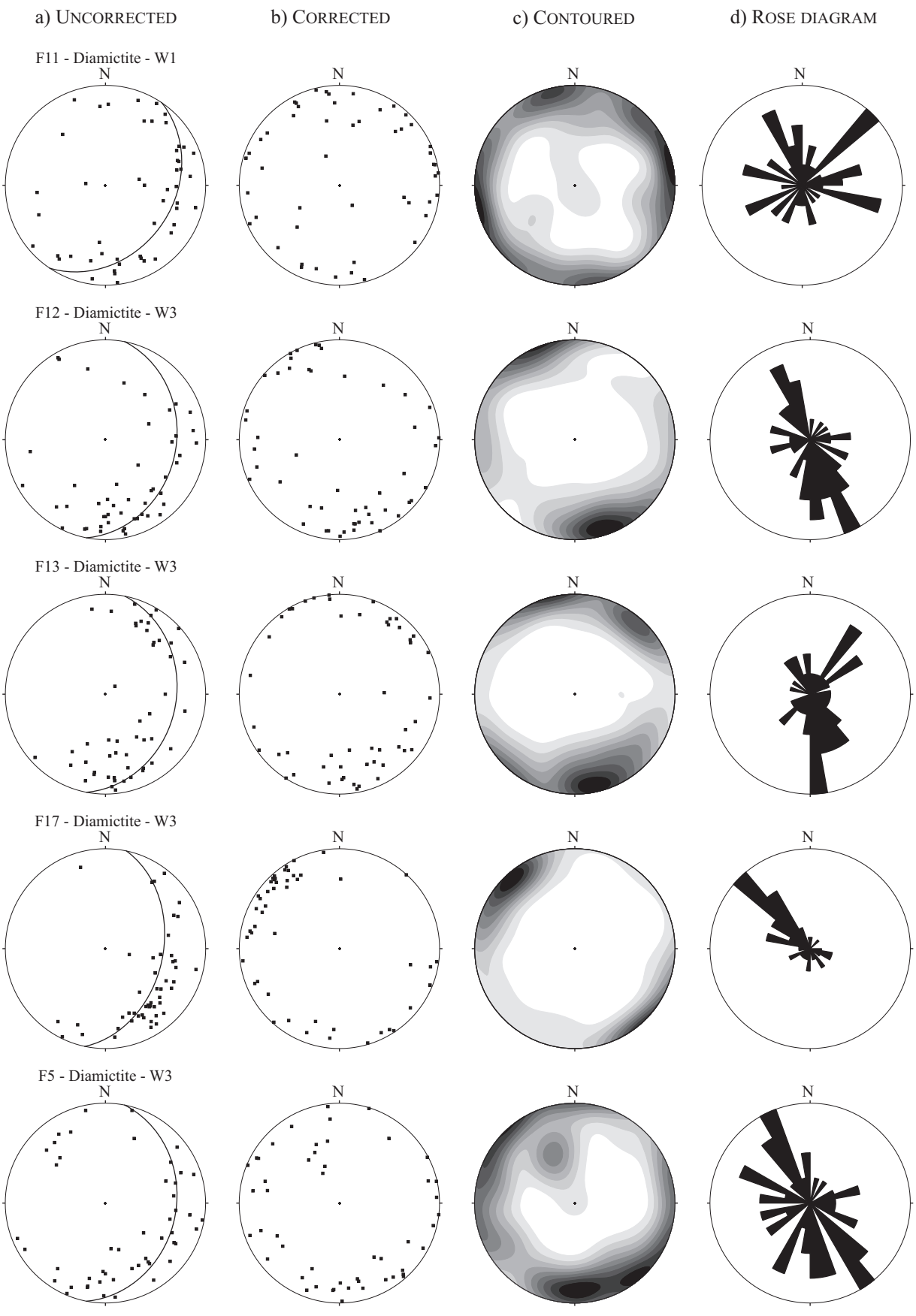
a) UNCORRECTED
b) CORRECTED
c) CONTOURED
d) ROSE DIAGRAM
F11 - Diamictite - W1
F12 - Diamictite - W3
F13 - Diamictite - W3
F17 - Diamictite - W3
F5 - Diamictite - W3
N

a) UNCORRECTED b) CORRECTED c) CONTOURED d) ROSE DIAGRAM

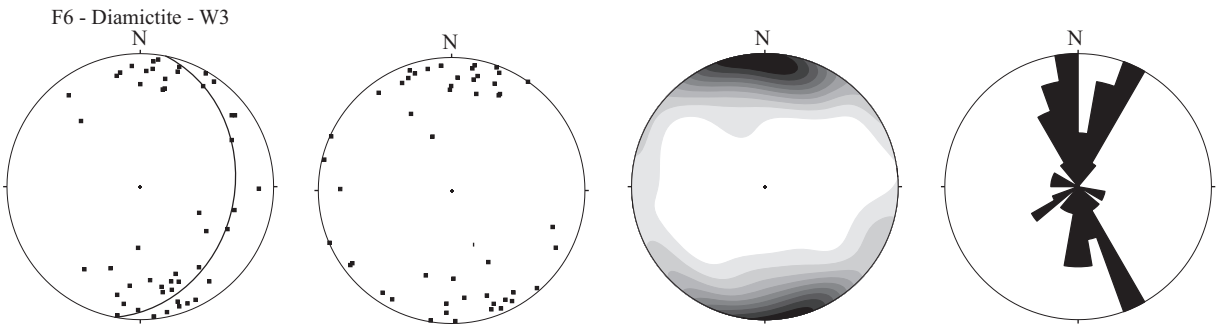

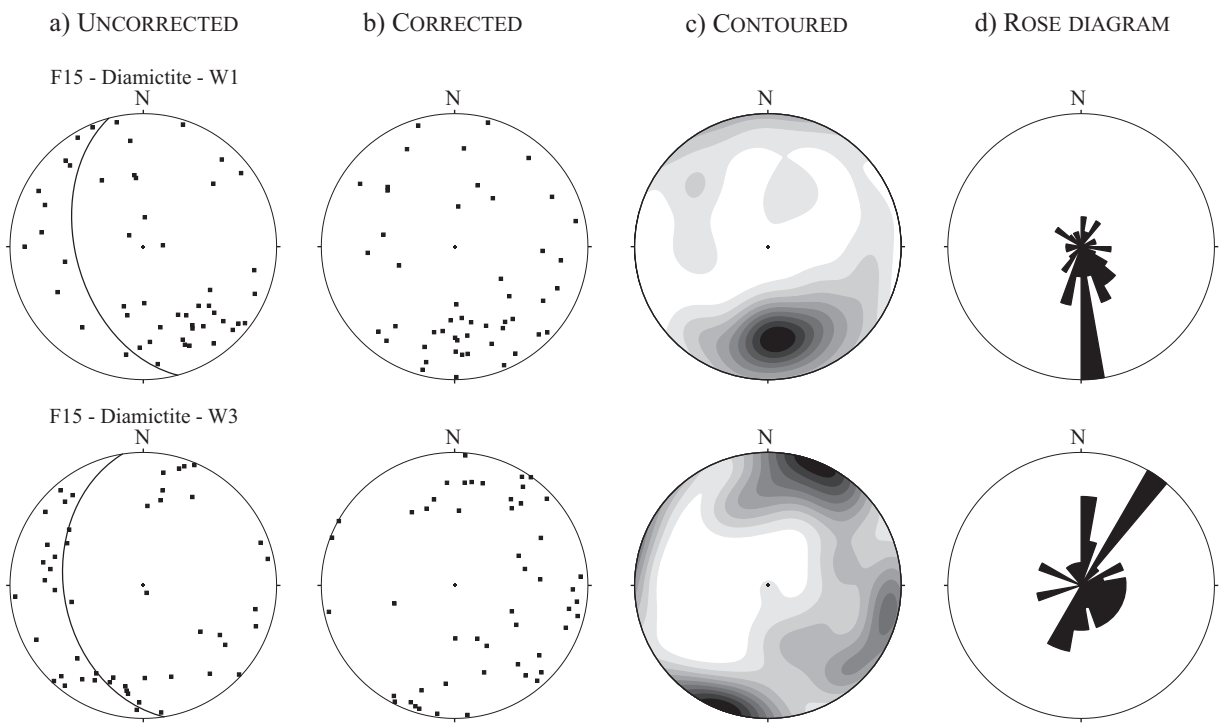
a) UNCORRECTED
b) CORRECTED
c) CONTOURED
d) ROSE DIAGRAM
F15 - Diamictite - W1
F15 - Diamictite - W3
N

APPENDIX D – COMPOSITE SEDIMENTARY LOGS OF THE WILSONBREEN FORMATION, SVALBARD

Detailed sedimentary logs of the Wilsonbreen Formation of NE Svalbard. Dracoisen and Ditlovtoppen logs are drafted from a composite of detailed data collected by MJH, DB, CTS, MSP, IJF and EAM during the summer 2010 field season. The MacDonaldryggen log is drafted from data from the spring 2011 field season. Logs from Andromedafjellet, Reinsryggen, Klofjellet, Backlundtoppen- Kvitfjella ridge, Pinnsvinfjellet, Slangen and Ormen are drafted from data collected during the summer 2011 field season. See logs for key.

APPENDIX E – COMPILATION GEOLOGICAL MAP OF NE SVALBARD WITH AMS RESULTS

Geological map of NE Svalbard. Constructed through a compilation of unpublished CASP maps from (formerly the Cambridge-Spitsbergen Expeditions) led by W. Brian Harland, Geological mapping of Galen Halverson, parts of which is published in Hoffman et al. (2012) and subsequent geological mapping undertaken during this thesis. AMS results, displaying the long (K_1), intermediate (K_2) and short (K_3) susceptibility axes are plotted as black squares, grey triangles and white circles respectively, on lower hemisphere, equal-area stereographic projections.

PUBLICATION 1 - MAGNETIC FABRICS IN THE BASAL ICE OF A SURGE-TYPE GLACIER

Fleming, E.J., Lovell, H., Stevenson, C.T.E., Petronis, M.S., Benn, D.I., Hambrey, M.J., and Fairchild, I.J., 2013, Magnetic fabrics in the basal ice of a surge-type glacier: Journal of Geophysical Research: Earth Surface, p. 2013JF002798.

Abstract:

Anisotropy of magnetic susceptibility (AMS) has been shown to provide specific useful information regarding the kinematics of deformation within subglacially deformed sediments. Here we present results from debris-rich basal glacier ice to examine deformation associated with glacier motion. Basal ice samples were collected from Tunabreen, a polythermal surge-type glacier in Svalbard. The magnetic fabrics recorded show strong correlation with structures within the ice, such as sheath folds and macroscopic stretching lineations. Thermomagnetic, low-temperature susceptibility, varying field susceptibility and isothermal remanent magnetism (IRM) acquisition experiments reveal that the debris-rich basal ice samples have a susceptibility and anisotropy dominated by paramagnetic phases within the detrital sediment. Sediment grains entrained within the basal ice are inferred to have rotated into a preferential alignment during deformation associated with flow of the glacier. An up-glacier directed plunge of magnetic lineations and subtle deviation from bulk glacier flow at the margins highlight the importance of non-coaxial strain during surge propagation. The results suggest that AMS can be used as an ice petrofabric indicator for investigations of glacier deformation and interactions with the bed.

PUBLICATION 2 - NEW INSIGHTS INTO THE DEFORMATION OF A MIDDLE PLEISTOCENE GLACIOTECTONISED SEQUENCE IN NORFOLK, ENGLAND THROUGH MAGNETIC AND STRUCTURAL ANALYSIS

Fleming, E.J., Stevenson, C.T.E., and Petronis, M.S., 2013, New insights into the deformation of a Middle Pleistocene glaciotectonised sequence in Norfolk, England through magnetic and structural analysis: Proceedings of the Geologists' Association, v. 124, p. 834-854.

Abstract:

North Norfolk is a classic area for the study of glacial sediments with a complex glaciotectonic deformational history, but the processes leading to the formation of some structures can be ambiguous. Anisotropy of magnetic susceptibility (AMS) analyses, providing quantitative fabric data, have been combined with the analysis of visible structures and applied to the Bacton Green Till Member, exposed at Bacton, Norfolk. Thermomagnetic curves, low temperature susceptibility and acquisition of isothermal remanent magnetism (IRM) reveal that the magnetic mineralogy is dominated by paramagnetic phases. The magnetic foliation is parallel to fold axial planes and weakly inclined to bedding, whilst the magnetic lineation is orientated parallel to stretching, indicated by the presence of stretching lineations and the trend of sheath folds. Variations in the orientation of the magnetic lineation suggest that the Bacton section has been subject to polyphase deformation. After subaqueous deposition, the sequence was overridden by ice and glaciotectonically deformed which involved stretching initially north–south, then east–west. These results show that AMS can be used to detect strain in three dimensions through a glaciotectonite where paramagnetic mineralogy is dominant. This approach therefore provides further support to the use of AMS as a fast, objective and accurate method of examining strain within deformed glacial sediments.

APPENDIX H - REFERENCES

Aber, J.S. & Ber, A. 2007. Glaciotectonism. Elsevier Science.

Allen, P.A. & Etienne, J.L. 2008. Sedimentary challenge to snowball Earth. *Nature Geoscience*, **1**, 817-825.

Alley, R.B. 1991. Deforming-bed origin for southern Laurentide till sheets? *Journal of Glaciology*, **37**, 125.

Alley, R.B., Blankenship, D.D., Bentley, C.R. & Rooney, S.T. 1986. Deformation of till beneath ice stream B, West Antarctica. *Nature*, **322**, 57-59.

Alley, R.B., Blankenship, D.D., Bentley, C.R. & Rooney, S.T. 1987. Till beneath ice Streams B 3. Till deformation: evidence and implications. *Journal of Geophysical Research*, **92**, 8921-8929.

Alsop, G.I. & Carreras, J. 2007. The structural evolution of sheath folds: A case study from Cap de Creus. *Journal of Structural Geology*, **29**, 1915-1930.

Alsop, G.I. & Holdsworth, R.E. 2004. The geometry and topology of natural sheath folds: a new tool for structural analysis. *Journal of Structural Geology*, **26**, 1561-1589.

Alsop, G.I., Holdsworth, R.E. & McCaffrey, K.J.W. 2007. Scale invariant sheath folds in salt, sediments and shear zones. *Journal of Structural Geology*, **29**, 1585-1604.

Anderson, J.B. 1999. Antarctic marine geology. Cambridge Univiversity Press, Cambridge.

Archanjo, C.J., Silva, M.G., Castro, J.C., Launeau, P., Trindade, R.I.F. & Macedo, J.W.P. 2006. AMS and grain shape fabric of the Late Palaeozoic diamictites of the Southeastern Parana Basin, Brazil. *Journal of Geological Society*, **163**, 95.

Argyle, K.S. & Dunlop, D.J. 1990. Low-temperature and high-temperature hysteresis of small multidomain magnetites (215–540 nm). *Journal of Geophysical Research: Solid Earth*, **95**, 7069-7082.

Arnaud, E. 2012. The paleoclimatic significance of deformation structures in Neoproterozoic successions. *Sedimentary Geology*, **243–244**, 33-56.

Arnaud, E. & Eyles, C.H. 2002. Catastrophic mass failure of a Neoproterozoic glacially influenced continental margin, the Great Breccia, Port Askaig Formation, Scotland. *Sedimentary Geology*, **151**, 313-333.

Atkins, C.B. & Dickinson, W.W. 2007. Landscape modification by meltwater channels at margins of cold-based glaciers, Dry Valleys, Antarctica. *Boreas*, **36**, 47-55.

Averbuch, O., Frizon de Lamotte, D. & Kissel, C. 1992. Magnetic fabric as a structural indicator of the deformation path within a fold-thrust structure: a test case from the Corbières (NE Pyrenees, France). *Journal of Structural Geology*, **14**, 461-474.

Bader, H. 1951. Introduction to ice petrofabrics. *The Journal of Geology*, **59**, 519-536.

Bailey, M.E. & Dunlop, D.J. 1983. Alternating field characteristics of pseudo-single-domain (2–14 μm) and multidomain magnetite. *Earth and Planetary Science Letters*, **63**, 335-352.

Ballet, O., Coey, J. & Burke, K. 1985. Magnetic properties of sheet silicates; 2: 1: 1 layer minerals. *Physics and Chemistry of Minerals*, **12**, 370-378.

Balsley, J.R. & Buddington, A.F. 1960. Magnetic susceptibility anisotropy and fabric of some Adirondack granites and orthogneisses. *American Journal of Science*, **2**, 6-20.

Bamber, J.L. 1987. Internal reflecting horizons in Spitsbergen glaciers. *Annals of Glaciology*, **9**, 5-10.

Banerjee, S.K. & Mellema, J.P. 1974. A new method for the determination of paleointensity from the A.R.M. properties of rocks. *Earth and Planetary Science Letters*, **23**, 177-184.

Banham, P.H. 1965. Pleistocene deposits at Weybourne: New data. *Proceedings of the Geologists' Association*, **76**, 77-81.

Banham, P.H. 1968. A preliminary note on the Pleistocene stratigraphy of north-east Norfolk. *Proceedings of the Geologists' Association*, **79**, 469-474.

Banham, P.H. 1975. Glacitectonic structures: a general discussion with particular reference to the contorted drift of Norfolk. *In*: Wright, A.E. & Moseley, F. (eds.) *Ice Ages: Ancient and Modern*. Seel House Press, Liverpool, 69–94.

Banham, P.H. 1977. Glacitectonites in till stratigraphy. *Boreas*, **6**, 101-105.

Banham, P.H. 1988. Polyphase glaciotectonic deformation in the Contorted Drift of Norfolk. *In*: Croot, D.G. (ed.) *Glaciotectonics; Forms and Processes*. Balkema, Rotterdam, 27-32.

Banham, P.H., Gibbard, P.L., Lunkka, J.P., Parfitt, S.A., Preece, R.C. & Turner, C. 2001. A critical assessment of 'A New Glacial Stratigraphy for Eastern England'. *Quaternary Newsletter*, **93**, 5-14.

Banham, P.H. & Ranson, C.E. 1965. Structural Study of the Contorted Drift and Disturbed Chalk at Weybourne, North Norfolk. *Geological Magazine*, **102**, 164-174.

Bao, H., Fairchild, I.J., Wynn, P.M. & Spotl, C. 2009. Stretching the envelope of past surface environments: Neoproterozoic glacial lakes from Svalbard. *Science*, **323**, 119.

Benediktsson, Í.Ö., Schomacker, A., Lokrantz, H. & Ingólfsson, Ó. 2010. The 1890 surge end moraine at Eyjabakkajökull, Iceland: a re-assessment of a classic glaciotectonic locality. *Quaternary Science Reviews*, **29**, 484-506.

Benn, D.I. 1994. Fabric shape and the interpretation of sedimentary fabric data. *Journal of Sedimentary Research*, **64**, 910-915.

Benn, D.I. 1995. Fabric signature of subglacial till deformation, Breidamerkurjökull, Iceland. *Sedimentology*, **42**, 735-747.

Benn, D.I. & Ballantyne, C.K. 1994. Reconstructing the transport history of glacigenic sediments: a new approach based on the co-variance of clast form indices. *Sedimentary Geology*, **91**, 215-227.

Benn, D.I. & Evans, D.J.A. 1996. The interpretation and classification of subglacially-deformed materials. *Quaternary Science Reviews*, **15**, 23-52.

Benn, D.I. & Evans, D.J.A. 2010. Glaciers and glaciation. second ed. Hodder Education.

Benn, D.I., Kristensen, L. & Gulley, J.D. 2009. Surge propagation constrained by a persistent subglacial conduit, BakaninbreenPaulabreen, Svalbard. *Annals of Glaciology*, **50**, 81-86.

Benn, D.I. & Prave, A.R. 2006. Subglacial and proglacial glacitectonic deformation in the Neoproterozoic Port Askaig Formation, Scotland. *Geomorphology*, **75**, 266-280.

Benn, D.I. & Ringrose, T.J. 2001. Random variation of fabric eigenvalues: implications for the use of a-axis fabric data to differentiate till facies. *Earth Surface Processes and Landforms*, **26**, 295-306.

Bennett, M.R. 2001. The morphology, structural evolution and significance of push moraines. *Earth-Science Reviews*, **53**, 197-236.

Bennett, M.R., Huddart, D. & Thomas, G.S.P. 2002. Facies architecture within a regional glaciolacustrine basin: Copper River, Alaska. *Quaternary Science Reviews*, **21**, 2237-2279.

Bennett, M.R., Waller, R.I., Glasser, N.F., Hambrey, M.J. & Huddart, D. 1999. Glacigenic clast fabrics: genetic fingerprint or wishful thinking? *Journal of Quaternary Science*, **14**,

125-135.

Biedermann, A.R., Lowrie, W. & Hirt, A.M. 2013. A method for improving the measurement of low-field magnetic susceptibility anisotropy in weak samples. *Journal of Applied Geophysics*, **88**, 122-130.

Borradaile, G.J. 1987. Anisotropy of magnetic susceptibility: rock composition versus strain. *Tectonophysics*, **138**, 327-329.

Borradaile, G.J. 1988. Magnetic susceptibility, petrofabrics and strain. *Tectonophysics*, **156**, 1-20.

Borradaile, G.J. 1991. Correlation of strain with anisotropy of magnetic susceptibility (AMS). *pure and applied geophysics*, **135**, 15-29.

Borradaile, G.J., Almqvist, B.S.G. & Geneviciene, I. 2012. Anisotropy of magnetic susceptibility (AMS) and diamagnetic fabrics in the Durness Limestone, NW Scotland. *Journal of Structural Geology*, **34**, 54-60.

Borradaile, G.J. & Henry, B. 1997. Tectonic applications of magnetic susceptibility and its anisotropy. *Earth-Science Reviews*, **42**, 49-93.

Borradaile, G.J. & Jackson, M. 2004. Anisotropy of magnetic susceptibility (AMS): magnetic petrofabrics of deformed rocks. *In*: Martin-Hernández, F., C, L., Aubourg, C. & Jackson, M. (eds.) *Magnetic fabric: methods and applications*. Geological Society, London, Special Publications, 299-360.

Borradaile, G.J. & Jackson, M. 2010. Structural geology, petrofabrics and magnetic fabrics (AMS, AARM, AIRM). *Journal of Structural Geology*, **32**, 1519-1551.

Borradaile, G.J., Mothersill, J., Tarling, D. & Alford, C. 1986. Sources of magnetic susceptibility in a slate. *Earth and Planetary Science Letters*, **76**, 336-340.

Borradaile, G.J. & Puumala, M.A. 1989. Synthetic magnetic fabrics in a plasticene medium. *Tectonophysics*, **164**, 73-78.

Borradaile, G.J. & Tarling, D. 1984. Strain partitioning and magnetic fabrics in particulate flow. *Canadian Journal of Earth Sciences*, **21**, 694-697.

Borradaile, G.J. & Tarling, D.H. 1981. The influence of deformation mechanisms on magnetic fabrics in weakly deformed rocks. *Tectonophysics*, **77**, 151-168.

Borradaile, G.J. & Werner, T. 1994. Magnetic anisotropy of some phyllosilicates.

Tectonophysics, **235**, 223-248.

Boulton, G.S. 1976. The origin of glacially fluted surfaces - observations and theory. *Journal of Glaciology*, **17**, 287-309.

Boulton, G.S. 1978. Boulder shapes and grain-size distributions of debris as indicators of transport paths through a glacier and till genesis. *Sedimentology*, **25**, 773-799.

Boulton, G.S. 1986. A paradigm shift in glaciology? *Nature*, **322**, 18.

Boulton, G.S. 1996. Theory of glacial erosion, transport and deposition as a consequence of subglacial sediment deformation. *Journal of Glaciology*, **42**, 43-62.

Boulton, G.S., Dobbie, K.E. & Zatsepin, S. 2001. Sediment deformation beneath glaciers and its coupling to the subglacial hydraulic system. *Quaternary International*, **86**, 3-28.

Boulton, G.S. & Hagdorn, M. 2006. Glaciology of the British Isles Ice Sheet during the last glacial cycle: form, flow, streams and lobes. *Quaternary Science Reviews*, **25**, 3359-3390.

Boulton, G.S. & Hindmarsh, R.C.A. 1987. Sediment deformation beneath glaciers: rheology and geological consequences. *Journal of Geophysical Research*, **92**, 9059-9082.

Bowen, D.Q., Rose, J., McCabe, A.M. & Sutherland, D.G. 1986. Correlation of Quaternary glaciations in England, Ireland, Scotland and Wales. *Quaternary Science Reviews*, **5**, 299-340.

Boyce, J.I. & Eyles, N. 2000. Architectural element analysis applied to glacial deposits: Internal geometry of a late Pleistocene till sheet, Ontario, Canada. *Geological Society of America Bulletin*, **112**, 98-118.

Bradák, B. 2009. Application of anisotropy of magnetic susceptibility (AMS) for the determination of paleo-wind directions and paleo-environment during the accumulation period of Bag Tephra, Hungary. *Quaternary International*, **198**, 77-84.

Busfield, M.E. & Le Heron, D.P. 2013. Glacitectonic deformation in the Chuos Formation of northern Namibia: implications for Neoproterozoic ice dynamics. *Proceedings of the Geologists' Association*, **124**, 778-789.

Butler, R.F. 1992. Paleomagnetism: magnetic domains to geologic terranes. Blackwell Scientific Publications, Boston.

Callot, J.P., Robion, P., Sassi, W., Guiton, M.L.E., Faure, J.L., Daniel, J.M., Mengus, J.M. & Schmitz, J. 2010. Magnetic characterisation of folded aeolian sandstones:

Interpretation of magnetic fabrics in diamagnetic rocks. *Tectonophysics*, **495**, 230-245.

Carr, S. 2001. Micromorphological criteria for discriminating subglacial and glacimarine sediments: evidence from a contemporary tidewater glacier, Spitsbergen. *Quaternary International*, **86**, 71-79.

Castelnau, O., Shoji, H., Mangeney, A., Milsch, H., Duval, P., Miyamoto, A., Kawada, K. & Watanabe, O. 1998. Anisotropic behavior of GRIP ices and flow in Central Greenland. *Earth and Planetary Science Letters*, **154**, 307-322.

Chernow, R.M., Frey, R.W. & Ellwood, B.B. 1986. Biogenic effects on development of magnetic fabrics in coastal Georgia sediments. *Journal of Sedimentary Research*, **56**, 160-172.

Chumakov, N.M. 1968. Okharaktere pozdnedokembriyskogo oledeneniya Shpitsbergena. [On the character of the Late Precambrian glaciation of Spitsbergen.] *Doklady An SSSR, Seriya geologicheskaya*, **180**, 1446-1449.

Chumakov, N.M. 1978. Dokembriyskiye tillity i tilloidy [Precambrian Tillites and Tilloids]. Nauka, Moscow.

Cifelli, F., Mattei, M., Chadima, M., Hirt, A.M. & Hansen, A. 2005. The origin of tectonic lineation in extensional basins: Combined neutron texture and magnetic analyses on "undeformed" clays. *Earth and Planetary Science Letters*, **235**, 62-78.

Cifelli, F., Mattei, M., Chadima, M., Lenser, S. & Hirt, A.M. 2009. The magnetic fabric in "undeformed clays": AMS and neutron texture analyses from the Rif Chain (Morocco). *Tectonophysics*, **466**, 79-88.

Clark, P.U. 1991. Striated clast pavements: Products of deforming subglacial sediment? *Geology*, **19**, 530.

Clark, P.U. 1994. Unstable Behavior of the Laurentide Ice Sheet over Deforming Sediment and Its Implications for Climate Change. *Quaternary Research*, **41**, 19-25.

Clark, P.U. & Walder, J.S. 1994. Subglacial drainage, eskers, and deforming beds beneath the Laurentide and Eurasian ice sheets. *Geological Society of America Bulletin*, **106**, 304-314.

Cobbold, P.R. & Quinquis, H. 1980. Development of sheath folds in shear regimes. *Journal of Structural Geology*, **2**, 119-126.

Collinson, D.W. 1983. Methods in rock magnetism and palaeomagnetism: techniques and instrumentation. Chapman and Hall.

Conway, H., Catania, G., Raymond, C.F., Gades, A.M., Scambos, T.A. & Engelhardt, H. 2002. Switch of flow direction in an Antarctic ice stream. *Nature*, **419**, 465-467.

Cook, S.J., Waller, R.I. & Knight, P.G. 2006. Glaciohydraulic supercooling: the process and its significance. *Progress in Physical Geography*, **30**, 577-588.

Copons, R., Parés, J.M., Dinarès-Turell, J. & Bordonau, J. 1997. Sampling induced AMS in soft sediments: A case study in Holocene (glaciolacustrine rhythmites from Lake Barrancs (central Pyrenees, Spain). *Physics and Chemistry of the Earth*, **22**, 137-141.

Cutbill, J.L. & Challinor, A. 1965. Revision of the Stratigraphical Scheme for the Carboniferous and Permian Rocks of Spitsbergen and Bjørnøya. *Geological Magazine*, **102**, 418-439.

Dall'olio, E., Felletti, F. & Muttoni, G. 2013. Magnetic-Fabric Analysis As A Tool To Constrain Mechanisms of Deep-Water Mudstone Deposition In the Marnoso Arenacea Formation (Miocene, Italy). *Journal of Sedimentary Research*, **83**, 170-182.

Davies, B.J., Hambrey, M.J., Smellie, J.L., Carrivick, J.L. & Glasser, N.F. 2012. Antarctic Peninsula Ice Sheet evolution during the Cenozoic Era. *Quaternary Science Reviews*, **31**, 30-66.

Day, R., Fuller, M. & Schmidt, V.A. 1977. Hysteresis properties of titanomagnetites: Grain-size and compositional dependence. *Physics of the Earth and Planetary Interiors*, **13**, 260-267.

de Wall, H., Bestmann, M. & Ullemeyer, K. 2000. Anisotropy of diamagnetic susceptibility in Thassos marble: A comparison between measured and modeled data. *Journal of Structural Geology*, **22**, 1761-1771.

Dowdeswell, J.A., Cofaigh, C.Ó., Noormets, R., Larter, R.D., Hillenbrand, C.D., Benetti, S., Evans, J. & Pudsey, C.J. 2008. A major trough-mouth fan on the continental margin of the Bellingshausen Sea, West Antarctica: The Belgica Fan. *Marine Geology*, **252**, 129-140.

Dowdeswell, J.A., Hambrey, M.J. & Ruitang, W. 1985. A comparison of clast fabric and shape in Late Precambrian and modern glacigenic sediments. *Journal of Sedimentary Research*, **55**, 691-704.

Dowdeswell, J.A., Kenyon, N.H., Elverhøi, A., Laberg, J.S., Hollender, F.J., Mienert, J. & Siegert, M.J. 1996. Large-scale sedimentation on the glacier-influenced polar North Atlantic Margins: Long-range side-scan sonar evidence. *Geophysical Research Letters*, **23**, 3535-3538.

Dowdeswell, J.A., Whittington, R.J. & Marienfeld, P. 1994. The origin of massive

diamicton facies by iceberg rafting and scouring, Scoresby Sund, East Greenland. *Sedimentology*, **41**, 21-35.

Drake, L.D. 1977. Human factor in till-fabric analysis. *Geology*, **5**, 180-184.

Dreimanis, A. 1984. Comments and Reply on "Sedimentation in a large lake: A reinterpretation of the late Pleistocene stratigraphy at Scarborough Bluffs, Ontario, Canada": COMMENT. *Geology*, **12**, 185-186.

Dreimanis, A. 1988. Tills: their genetic terminology and classification. *In*: Goldthwait, R.P. & Matsch, C.L. (eds.) *Genetic Classification of Glacigenic Deposits*. Balkema, Rotterdam, 17–83.

Dunlop, D.J., Hanes, J.A. & Buchan, K.L. 1973. Indices of multidomain magnetic behavior in basic igneous rocks: Alternating-field demagnetization, hysteresis, and oxide petrology. *Journal of Geophysical Research*, **78**, 1387-1393.

Dunlop, D.J. & Özdemir, O. 1997. Rock Magnetism: Fundamentals and Frontiers. Cambridge University Press, Cambridge.

Ellwood, B.B. 1980. Application of the anisotropy of magnetic susceptibility method as an indicator of bottom-water flow direction. *Marine Geology*, **34**, M83-M90.

Ellwood, B.B. 1982. Estimates of flow direction for calc-alkaline welded tuffs and paleomagnetic data reliability from anisotropy of magnetic susceptibility measurements: Central San Juan Mountains, southwest Colorado. *Earth and Planetary Science Letters*, **59**, 303-314.

Ellwood, B.B. & Ledbetter, M.T. 1977. Antarctic bottom water fluctuations in the Vema Channel: Effects of velocity changes on particle alignment and size. *Earth and Planetary Science Letters*, **35**, 189-198.

Etienne, J.L., Allen, P.A., Rieu, R. & Le Guerroué, E. 2009. Neoproterozoic Glaciated Basins: A Critical Review of the Snowball Earth Hypothesis by Comparison with Phanerozoic Glaciations. *Glacial Sedimentary Processes and Products*. Blackwell Publishing Ltd., 343-399.

Evans, D.J.A. 2005. Glacial Landsystems. Hodder Arnold.

Evans, D.J.A. & Benn, D.I. 2004. A practical guide to the study of glacial sediments. Arnold London, London.

Evans, D.J.A. & Campbell, I.A. 1995. Quaternary stratigraphy of the buried valleys of the lower Red Deer River, Alberta, Canada. *Journal of Quaternary Science*, **10**, 123-148.

Evans, D.J.A. & Hiemstra, J.F. 2005. Till deposition by glacier submarginal, incremental thickening. *Earth Surface Processes and Landforms*, **30**, 1633-1662.

Evans, D.J.A., Phillips, E.R., Hiemstra, J.F. & Auton, C.A. 2006. Subglacial till: formation, sedimentary characteristics and classification. *Earth-Science Reviews*, **78**, 115-176.

Eyles, C.H. & Eyles, N. 1983a. Glaciomarine model for upper Precambrian diamictites of the Port Askaig Formation, Scotland. *Geology*, **11**, 692.

Eyles, C.H. & Eyles, N. 1983b. Sedimentation in a large lake: A reinterpretation of the late Pleistocene stratigraphy at Scarborough Bluffs, Ontario, Canada. *Geology*, **11**, 146-152.

Eyles, C.H. & Eyles, N. 2000. Subaqueous mass flow origin for Lower Permian diamictites and associated facies of the Grant Group, Barbwire Terrace, Canning Basin, Western Australia. *Sedimentology*, **47**, 343-356.

Eyles, N., Day, T.E. & Gavican, A. 1987. Depositional controls on the magnetic characteristics of lodgement tills and other glacial diamict facies. *Canadian Journal of Earth Sciences*, **34**, 2436–2458.

Eyles, N., Eyles, C.H. & McCabe, A.M. 1989. Sedimentation in an ice-contact subaqueous setting: The mid-Pleistocene 'North Sea Drifts' of Norfolk, U.K. *Quaternary Science Reviews*, **8**, 57-74.

Eyles, N., Eyles, C.H. & Miall, A.D. 1983. Lithofacies types and vertical profile models; an alternative approach to the description and environmental interpretation of glacial diamict and diamictite sequences. *Sedimentology*, **30**, 393-410.

Eyles, N. & Januszczak, N. 2004. Zipper-rift': a tectonic model for Neoproterozoic glaciations during the breakup of Rodinia after 750 Ma. *Earth-Science Reviews*, **65**, 1-73.

Eyles, N. & Kocsis, S. 1988. Sedimentology and clast fabric of subaerial debris flow facies in a glacially-influenced alluvial fan. *Sedimentary Geology*, **59**, 15-28.

Fairchild, I.J. 1983. Effects of glacial transport and neomorphism on Precambrian dolomite crystal sizes. *Nature*, **304**, 714-716.

Fairchild, I.J. 1985. Comment and Reply on" Glaciomarine model for upper Precambrian diamictites of the Port Askaig Formation, Scotland": COMMENT. *Geology*, **13**, 89.

Fairchild, I.J. & Hambrey, M.J. 1984. The Vendian succession of northeastern Spitsbergen: Petrogenesis of a dolomite-tillite association. *Precambrian Research*, **26**, 111-167.

Fairchild, I.J. & Hambrey, M.J. 1995. Vendian basin evolution in East Greenland and NE Svalbard. *Precambrian Research*, **73**, 217-233.

Fairchild, I.J., Hambrey, M.J., Spiro, B. & Jefferson, T.H. 1989. Late Proterozoic glacial carbonates in northeast Spitsbergen: new insights into the carbonate–tillite association. *Geological Magazine*, **126**, 469-490.

Fairchild, I.J. & Kennedy, M.J. 2007. Neoproterozoic glaciation in the Earth System. *Journal of the Geological Society*, **164**, 895.

Ferré, E.C. 2002. Theoretical models of intermediate and inverse AMS fabrics. *Geophysical Research Letters*, **29**, 31-31.

Ferré, E.C., Martín-Hernández, F., Teyssier, C. & Jackson, M. 2004. Paramagnetic and ferromagnetic anisotropy of magnetic susceptibility in migmatites: measurements in high and low fields and kinematic implications. *Geophysical Journal International*, **157**, 1119-1129.

Fish, P.R. & Whiteman, C.A. 2001. Chalk micropalaeontology and the provenancing of middle Pleistocene Lowestoft Formation till in eastern England. *Earth Surface Processes and Landforms*, **26**, 953-970.

Fleming, E.J., Stevenson, C.T.E. & Petronis, M.S. 2013. New insights into the deformation of a Middle Pleistocene glaciotectonised sequence in Norfolk, England through magnetic and structural analysis. *Proceedings of the Geologists' Association*, **124**, 834-854.

Fleming, E.J.F., Lovell, H., Stevenson, C.T.E., Petronis, M.S., Benn, D.I., Hambrey, J.M. & Fairchild, I. in press. Magnetic fabrics in the basal ice of a surge-type glacier. *Journal of Geophysical Research*.

Flinn, D. 1962. On folding during three-dimensional progressive deformation. *Quarterly Journal of the Geological Society*, **118**, 385-428.

Flinn, D. 1965. On the symmetry principle and the deformation ellipsoid. *Geological Magazine*, **102**, 36-45.

Flint, R.F. 1971. Glacial and Quaternary Geology. John Wiley and Sons, New York.

Flint, R.F., Sanders, J.E. & Rodgers, J. 1960a. Diamictite, a substitute term for symmictite. *Geological Society of America Bulletin*, **71**, 1809-1810.

Flint, R.F., Sanders, J.E. & Rodgers, J. 1960b. Symmictite: a name for non sorted terrigenous sedimentary rocks that contain a wide range of particle sizes. *Geological Society of America Bulletin*, **71**, 507-510.

Fricker, H.A., Scambos, T., Bindschadler, R. & Padman, L. 2007. An Active Subglacial Water System in West Antarctica Mapped from Space. *Science*, **315**, 1544-1548.

Fritz, M., Wetterich, S., Meyer, H., Schirrmeister, L., Lantuit, H. & Pollard, W.H. 2011. Origin and characteristics of massive ground ice on Herschel Island (western Canadian Arctic) as revealed by stable water isotope and Hydrochemical signatures. *Permafrost and Periglacial Processes*, **22**, 26-38.

Fuller, M.D. 1962. A magnetic fabric in till. *Geological Magazine*, **99**, 233-237.

Gaillot, P., de Saint-Blanquat, M. & Bouchez, J.-L. 2006. Effects of magnetic interactions in anisotropy of magnetic susceptibility: Models, experiments and implications for igneous rock fabrics quantification. *Tectonophysics*, **418**, 3-19.

Gentoso, M.J., Evenson, E.B., Kodama, K.P., Iverson, N.R., Alley, R.B., Berti, C. & Kozlowski, A. 2012. Exploring till bed kinematics using AMS magnetic fabrics and pebble fabrics: the Weedsport drumlin field, New York State, USA. *Boreas*, **41**, 31-41.

Gibbard, P.L. & Clark, C.D. 2011. Chapter 7 - Pleistocene Glaciation Limits in Great Britain. *In*: Ehlers, J., Gibbard, P.L. & Hughes, P.D. (eds.) *Quaternary Glaciations-Extent and Chronology: A Closer Look, Developments in Quaternary Science* 75-93.

Girdler, R.W. 1961. The Measurement and Computation of Anisotropy of Magnetic Susceptibility of Rocks. *Geophysical Journal of the Royal Astronomical Society*, **5**, 34-44.

Goodsell, B., Hambrey, M.J. & Glasser, N.F. 2002. Formation of band ogives and associated structures at Bas Glacier d'Arolla, Valais, Switzerland. *Journal of Glaciology*, **48**, 287-300.

Goodwin, I. 1993. Basal ice accretion and debris entrainment within the coastal ice margin, Law Dome, Antarctica. *Journal of Glaciology*, **39**, 157-166.

Graham, D.J. & Midgley, N.G. 2000. Graphical representation of particle shape using triangular diagrams: an Excel spreadsheet method. *Earth Surface Processes and Landforms*, **25**, 1473-1477.

Graham, J.W. 1954. Magnetic susceptibility anisotropy, an unexploited petrofabric element. *Geological Society of America Bulletin*, **65**, 1257-1258.

Gravenor, C., Symons, D. & Coyle, D. 1984. Errors in the anisotropy of magnetic susceptibility and magnetic remanence of unconsolidated sediments produced by sampling methods. *Geophysical Research Letters*, **11**, 836-839.

Gravenor, C.P. 1986. Magnetic and pebble fabrics in subaquatic debris-flow deposits. *The Journal of Geology*, **94**, 683-698.

Griffiths, D.H., King, R.F. & Rees, A.I. 1962. The Relevance of Magnetic Measurements on Some Fine Grained Silts to the Study of Their Depositional Process. *Sedimentology*, **1**, 134-144.

Guerrero-Suarez, S. & Martín-Hernández, F. 2012. Magnetic anisotropy of hematite natural crystals: increasing low-field strength experiments. *International Journal of Earth Sciences*, **101**, 625-636.

Halverson, G.P. 2011. Glacial sediments and associated strata of the Polarisbreen Group, northeastern Svalbard. *Geological Society, London, Memoirs*, **36**, 571-579.

Halverson, G.P., Hoffman, P.F., Schrag, D.P., Maloof, A.C. & Rice, A.H.N. 2005. Toward a Neoproterozoic composite carbon-isotope record. *Geological Society of America Bulletin*, **117**, 1181-1207.

Halverson, G.P., Maloof, A.C. & Hoffman, P.F. 2004. The Marinoan glaciation (Neoproterozoic) in northeast Svalbard. *Basin Research*, **16**, 297-324.

Hamblin, R.J.O. 2000. A new glacial stratigraphy for Eastern England. *Mercian Geologist*, **15**, 19-62.

Hamblin, R.J.O., Moorlock, B.S.P., Rose, J., Lee, J.R., Riding, J.B., Booth, S.J. & Pawley, S.M. 2005. Revised Pre-Devensian glacial stratigraphy in Norfolk, England, based on mapping and till provenance. *Netherlands Journal of Geosciences*, **84**, 77-85.

Hambrey, J.M. & Glasser, N.F. 2003a. Glacial sediments: Processes, environments and facies. *In*: Middleton, G.V. (ed.) *Encyclopedia of Sediments and Sedimentary Rocks*. Kluwer, Dordrecht, 316-331.

Hambrey, M.J. 1982. Late Precambrian diamictites of northeastern Svalbard. *Geological Magazine*, **119**, 527-551.

Hambrey, M.J. 1994. Glacial environments. UCL Press, London.

Hambrey, M.J. & Barrett, P.J. 1993. Cenozoic sedimentary and climatic record, Ross Sea region, Antarctica. *The Antarctic Paleoenvironment: A Perspective on Global Change: Part Two*. AGU, Washington, DC, Antarctic Research Series, 91-124.

Hambrey, M.J., Barrett, P.J. & Powell, R.D. 2002. Late Oligocene and early Miocene glacimarine sedimentation in the SW Ross Sea, Antarctica: the record from offshore drilling. *Geological Society, London, Special Publications*, **203**, 105-128.

Hambrey, M.J. & Fitzsimons, S.J. 2010. Development of sediment–landform associations at cold glacier margins, Dry Valleys, Antarctica. *Sedimentology*, **57**, 857-882.

Hambrey, M.J. & Glasser, N.F. 2003b. The role of folding and foliation development in the genesis of medial moraines: examples from Svalbard glaciers. *The Journal of Geology*, **111**, 471-485.

Hambrey, M.J. & Glasser, N.F. 2012. Discriminating glacier thermal and dynamic regimes in the sedimentary record. *Sedimentary Geology*, **251–252**, 1-33.

Hambrey, M.J. & Harland, W.B. 1981. Earth's pre-Pleistocene glacial record. Cambridge University Press, Cambridge.

Hambrey, M.J. & Huddart, D. 1995. Englacial and proglacial glaciotectonic processes at the snout of a thermally complex glacier in Svalbard. *Journal of Quaternary Science*, **10**, 313-326.

Hambrey, M.J., Huddart, D., Bennett, M.R. & Glasser, N.F. 1997. Genesis of 'hummocky moraines' by thrusting in glacier ice: evidence from Svalbard and Britain. *Journal of the Geological Society*, **154**, 623.

Hambrey, M.J. & Lawson, W. 2000. Structural styles and deformation fields in glaciers: a review. *In*: Maltman, A., Hubbard, B. & Hambrey, J.M. (eds.) *Deformation of Glacial Materials*. Geological Society London Special Publications, 59-83.

Hambrey, M.J. & McKelvey, B. 2000. Neogene fjordal sedimentation on the western margin of the Lambert Graben, East Antarctica. *Sedimentology*, **47**, 577-607.

Hambrey, M.J., Murray, T., Glasser, N.F., Hubbard, A., Hubbard, B., Stuart, G., Hansen, S. & Kohler, J. 2005. Structure and changing dynamics of a polythermal valley glacier on a centennial timescale: Midre Lovénbreen, Svalbard. *Journal of Geophysical Research: Earth Surface*, **110**.

Hambrey, M.J. & Spencer, A.M. 1987. Late Precambrian glaciation of central east Greenland. Kommissionen for videnskabelige Undersøgelser i Grønland.

Hamilton, M.A. & Rees, A.I. 1970. The use of magnetic fabric in paleocurrent estimation. *In*: Runcorn, S.K. (ed.) *Paleogeophysics*. Academic Press, New York, 445-464.

Hamilton, N. 1963. Susceptibility Anisotropy Measurements on some Silurian Siltstones. *Nature*, **197**, 170-171.

Hamilton, T.D., Borradaile, G.J. & Lagroix, F. 2004. Sub-fabric identification by standardization of AMS: an example of inferred neotectonic structures from Cyprus. *Geological Society, London, Special Publications*, **238**, 527-540.

Hargraves, R.B., Johnson, D. & Chan, C.Y. 1991. Distribution anisotropy: The cause of AMS

in igneous rocks? *Geophysical Research Letters*, **18**, 2193-2196.

Harland, W.B. 1964. Critical evidence for a great Infra-Cambrian glaciation. *Geologische Rundschau*, **54**, 45-61.

Harland, W.B., Anderson, L.M., Manasrah, D. & Butterfield, N.J. 1997. The geology of Svalbard. Geological Society Publishing House.

Harland, W.B., Hambrey, J.M. & Waddams, P. 1993. Vendian geology of Svalbard. Norsk polarinstitutt.

Harland, W.B. & Wilson, C.B. 1956. The Hecla Hoek succession in Ny Friesland, Spitsbergen. *Geological Magazine*, **93**, 265-286.

Hart, J.K. 1990. Proglacial glaciotectonic deformation and the origin of the Cromer Ridge push moraine complex, North Norfolk, England. *Boreas*, **19**, 165-180.

Hart, J.K. 1998. The deforming bed/debris-rich basal ice continuum and its implications for the formation of glacial landforms (flutes) and sediments (melt-out till). *Quaternary Science Reviews*, **17**, 737-754.

Hart, J.K. 2007. An investigation of subglacial shear zone processes from Weybourne, Norfolk, UK. *Quaternary Science Reviews*, **26**, 2354-2374.

Hart, J.K. & Boulton, G.S. 1991. The interrelation of glaciotectonic and glaciodepositional processes within the glacial environment. *Quaternary Science Reviews*, **10**, 335-350.

Hart, J.K. & Roberts, D.H. 1994. Criteria to distinguish between subglacial glaciotectonic and glaciomarine sedimentation, I. Deformation styles and sedimentology. *Sedimentary Geology*, **91**, 191-213.

Hart, J.K. & Rose, J. 2001. Approaches to the study of glacier bed deformation. *Quaternary International*, **86**, 45-58.

Hart, J.K., Rose, K.C. & Martinez, K. 2011. Subglacial till behaviour derived from in situ wireless multi-sensor subglacial probes: Rheology, hydro-mechanical interactions and till formation. *Quaternary Science Reviews*, **30**, 234–247.

Heider, F., Dunlop, D.J. & Soffel, H.C. 1992. Low-temperature and alternating field demagnetization of saturation remanence and thermoremanence in magnetite grains (0.037 μm to 5 mm). *Journal of Geophysical Research: Solid Earth*, **97**, 9371-9381.

Herrington, P.M. & Fairchild, I.J. 1989. Carbonate shelf and slope facies evolution prior

to Vendian glaciation, central East Greenland. *The Caledonide geology of Scandinavia*. Graham Trotman, London, 285-297.

Hiemstra, J.F., Zaniewski, K., Powell, R.D. & Cowan, E.A. 2004. Strain Signatures of Fjord Sediment Sliding: Micro-Scale Examples from Yakutat Bay and Glacier Bay, Alaska, U.S.A. *Journal of Sedimentary Research*, **74**, 760-769.

Hirt, A.M., Lowrie, W., Clendenen, W.S. & Kligfield, R. 1993. Correlation of strain and the anisotropy of magnetic susceptibility in the Onaping Formation: evidence for a near-circular origin of the Sudbury Basin. *Tectonophysics*, **225**, 231-254.

Hodgkins, R. & Dowdeswell, J.A. 1994. Tectonic processes in Svalbard tide-water glacier surges: evidence from structural glaciology. *Journal of Glaciology*, **40**, 553-560.

Hoffman, P.F. 2009. Pan-glacial—a third state in the climate system. *Geology Today*, **25**, 100-107.

Hoffman, P.F., Halverson, G.P., Domack, E.W., Maloof, A.C., Swanson-Hysell, N.L. & Cox, G.M. 2012. Cryogenian glaciations on the southern tropical paleomargin of Laurentia (NE Svalbard and East Greenland), and a primary origin for the upper Russøya (Islay) carbon isotope excursion. *Precambrian Research*, **206–207**, 137-158.

Hoffman, P.F., Kaufman, A.J., Halverson, G.P. & Schrag, D.P. 1998. A Neoproterozoic snowball earth. *Science*, **281**, 1342.

Hoffmann, K. & Piotrowski, J.A. 2001. Till mélange at Amsdorf, central Germany: sediment erosion, transport and deposition in a complex, soft-bedded subglacial system. *Sedimentary Geology*, **140**, 215-234.

Holmes, C.D. 1941. Till fabric. *Bulletin of the Geological Society of America*, **52**, 1299-1354.

Hooyer, T.S., Iverson, N.R., Lagroix, F. & Thomason, J.F. 2008. Magnetic fabric of sheared till: A strain indicator for evaluating the bed deformation model of glacier flow. *Journal of Geophysical Research*, **113**, 1-15.

Hopkinson, J. 1890. Magnetic Properties of Alloys of Nickel and Iron. *Proceedings of the Royal Society of London*, **48**, 1-13.

Hrouda, F. 2002. Low-field variation of magnetic susceptibility and its effect on the anisotropy of magnetic susceptibility of rocks. *Geophysical Journal International*, **150**, 715-723.

Hrouda, F. 2004. Problems in interpreting AMS parameters in diamagnetic rocks. *In*: Martin-Hernández, F., Aubourg, C. & jackson, M. (eds.) *Magnetic fabric: methods and applications*. Geological Society, London, Special Publications, 49-59.

Hrouda, F. 2009. Determination of field-independent and field-dependent components of anisotropy of susceptibility through standard AMS measurement in variable low fields I: Theory. *Tectonophysics*, **466**, 114-122.

Hrouda, F. 2011. Anisotropy of Magnetic Susceptibility in Variable Low-Fields: A Review. *In*: Petrovský, E., Ivers, D., Harinarayana, T. & Herrero-Bervera, E. (eds.) *The Earth's Magnetic Interior*. Springer Netherlands, IAGA Special Sopron Book Series, 281-292.

Hrouda, F., Chlupácová, M. & Mrázová, S. 2006. Low-field variation of magnetic susceptibility as a tool for magnetic mineralogy of rocks. *Physics of the Earth and Planetary Interiors*, **154**, 323-336.

Hrouda, F., Jelínek, V. & Zapletal, K. 1997a. Refined technique for susceptibility resolution into ferromagnetic and paramagnetic components based on susceptibility temperature-variation measurement. *Geophysical Journal International*, **129**, 715-719.

Hrouda, F. & Kahan, š. 1991. The magnetic fabric relationship between sedimentary and basement nappes in the High Tatra Mountains, N. Slovakia. *Journal of Structural Geology*, **13**, 431-442.

Hrouda, F. & Kapička, A. 1986. The effect of quartz on the magnetic anisotropy of quartzite. *Studia Geophysica et Geodaetica*, **30**, 39-45.

Hrouda, F., Schulmann, K., Suppes, M., Ullemayer, K., de Wall, H. & Weber, K. 1997b. Quantitive relationship between low-field AMS and phyllosilicate fabric: A review. *Physics and Chemistry of the Earth*, **22**, 153-156.

Hubbard, A., Bradwell, T., Golledge, N., Hall, A., Patton, H., Sugden, D., Cooper, R. & Stoker, M. 2009a. Dynamic cycles, ice streams and their impact on the extent, chronology and deglaciation of the British–Irish ice sheet. *Quaternary Science Reviews*, **28**, 758-776.

Hubbard, B. 1991. Freezing-rate effects on the physical character istics of basal ice forlned by net adfreezing. *Journal of Glaciology*, **37**.

Hubbard, B., Cook, S. & Coulson, H. 2009b. Basal ice facies: a review and unifying approach. *Quaternary Science Reviews*, **28**, 1956-1969.

Hubbard, B. & Sharp, M. 1989. Basal ice formation and deformation: a review. *Progress in Physical Geography*, **13**, 529-558.

Hubbard, B. & Sharp, M. 1993. Weertman regelation, multiple refreezing events and the isotopic evolution of the basal ice layer. *Journal of Glaciology*, **39**, 275-291.

Hubbard, B. & Sharp, M. 1995. Basal ice facies and their formation in the western Alps. *Arctic and Alpine Research*, 301-310.

Hubbard, B., Tison, J.-L., Janssens, L. & Spiro, B. 2000. Ice-core evidence of the thickness and character of clear-facies basal ice: Glacier de Tsanfleuron, Switzerland. *Journal of Glaciology*, **46**, 140-150.

Huddart, D. & Hambrey, M.J. 1996. Sedimentary and tectonic development of a high-arctic, thrust-moraine complex: Comfortlessbreen, Svalbard. *Boreas*, **25**, 227-243.

Incoronato, A., Addison, F.T., Tarling, D.H., Nardi, G. & Pescatore, T. 1983. Magnetic fabric investigations of pyroclastic deposits from Phlegrean Fields, southern Italy. *Nature*, **306**, 461-463.

Iverson, N.R., Cohen, D., Hooyer, T.S., Fischer, U.H., Jackson, M., Moore, P.L., Lappegard, G. & Kohler, J. 2003. Effects of Basal Debris on Glacier Flow. *Science*, **301**, 81-84.

Iverson, N.R., Hooyer, T.S., Thomason, J.F., Graesch, M. & Shumway, J.R. 2008. The experimental basis for interpreting particle and magnetic fabrics of sheared till. *Earth Surface Processes and Landforms*, **33**, 627-645.

Jeffery, G.B. 1922. The motion of ellipsoidal particles immersed in a viscous fluid. *Proceedings of the Royal Society of London. Series A, Containing Papers of a Mathematical and Physical Character*, **102**, 161-179.

Jelínek, V. 1981. Characterization of the magnetic fabric of rocks. *Tectonophysics*, **79**, T63-T67.

Jelínek, V. & Kropáček, V. 1978. Statistical processing of anisotropy of magnetic susceptibility measured on groups of specimens. *Studia Geophysica et Geodaetica*, **22**, 50-62.

Jiskoot, H., Murray, T. & Boyle, P. 2000. Controls on the distribution of surge-type glaciers in Svalbard. *Journal of Glaciology*, **46**, 412-422.

Johnson, H.P., Lowrie, W. & Kent, D.V. 1975. Stability of Anhysteretic Remanent Magnetization in Fine and Coarse Magnetite and Maghemite Particles. *Geophysical Journal International*, **41**, 1-10.

Just, J. & Kontny, A. 2012. Thermally induced alterations of minerals during measurements of the temperature dependence of magnetic susceptibility: a case study from the hydrothermally altered Soultz-sous-Forêts granite, France. *International Journal of Earth Sciences*, **101**, 819-839.

Kazi, A. 1972. Clay Mineralogy of the North Sea Drift. *Nature*, **240**, 61-62.

Khan, M.A. 1962. The Anisotropy of Magnetic Susceptibility of Some Igneous and Metamorphic Rocks. *Journal of Geophysical Research*, **67**, 2873-2885.

King, R.F. 1955. The remanent magnetism of artificially deposited sediments. *Geophysical Journal International*, **7**, 115-134.

Kissel, C., Barrier, E., Laj, C. & Lee, T.Q. 1986. Magnetic fabric in "undeformed" marine clays from compressional zones. *Tectonics*, **5**, 769-781.

Kissel, C., Laj, C., Lehman, B., Labyrie, L. & Bout-Roumazeilles, V. 1997. Changes in the strength of the Iceland–Scotland Overflow Water in the last 200,000 years: Evidence from magnetic anisotropy analysis of core SU90-33. *Earth and Planetary Science Letters*, **152**, 25-36.

Kligfield, R., Owens, W.H. & Lowrie, W. 1981. Magnetic susceptibility anisotropy, strain, and progressive deformation in Permian sediments from the Maritime Alps (France). *Earth and Planetary Science Letters*, **55**, 181-189.

Kluiving, S.J., Rappol, M. & Wateren, D.v.d. 1991. Till stratigraphy and ice movements in eastern Overijssel, The Netherlands. *Boreas*, **20**, 193-205.

Knight, P.G. 1997. The basal ice layer of glaciers and ice sheets. *Quaternary Science Reviews*, **16**, 975-993.

Krumbein, W.C. 1941. Measurement and geological significance of shape and roundness of sedimentary particles. *Journal of Sedimentary Research*, **11**, 64-72.

Kulling, O. 1934. Scientific results of the Swedish^ Norwegian arctic expedition in the summer of 1931. *Geografiska Annaler*, **16**, 161-253.

Kurtz, D.D. & Anderson, J.B. 1979. Recognition and sedimentologic description of Recent debris flow deposits from the Ross and Weddell seas, Antarctica. *Journal of Sedimentary Research*, **49**, 1159-1169.

Laberg, J.S. & Vorren, T.O. 1995. Late Weichselian submarine debris flow deposits on the Bear Island Trough Mouth Fan. *Marine Geology*, **127**, 45-72.

Lagroix, F. & Banerjee, S.K. 2002. Paleowind directions from the magnetic fabric of loess profiles in central Alaska. *Earth and Planetary Science Letters*, **195**, 99-112.

Lanci, L., Kent, D.V., Biscaye, P.E. & Bory, A. 2001. Isothermal remanent magnetization of Greenland ice: Preliminary results. *Geophysical Research Letters*, **28**, 1639-1642.

Larsen, N.K., Kronborg, C., Yde, J.C. & Knudsen, N.T. 2010. Debris entrainment by basal freeze-on and thrusting during the 1995–1998 surge of Kuannersuit Glacier on Disko Island, west Greenland. *Earth Surface Processes and Landforms*, **35**, 561-574.

Lawson, W.J., Sharp, M.J. & Hambrey, M.J. 1994. The structural geology of a surge-type glacier. *Journal of Structural Geology*, **16**, 1447-1462.

Le Heron, D.P., Busfield, M.E. & Collins, A.S. 2013a. Bolla Bollana boulder beds: A Neoproterozoic trough mouth fan in South Australia? *Sedimentology*.

Le Heron, D.P., Busfield, M.E. & Kamona, F. 2013b. An interglacial on snowball Earth? Dynamic ice behaviour revealed in the Chuos Formation, Namibia. *Sedimentology*, **60**, 411-427.

Le Heron, D.P., Cox, G., Trundley, A. & Collins, A. 2011. Sea ice–free conditions during the Sturtian glaciation (early Cryogenian), South Australia. *Geology*, **39**, 31-34.

Le Heron, D.P., Sutcliffe, O.E., Whittington, R.J. & Craig, J. 2005. The origins of glacially related soft-sediment deformation structures in Upper Ordovician glaciogenic rocks: implication for ice-sheet dynamics. *Palaeogeography, Palaeoclimatology, Palaeoecology*, **218**, 75-103.

Lee, J.R. & Phillips, E.R. 2008. Progressive soft sediment deformation within a subglacial shear zone - a hybrid mosaic-pervasive deformation model for Middle Pleistocene glaciotectonised sediments from eastern England. *Quaternary Science Reviews*, **27**, 1350-1362.

Lee, J.R., Rose, J., Hamblin, R.J.O. & Moorlock, B.S.P. 2004. Dating the earliest lowland glaciation of eastern England: a pre-MIS 12 early Middle Pleistocene Happisburgh glaciation. *Quaternary Science Reviews*, **23**, 1551-1566.

Lee, J.R., Rose, J., Riding, J.B., Moorlock, B.S.P. & Hamblin, R.J.O. 2002. Testing the case for a Middle Pleistocene Scandinavian glaciation in Eastern England: evidence for a Scottish ice source for tills within the Corton Formation of East Anglia, UK. *Boreas*, **31**, 345-355.

Lefauconnier, B. & Hagen, J.O. 1991. Surging and calving glaciers in eastern Svalbard. *Norsk Polarinstitutt Meddelelser*, **116**, 412 - 422.

Lesemann, J.E., Alsop, G.I. & Piotrowski, J.A. 2010. Incremental subglacial meltwater sediment deposition and deformation associated with repeated ice-bed decoupling: a case study from the Island of Funen, Denmark. *Quaternary Science Reviews*, 3212-3229.

Licciardi, J.M., Clark, P.U., Jenson, J.W. & Macayeal, D.R. 1998. Deglaciation of a soft-

bedded Laurentide ice sheet. *Quaternary Science Reviews*, **17**, 427-448.

Liss, D., Hutton, D.H.W. & Owens, W.H. 2002. Ropy flow structures: A neglected indicator of magma-flow direction in sills and dikes. *Geology*, **30**, 715.

Lovell, H. 2014. *On the ice-sediment-landform associations of surging glaciers on Svalbard.* PhD, Queen Mary University of London.

Lowrie, W. 1990. Identification of ferromagnetic minerals in a rock by coercivity and unblocking temperature properties. *Geophysical Research Letters*, **17**, 159-162.

Lowrie, W. & Fuller, M. 1971. On the alternating field demagnetization characteristics of multidomain thermoremanent magnetization in magnetite. *Journal of Geophysical Research*, **76**, 6339-6349.

Lowrie, W. & Heller, F. 1982. Magnetic properties of marine limestones. *Reviews of Geophysics*, **20**, 171-192.

Lukas, S., Benn, D.I., Boston, C.M., Brook, M., Coray, S., Evans, D.J.A., Graf, A., Kellerer-Pirklbauer, A., Kirkbride, M.P., Krabbendam, M., Lovell, H., Machiedo, M., Mills, S.C., Nye, K., Reinardy, B.T.I., Ross, F.H. & Signer, M. 2013. Clast shape analysis and clast transport paths in glacial environments: A critical review of methods and the role of lithology. *Earth-Science Reviews*, **121**, 96-116.

Lüneburg, C.M., Lampert, S.A., Lebit, H.D., Hirt, A.M., Casey, M. & Lowrie, W. 1999. Magnetic anisotropy, rock fabrics and finite strain in deformed sediments of SW Sardinia (Italy). *Tectonophysics*, **307**, 51-74.

Lunkka, J.P. 1994. Sedimentation and Iithostratigraphy of the North Sea Drift and Lowestoft Till Formations in the Coastal cliffs of northeast Norfolk, England. *Journal of Quaternary Science*, **9**, 209-233.

MacAyeal, D.R. 1992. Irregular oscillations of the West Antarctic ice sheet. *Nature*, **359**, 29-32.

Maizels, J. 2002. 9 - Sediments and landforms of modern proglacial terrestrial environments. *In*: Menzies, J. (ed.) *Modern and Past Glacial Environments*. Butterworth-Heinemann, Oxford, 279-316.

Maloof, A., Halverson, G., Kirschvink, J., Schrag, D., Weiss, B. & Hoffman, P. 2006. Combined paleomagnetic, isotopic, and stratigraphic evidence for true polar wander from the Neoproterozoic Akademikerbreen Group, Svalbard, Norway. *Geological Society of America Bulletin*, **118**, 1099.

Maltman, A.J., Hubbard, B. & Hambrey, M.J. 2000. Deformation of glacial materials:

introduction and overview. *Geological Society London Special Publications*, **176**, 1.

Mansell, D., Luckman, A. & Murray, T. 2012. Dynamics of tidewater surge-type glaciers in northwest Svalbard. *Journal of Glaciology*, **58**, 110-118.

March, A. 1932. Mathematical theory on regulation according to the particle shape and affine deformation. *Zeitschrift Fur Kristallographie*, **81**, 285-297.

Mark, D.M. 1973. Analysis of Axial Orientation Data, Including Till Fabrics. *Geological Society of America Bulletin*, **84**, 1369-1374.

Martín-Hernández, F., Lüneburg, C.M., Aubourg, C. & Jackson, M. 2004. Magnetic fabric: methods and applications — an introduction. *Geological Society, London, Special Publications*, **238**, 1-7.

Mattei, M., Sagnotti, L., Faccenna, C. & Funiciello, R. 1997. Magnetic fabric of weakly deformed clay-rich sediments in the Italian peninsula: Relationship with compressional and extensional tectonics. *Tectonophysics*, **271**, 107-122.

McCabe, C., Jackson, M. & Ellwood, B.B. 1985. Magnetic anisotropy in the Trenton Limestone: Results of a new technique, anisotropy of anhysteretic susceptibility. *Geophysical Research Letters*, **12**, 333-336.

McClay, K.R. & Ellis, P.G. 1987. Geometries of extensional fault systems developed in model experiments. *Geology*, **15**, 341-344.

McKay, R., Browne, G., Carter, L., Cowan, E., Dunbar, G., Krissek, L., Naish, T., Powell, R., Reed, J. & Talarico, F. 2009. The stratigraphic signature of the late Cenozoic Antarctic Ice Sheets in the Ross Embayment. *Geological Society of America Bulletin*, **121**, 1537-1561.

Meier, M.F. & Post, A. 1969. What are glacier surges? *Canadian Journal of Earth Sciences*, **6**, 807-817.

Menzies, J. 1990. Sand intraclasts within a diamicton mélange, southern Niagara Peninsula, Ontario, Canada. *Journal of Quaternary Science*, **5**, 189-206.

Menzies, J. 2000. Micromorphological analyses of microfabrics and microstructures indicative of deformation processes in glacial sediments. *Geological Society London Special Publications*, **176**, 245.

Menzies, J. 2002. Modern and Past Glacial Environments. Butterworth-Heinemann.

Menzies, J., van der Meer, J.J.M. & Rose, J. 2006. Till as a glacial "tectomict", its internal architecture, and the development of a "typing" method for till differentiation. *Geomorphology*, **75**, 172-200.

Mercer, J.H. 1978. West Antarctic ice sheet and CO2 greenhouse effect: a threat of disaster. *Nature*, **271**, 321-325.

Miall, A.D. 1977. A review of the braided-river depositional environment. *Earth-Science Reviews*, **13**, 1-62.

Moncrieff, A.C.M. 1988. *The Vendian Stratigraphy and Sedimentology of East Greenland.* PhD, University of Cambridge.

Moncrieff, A.C.M. 1989. Classification of poorly-sorted sedimentary rocks. *Sedimentary Geology*, **65**, 191-194.

Moncrieff, A.C.M. & Hambrey, M.J. 1988. Late precambrian glacially-related grooved and striated surfaces in the Tillite Group of Central East Greenland. *Palaeogeography, Palaeoclimatology, Palaeoecology*, **65**, 183-200.

Moncrieff, A.C.M. & Hambrey, M.J. 1990. Marginal-marine glacial sedimentation in the late Precambrian succession of East Greenland. *Geological Society, London, Special Publications*, **53**, 387-410.

Moskowitz, B.M. 1991. Hitchhiker's Guide to Magnetism. *Environmental Magnetism Workshop*, Institute for Rock Magnetism.

Moskowitz, B.M., Frankel, R.B. & Bazylinski, D.A. 1993. Rock magnetic criteria for the detection of biogenic magnetite. *Earth and Planetary Science Letters*, **120**, 283-300.

Murray, T., Strozzi, T., Luckman, A., Jiskoot, H. & Christakos, P. 2003. Is there a single surge mechanism? Contrasts in dynamics between glacier surges in Svalbard and other regions. *Journal of Geophysical Research: Solid Earth*, **108**.

Nagata, T. 1961. Rock magnetism. Maruzen Tokyo.

Neves, S.P., da Silva, J.M.R. & Mariano, G. 2005. Oblique lineations in orthogneisses and supracrustal rocks: vertical partitioning of strain in a hot crust (eastern Borborema Province, NE Brazil). *Journal of Structural Geology*, **27**, 1513-1527.

Nordenskiöld, A.E. 1863. Geografisk och geognostisk beskrifning over noröstra delarna af Spetbergen och Hinlopen Strait [Geographic and geognostic descriptions of the northeast part of Spitsbergen and Hinlopen Straight]. *Kungliga Svenska Vetenskapsakademiens Handlingar*, Stockholm.

Nye, F. 1964. Physical properties of crystals. Clarendon Press Oxford.

O'Reilly, W. 1984. Rock and mineral magnetism. Blackie Glasgow.

Ó Cofaigh, C. & Dowdeswell, J.A. 2001. Laminated sediments in glacimarine environments: diagnostic criteria for their interpretation. *Quaternary Science Reviews*, **20**, 1411-1436.

Ó Cofaigh, C., Evans, J., Dowdeswell, J.A. & Larter, R.D. 2007. Till characteristics, genesis and transport beneath Antarctic paleo-ice streams. *Journal of Geophysical Research: Earth Surface*, **112**, F03006.

Owens, W.H. 1994. Laboratory drilling of field-orientated block samples. *Journal of Structural Geology*, **16**, 1719-1721.

Owens, W.H. 2000. Statistical applications to second-rank tensors in magnetic fabric analysis. *Geophysical Journal International*, **142**, 527-538.

Owens, W.H. & Rutter, E.H. 1978. The development of magnetic susceptibility anisotropy through crystallographic preferred orientation in a calcite rock. *Physics of the Earth and Planetary Interiors*, **16**, 215-222.

Parés, J.M., Hassold, N.J.C., Rea, D.K. & van der Pluijm, B.A. 2007. Paleocurrent directions from paleomagnetic reorientation of magnetic fabrics in deep-sea sediments at the Antarctic Peninsula Pacific margin (ODP Sites 1095, 1101). *Marine Geology*, **242**, 261-269.

Parés, J.M. & van der Pluijm, B.A. 2002. Evaluating magnetic lineations (AMS) in deformed rocks. *Tectonophysics*, **350**, 283-298.

Parés, J.M., van der Pluijm, B.A. & Dinarès-Turell, J. 1999. Evolution of magnetic fabrics during incipient deformation of mudrocks (Pyrenees, northern Spain). *Tectonophysics*, **307**, 1-14.

Perrin, R.M.S., Rose, J. & Davies, H. 1979. The Distribution, Variation and Origins of Pre-Devensian Tills in Eastern England. *Philosophical Transactions of the Royal Society of London. Series B, Biological Sciences*, **287**, 535-570.

Petronis, M.S., O'Driscoll, B. & Lindline, J. 2011. Late stage oxide growth associated with hydrothermal alteration of the Western Granite, Isle of Rum, NW Scotland. *Geochemistry, Geophysics, Geosystems*, **12**, Q01001.

Phillips, E., Everest, J. & Reeves, H. 2013. Micromorphological evidence for subglacial multiphase sedimentation and deformation during overpressurized fluid flow associated with hydrofracturing. *Boreas*, **42**, 395-427.

Phillips, E.R. & Auton, C.A. 2000. Micromorphological evidence for polyphase deformation of glaciolacustrine sediments from Strathspey, Scotland. *In*: Maltman, A.J., Hubbard, B. & Hambrey, J.M. (eds.) *Deformation of Glacial Materials*. Geological Society London Special Publications, 279–292.

Phillips, E.R., Evans, D.J.A. & Auton, C.A. 2002. Polyphase deformation at an oscillating ice margin following the Loch Lomond Readvance, central Scotland, UK. *Sedimentary Geology*, **149**, 157-182.

Phillips, E.R., Lee, J.R. & Burke, H. 2008. Progressive proglacial to subglacial deformation and syntectonic sedimentation at the margins of the Mid-Pleistocene British Ice Sheet: evidence from north Norfolk, UK. *Quaternary Science Reviews*, **27**, 1848-1871.

Phillips, E.R., Merritt, J., Auton, C. & Golledge, N. 2007. Microstructures in subglacial and proglacial sediments: understanding faults, folds and fabrics, and the influence of water on the style of deformation. *Quaternary Science Reviews*, **26**, 1499-1528.

Phillips, E.R., van der Meer, J.J.M. & Ferguson, A. 2011. A new 'microstructural mapping' methodology for the identification, analysis and interpretation of polyphase deformation within subglacial sediments. *Quaternary Science Reviews*, **30**, 2570-2596.

Piotrowski, J.A., Larsen, N.K. & Junge, F.W. 2004. Reflections on soft subglacial beds as a mosaic of deforming and stable spots. *Quaternary Science Reviews*, **23**, 993-1000.

Piotrowski, J.A., Mickelson, D.M., Tulaczyk, S., Krzyszkowski, D. & Junge, F.W. 2001. Were deforming subglacial beds beneath past ice sheets really widespread? *Quaternary International*, **86**, 139-150.

Piper, J.D.A., Elliot, M.T. & Kneller, B.C. 1996. Anisotropy of magnetic susceptibility in a Palaeozoic flysch basin: the Windermere Supergroup, northern England. *Sedimentary Geology*, **106**, 235-258.

Pokorný, J., Pokorný, P., Suza, P. & Hrouda, F. 2011. A Multi-Function Kappabridge for High Precision Measurement of the AMS and the Variations of Magnetic Susceptibility with Field, Temperature and Frequency. *In*: Petrovský, E., Ivers, D., Harinarayana, T. & Herrero-Bervera, E. (eds.) *The Earth's Magnetic Interior*. Springer Netherlands, IAGA Special Sopron Book Series, 293-301.

Potter, D.K. & Stephenson, A. 1988. Single-domain particles in rocks and magnetic fabric analysis. *Geophysical Research Letters*, **15**, 1097-1100.

Powell, R.D. 1984. Glacimarine processes and inductive lithofacies modelling of ice shelf and tidewater glacier sediments based on Quaternary examples. *Marine Geology*, **57**, 1-52.

Powell, R.D. 1990. Glacimarine processes at grounding-line fans and their growth to ice-contact deltas. *Geological Society, London, Special Publications*, **53**, 53-73.

Powell, R.D. & Domack, E. 1995. Modern glaciomarine environments. *In*: Menzies, J. (ed.) *Modern and Past Glacial Environments*. Elsevier, 445-486.

Preece, R.C., Parfitt, S.A., Coope, G.R., Penkman, K.E.H., Ponel, P. & Whittaker, J.E. 2009. Biostratigraphic and aminostratigraphic constraints on the age of the Middle Pleistocene glacial succession in north Norfolk, UK. *Journal of Quaternary Science*, **24**, 557-580.

Pueyo Anchuela, Ó., Ramajo Cordero, J., Gil Imaz, A. & Meléndez Hevia, G. 2013. Analysis of anisotropy of magnetic susceptibility in iron-oolitic beds: a potential tool for paleocurrent identification. *International Journal of Earth Sciences*, **102**, 1131-1149.

Ramsay, J.G. & Huber, M.I. 1983. The Techniques of Modern Structural Geology, Volume 1: Strain Analysis. Academic Press, London.

Rathore, J.S. 1979. Magnetic susceptibility anisotropy in the Cambrian slate belt of North Wales and correlation with strain. *Tectonophysics*, **53**, 83-97.

Rees, A.I. 1961. The Effect of Water Currents on the Magnetic Remanence and Anisotropy of Susceptibility of Some Sediments. *Geophysical Journal of the Royal Astronomical Society*, **5**, 235-251.

Rees, A.I. 1965. The use of anisotropy of magnetic susceptibility in the estimation of sedimentary fabric. *Sedimentology*, **4**, 257-271.

Rees, A.I., Von Rad, U. & Shepard, F.P. 1968. Magnetic fabric of sediments from the La Jolla submarine Canyon and Fan, California. *Marine Geology*, **6**, 145-178.

Rees, A.I. & Woodall, W.A. 1975. The magnetic fabric of some laboratory-deposited sediments. *Earth and Planetary Science Letters*, **25**, 121-130.

Richter, C. & van der Pluijm, B.A. 1994. Separation of paramagnetic and ferrimagnetic susceptibilities using low temperature magnetic susceptibilities and comparison with high field methods. *Physics of the Earth and Planetary Interiors*, **82**, 113-123.

Riedel, W. 1929. Zur Mechanik geologischer Brucherscheinungen. *Zentralblatt für Geologie und Paleontologie*, 354-368.

Rigsby, G.P. 1958. Fabrics of glacier and laboratory deformed ice. *Symposium on Physics of the Movement of the Ice, Symposium of Chamonix*, 16-24.

Roberts, D.H. & Hart, J.K. 2005. The deforming bed characteristics of a stratified till assemblage in north East Anglia, UK: investigating controls on sediment rheology and strain signatures. *Quaternary Science Reviews*, **24**, 123-140.

Rochette, P. 1987. Magnetic susceptibility of the rock matrix related to magnetic fabric studies. *Journal of Structural Geology*, **9**, 1015-1020.

Rochette, P. 1988. Inverse magnetic fabric in carbonate-bearing rocks. *Earth and Planetary Science Letters*, **90**, 229-237.

Rochette, P., Jackson, M. & Aubourg, C. 1992. Rock magnetism and the interpretation of anisotropy of magnetic susceptibility. *Reviews of Geophysics*, **30**, 209-226.

Rose, J., Moorlock, B.S.P. & Hamblin, R.J.O. 2001. Pre-Anglian fluvial and coastal deposits in Eastern England: lithostratigraphy and palaeoenvironments. *Quaternary International*, **79**, 5-22.

Samyn, D., Fitzsimons, S. & Lorrain, R. 2010. Rotating micro-structures in Antarctic cold basal ice: implications for glacier flow and its interpretation. *International Journal of Earth Sciences*, **99**, 1849-1857.

Samyn, D., Svensson, A. & Fitzsimons, S.J. 2008. Dynamic implications of discontinuous recrystallization in cold basal ice: Taylor Glacier, Antarctica. *Journal of Geophysical Research*, **113**, F03S90.

Scheib, A.J., Lee, J.R., Breward, N. & Riding, J.B. 2011. Reconstructing flow paths of the Middle Pleistocene British Ice Sheet in central-eastern England: the application of regional soil geochemical data. *Proceedings of the Geologists' Association*, **122**, 432-444.

Schermerhorn, L.J.G. 1974. Late Precambrian mixites: Glacial and/or nonglacial? *American Journal of Science*, **274**, 673.

Schieber, J. & Ellwood, B.B. 1988. The coincidence of macroscopic paleocurrent indicators and magnetic lineation in shales from the Precambrian Belt Basin. *Journal of Sedimentary Research*, **58**, 830-835.

Schieber, J. & Ellwood, B.B. 1993. Determination of basinwide paleocurrent patterns in a shale succession from anisotropy of magnetic susceptibility (AMS); a case study of the mid-Proterozoic Newland Formation, Montana. *Journal of Sedimentary Research*, **63**, 874-880.

Schwehr, K. & Tauxe, L. 2003. Characterization of soft-sediment deformation: Detection of cryptoslumps using magnetic methods. *Geology*, **31**, 203-206.

Sharp, M., Lawson, W. & Anderson, R.S. 1988. Tectonic processes in a surge-type glacier. *Journal of Structural Geology*, **10**, 499-515.

Shumway, J.R. & Iverson, N.R. 2009. Magnetic fabrics of the Douglas Till of the Superior lobe: exploring bed-deformation kinematics. *Quaternary Science Reviews*, **28**, 107-119.

Siegert, M.J., Carter, S., Tabacco, I., Popov, S. & Blankenship, D.D. 2005. A revised inventory of Antarctic subglacial lakes. *Antarctic Science*, **17**, 453-460.

Slater, G. 1926. Glacial tectonics as reflected in disturbed drift deposits. *Proceedings of the Geologists' Association*, **37**, 392 - 400.

Smith, J.V. 2000. Flow pattern within a Permian submarine slump recorded by oblique folds and deformed fossils, Ulladulla, south-eastern Australia. *Sedimentology*, **47**, 357-366.

Sneed, E.D. & Folk, R.L. 1958. Pebbles in the lower Colorado River, Texas a study in particle morphogenesis. *The Journal of Geology*, 114-150.

Souchez, R., Vandenschrick, G., Lorrain, R. & Tison, J.L. 2000. Basal ice formation and deformation in central Greenland: a review of existing and new ice core data. *Geological Society London Special Publications*, **176**, 13.

Spencer, A.M. 1971. Late Pre-Cambrian glaciation in Scotland. Geological Society of London.

Stacey, F.D. 1960. Magnetic anisotropy of igneous rocks. *Journal of Geophysical Research*, **65**, 2429-2442.

Stephenson, A. 1994. Distribution anisotropy: two simple models for magnetic lineation and foliation. *Physics of the Earth and Planetary Interiors*, **82**, 49-53.

Stephenson, A., Sadikun, S. & Potter, D.K. 1986. A theoretical and experimental comparison of the anisotropies of magnetic susceptibility and remanence in rocks and minerals. *Geophysical Journal of the Royal Astronomical Society*, **84**, 185-200.

Stevenson, C.T.E., Owens, W.H. & Hutton, D.H.W. 2007. Flow lobes in granite: The determination of magma flow direction in the Trawenagh Bay Granite, northwestern Ireland, using anisotropy of magnetic susceptibility. *Geological Society of America Bulletin*, **119**, 1368-1386.

Stewart, R.A., Bryant, D. & Sweat, M.J. 1988. Nature and origin of corrugated ground moraine of the Des Moines lobe, Story County, Iowa. *Geomorphology*, **1**, 111-130.

Stone, D.B. 1963. Anisotropic Magnetic Susceptibility Measurements on a Phonolite and on a

Folded Metamorphic Rock. *Geophysical Journal of the Royal Astronomical Society*, **7**, 375-390.

Stupavsky, M. & Gravenor, C.P. 1975. Magnetic fabric around boulders in till. *Bulletin of the Geological Society of America*, **86**, 1534-1536.

Stupavsky, M., Gravenor, C.P. & Symons, D.T.A. 1974a. Paleomagnetism and magnetic fabric of the Leaside and Sunnybrook Tills near Toronto, Ontario. *Bulletin of the Geological Society of America*, **85**, 1233 - 1236.

Stupavsky, M., Symons, D.T.A. & Gravenor, C.P. 1974b. Paleomagnetism of the Port Stanley Till, Ontario. *Geological Society of America Bulletin*, **85**, 141-144.

Syvitski, J.P.M., Andrews, J.T. & Dowdeswell, J.A. 1996. Sediment deposition in an iceberg-dominated glacimarine environment, East Greenland: basin fill implications. *Global and Planetary Change*, **12**, 251-270.

Taira, A. & Lienert, B.R. 1979. The comparative reliability of magnetic, photometric and microscopic methods of determining the orientations of sedimentary grains. *Journal of Sedimentary Research*, **49**, 759.

Tarling, D.H. 1983. Palaeomagnetism: Principles and applications in geology, geophysics, and archaeology. Chapman and Hall London.

Tarling, D.H. & Hrouda, F. 1993. The magnetic anisotropy of rocks. Chapman and Hall, London.

Tauxe, L. 1998. Paleomagnetic principles and practice. Kluwer, Dordecht.

Théveniaut, H. & Freyssinet, P. 1999. Paleomagnetism applied to lateritic profiles to assess saprolite and duricrust formation processes: the example of Mont Baduel profile (French Guiana). *Palaeogeography, Palaeoclimatology, Palaeoecology*, **148**, 209-231.

Thomas, G.S.P. & Connell, R.J. 1985. Iceberg drop, dump, and grounding structures from Pleistocene glacio-lacustrine sediments, Scotland. *Journal of Sedimentary Research*, **55**, 243-249.

Thomason, J.F. & Iverson, N.R. 2006. Microfabric and microshear evolution in deformed till. *Quaternary Science Reviews*, **25**, 1027-1038.

Thomason, J.F. & Iverson, N.R. 2009. Deformation of the Batestown till of the Lake Michigan lobe, Laurentide ice sheet. *Journal of Glaciology*, **55**, 131-146.

Tison, J.L. & Lorrain, R. 1987. A mechanism of basal ice-layer formation involving major ice-fabric changes. *Journal of Glaciology*, **33**, 47-50.

Tison, J.L., Thorsteinsson, T., Lorrain, R.D. & Kipfstuhl, J. 1994. Origin and development of textures and fabrics in basal ice at Summit, Central Greenland. *Earth and Planetary Science Letters*, **125**, 421-437.

Twiss, R.J. & Moores, E.M. 1992. Structural geology. WH Freeman, New York.

Tylmann, K., Piotrowski, J.A. & Wysota, W. 2012. The ice/bed interface mosaic: deforming spots intervening with stable areas under the fringe of the Scandinavian Ice Sheet at Sampława, Poland. *Boreas*.

van der Meer, J.M. 1993. Microscopic evidence of subglacial deformation. *Quaternary Science Reviews*, **12**, 553-587.

van der Wateren, F.M. 1999. Structural geology and sedimentology of the Heiligenhafen till section, Northern Germany. *Quaternary Science Reviews*, **18**, 1625-1639.

van der Wateren, F.M. 2002. Processes of glaciotectonism. *In*: Menzies, J. (ed.) *Modern and Past Glacial Environments*. Butterworth-Heinemann, Oxford, 417-443.

van der Wateren, F.M., Kluiving, S.J. & Bartek, L.R. 2000. Kinematic indicators of subglacial shearing. *In*: Maltman, A., Hubbard, B. & Hambrey, J.M. (eds.) *Deformation of Glacial Materials*. Geological Society London Special Publications, 259–291.

Verwey, E.J.W. 1939. Electronic conduction of magnetite (Fe3O4) and its transition point at low temperatures. *Nature*, **144**, 327-328.

Verwey, E.J.W. & Haayman, P.W. 1941. Electronic conductivity and transition point of magnetite ("Fe3O4"). *Physica*, **8**, 979-987.

Voight, W. & Kinoshita, S. 1907. Bestimmung absoluter Werte von Magnetiserungszahlen, inbesondere für Kristalle. *Annale der Physik*, **24**, 492-514.

Waller, R.I., Murton, J.B. & Knight, P.G. 2009. Basal glacier ice and massive ground ice: Different scientists, same science? *Geological Society, London, Special Publications*, **320**, 57-69.

Waller, R.I., Phillips, E.R., Murton, J., Lee, J.R. & Whiteman, C. 2011. Sand intraclasts as evidence of subglacial deformation of Middle Pleistocene permafrost, North Norfolk, UK. *Quaternary Science Reviews*, **30**, 3481-3500.

West, R.G. & Donner, J.J. 1956. The glaciations of East Anglia and the East Midlands: a differentiation based on stone-orientation measurements of the tills. *Quarterly Journal of the Geological Society*, **112**, 69-91.

Wilen, L.A., Diprinzio, C.L., Alley, R.B. & Azuma, N. 2003. Development, principles, and applications of automated ice fabric analyzers. *Microscopy Research and Technique*, **62**, 2-18.

Williams, P.F., Collins, A.R. & Wiltshire, R.G. 1969. Cleavage and Penecontemporaneous Deformation Structures in Sedimentary Rocks. *The Journal of Geology*, **77**, 415-425.

Wilson, C.B. & Harland, W.B. 1964. The Polarisbreen Series and other evidences of late Pre-Cambrian ice ages in Spitsbergen. *Geological Magazine*, **101**, 198-219.

Wilson, C.J.L. 2000. Experimental work on the effect of pre-existing anisotropy on fabric development in glaciers. *Geological Society London Special Publications*, **176**, 97.

Wilson, C.J.L. & Peternell, M. 2011. Evaluating ice fabrics using fabric analyser techniques in Sorsdal Glacier, East Antarctica. *Journal of Glaciology*, **57**, 881-894.

Wilson, C.J.L. & Sim, H.M. 2002. The localization of strain and c-axis evolution in anisotropic ice. *Journal of Glaciology*, **48**, 601-610.

Wingham, D.J., Siegert, M.J., Shepherd, A. & Muir, A.S. 2006. Rapid discharge connects Antarctic subglacial lakes. *Nature*, **440**, 1033-1036.

Xu, S. & Dunlop, D.J. 1995. Toward a better understanding of the Lowrie-Fuller test. *Journal of Geophysical Research: Solid Earth*, **100**, 22533-22542.

Zaniewski, K. & van der Meer, J.J.M. 2005. Quantification of plasmic fabric through image analysis. *CATENA*, **63**, 109-127.

Appendix D - Sedimentary Logs of the Wilsonbreen Formation, NE Svalbard

Ormen

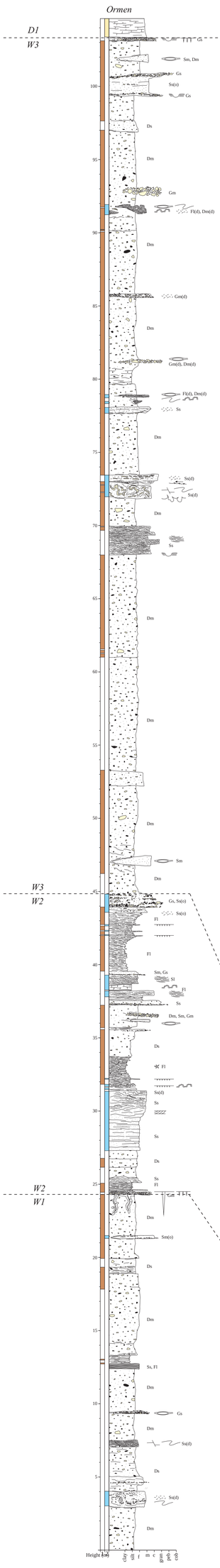

Pinnsvinfjellet

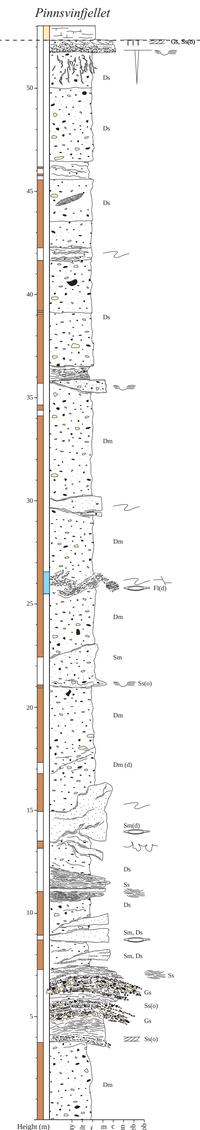

Backlundtoppen-Kvitfjella ridge

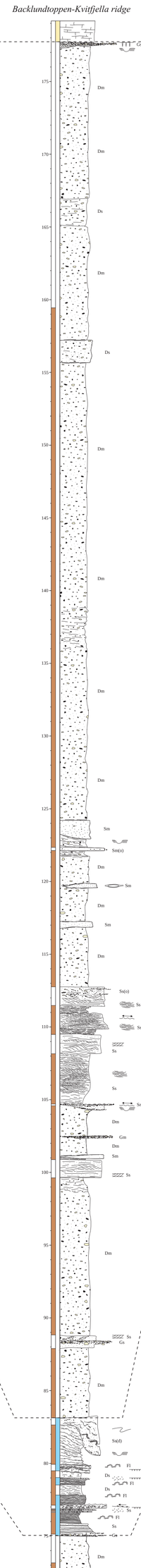

Klofjellet

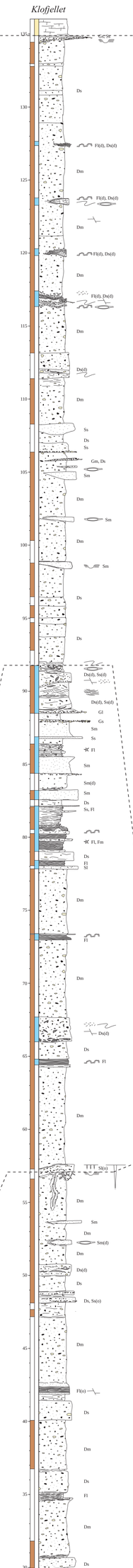
Ds
Fl(d), Ds(d)
Dm
Fl(d), Ds(d)
Dm
Fl(d), Ds(d)
Dm
Fl(d), Ds(d)
Dm
Ds(d)
Dm
Ss
Ds
Ss
Gm, Ds
Sm
Dm
Sm
Dm
Sm
Ds
Ds
Dm(d), Ss(d)
Dm(d), Ss(d)
Gl
Gs
Sm
Ss
Fl
Sm
Sm(d)
Sm
Ds
Ss, Fl
Fl
Sl
Fl, Fm
Ds
Fl
Sl
Dm
Fl
Dm
Dm
Ds(d)
Fl
Dm
Ss
Ds
Fl
Ss
Ss
Sm(o)
Dm
Gm
Dm
Sm
Dm
Sm(d)
Dm
Ds(d)
Ds
Ds, Ss(o)
Ss
Gs
Dm
Gs(d)
Sl(d)
Sm
Ss
Fl
Sm
Sm(d)
Sm
Ds
Ss, Fl
Fl
Sl
Dm
Ds
Ds
Fl
Ss
Fl
Dm
Ds
Ds
Ds
Fl
Ss
Fl
Dm
Ds
Ds
Fl
Ss
Fl
Dm
Ds
Ds
Fl
Ss
Fl
Dm

Appendix E - Geological Map and Anisotropy of Magnetic Susceptibility of the Wilsonbreen Formation, NE Svalbard